109.9. Extensions beyond the MSSM

Extensions of the MSSM have been proposed to solve a variety of theoretical problems. One such problem involves the μ parameter of the MSSM. Although μ is a supersymmetry-*preserving* parameter, it must be of order the effective supersymmetry-breaking scale of the MSSM to yield a consistent supersymmetric phenomenology [228]. Any natural solution to the so-called μ-problem must incorporate a symmetry that enforces $\mu = 0$ and a small symmetry-breaking parameter that generates a value of μ that is not parametrically larger than the effective supersymmetry-breaking scale [229]. A number of proposed mechanisms in the literature (*e.g.*, see Refs. 228–231) provide concrete examples of a natural solution to the μ-problem of the MSSM.

In extensions of the MSSM, new compelling solutions to the μ-problem are possible. For example, one can replace μ by the vacuum expectation value of a new SU(3)×SU(2)×U(1) singlet scalar field. This is the NMSSM, which yields phenomena that were briefly discussed in Section 109.4–Section 109.7. The NMSSM superpotential consists only of trilinear terms whose coefficients are dimensionless. There are some advantages to extending the NMSSM further to the USSM [98] by adding a new broken U(1) gauge symmetry [232], under which the singlet field is charged.

Alternatively, one can consider a generalized version of the NMSSM (called the GNMSSM in Ref. 180), where all possible renormalizable terms in the superpotential are allowed, which yields new supersymmetric mass terms (analogous to the μ term of the MSSM). A discussion of the parameters of the GNMSSM can be found in Ref. 76. Although the GNMSSM does not solve the μ-problem, it does exhibit regions of parameter space in which the degree of fine-tuning is relaxed, as discussed in Section 109.7.1.

The generation of the μ term may be connected with the solution to the strong CP problem [233]. Models of this type, which include new gauge singlet fields that are charged under the Peccei-Quinn (PQ) symmetry [234], were first proposed in Ref. 228. The breaking of the PQ symmetry is thus intimately tied to supersymmetry breaking, while naturally yielding a value of μ that is of order the electroweak symmetry breaking scale [235].

It is also possible to add higher dimensional Higgs multiplets, such as Higgs triplet superfields [236], provided a custodial-symmetric model (in which the ρ-parameter of precision electroweak physics is close to 1 [201]) can be formulated. Such models can provide a rich phenomenology of new signals for future LHC studies.

All supersymmetric models discussed so far in this review possess self-conjugate fermions—the Majorana gluinos and neutralinos. However, it is possible to add additional chiral superfields in the adjoint representation. The spin-1/2 components of these new superfields can pair up with the gauginos to form Dirac gauginos [237,238]. Such states appear in models of so-called supersoft supersymmetry breaking [239], in some generalized GMSB models [240] and in R-symmetric supersymmetry [241,242]. Such approaches often lead to improved naturalness and/or significantly relaxed flavor constraints. The implications of models of Dirac gauginos on the observed Higgs boson mass and its properties is addressed in Ref. 243.

For completeness, we briefly note other MSSM extensions considered in the literature. These include an enlarged electroweak gauge group beyond SU(2)×U(1) [244]; and/or the addition of new (possibly exotic) matter supermultiplets such as vector-like fermions and their superpartners [181,245].

References:

1. The early history of supersymmetry and a guide to the original literature can be found in *The Supersymmetric World—The Beginnings of the Theory*, edited by G. Kane and M. Shifman (World Scientific, Singapore, 2000).
2. R. Haag, J.T. Lopuszanski, and M. Sohnius, Nucl. Phys. **B88**, 257 (1975);
   S.R. Coleman and J. Mandula, Phys. Rev. **159**, 1251 (1967).
3. H.P. Nilles, Phys. Reports **110**, 1 (1984).
4. S. Weinberg, *The Quantum Theory of Fields, Volume III: Supersymmetry* (Cambridge University Press, Cambridge, UK, 2000);
   P. Binétruy, *Supersymmetry : Theory, Experiment, and Cosmology* (Oxford University Press, Oxford, UK, 2006).
5. P. Nath, *Supersymmetry, Supergravity, and Unification* (Cambridge University Press, Cambridge, UK, 2017).
6. S.P. Martin, in *Perspectives on Supersymmetry II*, edited by G.L. Kane (World Scientific, Singapore, 2010) pp. 1–153; see arXiv:hep-ph/9709356 for the latest version and `http://www.niu.edu/spmartin/primer/` for the most recent errata.
7. E. Witten, Nucl. Phys. **B188**, 513 (1981).
8. S. Dimopoulos and H. Georgi, Nucl. Phys. **B193**, 150 (1981).
9. N. Sakai, Z. Phys. **C11**, 153 (1981);
   R.K. Kaul, Phys. Lett. **109B**, 19 (1982);
   R.K. Kaul and M. Parthasarathi, Nucl. Phys. **B199**, 36 (1982).
10. L. Susskind, Phys. Reports **104**, 181 (1984).
11. L. Girardello and M. Grisaru, Nucl. Phys. **B194**, 65 (1982).
12. L.J. Hall and L. Randall, Phys. Rev. Lett. **65**, 2939 (1990);
    I. Jack and D.R.T. Jones, Phys. Lett. **B457**, 101 (1999).
13. O. Buchmüller and P. de Jong, *"Supersymmetry Part II (Experiment),"* and associated *Particle Listings: Other Searches–Supersymmetric Particles,* in the web edition of the *Review of Particle Physics* at `http://pdg.lbl.gov`.
14. V.F. Weisskopf, Phys. Rev. **56**, 72 (1939).
15. For a review, see *e.g.*, N. Polonsky, *Supersymmetry: Structure and phenomena. Extensions of the standard model*, Lect. Notes Phys. **M68**, 1 (2001).
16. G. Bertone, D. Hooper, and J. Silk, Phys. Reports **405**, 279 (2005).
17. D. Hooper, "TASI 2008 Lectures on Dark Matter," in *The Dawn of the LHC Era, Proceedings of the 2008 Theoretical and Advanced Study Institute in Elementary Particle Physics,* Boulder, Colorado, 2–27 June 2008, edited by Tao Han (World Scientific, Singapore, 2009).
18. H. Pagels and J.R. Primack, Phys. Rev. Lett. **48**, 223 (1982).
19. H. Goldberg, Phys. Rev. Lett. **50**, 1419 (1983) [Erratum: **103**, 099905 (2009)].
20. J. Ellis *et al.*, Nucl. Phys. **B238**, 453 (1984).
21. G. Jungman, M. Kamionkowski, and K. Griest, Phys. Reports **267**, 195 (1996);
    K. Griest and M. Kamionkowski, Phys. Reports **333**, 167 (2000).
22. F.D. Steffen, Eur. Phys. J. **C59**, 557 (2009).
23. M. Drees and G. Gerbier, *"Dark Matter,"* in the web edition of the *Review of Particle Physics* at `http://pdg.lbl.gov`.
24. H.E. Haber and G.L. Kane, Phys. Reports **117**, 75 (1985).
25. M. Drees, R. Godbole, and P. Roy, *Theory and Phenomenology of Sparticles* (World Scientific, Singapore, 2005);
    H. Baer and X. Tata, *Weak Scale Supersymmetry: from Superfields to Scattering Events* (Cambridge University Press, Cambridge, UK, 2006);
    I.J.R. Aitchison, *Supersymmetry in Particle Physics: an elementary introduction* (Cambridge University Press, Cambridge, UK, 2007).
26. Our notation for the charge-conjugated fields follows the notation of P. Langacker, *The Standard Model and Beyond*, 2nd edition (CRC Press, Boca Raton, FL, 2017).
27. H. Georgi and S.L. Glashow, Phys. Rev. **D6**, 429 (1972).
28. P. Fayet, Nucl. Phys. **B90**, 104 (1975).
29. K. Inoue *et al.*, Prog. Theor. Phys. **67**, 1889 (1982);
    R. Flores and M. Sher, Ann. Phys. (NY) **148**, 95 (1983).
30. J.F. Gunion and H.E. Haber, Nucl. Phys. **B272**, 1 (1986) [Erratum: **B402**, 567 (1993)].
31. J. Wess and J. Bagger, *Supersymmetry and Supergravity* (Princeton University Press, Princeton, NJ, 1992).
32. I. Buchbinder, S. Kuzenko, and J. Yarevskaya, Nucl. Phys. **B411**, 665 (1994);
    I. Antoniadis, E. Dudas, and D.M. Ghilencea, JHEP **0803**, 045 (2008).

33. For an overview of the theory and models of the soft-supersymmetry-breaking Lagrangian, see D.J.H. Chung *et al.*, Phys. Reports **407**, 1 (2005).
34. J. Ellis *et al.*, Phys. Rev. **D39**, 844 (1989);
U. Ellwanger and C. Hugonie, Eur. Phys. J. **C25**, 297 (2002);
U. Ellwanger, C. Hugonie, and A.M. Teixeira, Phys. Reports **496**, 1 (2010);
M. Maniatis, Int. J. Mod. Phys. **A25**, 3505 (2010).
35. S. Weinberg, Phys. Rev. Lett. **43**, 1566 (1979); Phys. Rev. **D22**, 1694 (1980);
F. Wilczek and A. Zee, Phys. Rev. Lett. **43**, 1571 (1979);
H.A. Weldon and A. Zee, Nucl. Phys. **B173**, 269 (1980).
36. P. Fayet, Phys. Lett. **69B**, 489 (1977);
G. Farrar and P. Fayet, Phys. Lett. **76B**, 575 (1978).
37. P. Fayet, Phys. Lett. **84B**, 421 (1979); Phys. Lett. **86B**, 272 (1979).
38. D.Z. Freedman and A. Van Proeyen, *Supergravity* (Cambridge University Press, Cambridge, UK, 2012).
39. S. Deser and B. Zumino, Phys. Rev. Lett. **38**, 1433 (1977);
E. Cremmer *et al.*, Phys. Lett. **79B**, 231 (1978).
40. R. Casalbuoni *et al.*, Phys. Lett. **B215**, 313 (1988); Phys. Rev. **D39**, 2281 (1989);
A.L. Maroto and J.R. Pelaez, Phys. Rev. **D62**, 023518 (2000).
41. Z. Komargodski and N. Seiberg, JHEP **0909**, 066 (2009);
I. Antoniadis *et al.*, Theor. Math. Phys. **170**, 26 (2012).
42. K. Benakli and C. Moura, Nucl. Phys. **B791**, 125 (2008);
C. Cheung, Y. Nomura, and J. Thaler, JHEP **1003**, 073 (2010);
N. Craig, J. March-Russell, and M. McCullough, JHEP **1010**, 095 (2010);
R. Argurio, Z. Komargodski and A. Mariotti, Phys. Rev. Lett. **107**, 061601 (2011).
43. A.H. Chamseddine, R. Arnowitt, and P. Nath, Phys. Rev. Lett. **49**, 970 (1982);
R. Barbieri, S. Ferrara, and C.A. Savoy, Phys. Lett. **119B**, 343 (1982);
L. Ibáñez, Nucl. Phys. **B218**, 514 (1982);
H.-P. Nilles, M. Srednicki, and D. Wyler, Phys. Lett. **120B**, 346 (1983); Phys. Lett. **124B**, 337 (1983);
E. Cremmer, P. Fayet, and L. Girardello, Phys. Lett. **122B**, 41 (1983);
N. Ohta, Prog. Theor. Phys. **70**, 542 (1983).
44. L. Alvarez-Gaumé, J. Polchinski, and M.B. Wise, Nucl. Phys. **B221**, 495 (1983).
45. L.J. Hall, J. Lykken, and S. Weinberg, Phys. Rev. **D27**, 2359 (1983).
46. S.K. Soni and H.A. Weldon, Phys. Lett. **126B**, 215 (1983);
Y. Kawamura, H. Murayama, and M. Yamaguchi, Phys. Rev. **D51**, 1337 (1995).
47. See, *e.g.*, A. Brignole, L.E. Ibáñez, and C. Munoz, in *Perspectives on Supersymmetry II*, edited by G.L. Kane (World Scientific, Singapore, 2010) pp. 244–268.
48. A.B. Lahanas and D.V. Nanopoulos, Phys. Reports **145**, 1 (1987).
49. J.L. Feng, A. Rajaraman, and F. Takayama, Phys. Rev. Lett. **91**, 011302 (2003); Phys. Rev. **D68**, 063504 (2003); Gen. Rel. Grav. **36**, 2575 (2004).
50. L. Randall and R. Sundrum, Nucl. Phys. **B557**, 79 (1999).
51. F. D'Eramo, J. Thaler, and Z. Thomas, JHEP **1206**, 151 (2012); JHEP **1309**, 125 (2013);
S.P. de Alwis, Phys. Rev. **D77**, 105020 (2008); JHEP **1301**, 006 (2013);
K. Harigaya and M. Ibe, Phys. Rev. **D90**, 085028 (2014).
52. See *e.g.*, I. Jack, D.R.T. Jones, and R. Wild, Phys. Lett. **B535**, 193 (2002);
B. Murakami and J.D. Wells, Phys. Rev. **D68**, 035006 (2003);
R. Kitano, G.D. Kribs, and H. Murayama, Phys. Rev. **D70**, 035001 (2004);
R. Hodgson *et al.*, Nucl. Phys. **B728**, 192 (2005);
D.R.T. Jones and G.G. Ross, Phys. Lett. **B642**, 540 (2006).
53. S. Asai *et al.*, Phys. Lett. **B653**, 81 (2007).
54. M. Dine, W. Fischler, and M. Srednicki, Nucl. Phys. **B189**, 575 (1981);
S. Dimopoulos and S. Raby, Nucl. Phys. **B192**, 353 (1982); Nucl. Phys. **B219**, 479 (1983);
M. Dine and W. Fischler, Phys. Lett. **110B**, 227 (1982);
C. Nappi and B. Ovrut, Phys. Lett. **113B**, 175 (1982);
L. Alvarez-Gaumé, M. Claudson, and M. Wise, Nucl. Phys. **B207**, 96 (1982).
55. M. Dine and A.E. Nelson, Phys. Rev. **D48**, 1277 (1993);
M. Dine, A.E. Nelson, and Y. Shirman, Phys. Rev. **D51**, 1362 (1995);
M. Dine *et al.*, Phys. Rev. **D53**, 2658 (1996).
56. G.F. Giudice and R. Rattazzi, Phys. Reports **322**, 419 (1999).
57. E. Poppitz and S.P. Trivedi, Phys. Rev. **D55**, 5508 (1997);
H. Murayama, Phys. Rev. Lett. **79**, 18 (1997);
M.A. Luty and J. Terning, Phys. Rev. **D57**, 6799 (1998);
K. Agashe, Phys. Lett. **B435**, 83 (1998);
N. Arkani-Hamed, J. March-Russell, and H. Murayama, Nucl. Phys. **B509**, 3 (1998);
C. Csaki, Y. Shirman, and J. Terning, JHEP **0705**, 099 (2007);
M. Ibe and R. Kitano, Phys. Rev. **D77**, 075003 (2008).
58. M. Kawasaki *et al.*, Phys. Rev. **D78**, 065011 (2008).
59. M.J. Strassler and K.M. Zurek, Phys. Lett. **B651**, 374 (2007);
T. Han *et al.*, JHEP **0807**, 008 (2008).
60. M.J. Strassler, `arXiv:hep-ph/0607160`;
K.M. Zurek, Phys. Rev. **D79**, 115002 (2009).
61. See *e.g.*, M. Quiros, in *Particle Physics and Cosmology: The Quest for Physics Beyond the Standard Model(s), Proceedings of the 2002 Theoretical Advanced Study Institute in Elementary Particle Physics (TASI 2002),* edited by H.E. Haber and A.E. Nelson (World Scientific, Singapore, 2004) pp. 549–601;
C. Csaki, in *ibid.*, pp. 605–698.
62. See, *e.g.*, J. Parsons and A. Pomarol, "Extra Dimensions," in the web edition of the *Review of Particle Physics* at `http://pdg.lbl.gov`.
63. See *e.g.*, V.A. Rubakov, Sov. Phys. Usp. **44**, 871 (2001);
J. Hewett and M. Spiropulu, Ann. Rev. Nucl. and Part. Sci. **52**, 397 (2002).
64. Z. Chacko, M.A. Luty, and E. Ponton, JHEP **0007**, 036 (2000);
D.E. Kaplan, G.D. Kribs, and M. Schmaltz, Phys. Rev. **D62**, 035010 (2000);
Z. Chacko *et al.*, JHEP **0001**, 003 (2000).
65. J. Scherk and J.H. Schwarz, Phys. Lett. **82B**, 60 (1979); Nucl. Phys. **B153**, 61 (1979).
66. See, *e.g.*, R. Barbieri, L.J. Hall, and Y. Nomura, Phys. Rev. **D66**, 045025 (2002); Nucl. Phys. **B624**, 63 (2002);
I.G. Garcia, K. Howe, and J. March-Russell, JHEP **1512**, 005 (2015).
67. J. Wells, `arXiv:hep-ph/0306127`; Phys. Rev. **D71**, 015013 (2005).
68. N. Arkani-Hamed and S. Dimopoulos, JHEP **0506**, 073 (2005);
G.F. Giudice and A. Romanino, Nucl. Phys. **B699**, 65 (2004) [Erratum: **B706**, 487 (2005)].
69. G. Aad *et al.* [ATLAS and CMS Collab.] Phys. Rev. Lett. **114**, 191803 (2015).
70. G.F. Giudice and A. Strumia, Nucl. Phys. **B858**, 63 (2012).
71. A. Arvanitaki *et al.*, JHEP **1302**, 126 (2013);
N. Arkani-Hamed *et al.*, `arXiv:1212.6971`(2012).
72. J.P. Vega and G. Villadoro, JHEP **1507**, 159 (2015).
73. Y. Kahn, M. McCullough and J. Thaler, JHEP **1311**, 161 (2013).
74. L.J. Hall and Y. Nomura, JHEP **1201**, 082 (2012);
M. Ibe and T.T. Yanagida, Phys. Lett. **B709**, 374 (2012).
75. H.E. Haber, in *Recent Directions in Particle Theory, Proceedings of the 1992 Theoretical Advanced Study Institute in Particle Physics*, edited by J. Harvey and J. Polchinski (World Scientific, Singapore, 1993) pp. 589–686.
76. B.C. Allanach *et al.*, Comp. Phys. Comm. **180**, 8 (2009).
77. J.M. Frere, D.R.T. Jones, and S. Raby, Nucl. Phys. **B222**, 11 (1983);
J.P. Derendinger and C.A. Savoy, Nucl. Phys. **B237**, 307

(1984);
J.F. Gunion, H.E. Haber, and M. Sher, Nucl. Phys. **B306**, 1 (1988);
D. Chowdhury *et al.*, JHEP **1402**, 110 (2014);
W.G. Hollik, JHEP **1608**, 126 (2016).
78. J.A. Casas, A. Lleyda, and C. Munoz, Nucl. Phys. **B471**, 3 (1996).
79. C.S. Ün *et al.*, Phys. Rev. **D91**, 105033 (2015);
U. Chattopadhyay and A. Dey, JHEP **1610**, 027 (2016).
80. G.G. Ross, K. Schmidt-Hoberg and F. Staub, Phys. Lett. **B759**, 110 (2016).
81. G.G. Ross, K. Schmidt-Hoberg and F. Staub, JHEP **1703**, 021 (2017).
82. S.P. Martin, Phys. Rev. **D61**, 035004 (2000).
83. S. Dimopoulos and D. Sutter, Nucl. Phys. **B452**, 496 (1995);
D.W. Sutter, Stanford Ph. D. thesis, `arXiv:hep-ph/9704390`.
84. H.E. Haber, Nucl. Phys. B (Proc. Suppl.) **62A-C**, 469 (1998).
85. R.M. Barnett, J.F. Gunion, and H.E. Haber, Phys. Lett. **B315**, 349 (1993);
H. Baer, X. Tata, and J. Woodside, Phys. Rev. **D41**, 906 (1990).
86. S.M. Bilenky, E.Kh. Khristova, and N.P. Nedelcheva, Phys. Lett. **B161**, 397 (1985); Bulg. J. Phys. **13**, 283 (1986);
G. Moortgat-Pick and H. Fraas, Eur. Phys. J. **C25**, 189 (2002).
87. J. Rosiek, Phys. Rev. **D41**, 3464 (1990) [Erratum: `arXiv:hep-ph/9511250`]. The most recent corrected version of this manuscript can be found on the author's webpage, `www.fuw.edu.pl/~rosiek/physics/prd41.html`.
88. J. Alwall *et al.*, JHEP **0709**, 028 (2007). See also the MadGraph homepage, `http://madgraph.physics.illinois.edu`.
89. T. Hahn, Comp. Phys. Comm. **140**, 418 (2001);
T. Hahn and C. Schappacher, Comp. Phys. Comm. **143**, 54 (2002). The FeynArts homepage is located at `http://www.feynarts.de`.
90. A. Pukhov *et al.*, INP MSU report 98-41/542 (`arXiv:hep-ph/9908288`);
E. Boos *et al.* [CompHEP Collab.], Nucl. Instrum. Methods **A534**, 50 (2004); CompHEP webpage, `theory.sinp.msu.ru/dokuwiki/doku.php/comphep/news`.
91. D.M. Pierce *et al.*, Nucl. Phys. **B491**, 3 (1997).
92. P. Skands *et al.*, JHEP **0407**, 036 (2004). The Supersymmetry Les Houches Accord homepage is `skands.physics.monash.edu/slha/`.
93. For further details, see *e.g.*, Appendix C of Ref. 24 and Appendix A of Ref. 30.
94. J.L. Kneur and G. Moultaka, Phys. Rev. **D59**, 015005 (1999).
95. R.A. Horn and C.R. Johnson, *Matrix Analysis*, 2nd Edition (Cambridge University Press, Cambridge, UK, 2003).
96. H.K. Dreiner, H.E. Haber, and S.P. Martin, Phys. Reports **494**, 1 (2010).
97. T. Takagi, Japan J. Math. **1**, 83 (1925).
98. S.Y. Choi *et al.*, Nucl. Phys. **B778**, 85 (2007).
99. S.Y. Choi *et al.*, Eur. Phys. J. **C22**, 563 (2001); Eur. Phys. J. **C23**, 769 (2002).
100. M.M. El Kheishen, A.A. Aboshousha, and A.A. Shafik, Phys. Rev. **D45**, 4345 (1992);
M. Guchait, Z. Phys. **C57**, 157 (1993) [Erratum: **C61**, 178 (1994)].
101. T. Hahn, preprint MPP-2006-85, `physics/0607103`.
102. K. Hikasa and M. Kobayashi, Phys. Rev. **D36**, 724 (1987);
F. Gabbiani and A. Masiero, Nucl. Phys. **B322**, 235 (1989);
Ph. Brax and C.A. Savoy, Nucl. Phys. **B447**, 227 (1995).
103. J. Ellis and S. Rudaz, Phys. Lett. **128B**, 248 (1983);
F. Browning, D. Chang, and W.Y. Keung, Phys. Rev. **D64**, 015010 (2001);
A. Bartl *et al.*, Phys. Lett. **B573**, 153 (2003); Phys. Rev. **D70**, 035003 (2004).
104. J.F. Gunion *et al.*, *The Higgs Hunter's Guide* (Westview Press, Boulder, CO, 2000);
M. Carena and H.E. Haber, Prog. in Part. Nucl. Phys. **50**, 63 (2003);
A. Djouadi, Phys. Reports **459**, 1 (2008).
105. P. Bechtle *et al.*, Eur. Phys. J. **C77**, 67 (2017).
106. H.E. Haber and M. Sher, Phys. Rev. **D35**, 2206 (1987).
107. L.J. Hall, D. Pinner, and J.T. Ruderman, JHEP **1204**, 131 (2012).
108. L.J. Hall and M.B. Wise, Nucl. Phys. **B187**, 397 (1981).
109. H.E. Haber and R. Hempfling, Phys. Rev. Lett. **66**, 1815 (1991);
Y. Okada, M. Yamaguchi, and T. Yanagida, Prog. Theor. Phys. **85**, 1 (1991);
J. Ellis, G. Ridolfi, and F. Zwirner, Phys. Lett. **B257**, 83 (1991).
110. For a recent review, see P. Draper and H. Rzehak, Phys. Reports **619**, 1 (2016).
111. A. Pilaftsis and C.E.M. Wagner, Nucl. Phys. **B553**, 3 (1999);
D.A. Demir, Phys. Rev. **D60**, 055006 (1999);
S.Y. Choi, M. Drees, and J.S. Lee, Phys. Lett. **B481**, 57 (2000);
M. Carena *et al.*, Nucl. Phys. **B586**, 92 (2000); Phys. Lett. **B495**, 155 (2000); Nucl. Phys. **B625**, 345 (2002);
M. Frank *et al.*, JHEP **0702**, 047 (2007);
S. Heinemeyer *et al.*, Phys. Lett. **B652**, 300 (2007).
112. H.E. Haber and J.D. Mason, Phys. Rev. **D77**, 115011 (2008).
113. M. Carena *et al.*, Phys. Rev. **D93**, 035013 (2016).
114. S. Khalil, Int. J. Mod. Phys. **A18**, 1697 (2003).
115. W. Fischler, S. Paban, and S. Thomas, Phys. Lett. **B289**, 373 (1992);
S.M. Barr, Int. J. Mod. Phys. **A8**, 209 (1993);
T. Ibrahim and P. Nath, Phys. Rev. **D58**, 111301 (1998) [Erratum: **D60**, 099902 (1999)];
M. Brhlik, G.J. Good, and G.L. Kane, Phys. Rev. **D59**, 115004 (1999);
V.D. Barger *et al.*, Phys. Rev. **D64**, 056007 (2001);
S. Abel, S. Khalil, and O. Lebedev, Nucl. Phys. **B606**, 151 (2001);
K.A. Olive *et al.*, Phys. Rev. **D72**, 075001 (2005);
G.F. Giudice and A. Romanino, Phys. Lett. **B634**, 307 (2006).
116. A. Masiero and L. Silvestrini, in *Perspectives on Supersymmetry*, edited by G.L. Kane (World Scientific, Singapore, 1998) pp. 423–441.
117. M. Pospelov and A. Ritz, Ann. Phys. **318**, 119 (2005).
118. See, *e.g.*, F. Gabbiani *et al.*, Nucl. Phys. **B477**, 321 (1996);
A. Masiero, and O. Vives, New J. Phys. **4**, 1 (2002).
119. For a review and references to the original literature, see: M.J. Ramsey-Musolf and S. Su, Phys. Reports **456**, 1 (2008).
120. M. Carena, A. Menon, and C.E.M. Wagner, Phys. Rev. **D79**, 075025 (2009);
S. Jager, Eur. Phys. J. **C59**, 497 (2009);
W. Altmannshofer *et al.*, Nucl. Phys. **B830**, 17 (2010).
121. M.B. Einhorn and D.R.T. Jones, Nucl. Phys. **B196**, 475 (1982).
122. For a review, see R.N. Mohapatra, in *Particle Physics 1999*, ICTP Summer School in Particle Physics, Trieste, Italy, edited by G. Senjanovic and A.Yu. Smirnov (World Scientific, Singapore, 2000) pp. 336–394;
W.J. Marciano and G. Senjanovic, Phys. Rev. **D25**, 3092 (1982).
123. R.M. Fonseca *et al.*, Nucl. Phys. **B854**, 28 (2012);
F. Staub, Comp. Phys. Comm. **182**, 808 (2011).
124. Comp. Phys. Comm. **185**, 1773 (2014); Adv. High Energy Phys. **2015**, 840780 (2015); the SARAH homepage is `sarah.hepforge.org/`.
125. B.C. Allanach, Comput. Phys. Commun. **143** 305 (2002); the SOFTSUSY homepage is `softsusy.hepforge.org/`.
126. P. Athron *et al.*, Comput. Phys. Commun. **190** 139 (2015); the FlexibleSUSY homepage is `flexiblesusy.hepforge.org/`.
127. L.E. Ibáñez and G.G. Ross, Phys. Lett. **B110**, 215 (1982).
128. J. Abdullah *et al.* [DELPHI Collab.], Eur. Phys. J. **C31**, 421 (2004).
129. H.K. Dreiner *et al.*, Eur. Phys. J. **C62**, 547 (2009).

130. G.F. Giudice *et al.*, JHEP **9812**, 027 (1998); A. Pomarol and R. Rattazzi, JHEP **9905**, 013 (1999); D.W. Jung and J.Y. Lee, JHEP **0903**, 123 (2009).
131. J.F. Gunion and H.E. Haber, Phys. Rev. **D37**, 2515 (1988); S.Y. Choi, M. Drees, and B. Gaissmaier, Phys. Rev. **D70**, 014010 (2004).
132. J.L. Feng *et al.*, Phys. Rev. Lett. **83**, 1731 (1999); J.F. Gunion and S. Mrenna, Phys. Rev. **D62**, 015002 (2000).
133. T. Gherghetta, G.F. Giudice, and J.D. Wells, Nucl. Phys. **B559**, 27 (1999).
134. M. Endo, M. Yamaguchi, and K. Yoshioka, Phys. Rev. **D72**, 015004 (2005); K. Choi, K.S. Jeong, and K.-I. Okumura, JHEP **0509**, 039 (2005); O. Loaiza-Brito *et al.*, AIP Conf. Proc. **805**, 198 (2006).
135. See *e.g.*, G. D'Ambrosio *et al.*, Nucl. Phys. **B465**, 155 (2002).
136. For a review of minimal flavor violation in supersymmetric theories, see C. Smith, Acta Phys. Polon. Supp. **3**, 53 (2010).
137. M. Drees and S.P. Martin, in *Electroweak Symmetry Breaking and New Physics at the TeV Scale*, edited by T. Barklow *et al.* (World Scientific, Singapore, 1996) pp. 146–215.
138. G.L. Kane *et al.*, Phys. Rev. **D49**, 6173 (1994).
139. J.R. Ellis *et al.*, Phys. Lett. **B573**, 162 (2003); Phys. Rev. **D70**, 055005 (2004).
140. L.E. Ibáñez and D. Lüst, Nucl. Phys. **B382**, 305 (1992); B. de Carlos, J.A. Casas, and C. Munoz, Phys. Lett. **B299**, 234 (1993); V. Kaplunovsky and J. Louis, Phys. Lett. **B306**, 269 (1993); A. Brignole, L.E. Ibáñez, and C. Munoz, Nucl. Phys. **B422**, 125 (1994) [Erratum: **B436**, 747 (1995)].
141. A. Arbey *et al.*, Phys. Rev. **D87**, 115020 (2013).
142. G.R. Dvali, G.F. Giudice and A. Pomarol, Nucl. Phys. **B478**, 31 (1996).
143. P. Draper *et al.*, Phys. Rev. **D85**, 095007 (2012).
144. P. Meade, N. Seiberg, and D. Shih, Prog. Theor. Phys. Supp. **177**, 143 (2009); M. Buican *et al.*, JHEP **0903**, 016 (2009).
145. A. Rajaraman *et al.*, Phys. Lett. **B678**, 367 (2009); L.M. Carpenter *et al.*, Phys. Rev. **D79**, 035002 (2009).
146. S. Ambrosanio, G.D. Kribs, and S.P. Martin, Nucl. Phys. **B516**, 55 (1998).
147. For a review and guide to the literature, see J.F. Gunion and H.E. Haber, in *Perspectives on Supersymmetry II*, edited by G.L. Kane (World Scientific, Singapore, 2010) pp. 420–445.
148. T.S. Roy and M. Schmaltz, Phys. Rev. **D77**, 095008 (2008); S. Knapen and D. Shih, JHEP **1408**, 136 (2014).
149. A. de Gouvea, A. Friedland, and H. Murayama, Phys. Rev. **D57**, 5676 (1998).
150. T. Han, D. Marfatia, and R.-J. Zhang, Phys. Rev. **D61**, 013007 (2000); Z. Chacko and E. Ponton, Phys. Rev. **D66**, 095004 (2002); A. Delgado, G.F. Giudice, and P. Slavich, Phys. Lett. **B653**, 424 (2007); T. Liu and C.E.M. Wagner, JHEP **0806**, 073 (2008).
151. B. Allanach *et al.*, Phys. Rev. **D92**, 015006 (2015).
152. A. Djouadi, J.L. Kneur, and G. Moultaka, Comp. Phys. Comm. **176**, 426 (2007); C.F. Berger *et al.*, JHEP **0902**, 023 (2009).
153. J. Berger *et al.*, Phys. Rev. **D93**, 035017 (2016).
154. K.J. de Vries *et al.*, Eur. Phys. J. **C75**, 422 (2015).
155. M. Cahill-Rowley *et al.*, Phys. Rev. **D90**, 095017 (2014); Phys. Rev. **D91**, 055002 (2015); A. Barr and J. Liu, Eur. Phys. J. **C77**, 202 (2017).
156. G. Bertone *et al.*, JCAP **1604**, 037 (2016).
157. N. Arkani-Hamed *et al.*, `arXiv:hep-ph/0703088`; J. Alwall *et al.*, Phys. Rev. **D79**, 015005 (2009); J. Alwall, P. Schuster, and N. Toro, Phys. Rev. **D79**, 075020 (2009); D.S.M. Alves, E. Izaguirre, and J.G. Wacker, Phys. Lett. **B702**, 64 (2011); JHEP **1110**, 012 (2011); D. Alves *et al.*, J. Phys. **G39**, 105005 (2012).
158. F. Ambrogi *et al.*, Eur. Phys. J. **C78**, 215 (2018).
159. R. Barbieri and G.F. Giudice, Nucl. Phys. **B305**, 63 (1988).
160. J.R. Ellis *et al.*, Mod. Phys. Lett. **A1**, 57 (1986).
161. G.W. Anderson and D.J. Castano, Phys. Lett. **B347**, 300 (1995); Phys. Rev. **D52**, 1693 (1995); Phys. Rev. **D53**, 2403 (1996); J.L. Feng, K.T. Matchev, and T. Moroi, Phys. Rev. **D61**, 075005 (2000); P. Athron and D.J. Miller, Phys. Rev. **D76**, 075010 (2007); M.E. Cabrera, J.A. Casas, and R.R. de Austri, JHEP **0903**, 075 (2009) (2009); H. Baer *et al.*, Phys. Rev. Lett. **109**, 161802 (2012).
162. D.M. Ghilencea and G.G. Ross, Nucl. Phys. **B868**, 65 (2013).
163. G.L. Kane and S.F. King, Phys. Lett. **B451**, 113 (1999); M. Bastero-Gil, G.L. Kane, and S.F. King, Phys. Lett. **B474**, 103 (2000); J.A. Casas, J.R. Espinosa, and I, Hidalgo, JHEP **0401**, 008 (2004); J. Abe, T. Kobayashi, and Y. Omura, Phys. Rev. **D76**, 015002 (2007); R. Essig and J.-F. Fortin, JHEP **0804**, 073 (2008).
164. O. Buchmüller *et al.*, Eur. Phys. J. **C74**, 2922 (2014).
165. P. Bechtle *et al.*, Eur. Phys. J. **C76**, 96 (2016).
166. H. Baer *et al.*, Phys. Rev. **D89**, 115019 (2014).
167. R. Barbieri and A. Strumia, `arXiv:hep-ph/0007265`.
168. L. Giusti, A. Romanino, and A. Strumia, Nucl. Phys. **B550**, 3 (1999); H.C. Cheng and I. Low, JHEP **0309**, 051 (2003); JHEP **0408**, 061 (2004); R. Harnik *et al.*, Phys. Rev. **D70**, 015002 (2004).
169. H. Baer, V. Barger, and D. Mickelson, Phys. Rev. **D88**, 095013 (2013).
170. B. de Carlos and J. A. Casas, Phys. Lett. **B309**, 320 (1993); S. Cassel, D.M. Ghilencea, and G.G. Ross, Nucl. Phys. **B825**, 203 (2010); **B835**, 110 (2010).
171. H. Baer *et al.*, Phys. Rev. **D87**, 035017 (2013); Phys. Rev. **D87**, 115028 (2013); Ann. Rev. Nucl. and Part. Sci. **63**, 351 (2013).
172. J. Feng, K. Matchev, and T. Moroi, Phys. Rev. Lett. **84**, 2322 (2000); Phys. Rev. **D61**, 075005 (2000); J. Feng and F. Wilczek, Phys. Lett. **B631**, 170 (2005); D. Horton and G.G. Ross, Nucl. Phys. **B830**, 221 (2010).
173. M. Drees, Phys. Rev. **D33**, 1468 (1986); S. Dimopoulos and G.F. Giudice, Phys. Lett. **B357**, 573 (1995); A. Pomarol and D. Tommasini, Nucl. Phys. **B466**, 3 (1996).
174. M. Dine, A. Kagan, and S. Samuel, Phys. Lett. **B243**, 250 (1990); A.G. Cohen, D.B. Kaplan, and A.E. Nelson, Phys. Lett. **B388**, 588 (1996).
175. C. Brust *et al.*, JHEP **1203**, 103 (2012); M. Papucci, J.T. Ruderman, and A. Weiler, JHEP **1209**, 035 (2012); H.K. Dreiner, M. Kramer, and J. Tattersall, Europhys. Lett. **99**, 61001 (2012); H. Baer *et al.*, JHEP **1205**, 109 (2012).
176. S.P. Martin, Phys. Rev. **D75**, 115005 (2007); Phys. Rev. **D78**, 055019 (2009).
177. J. Fan, M. Reece, and J.T. Ruderman, JHEP **1111**, 012 (2011); JHEP **1207**, 196 (2012).
178. H. Murayama, Y. Nomura and D. Poland, Phys. Rev. **D77**, 015005 (2008); G. Perez, T.S. Roy, and M. Schmaltz, Phys. Rev. **D79**, 095016 (2009).
179. R. Dermisek and J.F. Gunion, Phys. Rev. Lett. **95**, 041801 (2005); Phys. Rev. **D75**, 095019 (2007); Phys. Rev. **D76**, 095006 (2007).
180. G.G. Ross and K. Schmidt-Hoberg, Nucl. Phys. **B862**, 710 (2012); JHEP **1208**, 074 (2012); A. Kaminska, G.G. Ross, and K. Schmidt-Hoberg, JHEP **1311**, 209 (2013).
181. S.P. Martin and J.D. Wells, Phys. Rev. **D86**, 035017 (2012).

182. B. Bellazzini *et al.*, Phys. Rev. **D79**, 095003 (2009).
183. H. Baer, V. Barger, and M. Savoy, Phys. Rev. **D93**, 035016 (2016).
184. M.L. Mangano, editor, *Physics at the FCC-hh, a 100 TeV pp collider*, CERN Yellow Report, CERN-2017-003-M (2017).
185. D. Stockinger, J. Phys. **G34**, R45 (2007);
P. Athron *et al.*, Eur. Phys. J. **C76**, 62 (2016).
186. F. Jegerlehner, EPJ Web Conf. **166**, 00022 (2018);
M. Davier *et al.*, Eur. Phys. J. **C77**, 827 (2017);
K. Hagiwara *et al.*, Nucl. Part. Phys. Proc. **287-288**, 33 (2017).
187. M. Ibe, T. T. Yanagida, and N. Yokozaki, JHEP **1308**, 067 (2013).
188. A. Limosani *et al.* [Belle Collab.], Phys. Rev. Lett. **103**, 241801 (2009);
J.P. Lees *et al.* [BaBar Collab.], Phys. Rev. Lett. **109**, 191801 (2012); Phys. Rev. **D86**, 112008 (2012).
189. M. Misiak *et al.*, Phys. Rev. Lett. **114**, 221801 (2015);
M. Czakon *et al.*, JHEP **1504**, 168 (2015).
190. See, *e.g.*, M. Ciuchini *et al.*, Phys. Rev. **D67**, 075016 (2003);
T. Hurth, Rev. Mod. Phys. **75**, 1159 (2003);
F. Mahmoudi, JHEP **0712**, 026 (2007);
K.A. Olive and L. Velasco-Sevilla, JHEP **0805**, 052 (2008).
191. S.R. Choudhury and N. Gaur, Phys. Lett. **B451**, 86 (1999);
K.S. Babu and C.F. Kolda, Phys. Rev. Lett. **84**, 228 (2000);
G. Isidori and A. Retico, JHEP **0111**, 001 (2001); JHEP **0209**, 063 (2002).
192. The CMS and LHCb Collab., Nature **522**, 68 (2015);
ATLAS Collab., Eur. Phys. J. **C76**, 513 (2016);
LHCb Collab., Phys. Rev. Lett. **118**, 191801 (2017).
193. C. Bobeth *et al.*, Phys. Rev. Lett. **112**, 101801 (2014).
194. K. Hara *et al.* [Belle Collab.], Phys. Rev. Lett. **110**, 131801 (2013);
J.P. Lees *et al.* [BaBar Collab.], Phys. Rev. **D88**, 031102 (R)(2013).
195. J.P. Lees *et al.* [BaBar Collab.], Phys. Rev. Lett. **109**, 101802 (2012);
Phys. Rev. **D88**, 072012 (2013).
196. R. Aaij *et al.* [LHCb Collab.], Phys. Rev. Lett. **115**, 111803 (2015); Phys. Rev. Lett. **120**, 171802 (2018);
M. Huschle *et al.* [Belle Collab.], Phys. Rev. **D92**, 072014 (2015);
Y. Sato *et al.* [Belle Collab.], Phys. Rev. **D94**, 072007 (2016);
S. Hirose *et al.* [Belle Collab.], Phys. Rev. Lett. **118**, 211801 (2017); Phys. Rev. **D97**, 012004 (2018).
197. G. Ciezarek *et al.*, Nature **546**, 227 (2017).
198. D. Boubaa, S. Khalil and S. Moretti, `arXiv:1604.03416`.
199. R. Aaij *et al.* [LHCb Collaboration], JHEP **1708**, 055 (2017).
200. F. Mahmoudi, S. Neshatpour, and J. Orloff, JHEP **1208**, 092 (2012);
A. Arbey *et al.*, Phys. Rev. **D87**, 035026 (2013).
201. J. Erler and A. Freitas, "Electroweak Model and Constraints on New Physics," in the web edition of the *Review of Particle Physics* at `http://pdg.lbl.gov`.
202. J.R. Ellis *et al.*, JHEP **0708**, 083 (2007);
S. Heinemeyer *et al.*, JHEP **0808**, 087 (2008);
G.-C. Cho *et al.*, JHEP **1111**, 068 (2011).
203. See the section on neutrinos in "Particle Listings—Leptons" in the web edition of the *Review of Particle Physics* at `http://pdg.lbl.gov`;
An updated global analysis of neutrino oscillation measurements is provided by the NuFIT collaboration at `http://www.nu-fit.org`.
204. J. Bergstrom *et al.*, JHEP **1701**, 087 (2017).
205. K. Zuber, Phys. Reports **305**, 295 (1998);
S.F. King, J. Phys. **G42**, 123001 (2015).
206. For a review of neutrino masses in supersymmetry, see *e.g.*, B. Mukhopadhyaya, *Proc. Indian National Science Academy* **A70**, 239 (2004);
M. Hirsch and J.W.F. Valle, New J. Phys. **6**, 76 (2004).
207. F. Borzumati and Y. Nomura, Phys. Rev. **D64**, 053005 (2001).
208. P. Minkowski, Phys. Lett. **67B**, 421 (1977);
M. Gell-Mann, P. Ramond, and R. Slansky, in *Supergravity*, edited by D. Freedman and P. van Nieuwenhuizen (North Holland, Amsterdam, 1979) p. 315;
T. Yanagida, Prog. Theor. Phys. **64**, 1103 (1980);
R. Mohapatra and G. Senjanovic, Phys. Rev. Lett. **44**, 912 (1980); Phys. Rev. **D23**, 165 (1981).
209. J. Hisano *et al.*, Phys. Lett. **B357**, 579 (1995);
J. Hisano *et al.*, Phys. Rev. **D53**, 2442 (1996);
J.A. Casas and A. Ibarra, Nucl. Phys. **B618**, 171 (2001);
J. Ellis *et al.*, Phys. Rev. **D66**, 115013 (2002);
A. Masiero, S.K. Vempati, and O. Vives, New J. Phys. **6**, 202 (2004);
E. Arganda *et al.*, Phys. Rev. **D71**, 035011 (2005);
F.R. Joaquim and A. Rossi, Phys. Rev. Lett. **97**, 181801 (2006);
J.R. Ellis and O. Lebedev, Phys. Lett. **B653**, 411 (2007).
210. Y. Grossman and H.E. Haber, Phys. Rev. Lett. **78**, 3438 (1997);
A. Dedes, H.E. Haber, and J. Rosiek, JHEP **0711**, 059 (2007).
211. M. Hirsch, H.V. Klapdor-Kleingrothaus, and S.G. Kovalenko, Phys. Lett. **B398**, 311 (1997);
L.J. Hall, T. Moroi, and H. Murayama, Phys. Lett. **B424**, 305 (1998);
K. Choi, K. Hwang, and W.Y. Song, Phys. Rev. Lett. **88**, 141801 (2002);
T. Honkavaara, K. Huitu, and S. Roy, Phys. Rev. **D73**, 055011 (2006).
212. L. Basso *et al.*, Comp. Phys. Comm. **184**, 698 (2013).
213. M. Chemtob, Prog. in Part. Nucl. Phys. **54**, 71 (2005);
R. Barbier *et al.*, Phys. Reports **420**, 1 (2005).
214. H. Dreiner, in *Perspectives on Supersymmetry II*, edited by G.L. Kane (World Scientific, Singapore, 2010) pp. 565–583.
215. B.C. Allanach, A. Dedes, and H.K. Dreiner, Phys. Rev. **D60**, 075014 (1999).
216. L.E. Ibáñez and G.G. Ross, Nucl. Phys. **B368**, 3 (1992);
L.E. Ibáñez, Nucl. Phys. **B398**, 301 (1993).
217. A. Dedes, S. Rimmer, and J. Rosiek, JHEP **0608**, 005 (2006);
B.C. Allanach and C.H. Kom, JHEP **0804**, 081 (2008);
H.K. Dreiner *et al.*, Phys. Rev. **D84**, 113005 (2011).
218. L.E. Ibáñez and G.G. Ross, Nucl. Phys. **B368**, 3 (1992).
219. H.K. Dreiner, C. Luhn, and M. Thormeier Phys. Rev. **D73**, 075007 (2006).
220. K. Tamvakis, Phys. Lett. **B382**, 251 (1996);
G. Eyal and Y. Nir, JHEP **9906**, 024 (1999);
A. Florez *et al.*, Phys. Rev. **D87**, 095010 (2013).
221. D. Dercks *et al.*, Eur. Phys. J. **C77**, 856 (2017).
222. B.C. Allanach and B. Gripaios, JHEP **1205**, 062 (2012);
M. Asano, K. Rolbiecki, and K. Sakurai, JHEP **1301**, 128 (2013);
N. Chamoun *et al.*, JHEP **1408**, 142 (2014).
223. See *e.g.*, J.C. Romao, Nucl. Phys. (Proc. Supp.) **81**, 231 (2000);
Y. Grossman and S. Rakshit, Phys. Rev. **D69**, 093002 (2004).
224. R.N. Mohapatra, Phys. Rev. **D34**, 3457 (1986);
K.S. Babu and R.N. Mohapatra, Phys. Rev. Lett. **75**, 2276 (1995);
M. Hirsch, H.V. Klapdor-Kleingrothaus, and S.G. Kovalenko, Phys. Rev. Lett. **75**, 17 (1995); Phys. Rev. **D53**, 1329 (1996).
225. Y. Grossman and H.E. Haber, Phys. Rev. **D59**, 093008 (1999).
226. S. Dimopoulos and L.J. Hall, Phys. Lett. **B207**, 210 (1988);
J. Kalinowski *et al.*, Phys. Lett. **B406**, 314 (1997);
J. Erler, J.L. Feng, and N. Polonsky, Phys. Rev. Lett. **78**, 3063 (1997).
227. H.K. Dreiner, P. Richardson, and M.H. Seymour, Phys. Rev. **D63**, 055008 (2001).
228. J.E. Kim and H.P. Nilles, Phys. Lett. **B138**, 150 (1984).
229. J.E. Kim and H.P. Nilles, Mod. Phys. Lett. **A9**, 3575 (1994).
230. G.F. Giudice and A. Masiero, Phys. Lett. **B206**, 480 (1988).
231. J.A. Casas and C. Munoz, Phys. Lett. **B306**, 288 (1993).
232. M. Cvetič *et al.*, Phys. Rev. **D56**, 2861 (1997) [Erratum: **D58**, 119905 (1998)].

233. For a review see e.g., R. D. Peccei, Lect. Notes Phys. **741**, 3 (2008).
234. R. Peccei and H. Quinn, Phys. Rev. Lett. **38**, 1440 (1977); Phys. Rev. **D16**, 1791 (1977).
235. H. Murayama, H. Suzuki, and T. Yanagida, Phys. Lett. **B291**, 418 (1992);
T. Gherghetta, G.L. Kane, Phys. Lett. **B354**, 300 (1995);
K.J. Bae, H. Baer, and H. Serce, Phys. Rev. **D91**, 015003 (2015).
236. A. Delgado, G. Nardini, and M. Quiros, Phys. Rev. **D86**, 115010 (2012).
237. P. Fayet, Phys. Lett. **78B**, 417 (1978).
238. For a review, see *e.g.*, K. Benakli, Fortsch. Phys. **59**, 1079 (2011).
239. P.J. Fox, A.E. Nelson, and N. Weiner, JHEP **0208**, 035 (2002).
240. K. Benakli and M.D. Goodsell, Nucl. Phys. **B816**, 185 (2009); Nucl. Phys. **B840**, 1 (2010).
241. U. Sarkar and R. Adhikari, Phys. Rev. **D55**, 3836 (1997); R. Fok *et al.*, Phys. Rev. **D87**, 055018 (2013).
242. G.D. Kribs, E. Poppitz, and N. Weiner, Phys. Rev. **D78**, 055010 (2008).
243. K. Benakli, M.D. Goodsell, and F. Staub, JHEP **1306**, 073 (2013).
244. See *e.g.*, J.L. Hewett and T.G. Rizzo, Phys. Reports **183**, 193 (1989).
245. S.F. King, S. Moretti, and R. Nevzorov, Phys. Lett. **B634**, 278 (2006); Phys. Rev. **D73**, 035009 (2006).

110. Supersymmetry, Part II (Experiment)

Updated September 2017 by O. Buchmueller (Imperial College London) and P. de Jong (Nikhef and University of Amsterdam).

110.1. Introduction

Supersymmetry (SUSY), a transformation relating fermions to bosons and vice versa [1–9], is one of the most compelling possible extensions of the Standard Model of particle physics (SM).

On theoretical grounds SUSY is motivated as a generalization of space-time symmetries. A low-energy realization of SUSY, *i.e.*, SUSY at the TeV scale, is, however, not a necessary consequence. Instead, low-energy SUSY is motivated by the possible cancellation of quadratic divergences in radiative corrections to the Higgs boson mass [10–15]. Furthermore, it is intriguing that a weakly interacting, (meta)stable supersymmetric particle might make up some or all of the dark matter in the universe [16–18]. In addition, SUSY predicts that gauge couplings, as measured experimentally at the electroweak scale, unify at an energy scale $\mathcal{O}(10^{16})$ GeV ("GUT scale") near the Planck scale [19–25].

In the minimal supersymmetric extension to the Standard Model, the so called MSSM [11,26,27], a supersymmetry transformation relates every fermion and gauge boson in the SM to a supersymmetric partner with half a unit of spin difference, but otherwise with the same properties (such as mass) and quantum numbers. These are the "sfermions": squarks ($\tilde{q}$) and sleptons ($\tilde{\ell}$, $\tilde{\nu}$), and the "gauginos". The MSSM Higgs sector contains two doublets, for up-type quarks and for down-type quarks and charged leptons respectively. After electroweak symmetry breaking, five Higgs bosons arise, of which two are charged. The supersymmetric partners of the Higgs doublets are known as "higgsinos." The weak gauginos and higgsinos mix, giving rise to charged mass eigenstates called "charginos" ($\tilde{\chi}^{\pm}$), and neutral mass eigenstates called "neutralinos" ($\tilde{\chi}^0$). The SUSY partners of the gluons are known as "gluinos" ($\tilde{g}$). The fact that such particles are not yet observed leads to the conclusion that, if supersymmetry is realized, it is a broken symmetry. A description of SUSY in the form of an effective Lagrangian with only "soft" SUSY breaking terms and SUSY masses at the TeV scale maintains cancellation of quadratic divergences in particle physics models.

The phenomenology of SUSY is to a large extent determined by the SUSY breaking mechanism and the SUSY breaking scale. This determines the SUSY particle masses, the mass hierarchy, the field contents of physical particles, and their decay modes. In addition, phenomenology crucially depends on whether the multiplicative quantum number of R-parity [27], $R = (-1)^{3(B-L)+2S}$, where B and L are baryon and lepton numbers and S is the spin, is conserved or violated. If R-parity is conserved, SUSY particles (sparticles), which have odd R-parity, are produced in pairs and the decays of each SUSY particle must involve an odd number of lighter SUSY particles. The lightest SUSY particle (LSP) is then stable and often assumed to be a weakly interacting massive particle (WIMP). If R-parity is violated, new terms λ_{ijk}, λ'_{ijk} and λ''_{ijk} appear in the superpotential, where ijk are generation indices; λ-type couplings appear between lepton superfields only, λ''-type are between quark superfields only, and λ'-type couplings connect the two. R-parity violation implies lepton and/or baryon number violation. More details of the theoretical framework of SUSY are discussed elsewhere in this volume [28].

Today, low-energy data from flavor physics experiments, high-precision electroweak observables as well as astrophysical data impose strong constraints on the allowed SUSY parameter space. Recent examples of such data include measurements of the rare B-meson decay $B_s \to \mu^+\mu^-$ [29,30], measurements of the anomalous magnetic moment of the muon [31], and accurate determinations of the cosmological dark matter relic density constraint [32,33].

These indirect constraints are often more sensitive to higher SUSY mass scales than experiments searching for direct sparticle production at colliders, but the interpretation of these results is often strongly model dependent. In contrast, direct searches for sparticle production at collider experiments are less subject to interpretation ambiguities and therefore they play a crucial role in the search for SUSY.

The discovery of a Higgs boson with a mass around 125 GeV imposes constraints on SUSY, which are discussed elsewhere [28,34].

In this review we limit ourselves to direct searches, covering data analyses at LEP, HERA, the Tevatron and the LHC, with emphasis on the latter. For more details on LEP and Tevatron constraints, see earlier PDG reviews [35].

110.2. Experimental search program

The electron-positron collider LEP was operational at CERN between 1989 and 2000. In the initial phase, center-of-mass energies around the Z-peak were probed, but after 1995 the LEP experiments collected a significant amount of luminosity at higher center-of-mass energies, some 235 pb^{-1} per experiment at $\sqrt{s} \geq 204$ GeV , with a maximum $\sqrt{s}$ of 209 GeV .

Searches for new physics at e^+e^- colliders benefit from the clean experimental environment and the fact that momentum balance can be measured not only in the plane transverse to the beam, but also in the direction along the beam (up to the beam pipe holes), defined as the longitudinal direction. Searches at LEP are dominated by the data samples taken at the highest center-of-mass energies.

Constraints on SUSY have been set by the CDF and D0 experiments at the Tevatron, a proton-antiproton collider at a center-of-mass energy of up to 1.96 TeV. CDF and D0 have collected integrated luminosities between 10 and 11 fb^{-1} each up to the end of collider operations in 2011.

The electron-proton collider HERA provided collisions to the H1 and ZEUS experiments between 1992 and 2007, at a center-of-mass energy up to 318 GeV . A total integrated luminosity of approximately 0.5 fb^{-1} was collected by each experiment. Since in ep collisions no annihilation process takes place, SUSY searches at HERA typically look for R-parity violating production of single SUSY particles.

The Large Hadron Collider (LHC) at CERN started proton-proton operation at a center-of-mass energy of 7 TeV in 2010. By the end of 2011 the experiments ATLAS and CMS had collected about 5 fb^{-1} of integrated luminosity each, and the LHCb experiment had collected approximately 1 fb^{-1}. In 2012, the LHC operated at a center-of-mass energy of 8 TeV, and ATLAS and CMS collected approximately 20 fb^{-1} each, whereas LHCb collected 2 fb^{-1}. In 2015, the LHC started Run 2, with a center-of-mass energy of 13 TeV. At the end of 2016, ATLAS and CMS had both collected approximately 36 fb^{-1}, and LHCb had collected 2 fb^{-1}.

Proton-(anti)proton colliders produce interactions at higher center-of-mass energies than those available at LEP, and cross sections of QCD-mediated processes are larger, which is reflected in the higher sensitivity for SUSY particles carrying color charge: squarks and gluinos. Large background contributions from Standard Model processes, however, pose challenges to trigger and analysis. Such backgrounds are dominated by multijet production processes, including, particularly at the LHC, those of top quark production, as well as jet production in association with vector bosons. The proton momentum is shared between its parton constituents, and in each collision only a fraction of the total center-of-mass energy is available in the hard parton-parton scattering. Since the parton momenta in the

longitudinal direction are not known on an event-by-event basis, use of momentum conservation constraints in an analysis is restricted to the transverse plane, leading to the definition of transverse variables, such as the missing transverse momentum, and the transverse mass. Proton-proton collisions at the LHC differ from proton-antiproton collisions at the Tevatron in the sense that there are no valence anti-quarks in the proton, and that gluon-initiated processes play a more dominant role. The increased center-of-mass energy of the LHC compared to the Tevatron, as well as the increase at the LHC between Run 1 and Run 2, significantly extends the kinematic reach for SUSY searches. This is reflected foremost in the sensitivity for squarks and gluinos, but also for other SUSY particles.

The main production mechanisms of massive colored sparticles at hadron colliders are squark-squark, squark-gluino and gluino-gluino production; when "squark" is used "antisquark" is also implied. The typical SUSY search signature at hadron colliders contains high-p_{T} jets, which are produced in the decay chains of heavy squarks and gluinos, and significant missing momentum originating from the two LSPs produced at the end of the decay chain. Assuming R-parity conservation, the LSPs are expected to be neutral and weakly interacting massive particles, since otherwise the model contradicts standard cosmology. These particles then escape detection at colliders. Standard Model backgrounds with missing transverse momentum include leptonic W/Z-boson decays, heavy-flavor decays to neutrinos, and multijet events that may be affected by instrumental effects such as jet mismeasurement.

Selection variables designed to separate the SUSY signal from the Standard Model backgrounds include H_{T}, $E_{\mathrm{T}}^{\mathrm{miss}}$, and m_{eff}. The quantities H_{T} and $E_{\mathrm{T}}^{\mathrm{miss}}$ refer to the measured transverse energy and missing transverse momentum in the event, respectively. They are usually defined as the scalar sum of the transverse jet momenta or calorimeter clusters transverse energies measured in the event (H_{T}), or the negative vector sum of transverse momenta of reconstructed objects like jets and leptons in the event ($E_{\mathrm{T}}^{\mathrm{miss}}$). The quantity m_{eff} is referred to as the effective mass of the event and is defined as $m_{\mathrm{eff}} = H_{\mathrm{T}} + |E_{\mathrm{T}}^{\mathrm{miss}}|$. The peak of the m_{eff} distribution for SUSY signal events correlates with the SUSY mass scale, in particular with the mass difference between the primary produced SUSY particle and the LSP [36], whereas the Standard Model backgrounds dominate at low m_{eff}. Additional reduction of multijet backgrounds can be achieved by demanding isolated leptons or photons in the final states; in such events the lepton or photon transverse momentum may be added to H_{T} or m_{eff} for further signal-background separation.

At the LHC, alternative approaches have been developed to increase the sensitivity to pair production of heavy sparticles with TeV-scale masses focusing on the kinematics of their decays, and to further suppress the background from multijet production. Prominent examples of these new approaches are searches using the α_{T} [37–41], *razor* [42], *stransverse mass* (m_{T2}) [43], and *contransverse mass* (m_{CT}) [44] variables. Recently, the topological event reconstruction methods have expanded with the *super-razor* [45] and *recursive jigsaw reconstruction* [46] techniques. Furthermore, frequently the searches for massive SUSY particles attempt to identify their decay into top quarks or vector bosons, which are themselves unstable. If these are produced with a significant boost, jets from their decay will typically overlap, and such topologies are searched for with *jet-substructure* [47] techniques.

110.3. Interpretation of results

Since the mechanism by which SUSY is broken is unknown, a general approach to SUSY via the most general soft SUSY breaking Lagrangian adds a significant number of new free parameters. For the minimal supersymmetric standard model, MSSM, *i.e.*, the model with the minimal particle content, these comprise 105 new parameters. A phenomenological analysis of SUSY searches leaving all these parameters free is not feasible. For the practical interpretation of SUSY searches at colliders several approaches are taken to reduce the number of free parameters.

One approach is to assume a SUSY breaking mechanism and lower the number of free parameters through the assumption of additional constraints. Before the start of the LHC, interpretations of experimental results were predominately performed in constrained models of gravity mediated [48,49], gauge-mediated [50–52], and anomaly mediated [53,54] SUSY breaking. The most popular model was the constrained MSSM (CMSSM) [48,55,56], which in the literature is also referred to as minimal supergravity, or MSUGRA.

These constrained SUSY models are theoretically well motivated and provide a rich spectrum of experimental signatures. However, with universality relations imposed on the soft SUSY breaking parameters, they do not cover all possible kinematic signatures and mass relations of SUSY. In such scenarios the squarks are often nearly degenerate in mass, in particular for the first and second generation. The exclusion of parameter space in the CMSSM and in CMSSM-inspired models is mainly driven by first and second generation squark production together with gluino production. As shown in Fig. 110.1 [57] these processes possess the largest production cross sections in proton-proton collisions, and thus the LHC searches typically provide the tightest mass limits on these colored sparticles. This, however, implies that the allowed parameter space of constrained SUSY models today has been restrained significantly by searches from ATLAS and CMS. Furthermore, confronting the remaining allowed parameter space with other collider and non-collider measurements, which are directly or indirectly sensitive to contributions from SUSY, the overall compatibility of these models with all data is significantly worse than in the pre-LHC era (see section II.8 for further discussion), indicating that very constrained models like the CMSSM are no longer be good benchmark scenarios to solely characterize the results of SUSY searches at the LHC.

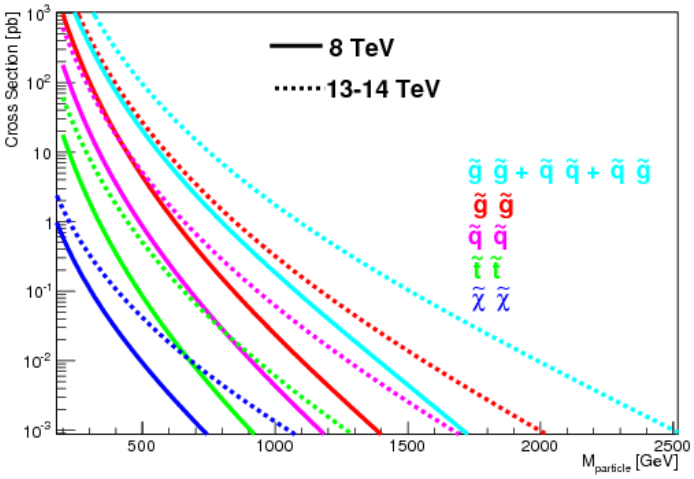

Figure 110.1: Cross sections for pair production of different sparticles as a function of their mass at the LHC for a center-of-mass energy of 8 TeV (solid curves) and 13-14 TeV (dotted curves), taken from Ref. [57]. Typically the production cross section of colored squarks and gluinos, calculated with NLL-FAST [58] at $\sqrt{s}$ =8 and 13 TeV, is several orders of magnitude larger than the one for electroweak gauginos, calculated with PROSPINO [59] at $\sqrt{s}$ =8 and 14 TeV for higgsino-like neutralinos. Except for the explicitly shown pair production of stops, production cross sections for squarks assumes mass degeneracy of left- and right-handed u, d, s, c and b squarks.

For these reasons, an effort has been made in the past years to complement the traditional constrained models with more flexible approaches.

One approach to study a broader and more comprehensive subset of the MSSM is via the phenomenological-MSSM, or pMSSM [60–62]. It is derived from the MSSM, using experimental data to eliminate parameters that are free in principle but have already been highly constrained by measurements of *e.g.*, flavor mixing and CP-violation. This effective approach reduces the number of free parameters in the

MSSM to typically 19 or even less, making it a practical compromise between the full MSSM and highly constrained models such as the CMSSM.

Even less dependent on fundamental assumptions are interpretations in terms of so-called simplified models [63–66]. Such models assume a limited set of SUSY particle production and decay modes and leave open the possibility to vary masses and other parameters freely. Therefore, simplified models enable comprehensive studies of individual SUSY topologies, and are useful for optimization of the experimental searches over a wide parameter space without limitations on fundamental kinematic properties such as masses, production cross sections, and decay modes.

As a consequence, ATLAS and CMS have adopted simplified models as the primary framework to provide interpretations of their searches. In addition to using simplified models that describe prompt decays of SUSY particles, the experiments are now also focusing more on the use simplified models that allow for decays of long-lived SUSY particles as they can arise in different SUSY scenarios (see section II.7 for further discussion). Today, almost every individual search provides interpretations of their results in one or even several simplified models that are characteristic of SUSY topologies probed by the analysis.

However, while these models are very convenient for the interpretation of individual SUSY production and decay topologies, care must be taken when applying these limits to more complex SUSY spectra. Therefore, in practice, simplified model limits are often used as an approximation of the constraints that can be placed on sparticle masses in more complex SUSY spectra. Yet, depending on the assumed SUSY spectrum, the sparticle of interest, and the considered simplified model limit, this approximation can lead to a significant mistake, typically an overestimation, in the assumed constraint on the sparticle mass (see for example [67]) . Only on a case-by-case basis can it be determined whether the limit of a given simplified model represents a good approximation of the true underlying constraint that can be applied on a sparticle mass in a complex SUSY spectrum. In the following, we will point out explicitly the assumptions that have entered the limits when quoting interpretations from simplified models.

This review covers results up to September 2017 and since none of the searches performed so far have shown significant excess above the SM background prediction, the interpretation of the presented results are exclusion limits on SUSY parameter space.

110.4. Exclusion limits on gluino and squark masses

Gluinos and squarks are the SUSY partners of gluons and quarks, and thus carry color charge. Limits on squark masses of the order 100 GeV have been set by the LEP experiments [68], in the decay to quark plus neutralino, and for a mass difference between squark and quark plus neutralino of typically at least a few GeV . However, due to the colored production of these particles at hadron colliders (see e.g. Fig. 110.1), hadron collider experiments are able to set much tighter mass limits.

Pair production of these massive colored sparticles at hadron colliders generally involve both the s-channel and t-channel parton-parton interactions. Since there is a negligible amount of bottom and top quark content in the proton, top- and bottom squark production proceeds through s-channel diagrams only. In the past, experimental analyses of squark and/or gluino production typically assumed the first and second generation squarks to be approximately degenerate in mass. However, in order to have even less model dependent interpretations of the searches, the experiments have started to also provide simplified model limits on individual first or second generation squarks.

Assuming R-parity conservation and assuming gluinos to be heavier than squarks, squarks will predominantly decay to a quark and a neutralino or chargino, if kinematically allowed. The decay may involve the lightest neutralino (typically the LSP) or chargino, but, depending on the masses of the gauginos, may involve heavier neutralinos or charginos. For pair production of first and second generation squarks, the simplest decay modes involve two jets and missing momentum, with potential extra jets stemming from initial state or final state radiation (ISR/FSR) or from decay modes with longer cascades. Similarly, gluino pair production leads to four jets and missing momentum, and possibly additional jets from ISR/FSR or cascades. Associated production of a gluino and a (anti-)squark is also possible, in particular if squarks and gluinos have similar masses, typically leading to three or more jets in the final state. In cascades, isolated photons or leptons may appear from the decays of sparticles such as neutralinos or charginos. Final states are thus characterized by significant missing transverse momentum, and at least two, and possibly many more high p_{T} jets, which can be accompanied by one or more isolated objects like photons or leptons, including τ leptons, in the final state. Table 110.1 shows a schematic overview of characteristic final state signatures of gluino and squark production for different mass hierarchy hypotheses and assuming decays involving the lightest neutralino.

Table 110.1: Typical search signatures at hadron colliders for direct gluino and first- and second-generation squark production assuming different mass hierarchies.

Mass Hierarchy	Main Production	Dominant Decay	Typical Signature
$m_{\tilde{q}} \ll m_{\tilde{g}}$	$\tilde{q}\bar{\tilde{q}}, \tilde{q}\tilde{\bar{q}}$	$\tilde{q} \to q\tilde{\chi}_1^0$	≥ 2 jets + $E_{\mathrm{T}}^{\mathrm{miss}}$ + X
$m_{\tilde{q}} \approx m_{\tilde{g}}$	$\tilde{q}\tilde{g}, \bar{\tilde{q}}\tilde{g}$	$\tilde{q} \to q\tilde{\chi}_1^0$ $\tilde{g} \to q\bar{q}\tilde{\chi}_1^0$	≥ 3 jets + $E_{\mathrm{T}}^{\mathrm{miss}}$ + X
$m_{\tilde{q}} \gg m_{\tilde{g}}$	$\tilde{g}\tilde{g}$	$\tilde{g} \to q\bar{q}\tilde{\chi}_1^0$	≥ 4 jets + $E_{\mathrm{T}}^{\mathrm{miss}}$ + X

110.4.1. *Exclusion limits on the gluino mass* :

Limits set by the Tevatron experiments on the gluino mass assume the framework of the CMSSM, with $\tan\beta = 5$ (CDF) or $\tan\beta = 3$ (D0), where $\tan\beta$ is the ratio of vacuum expectation values of the Higgs fields for up-type and down-type fermions. Furthermore, $A_0 = 0$ and $\mu < 0$ is assumed, and the resulting lower mass limits are about 310 GeV for all squark masses, or 390 GeV for the case $m_{\tilde{q}} = m_{\tilde{g}}$ [69,70]. These limits have been superseded by those provided by ATLAS and CMS, and the tightest constraints have been set with up to approximately 36 fb^{-1} of data recorded at the LHC at a center-of-mass energy of 13 TeV.

Limits on the gluino mass have been established in the framework of simplified models. Assuming only gluino pair production, in particular three primary decay chains of the gluino have been considered by the LHC experiments for interpretations of their search results. The first decay chain $\tilde{g} \to q\bar{q}\tilde{\chi}_1^0$ assumes gluino mediated production of first and second generation squarks (on-shell or off-shell) which leads to four light flavor quarks in the final state. Therefore, inclusive all-hadronic analyses searching for multijet plus $E_{\mathrm{T}}^{\mathrm{miss}}$ final states are utilized to put limits on this simplified model. These limits are derived as a function of the gluino and neutralino (LSP) mass. As shown in Fig. 110.2 (upper left), using the cross section from next-to-leading order QCD corrections and the resummation of soft gluon emission at next-to-leading-logarithmic accuracy as reference [58], the ATLAS collaboration [71] excludes in this simplified model gluino masses below approximately 2000 GeV , for a massless neutralino. In scenarios where neutralinos are not very light, the efficiency of the analyses is reduced by the fact that jets are less energetic, and there is less missing transverse momentum in the event. This leads to weaker limits when the mass difference $\Delta m = m_{\tilde{g}} - m_{\tilde{\chi}_1^0}$ is reduced. For example, for neutralino masses above about 1000 GeV no limit on the gluino mass can be set for this decay chain. Therefore, limits on gluino masses are strongly affected by the assumption of the neutralino mass. Similar results for this simplified model have been obtained by CMS [72,73].

The second important decay chain of the gluino considered for interpretation in a simplified model is $\tilde{g} \to b\bar{b}\tilde{\chi}_1^0$. Here the decay is mediated via bottom squarks and thus leads to four jets from b quarks and $E_{\mathrm{T}}^{\mathrm{miss}}$ in the final state. Also for this topology inclusive all-hadronic searches provide the highest sensitivity. However, with four b quarks in the final state, the use of secondary vertex reconstruction for the identification of jets originating from b quarks provides a powerful handle on the SM background. Therefore, in addition to a multijet

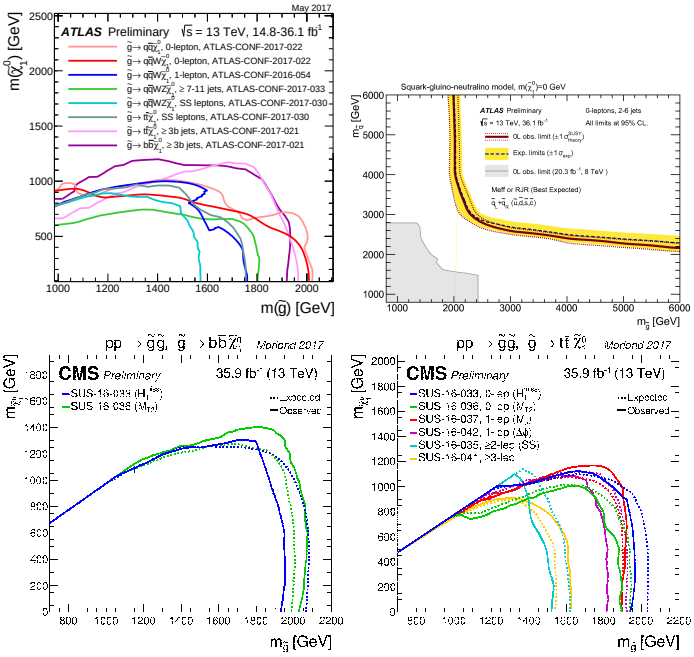

Figure 110.2: Upper left and lower left and right plots: lower mass limits, at 95% C.L., on gluino pair production for various decay chains. The upper left plot shows limits from the ATLAS collaboration; the lower plots display CMS results for the decay chains $\tilde{g} \to b\bar{b}\tilde{\chi}_1^0$ (lower left) and $\tilde{g} \to t\bar{t}\tilde{\chi}_1^0$ (lower right). The limits are defined in the framework of simplified models assuming a single decay chain, i.e. a 100% branching fraction. The upper right plot shows 95% C.L. mass limits on gluinos and squarks assuming gluino and squark production and massless neutralinos.

plus $E_{\mathrm{T}}^{\mathrm{miss}}$ signature these searches also require several jets to be tagged as b-jets. As shown in Fig. 110.2 (lower left), for this simplified model CMS [72] excludes gluino masses below ≈ 2000 GeV for a massless neutralino, while for neutralino masses above ≈ 1400 GeV no limit on the gluino mass can be set. Comparable limits for this simplified model are provided by searches from ATLAS [74].

Gluino decays are not limited to first and second generation squarks or bottom squarks, if kinematically allowed, top squarks via the decay $\tilde{g} \to \tilde{t}t$ are also possible. This leads to a "four tops" final state $tttt\tilde{\chi}_1^0\tilde{\chi}_1^0$ and defines the third important simplified model, $\tilde{g} \to t\bar{t}\tilde{\chi}_1^0$, characterizing gluino pair production. The topology of this decay is very rich in different experimental signatures: as many as four isolated leptons, four b-jets, several light flavor quark jets, and significant missing momentum from the neutrinos in the W decay and from the two neutralinos. As shown in Fig. 110.2 (lower right), the CMS inclusive H_{T} based search [73] and a search requiring one isolated lepton and large-radius jets [75] rule out gluinos with masses below ≈ 1900 GeV for massless neutralinos in this model. For neutralino masses above ≈ 1100 GeV , no limit can be placed on the gluino mass. The ATLAS multiple b-jets search [74] obtains similar limits.

The ATLAS collaboration also provides limits in a pMSSM-inspired model with only gluinos and first and second generation squarks, and a bino-like $\tilde{\chi}_1^0$ [71]. As shown in Fig. 110.2 (upper right), assuming $m_{\tilde{\chi}_1^0} = 0$ GeV , gluinos with masses below ≈ 2000 GeV are excluded for any squark mass and vice versa. For $m_{\tilde{q}} \approx m_{\tilde{g}}$, the mass exclusion is about 2700 GeV .

R-parity violating gluino decays are searched for in a number of final states. Searches in multilepton final states set lower mass limits of 1 to 1.4 TeV, depending on neutralino mass and lepton flavor, on decays mediated by λ and λ' couplings [76,77], assuming prompt decays. Searches for displaced vertices are sensitive to non-prompt decays [78]. Multijet final states have been used to search for fully hadronic gluino decays involving λ'', by CDF [79], ATLAS [80,81] and CMS [82,83]. Lower mass limits range between 600 and 2000 GeV depending on neutralino mass and flavor content of the final state.

110.4.2. *Exclusion limits squark masses* :

Limits on first and second generation squark masses set by the Tevatron experiments assume the CMSSM model, and amount to lower limits of about 380 GeV for all gluino masses, or 390 GeV for the case $m_{\tilde{q}} = m_{\tilde{g}}$ [69,70].

At the LHC, limits on squark masses have been set using up to approximately 36 fb^{-1} of data at 13 TeV. Interpretations in simplified models typically characterize squark pair production with only one decay chain of $\tilde{q} \to q\tilde{\chi}_1^0$. Here it is assumed that the left and right-handed $\tilde{u}$, $\tilde{d}$, $\tilde{s}$ and $\tilde{c}$ squarks are degenerate in mass. Furthermore, it is assumed that the mass of the gluino is very high and thus contributions of the corresponding t-channel diagrams to squark pair production are negligible. Therefore, the total production cross section for this simplified model is eight times the production cross section of an individual squark (e.g. $\tilde{u}_L$). The CMS collaboration provides interpretations using different all-hadronic searches for this simplified model. As displayed in the upper plot of Fig. 110.3, best observed exclusion is obtained from the analysis using the m_{T2} variable [72], which excludes squark masses just below 1550 GeV for a light neutralino. The effects of heavy neutralinos on squark limits are similar to those discussed in the gluino case (see section II.4.1) and only for neutralino masses below ≈ 800 GeV can any squark masses be excluded. Results from the ATLAS collaboration [71] for this simplified model are similar.

For the same analysis ATLAS also provides an interpretation of their search result in the aforementioned pMSSM-inspired model with only gluinos and first and second generation squarks, and a bino-like $\tilde{\chi}_1^0$ [71]. In this model, squark production can take place with non-decoupled gluinos, enhancing the squark production cross section through gluino exchange diagrams. For example, for gluinos of 6 TeV, squark masses up to 2.2 TeV are excluded, much higher than in the simplified model under consideration.

If the assumption of mass degenerate first and second generation squarks is dropped and only the production of a single light squark is assumed, the limits weaken significantly. This is shown as the much smaller exclusion region in the upper plot of Fig. 110.3, which represents the 95% C.L. limit on pair production of a single light squark, with the gluino and all other squarks decoupled to very high masses. Under this assumption, the lower limit on squark masses is only ≈ 1050 GeV for a massless neutralino, and for neutralinos heavier than ≈ 450 GeV no squark mass limit can be placed. It should be noted that this limit is not a result of a simple scaling of the above mentioned mass limits assuming eightfold mass degeneracy but it also takes into account that for an eight times lower production cross section the analyses must probe kinematic regions of phase space that are closer to the ones of SM background production. Since signal acceptance and the ratio of expected signal to SM background events of the analyses are typically worse in this region of phase space not only the 1/8 reduction in production cross section but also a worse analysis sensitivity are responsible for the much weaker limit on single squark pair production.

For single light squarks ATLAS also reports results of a dedicated search, at $\sqrt{s} = 8$ TeV, for pair production of scalar partners of charm quarks [84]. Assuming that the scalar-charm state exclusively decays into a charm quark and a neutralino, scalar-charm masses up to 490 GeV are excluded for neutralino masses below 200 GeV .

Besides placing stringent limits on first and second generation squark masses, the LHC experiments also search for the production of third generation squarks. SUSY at the TeV-scale is often motivated by naturalness arguments, most notably as a solution to stabilize quadratic divergences in radiative corrections to the Higgs boson mass. In this context, the most relevant terms for SUSY phenomenology arise from the interplay between the masses of the third generation squarks and the Yukawa coupling of the top quark to the Higgs boson. This motivates a potential constraint on the masses of the top squarks and the left-handed bottom squark. Due to the large top quark mass, significant mixing between $\tilde{t}_{\mathrm{L}}$ and $\tilde{t}_{\mathrm{R}}$ is expected, leading to a lighter mass state $\tilde{t}_1$ and a heavier mass state $\tilde{t}_2$. In the MSSM, the lightest top squark ($\tilde{t}_1$) can be the lightest squark.

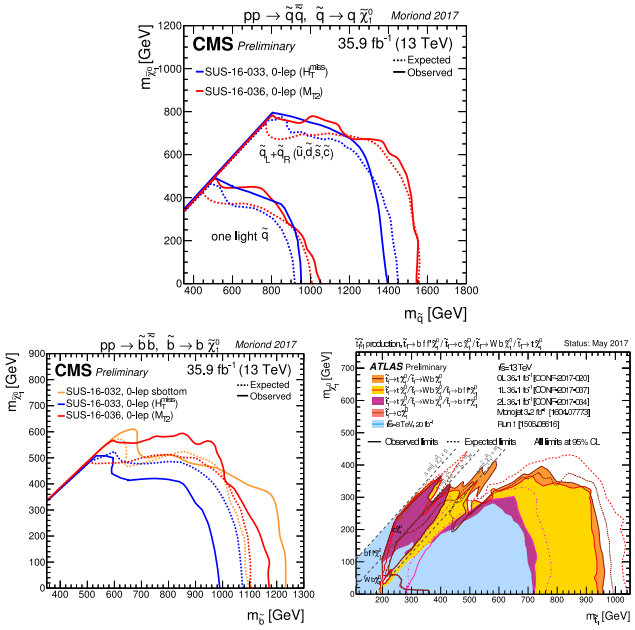

Figure 110.3: The upper plot shows 95% C.L. exclusion contours in the squark-neutralino mass plane defined in the framework of simplified models assuming a single decay chain of $\tilde{q} \to q\tilde{\chi}_1^0$ [72]. Two assumptions for the squark pair production cross sections are displayed; a) eightfold degeneracy for the masses of the first and second generation squarks and b) only one light flavor squark. The lower left plot shows the 95% C.L. exclusion contours in the sbottom-neutralino mass plane defined in the framework of a simplified model assuming a single decay chain of $\tilde{b} \to b\tilde{\chi}_1^0$ as obtained by CMS. The lower right plot shows the 95% C.L. exclusion contours in the stop-neutralino mass plane defined in various simplified models of stop decay, as obtained by ATLAS.

Bottom squarks are expected to decay predominantly to $b\tilde{\chi}^0$ giving rise to the characteristic multi b-jet and $E_{\mathrm{T}}^{\mathrm{miss}}$ signature. Direct production of bottom squark pairs has been studied at the Tevatron and at the LHC. Limits from the Tevatron are $m_{\tilde{b}} > 247$ GeV for a massless neutralino [85,86]. The LHC experiments have surpassed these limits, and the latest results are based on 36 fb^{-1} of data collected at $\sqrt{s} = 13$ TeV. As shown in the lower left plot of Fig. 110.3, using inclusive all-hadronic searches [72,73] as well as a search requiring significant $E_{\mathrm{T}}^{\mathrm{miss}}$ and two jets reconstructed as b-jets [87], CMS has set a lower limit of $m_{\tilde{b}} > \approx 1200$ GeV for massless neutralinos in this model. For $m_{\tilde{\chi}_1^0} \approx 550$ GeV or higher no limit can be placed on direct bottom squark pair production in this simplified model. Limits from ATLAS are comparable [88]. Further bottom squark decay modes have also been studied by ATLAS [88,89] and CMS [87,90].

The top squark decay modes depend on the SUSY mass spectrum, and on the $\tilde{t}_{\mathrm{L}}$-$\tilde{t}_{\mathrm{R}}$ mixture of the top squark mass eigenstate. If kinematically allowed, the two-body decays $\tilde{t} \to t\tilde{\chi}^0$ (which requires $m_{\tilde{t}} - m_{\tilde{\chi}^0} > m_t$) and $\tilde{t} \to b\tilde{\chi}^{\pm}$ (which requires $m_{\tilde{t}} - m_{\tilde{\chi}^{\pm}} > m_b$) are expected to dominate. If not, the top squark decay may proceed either via the two-body decay $\tilde{t} \to c\tilde{\chi}^0$ or through $\tilde{t} \to bf\bar{f}'\tilde{\chi}^0$ (where f and $\bar{f}'$ denote a fermion-antifermion pair with appropriate quantum numbers). For $m_{\tilde{t}} - m_{\tilde{\chi}^0} > m_b$ the latter decay chain represents a four-body decay with a W boson, charged Higgs H, slepton $\tilde{\ell}$, or light flavor squark $\tilde{q}$, exchange. If the exchanged W boson and/or sleptons are kinematically allowed to be on-shell ($m_{\tilde{t}} - m_{\tilde{\chi}^{\pm}} > m_b + m_W$ and/or $m_{\tilde{t}} - m_{\tilde{\ell}} > m_b$), the three-body decays $\tilde{t} \to Wb\tilde{\chi}^0$ and/or $\tilde{t} \to bl\tilde{\ell}$ will become dominant. For further discussion on top squark decays see for example Ref. [91].

Limits from LEP on the $\tilde{t}_1$ mass are $m_{\tilde{t}} > 96$ GeV in the charm plus neutralino final state, and > 93 GeV in the lepton, b-quark and sneutrino final state [68].

The Tevatron experiments have performed a number of searches for top squarks, often assuming direct pair production. In the $b\ell\tilde{\nu}$ decay channel, and assuming a 100% branching fraction, limits are set as $m_{\tilde{t}} > 210$ GeV for $m_{\tilde{\nu}} < 110$ GeV and $m_{\tilde{t}} - m_{\tilde{\nu}} > 30$ GeV , or $m_{\tilde{t}} > 235$ GeV for $m_{\tilde{\nu}} < 50$ GeV [92,93]. In the $\tilde{t} \to c\tilde{\chi}^0$ decay mode, a top squark with a mass below 180 GeV is excluded for a neutralino lighter than 95 GeV [94,95]. In both analyses, no limits on the top squark can be set for heavy sneutrinos or neutralinos. In the $\tilde{t} \to b\tilde{\chi}_1^{\pm}$ decay channel, searches for a relatively light top squark have been performed in the dilepton final state [96,97]. The CDF experiment sets limits in the $\tilde{t} - \tilde{\chi}_1^0$ mass plane for various branching fractions of the chargino decay to leptons and for two value of $m_{\tilde{\chi}_1^{\pm}}$. For $m_{\tilde{\chi}_1^{\pm}} = 105.8$ GeV and $m_{\tilde{\chi}_1^0} = 47.6$ GeV , top squarks between 128 and 135 GeV are excluded for W-like leptonic branching fractions of the chargino.

The LHC experiments have improved these limits substantially. As shown in the right plot of Fig. 110.3, limits on the top squark mass assuming a simplified model with a single decay chain of $\tilde{t} \to t\tilde{\chi}_1^0$ now approach or surpass 1 TeV. The most important searches for this top squark decay topology are dedicated searches requiring zero or one isolated lepton, modest $E_{\mathrm{T}}^{\mathrm{miss}}$, and four or more jets out of which at least one jet must be reconstructed as a b-jet [98–101]. For example, CMS excludes top squarks with masses below about 1100 GeV in this model for massless neutralinos, while for $m_{\tilde{\chi}_1^0} >$ 500 GeV no limits can be provided.

Assuming that the top squark decay exclusively proceeds via the chargino mediated decay chain $\tilde{t} \to b\tilde{\chi}_1^{\pm}$, $\tilde{\chi}_1^{\pm} \to W^{\pm(*)}\tilde{\chi}_1^0$ yields stop mass exclusion limits that vary strongly with the assumptions made on the $\tilde{t}-\tilde{\chi}_1^{\pm}-\tilde{\chi}_1^0$ mass hierarchy. For example, for $m_{\tilde{\chi}_1^{\pm}} = (m_{\tilde{t}}+m_{\tilde{\chi}_1^0})/2$, a stop mass below ≈ 1000 GeV for a light $\tilde{\chi}_1^0$ is excluded, while no limit can be placed for $m_{\tilde{\chi}_1^0} > 500$ GeV [98]. These limits, however, can weaken significantly when other assumptions about the mass hierarchy are imposed. For example, if the chargino becomes nearly mass degenerate with the top squark the key experimental signature turns from an all-hadronic final state with b-jets and $E_{\mathrm{T}}^{\mathrm{miss}}$ into a multi-lepton and $E_{\mathrm{T}}^{\mathrm{miss}}$ topology yielding typically weaker limits for this top squark decay (see e.g. [99,101,102]) .

If the decays $\tilde{t} \to t\tilde{\chi}_1^0$ and $\tilde{t} \to b\tilde{\chi}_1^{\pm}$, $\tilde{\chi}_1^{\pm} \to W^{\pm(*)}\tilde{\chi}_1^0$ are kinematically forbidden, the decay chains $\tilde{t} \to Wb\tilde{\chi}^0$ and $\tilde{t} \to c\tilde{\chi}^0$ can become important. As shown in the lower right plot of Fig. 110.3, the zero-lepton ATLAS search provides for the kinematic region $m_{\tilde{t}} - m_{\tilde{\chi}^{\pm}} > m_b + m_W$ lower limits on the top squark mass of ≈ 400 GeV for a neutralino lighter than ≈ 300 GeV [100], while the corresponding CMS analyses [72,73,98] push this limit to about 550 GeV for neutralino masses below ≈ 400 GeV . Furthermore, analyses with one or two lepton final states [99,101–103] also place significant constraints on this decay channel.

For the kinematic region in which even the production of real W bosons is not allowed, ATLAS and CMS improve the Tevatron limit on $\tilde{t} \to c\tilde{\chi}^0$ substantially. Based on a monojet analysis [104] ATLAS excludes top squark masses below $m_{\tilde{\chi}_1^0} \approx 450$ GeV along the kinematic boundary for the $\tilde{t} \to c\tilde{\chi}^0$ decay. The CMS collaboration uses the hadronic searches [72,98] to place constraints on this particular stop decay and excludes $m_{\tilde{t}} \approx 550$ GeV for $m_{\tilde{\chi}_1^0}$ below 450 GeV . The exclusion at the diagonal $m_{\tilde{t}} \approx m_{\tilde{\chi}_1^0}$ is also about 550 GeV .

The other decay chain relevant in this phase region is $\tilde{t} \to bf\bar{f}'\tilde{\chi}^0$. Here the ATLAS one-lepton search [101] excludes up to $m_{\tilde{t}} \approx$ 350 GeV for $m_{\tilde{\chi}_1^0}$ below 250 GeV , while the monojet analysis [104] excludes at the kinematic boundary top squarks below 400 GeV . As for the $\tilde{t} \to c\tilde{\chi}^0$ decay, CMS uses the zero-lepton searches [72,98] to also place constraints on $\tilde{t} \to bf\bar{f}'\tilde{\chi}^0$. Also in this case CMS excludes $m_{\tilde{t}} \approx 550$ GeV for $m_{\tilde{\chi}_1^0}$ below 450 GeV .

In general, the variety of top squark decay chains in the phase space region where $\tilde{t} \to t\tilde{\chi}_1^0$ is kinematically forbidden represents a

challenge for the experimental search program and more data and refined analyses will be required to further improve the sensitivity in this difficult but important region of SUSY parameter space.

R-parity violating production of single squarks via a λ'-type coupling has been studied at HERA. In such models, a lower limit on the squark mass of the order of 275 GeV has been set for electromagnetic-strength-like couplings $\lambda' = 0.3$ [105]. At the LHC, both prompt [76,77] and non-prompt [78,106] R-parity violating squark decays have been searched for, but no signal was found. Squark mass limits are very model-dependent.

R-parity violating production of single top squarks has been searched for at LEP, HERA, and the Tevatron. For example, an analysis from the ZEUS collaboration [107] makes an interpretation of its search result assuming top squarks to be produced via a λ' coupling and decay either to $b\tilde{\chi}_1^{\pm}$ or R-parity-violating to a lepton and a jet. Limits are set on λ'_{131} as a function of the top squark mass in an MSSM framework with gaugino mass unification at the GUT scale.

The search for top squark pair production in the context of R-parity violating supersymmetry has now also become a focus point for searches at the LHC. The CMS collaboration has performed a search for top squarks using a variety of multilepton final states [108]. It provides lower limits on the top squark mass in models with non-zero leptonic R-parity violating couplings λ_{122} and λ_{233}. For a bino mass of 200 GeV , these limits are 1020 GeV and 820 GeV , respectively. The analysis also provides limits in a model with the semileptonic R-parity violating coupling λ'_{233}. The λ'-mediated top squark decay $\tilde{t} \to b\ell$ has been studied by ATLAS for prompt decays [109], and by CMS for non-prompt decays [110]. CMS also searched for the λ'-mediated decay $\tilde{t} \to b\ell qq$, setting lower stop mass limits of 890 GeV (e) or 1000 GeV (μ) [111]. The fully hadronic R-parity violating top squark decays $\tilde{t} \to bs$ and $\tilde{t} \to ds$, involving λ'', have been searched for by ATLAS [112], and lower top squark mass limits between 410 and 610 GeV were set. CMS [113] have searched for a top squark decay to a bottom quark and a light-flavor quark, and excludes top squarks with masses between 200 and 385 GeV in this decay mode.

It should be noted that limits discussed in this section belong to different top and bottom squark decay channels, different sparticle mass hierarchies, and different simplified decay scenarios. Therefore, care must be taken when interpreting these limits in the context of more complete SUSY models.

110.4.3. *Summary of exclusion limits on squarks and gluinos assuming R-Parity conservation* :

A summary of the most important squark and gluino mass limits for different interpretation approaches assuming R-parity conservation is shown in Table 110.2.

For gluino masses rather similar limits of about 2 TeV are obtained from different model assumptions, indicating that the LHC is indeed probing direct gluino production at the TeV scale and beyond. However, for neutralino masses above approximately 1 to 1.4 TeV, in the best case scenarios, ATLAS and CMS searches cannot place any limits on the gluino mass.

Limits on direct squark production, on the other hand, depend strongly on the chosen model. Especially for direct production of top squarks there are still large regions in parameter space where masses below 1 TeV cannot be excluded. This is also true for first and second generation squarks when only one single squark is considered. Furthermore, for neutralino masses above ≈ 500 GeV no limit on any direct squark production scenario can be placed by the LHC.

110.5. Exclusion limits on the masses of charginos and neutralinos

Charginos and neutralinos result from mixing of the charged wino and higgsino states, and the neutral bino, wino and higgsino states, respectively. The mixing is determined by a limited number of parameters. For charginos these are the wino mass parameter M_2, the higgsino mass parameter μ, and $\tan\beta$, and for neutralinos these are the same parameters plus the bino mass parameter M_1. If any of the parameters M_1, M_2 or μ happened to be substantially smaller than the others, the chargino and neutralino composition would be dominated by specific states, which are referred to as bino-like ($M_1 \ll M_2, \mu$), wino-like ($M_2 \ll M_1, \mu$), or higgsino-like ($\mu \ll M_1, M_2$). If gaugino mass unification at the GUT scale is assumed, a relation between M_1 and M_2 at the electroweak scale follows: $M_1 = 5/3 \tan^2\theta_W M_2 \approx 0.5 M_2$, with θ_W the weak mixing angle. Charginos and neutralinos carry no color charge.

Table 110.2: Summary of squark mass and gluino mass limits using different interpretation approaches assuming R-parity conservation. Masses in this table are provided in GeV . Further details about assumption and analyses from which these limits are obtained are discussed in the corresponding sections of the text.

Model	Assumption	$m_{\tilde{q}}$	$m_{\tilde{g}}$
Simplified model	$m_{\tilde{\chi}_1^0}$= 0, $m_{\tilde{q}} \approx m_{\tilde{g}}$	$\approx$ 2700	$\approx$ 2700
$\tilde{g}\tilde{q}, \tilde{g}\bar{\tilde{q}}$	$m_{\tilde{\chi}_1^0}$= 0, all $m_{\tilde{q}}$	-	$\approx$ 2000
	$m_{\tilde{\chi}_1^0}$= 0, all $m_{\tilde{g}}$	$\approx$ 2000	-
Simplified models $\tilde{g}\tilde{g}$			
$\tilde{g} \to q\bar{q}\tilde{\chi}_1^0$	$m_{\tilde{\chi}_1^0}$ =0	-	$\approx$ 2000
	$m_{\tilde{\chi}_1^0} > \approx$ 1000	-	no limit
$\tilde{g} \to b\bar{b}\tilde{\chi}_1^0$	$m_{\tilde{\chi}_1^0}$ =0	-	$\approx$ 2000
	$m_{\tilde{\chi}_1^0} > \approx$ 1400	-	no limit
$\tilde{g} \to t\bar{t}\tilde{\chi}_1^0$	$m_{\tilde{\chi}_1^0}$ =0	-	$\approx$ 1900
	$m_{\tilde{\chi}_1^0} > \approx$ 1100	-	no limit
Simplified models $\tilde{q}\bar{\tilde{q}}$			
$\tilde{q} \to q\tilde{\chi}_1^0$	$m_{\tilde{\chi}_1^0}$ =0	$\approx$ 1550	-
	$m_{\tilde{\chi}_1^0} > \approx$ 800	no limit	-
$\tilde{u}_L \to q\tilde{\chi}_1^0$	$m_{\tilde{\chi}_1^0}$ =0	$\approx$ 1050	-
	$m_{\tilde{\chi}_1^0} > \approx$ 450	no limit	-
$\tilde{b} \to b\tilde{\chi}_1^0$	$m_{\tilde{\chi}_1^0}$ =0	$\approx$ 1200	-
	$m_{\tilde{\chi}_1^0} > \approx$ 550	no limit	-
$\tilde{t} \to t\tilde{\chi}_1^0$	$m_{\tilde{\chi}_1^0}$ =0	$\approx$ 1100	-
	$m_{\tilde{\chi}_1^0} > \approx$ 500	no limit	-
$\tilde{t} \to b\tilde{\chi}_1^{\pm}$	$m_{\tilde{\chi}_1^0}$ =0	$\approx$ 1000	-
$[m_{\tilde{\chi}_1^{\pm}} = (m_{\tilde{t}} - m_{\tilde{\chi}_1^0})/2]$	$m_{\tilde{\chi}_1^0} > \approx$ 500	no limit	-
$\tilde{t} \to Wb\tilde{\chi}_1^0$	$m_{\tilde{\chi}_1^0} < \approx$ 400	$\approx$ 550	-
$[m_W < m_{\tilde{t}} - m_{\tilde{\chi}^0} < m_t]$			
$\tilde{t} \to c\tilde{\chi}_1^0$	$m_{\tilde{\chi}_1^0} < \approx$ 450	$\approx$ 550	-
	$m_{\tilde{t}} \approx m_{\tilde{\chi}_1^0}$	$\approx$ 550	-
$\tilde{t} \to bff'\tilde{\chi}_1^0$	$m_{\tilde{\chi}_1^0} < \approx$ 450	$\approx$ 550	-
	$m_{\tilde{t}} \approx m_{\tilde{\chi}_1^0}$	$\approx$ 550	-
$[m_{\tilde{t}} - m_{\tilde{\chi}^0} < m_W]$			

110.5.1. *Exclusion limits on chargino masses* :

If kinematically allowed, two body decay modes such as $\tilde{\chi}^{\pm} \to \tilde{f}\bar{f}'$ (including $\ell\tilde{\nu}$ and $\tilde{\ell}\nu$) are dominant. If not, three body decay $\tilde{\chi}^{\pm} \to f\bar{f}'\tilde{\chi}^0$ are mediated through virtual W bosons or sfermions. If sfermions are heavy, the W mediation dominates, and $f\bar{f}'$ are distributed with branching fractions similar to W decay products (barring phase space effects for small mass gaps between $\tilde{\chi}^{\pm}$ and $\tilde{\chi}^0$). If, on the other hand, sleptons are light enough to play a significant role in the decay mediation, leptonic final states will be enhanced.

At LEP, charginos have been searched for in fully-hadronic, semi-leptonic and fully leptonic decay modes [114,115]. A general lower

limit on the lightest chargino mass of 103.5 GeV is derived, except in corners of phase space with low electron sneutrino mass, where destructive interference in chargino production, or two-body decay modes, play a role. The limit is also affected if the mass difference between $\tilde{\chi}_1^{\pm}$ and $\tilde{\chi}_1^0$ is small; dedicated searches for such scenarios set a lower limit of 92 GeV .

At the Tevatron, charginos have been searched for via associated production of $\tilde{\chi}_1^{\pm}\tilde{\chi}_2^0$ [116,117]. Decay modes involving multilepton final states provide the best discrimination against the large multijet background. Analyses have looked for at least three charged isolated leptons, for two leptons with missing transverse momentum, or for two leptons with the same charge. Depending on the $(\tilde{\chi}_1^{\pm} - \tilde{\chi}_1^0)$ and/or $(\tilde{\chi}_2^0 - \tilde{\chi}_1^0)$ mass differences, leptons may be soft.

At the LHC, the search strategy is similar to that at the Tevatron. As shown in Fig. 110.1, the cross section of pair production of electroweak gauginos at the LHC, for masses of several hundreds of GeV, is at least two orders of magnitude smaller than for colored SUSY particles (e.g. top squark pair production). For this reason a high statistics data sample is required to improve the sensitivity of LEP and Tevatron searches for direct chargino/neutralino production. With the full LHC Run 1 data and the first set of Run 2 data, ATLAS and CMS have started to surpass the limits from LEP and Tevatron in regions of SUSY parameter space.

Chargino pair production is searched for in the dilepton plus missing momentum final state. In the simplified model interpretation of the results, assuming mediation of the chargino decay by light sleptons, ATLAS [118] sets limits on the chargino mass up to 740 GeV for massless LSPs, but no limits on the chargino mass can be set for $\tilde{\chi}_1^0$ heavier than 350 GeV . Limits are fairly robust against variation of the slepton mass, unless the mass gap between chargino and slepton becomes small. At 8 TeV, first limits were also set on charginos decaying via a W boson [119]: chargino masses below 180 GeV are excluded for massless LSPs, but no limits are set for LSPs heavier than 25 GeV .

The trilepton plus missing momentum final state is used to set limits on $\tilde{\chi}_1^{\pm}\tilde{\chi}_2^0$ production, assuming wino-like $\tilde{\chi}^{\pm}$ and $\tilde{\chi}_2^0$, bino-like $\tilde{\chi}_1^0$, and $m_{\tilde{\chi}^{\pm}} = m_{\tilde{\chi}_2^0}$, leaving $m_{\tilde{\chi}^{\pm}}$ and $m_{\tilde{\chi}_1^0}$ free. Again, the branching fraction of leptonic final states is determined by the slepton masses. If the decay is predominantly mediated by a light $\tilde{\ell}_{\mathrm{L}}$, i.e. $\tilde{\ell}_{\mathrm{R}}$ is assumed to be heavy, the three lepton flavors will be produced in equal amounts. It is assumed that $\tilde{\ell}_{\mathrm{L}}$ and sneutrino masses are equal, and diagrams with sneutrinos are included. In this scenario, ATLAS [118] and CMS [120] exclude chargino masses below 1140 GeV for massless LSPs; no limits are set for LSP masses above 700 GeV . If the decay is dominated by a light $\tilde{\ell}_{\mathrm{R}}$, the chargino cannot be a pure wino but needs to have a large higgsino component, preferring the decays to tau leptons. Limits are set in various scenarios. If, like for $\tilde{\ell}_{\mathrm{L}}$, a flavor-democratic scenario is assumed, CMS sets limits of 1060 GeV on the chargino mass for massless LSPs, but under the assumption that both $\tilde{\chi}^{\pm}$ and $\tilde{\chi}_2^0$ decay leads to tau leptons in the final state, the chargino mass limit deteriorates to 620 GeV for massless LSPs [120]. ATLAS assumes a simplified model in which staus are significantly lighter than the other sleptons in order to search for a similar multi-tau final state, and sets a lower limit on the chargino mass of 760 GeV in this model [121].

If sleptons are heavy, the chargino is assumed to decay to a W boson plus LSP, and the $\tilde{\chi}_2^0$ into Z plus LSP or H plus LSP. In the WZ channel, ATLAS [118] and CMS [122] limits on the chargino mass reach 610 GeV for massless LSPs, but no limits are set for LSPs heavier than 250 GeV . In the WH channel, for $m_H = 125$ GeV and using Higgs decays to $b\bar{b}$, $\gamma\gamma$ and WW (ATLAS [123]) , or Higgs decays to $b\bar{b}$, $\gamma\gamma$, WW, ZZ and $\tau^+\tau^-$ (CMS [122]) , assuming a SM-like branching fraction in these final states, chargino mass limits extend up to 480 GeV for massless LSPs, but vanish for LSP masses above 100 GeV .

The results on electroweak gaugino searches interpreted in simplified models are summarized in Fig. 110.4 for the two cases of light or decoupled sleptons. For both cases, ATLAS and CMS have comparable limits.

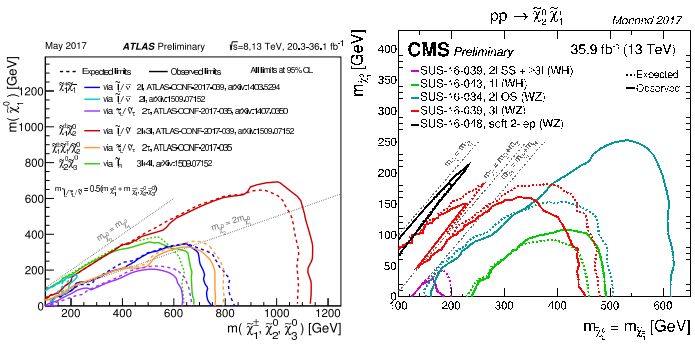

Figure 110.4: LHC exclusion limits on chargino and neutralino masses in a number of simplified models. Left: limits on chargino and neutralino masses for pair production of charginos, pair production of heavier neutralinos, or pair production of chargino and neutralino, under the assumption of light sleptons mediating the decays. Right: limits on chargino and neutralino masses for pair production of chargino and neutralino, under the assumption of decoupled sleptons, and chargino/neutralino decay through W^*, Z^* or H.

In both the wino region (a characteristic of anomaly-mediated SUSY breaking models) and the higgsino region of the MSSM, the mass splitting between $\tilde{\chi}_1^{\pm}$ and $\tilde{\chi}_1^0$ is small. The chargino decay products are very soft and may escape detection. These compressed spectra are very hard to find, and have triggered dedicated search strategies, which, however, still have limited sensitivity. Photons or jets from initial state radiation may be used to tag such decays. An alternative production mode of electroweak gauginos is provided by vector-boson-fusion, where two additional jets with a large rapidity gap can be used to select events and suppress backgrounds [124,125].

110.5.2. *Exclusion limits on neutralino masses* :

In a considerable part of the MSSM parameter space, and in particular when demanding that the LSP carries no electric or color charge, the lightest neutralino $\tilde{\chi}_1^0$ is the LSP. If R-parity is conserved, such a $\tilde{\chi}_1^0$ is stable. Since it is weakly interacting, it will typically escape detectors unseen. Limits on the invisible width of the Z boson apply to neutralinos with a mass below 45.5 GeV , but depend on the Z-neutralino coupling. Such a coupling could be small or even absent; in such a scenario there is no general lower limit on the mass of the lightest neutralino [126]. In models with gaugino mass unification and sfermion mass unification at the GUT scale, a lower limit on the neutralino mass is derived from limits from direct searches, notably for charginos and sleptons, and amounts to 47 GeV [127]. Assuming a constraining model like the CMSSM, this limit increases to 50 GeV at LEP; however the strong constraints now set by the LHC increase such CMSSM-derived $\tilde{\chi}_1^0$ mass limits to well above 200 GeV [128].

In gauge-mediated SUSY breaking models (GMSB), the LSP is typically a gravitino, and the phenomenology is determined by the nature of the next-to-lightest supersymmetric particle (NLSP). A NLSP neutralino will decay to a gravitino and a SM particle whose nature is determined by the neutralino composition. Final states with two high p_{T} photons and missing momentum are searched for, and interpreted in gauge mediation models with bino-like neutralinos [129–133].

Assuming the production of at least two neutralinos per event, neutralinos with large non-bino components can also be searched for by their decay in final states with missing momentum plus any two bosons out of the collection γ, Z, H. A number of searches at the LHC have tried to cover the rich phenomenology of the various Z and H decay modes [120,132–135].

Heavier neutralinos, in particular $\tilde{\chi}_2^0$, have been searched for in their decays to the lightest neutralino plus a γ, a Z boson or a Higgs boson. Limits on electroweak production of $\tilde{\chi}_2^0$ plus $\tilde{\chi}_1^{\pm}$ from trilepton analyses have been discussed in the section on charginos; the assumption of equal mass of $\tilde{\chi}_2^0$ and $\tilde{\chi}_1^{\pm}$ make the limits on

chargino masses apply to $\tilde{\chi}_2^0$ as well. Multilepton analyses have also been used to set limits on $\tilde{\chi}_2^0\tilde{\chi}_3^0$ production; assuming equal mass and decay through light sleptons, limits are set up to 680 GeV for massless LSPs [124]. Again, compressed spectra with small mass differences between the heavier neutralinos and the LSP form the most challenging region.

In $\tilde{\chi}_2^0$ decays to $\tilde{\chi}_1^0$ and a lepton pair, the lepton pair invariant mass distribution may show a structure that can be used to measure the $\tilde{\chi}_2^0 - \tilde{\chi}_1^0$ mass difference in case of a signal [36]. This structure, however, can also be used in the search strategy itself, as demonstrated by ATLAS [134] and CMS [136].

In models with R-parity violation, the lightest neutralino can decay even if it is the lightest supersymmetric particle. If the decay involves a non-zero λ coupling, the final state will be a multi-lepton one. Searches for events with four or more isolated charged leptons by ATLAS [76,137] and CMS [77] are interpreted in such models. With very small coupling values, the neutralino would be long-lived, leading to lepton pairs with a displaced vertex, which have also been searched for [78,106].

Searches for events with a displaced hadronic vertex, with or without a matched lepton, are interpreted in a model with R-parity violating neutralino decay involving a non-zero λ' coupling [78,138]. Neutralino decays involving non-zero λ'' lead to fully hadronic final states, and searches for jet-pair resonances are used to set limits, typically on the production of colored particles like top squarks or gluinos, which are assumed to be the primary produced sparticles in these interpretations, as discussed earlier.

The limits on weak gauginos in simplified models are summarized in Table 110.3. Interpretations of the search results outside simplified models, such as in the phenomenological MSSM [139–141], show that the simplified model limits must be interpreted with care. Electroweak gauginos in models that are compatible with the relic density of dark matter in the universe, for example, have particularly tuned mixing parameters and mass spectra, which are not always captured by the simplified models used.

Table 110.3: Summary of weak gaugino mass limits in simplified models, assuming R-parity conservation. Masses in the table are provided in GeV. Further details about assumptions and analyses from which these limits are obtained are discussed in the text.

Assumption	m_χ
$\tilde{\chi}_1^\pm$, all $\Delta m(\tilde{\chi}_1^\pm, \tilde{\chi}_1^0)$	> 92
$\tilde{\chi}_1^\pm$ $\Delta m > 5$, $m_{\tilde{\nu}} > 300$	> 103.5
$\tilde{\chi}_1^\pm$, $m_{(\tilde{\ell},\tilde{\nu})} = (m_{\tilde{\chi}_1^\pm} + m_{\tilde{\chi}_1^0})/2$	
$m_{\tilde{\chi}_1^0} \approx 0$	> 740
$\tilde{\chi}_1^\pm$, $m_{\tilde{\chi}_1^0} > 350$	no LHC limit
$\tilde{\chi}_1^\pm$, $m_{\tilde{\ell}} > m_{\tilde{\chi}_1^\pm}$	
$m_{\tilde{\chi}_1^0} \approx 0$	> 180
$\tilde{\chi}_1^\pm$, $m_{\tilde{\chi}_1^0} > 25$	no LHC limit
$m_{\tilde{\chi}_1^\pm} = m_{\tilde{\chi}_2^0}$, $m_{\tilde{\ell}_L} = (m_{\tilde{\chi}_1^\pm} + m_{\tilde{\chi}_1^0})/2$	
$m_{\tilde{\chi}_1^0} \approx 0$	> 1140
$m_{\tilde{\chi}_1^0} > 700$	no LHC limit
$m_{\tilde{\chi}_1^\pm} = m_{\tilde{\chi}_2^0}$, $m_{\tilde{\ell}_R} = (m_{\tilde{\chi}_1^\pm} + m_{\tilde{\chi}_1^0})/2$	flavor-democratic
$m_{\tilde{\chi}_1^0} \approx 0$	> 1060
$m_{\tilde{\chi}_1^0} > 600$	no LHC limit
$m_{\tilde{\chi}_1^\pm} = m_{\tilde{\chi}_2^0}$, $m_{\tilde{\tau}} = (m_{\tilde{\chi}_1^\pm} + m_{\tilde{\chi}_1^0})/2$	$\tilde{\tau}$-dominated
$m_{\tilde{\chi}_1^0} \approx 0$	> 620
$m_{\tilde{\chi}_1^0} > 260$	no LHC limit
$m_{\tilde{\chi}_1^\pm} = m_{\tilde{\chi}_2^0}$, $m_{\tilde{\ell}} > m_{\tilde{\chi}_1^\pm}$, BF$(WZ) = 1$	
$m_{\tilde{\chi}_1^0} \approx 0$	> 610
$m_{\tilde{\chi}_1^0} > 250$	no LHC limit
$m_{\tilde{\chi}_1^\pm} = m_{\tilde{\chi}_2^0}$, $m_{\tilde{\ell}} > m_{\tilde{\chi}_1^\pm}$, BF$(WH) = 1$	
$m_{\tilde{\chi}_1^0} \approx 0$	> 480
$m_{\tilde{\chi}_1^0} > 100$	no LHC limit

110.6. Exclusion limits on slepton masses

In models with slepton and gaugino mass unification at the GUT scale, the right-handed slepton, $\tilde{\ell}_R$, is expected to be lighter than the left-handed slepton, $\tilde{\ell}_L$. For tau sleptons there may be considerable mixing between the L and R states, leading to a significant mass difference between the lighter $\tilde{\tau}_1$ and the heavier $\tilde{\tau}_2$.

110.6.1. *Exclusion limits on the masses of charged sleptons* :

The most model-independent searches for selectrons, smuons and staus originate from the LEP experiments [142]. Smuon production only takes place via s-channel γ^*/Z exchange. Search results are often quoted for $\tilde{\mu}_R$, since it is typically lighter than $\tilde{\mu}_L$ and has a weaker coupling to the Z boson; limits are therefore conservative. Decays are expected to be dominated by $\tilde{\mu}_R \to \mu\tilde{\chi}_1^0$, leading to two non-back-to-back muons and missing momentum. Slepton mass limits are calculated in the MSSM under the assumption of gaugino mass unification at the GUT scale, and depend on the mass difference between the smuon and $\tilde{\chi}_1^0$. A $\tilde{\mu}_R$ with a mass below 94 GeV is excluded for $m_{\tilde{\mu}_R} - m_{\tilde{\chi}_1^0} > 10$ GeV. The selectron case is similar to the smuon case, except that an additional production mechanism is provided by t-channel neutralino exchange. The $\tilde{e}_R$ lower mass limit is 100 GeV for $m_{\tilde{\chi}_1^0} < 85$ GeV. Due to the t-channel neutralino exchange, $\tilde{e}_R\tilde{e}_L$ pair production was possible at LEP, and a lower limit of 73 GeV was set on the selectron mass regardless of the neutralino mass by scanning over MSSM parameter space [143]. The potentially large mixing between $\tilde{\tau}_L$ and $\tilde{\tau}_R$ not only makes the $\tilde{\tau}_1$ light, but can also make its coupling to the Z boson small. LEP lower limits on the $\tilde{\tau}$ mass range between 87 and 93 GeV depending on the $\tilde{\chi}_1^0$ mass, for $m_{\tilde{\tau}} - m_{\tilde{\chi}_1^0} > 7$ GeV [142].

At the LHC, pair production of sleptons is not only heavily suppressed with respect to pair production of colored SUSY particles but the cross section is also almost two orders of magnitude smaller than the one of pair production of charginos and neutralinos. Only with the full Run 1 LHC data set and the first data of Run 2, ATLAS and CMS have started to surpass the sensitivity of the LEP analyses under certain assumptions.

ATLAS and CMS have searched for direct production of selectron pairs and smuon pairs at the LHC, with each slepton decaying to its corresponding SM partner lepton and the $\tilde{\chi}_1^0$ LSP. In simplified models, ATLAS [118] and CMS [120] set lower mass limits on sleptons of 500 GeV for degenerate $\tilde{\ell}_L$ and $\tilde{\ell}_R$, for a massless $\tilde{\chi}_1^0$ and assuming equal selectron and smuon masses, as shown in Fig. 110.5. The limits deteriorate with increasing $\tilde{\chi}_1^0$ mass due to decreasing missing momentum and lepton momentum. As a consequence, no limits are set for $\tilde{\chi}_1^0$ masses above 270 GeV.

In gauge-mediated SUSY breaking models, sleptons can be (co-)NLSPs, *i.e.*, the next-to-lightest SUSY particles and almost degenerate in mass, decaying to a lepton and a gravitino. This decay can either be prompt, or the slepton can have a non-zero lifetime. Combining several analyses, lower mass limits on $\tilde{\mu}_R$ of 96.3 GeV and on $\tilde{e}_R$ of 66 GeV are set for all slepton lifetimes at LEP [144]. In a considerable part of parameter space in these models, the $\tilde{\tau}$ is the NLSP. The LEP experiments have set lower limits on the mass of such a $\tilde{\tau}$ between 87 and 97 GeV, depending on the $\tilde{\tau}$ lifetime. ATLAS has searched for final states with τs, jets and missing transverse momentum, and has interpreted the results in GMSB models setting limits on the model parameters [145]. CMS has interpreted a multilepton analysis in terms of limits on gauge mediation models with slepton NLSP [146]. CDF has put limits on gauge mediation models at high $\tan\beta$ and slepton NLSP using an analysis searching for like-charge light leptons and taus [147].

Limits also exist on sleptons in R-parity violating models, both from LEP and the Tevatron experiments. From LEP, lower limits on

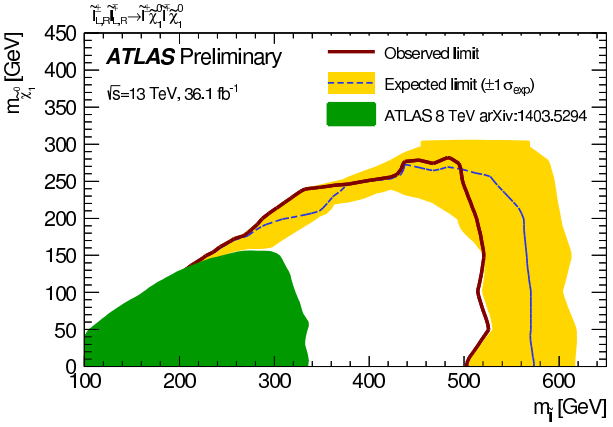

Figure 110.5: LHC exclusion limits on slepton (selectron and smuon) masses, assuming equal masses of selectrons and smuons, degeneracy of $\tilde{\ell}_{\rm L}$ and $\tilde{\ell}_{\rm R}$, and a 100% branching fraction for $\tilde{\ell} \to \ell\tilde{\chi}_1^0$ [118].

$\tilde{\mu}_{\rm R}$ and $\tilde{e}_{\rm R}$ masses in such models are 97 GeV , and the limits on the stau mass are very close: 96 GeV [148].

110.6.2. *Exclusion limits on sneutrino masses* :

The invisible width of the Z boson puts a lower limit on the sneutrino mass of about 45 GeV . Tighter limits are derived from other searches, notably for gauginos and sleptons, under the assumption of gaugino and sfermion mass universality at the GUT scale, and amount to approximately 94 GeV in the MSSM [149]. It is possible that the lightest sneutrino is the LSP; however, a left-handed sneutrino LSP is ruled out as a cold dark matter candidate [150,151].

Production of pairs of sneutrinos in R-parity violating models has been searched for at LEP [148]. Assuming fully leptonic decays via λ-type couplings, lower mass limits between 85 and 100 GeV are set. At the Tevatron [152,153] and at the LHC [154,155], searches have focused on scenarios with resonant production of a sneutrino, decaying to $e\mu$, $\mu\tau$ and $e\tau$ final states. No signal has been seen, and limits have been set on sneutrino masses as a function of the value of relevant RPV couplings. As an example, the LHC experiments exclude a resonant tau sneutrino with a mass below 1500 GeV for $\lambda_{312} > 0.07$ and $\lambda'_{311} > 0.01$.

The limits on sleptons in simplified models are summarized in Table 110.4.

Table 110.4: Summary of slepton mass limits from LEP and LHC, assuming R-parity conservation and 100% branching fraction for $\tilde{\ell} \to \ell\tilde{\chi}_1^0$. Masses in this table are provided in GeV .

Assumption	$m_{\tilde{\ell}}$
$\tilde{\mu}_{\rm R}$, $\Delta m(\tilde{\mu}_{\rm R}, \tilde{\chi}_1^0) > 10$	> 94
$\tilde{e}_{\rm R}$, $\Delta m(\tilde{e}_{\rm R}, \tilde{\chi}_1^0) > 10$	> 94
$\tilde{e}_{\rm R}$, any Δm	> 73
$\tilde{\tau}_{\rm R}$, $\Delta m((\tilde{\tau}_{\rm R}, \tilde{\chi}_1^0) > 7$	> 87
$\tilde{\nu}_e$, $\Delta m(\tilde{e}_{\rm R}, \tilde{\chi}_1^0) > 10$	> 94
$m_{\tilde{e}_{\rm L,R}} = m_{\tilde{\mu}_{\rm L,R}}$, $m_{\tilde{\chi}_1^0} \approx 0$	> 500
$m_{\tilde{\chi}_1^0} >\approx 270$	no LHC limit

110.7. Exclusion limits on long-lived sparticles

Long-lived sparticles arise in many different SUSY models. In particular in co-annihilation scenarios, where the NLSP and LSP are nearly mass-degenerate, this is rather common in order to obtain the correct Dark Matter relic density. Prominent examples are scenarios featuring $\tilde{\tau}$ co-annihilation, or models of SUSY breaking, e.g. minimal anomaly-mediated SUSY breaking, in which the appropriate Dark Matter density is obtained by co-annihilation of the LSP with an almost degenerate long-lived wino. However, in general, also other sparticles can be long-lived and it is desirable to establish a comprehensive search programme for these special long-lived cases, which lead to distinct experimental search signatures, including displaced vertices or disappearing tracks, etc.

Already in the past experiments performed dedicated searches for long-lived SUSY signatures, but with the absence of any experimental evidence for SUSY so far, it is expected that in the future even more effort and focus will be placed on SUSY scenarios involving long-lived sparticles. As for the interpretation of the canonical SUSY searches, also for long-lived scenarios simplified models are a convenient tool to benchmark these special cases (see e.g. [156,157]) .

In the following we give an overview of the most recent and relevant results for dedicated long-lived SUSY searches.

If the decay of gluinos is suppressed, for example if squark masses are high, gluinos may live longer than typical hadronization times. It is expected that such gluinos will hadronize to long-living strongly interacting particles known as R-hadrons. In particular, if the suppression of the gluino decay is highly significant, as in the case that the squark masses are much higher than the TeV scale, these R-hadrons can be (semi-)stable in collider timescales. Searches for such R-hadrons exploit the typical signature of stable charged massive particles in the detector. As shown in the upper left plot of Fig. 110.6, the CMS experiment excludes semi-stable gluino R-hadrons with masses below approximately 1.6 TeV [158]. The limits depend on the probability for gluinos to form bound states known as gluinoballs, as these are neutral and not observed in the tracking detectors. Similar limits are obtained by the ATLAS experiment [159]. Limits ranging between 1 and 1.6 TeV are set in the scenario of R-hadron decays inside the detector, using dE/dx measurements and searches for displaced vertices, for $c\tau$ ranging from 1 mm to more than 10 m, as shown in Fig. 110.6 (bottom left).

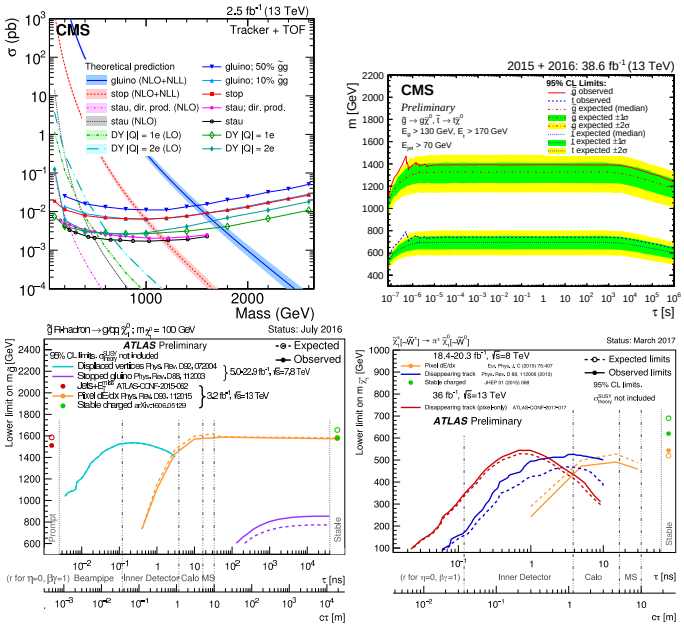

Figure 110.6: The upper left plot shows the observed 95% C.L. upper limits on the cross section for various long-lived charged sparticles. For gluinos, different fractions of gluinoball states produced after hadronization scenarios are indicated. The observed limits are compared with the predicted theoretical cross sections where the bands represent the theoretical uncertainties on the cross section values. The other plots show observed 95% C.L. lower limits on different sparticle masses in the mass-vs-lifetime plane for gluino R-hadrons (bottom left), stopped R-hadrons (top right) or charginos (bottom right).

Alternatively, since such R-hadrons are strongly interacting, they may be stopped in the calorimeter or in other material, and decay later into energetic jets. These decays are searched for by identifying the jets [160–162] or muons [163] outside the time window associated with bunch-bunch collisions. As shown in the upper right plot of Fig. 110.6, the CMS collaboration sets limits on such stopped R-hadrons over 13 orders of magnitude in gluino lifetime, up to masses of 1385 GeV [162]. A summary of a variety of different ATLAS searches for long-lived gluinos is shown in the lower left plot of Fig. 110.6. It displays constraints on the gluino mass-vs-lifetime plane for a split-supersymmetry model with the gluino R-hadron decaying into a gluon or light quarks and a neutralino with mass of 100 GeV .

Top squarks can also be long-lived and hadronize to a R-hadron, for example in the scenario where the top squark is the next-to-lightest SUSY particle (NLSP), with a small mass difference to the LSP. Searches for massive stable charged particles are sensitive to such top squarks. Displayed in the upper left plot of Fig. 110.6 are the results of the CMS analysis [158], which sets limits $m_{\tilde{t}} > 800$ GeV in such scenarios, while ATLAS [159] reports limits of $m_{\tilde{t}} > 900$ GeV . Limits from the Tevatron are about $m_{\tilde{t}} > 300$ GeV [164,165].

In addition to colored sparticles, also sparticles like charginos may be long-lived, especially in scenarios with compressed mass spectra. Charginos decaying in the detectors away from the primary vertex could lead to signatures such as kinked-tracks, or apparently disappearing tracks, since, for example, the pion in $\tilde{\chi}_1^{\pm} \to \pi^{\pm}\tilde{\chi}_1^0$ might be too soft to be reconstructed. At the LHC, searches have been performed for such disappearing tracks, and interpreted within anomaly-mediated SUSY breaking models [166–168]. The lower right plot of Fig. 110.6 shows constraints for different ATLAS searches on the chargino mass-vs-lifetime plane for an Anomaly Mediated SUSY Breaking (AMSB) model with $\tan\beta = 5$ and $\mu > 0$. It is assumed that wino-like charginos are pair-produced and decay to wino-like neutralinos and very soft charged pions. For example, for specific AMSB parameters, charginos with lifetimes between 0.1 and 10 ns are excluded for chargino masses up to 500 GeV . Within AMSB models, a lower limit on the chargino mass of 430 GeV is set, for a mass difference with the LSP of 160 MeV and a lifetime of 0.2 ns. Furthermore, charginos with a lifetime longer than the time needed to pass through the detector appear as charged stable massive particles. Limits have been derived by the LEP experiments [169], by D0 at the Tevatron [165], and by the LHC experiments [159,170,171]. For lifetimes above 100 ns, charginos below some 800 GeV are excluded.

In gauge mediation models, NLSP neutralino decays need not be prompt, and experiments have searched for late decays with photons in the final state. CDF have searched for delayed $\tilde{\chi}_1^0 \to \gamma\tilde{G}$ decays using the timing of photon signals in the calorimeter [172]. CMS has used the same technique at the LHC [173]. Results are given as upper limits on the neutralino production cross section as a function of neutralino mass and lifetime. D0 has looked at the direction of showers in the electromagnetic calorimeter with a similar goal [174], and ATLAS has searched for photon candidates that do not point back to the primary vertex, as well as for delayed photons [175].

Charged slepton decays may be kinematically suppressed, for example in the scenario of a NLSP slepton with a very small mass difference to the LSP. Such a slepton may appear to be a stable charged massive particle. Interpretation of searches at LEP for such signatures within GMSB models with stau NLSP or slepton co-NLSP exclude masses up to 99 GeV [169]. Searches of stable charged particles at the Tevatron [164,165] and at the LHC [158,159] are also interpreted in terms of limits on stable charged sleptons. The limits obtained at the LHC exclude stable staus with masses below 240 GeV when produced directly in pairs, and below 490 GeV when staus are produced both directly and indirectly in the decay of other particles in a GMSB model [158].

110.8. Global interpretations

Apart from the interpretation of direct searches for sparticle production at colliders in terms of limits on masses of individual SUSY particles, model-dependent interpretations of allowed SUSY parameter space are derived from global SUSY fits. Typically these fits combine the results from collider experiments with indirect constraints on SUSY as obtained from low-energy experiments, flavor physics, high-precision electroweak results, and astrophysical data.

In the pre-LHC era these fits were mainly dominated by indirect constraints. Even for very constrained models like the CMSSM, the allowed parameter space, in terms of squark and gluino masses, ranged from several hundreds of GeV to a few TeV. Furthermore, these global fits indicated that squarks and gluino masses in the range of 500 to 1000 GeV were the preferred region of parameter space, although values as high as few TeV were allowed with lower probabilities [176].

With ATLAS and CMS now probing mass scales around 1 TeV and even beyond, the importance of the direct searches for global analyses of allowed SUSY parameter space has strongly increased. For example, imposing the new experimental limits on constrained supergravity models pushes the most likely values of first generation squark and gluino masses significantly beyond 2 TeV, typically resulting in overall values of fit quality much worse than those in the pre-LHC era [128]. Although these constrained models are not yet ruled out, the extended experimental limits impose very tight constraints on the allowed parameter space.

For this reason, the emphasis of global SUSY fits has shifted towards less-constrained SUSY models. Especially interpretations in the pMSSM [170,139–141] but also in simplified models have been useful to generalize SUSY searches, for example to redesign experimental analyses in order to increase their sensitivity for compressed spectra, where the mass of the LSP is much closer to squark and gluino masses than predicted, for example, by the CMSSM. As shown in Table 110.2, for neutralino masses above approximately 0.5 TeV the current set of ATLAS and CMS searches, interpreted in simplified models, cannot exclude the existence of squarks or gluinos with masses only marginally above the neutralino mass. However, as these exclusion limits are defined in the context of simplified models, they are only valid for the assumptions in which these models are defined.

As an alternative approach, both ATLAS [139] and CMS [140] have performed an analysis of the impact of their searches on the parameter space of the pMSSM. Fig. 110.7 shows graphically the LHC exclusion power in the pMSSM based on searches performed at $\sqrt{s} =$ 7 and 8 TeV. The plot on the left shows the survival probability in the gluino-neutralino mass plane, which is a measure of the parameter space that remains after inclusion of the relevant CMS search results. As can be seen, gluino masses below about 1.2 TeV are almost fully excluded. This result agrees well with the typical exclusion obtained in simplified models for gluino production. However, as shown in the right plot of Fig. 110.7, when a similar analysis for other sparticles is performed it becomes apparent that exclusions on the pMSSM parameter can be significantly less stringent than simplified model limits might suggest. This is especially apparent for the electroweak sector, where even at rather low masses several of the pMSSM test points still survive the constraint of ATLAS searches at $\sqrt{s} = 7$ and 8 TeV. This again indicates that care must be taken when interpreting results from the LHC searches and there are still several scenarios where sparticles below the 1 TeV scale are not excluded, even when considering the most recent results at $\sqrt{s} = 13$ TeV.

Furthermore, the discovery of a Higgs boson with a mass around 125 GeV has triggered many studies regarding the compatibility of SUSY parameter space with this new particle. Much of it is still work in progress and it will be interesting to see how the interplay between the results from direct SUSY searches and more precise measurements of the properties of the Higgs boson will unfold in the future.

110.9. Summary and Outlook

The absence of any observation of new phenomena at the first run of the LHC at $\sqrt{s} = 7/8$ TeV, and now also during operation at $\sqrt{s} = 13$ TeV, place significant constraints on SUSY parameter space. Today, inclusive searches probe production of gluinos at about 2 TeV, first and second generation squarks in the range of about 1 to 1.6 TeV, third generation squarks at scales around 600 GeV to 1 TeV, electroweak gauginos at scales around $300 - 800$ GeV , and

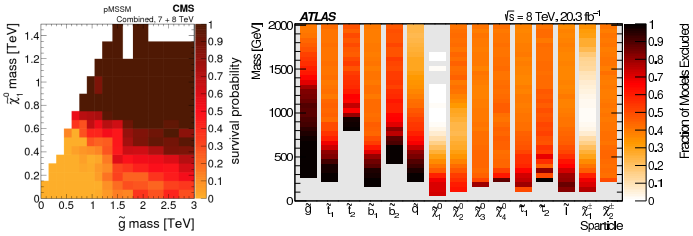

Figure 110.7: The plot on the left shows the survival probability of a pMSSM parameter space model in the gluino-neutralino mass plane after the application of the relevant CMS search results. The plot on the right shows a graphical representation of the ATLAS exclusion power in a pMSSM model. Each vertical bar is a one-dimensional projection of the fraction of models points excluded for each sparticle by ATLAS analyses. The experimental results are obtained from data taken at $\sqrt{s} = 7$ and 8 TeV.

sleptons around 500 GeV . However, depending on the assumptions made on the underlying SUSY spectrum these limits can also weaken considerably.

Fig. 110.8 shows a comparison of the results from the first run of the LHC (about 20 fb^{-1} of data at $\sqrt{s} = 7/8$ TeV) with the new results obtained from about 36 fb^{-1} taken at $\sqrt{s} = 13$ TeV. Based on the example of a selected set of simplified model limits discussed in this review, it becomes apparent that for all sparticle sectors the new LHC results push sensitivity deep into new territory. This is especially apparent for limits on colored sparticles, which typically benefit most from the energy increase, but also limits on electroweakly produced sparticles have strengthened significantly since the last run period.

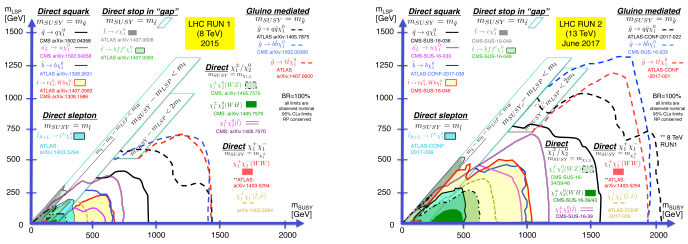

Figure 110.8: Comparison of a selected set of simplified model limits based on about 20 fb^{-1}) taken at $\sqrt{s} = 7/8$ TeV, with the same limits derived from 36 fb^{-1} taken at $\sqrt{s} = 13$ TeV. Further details about the different simplified models displaced here are provided in the text.

With the LHC having reached almost its maximum energy of about $\sqrt{s} = 14$ TeV, future sensitivity improvement will have to originate from more data and improvement of experimental analysis techniques. Therefore, it is expected that the current landscape of SUSY searches and corresponding exclusion limits at the LHC, as, for example, shown in Fig. 110.9 from the ATLAS experiment [177], will not change as rapidly anymore as it did in the past, when the LHC underwent several successive increases of collision energy.

The interpretation of results at the LHC has moved away from constrained models like the CMSSM towards a large set of simplified models, or the pMSSM. On the one hand this move is because the LHC limits have put constrained models like the CMSSM under severe pressure, while on the other hand simplified models leave more freedom to vary parameters and form a better representation of the underlying sensitivity of analyses. However, these interpretations in simplified models do not come without a price: the decomposition of a potentially complicated reality in a limited set of individual decay chains can be significantly incomplete. Therefore, quoted limits in simplified models are only valid under the explicit assumptions

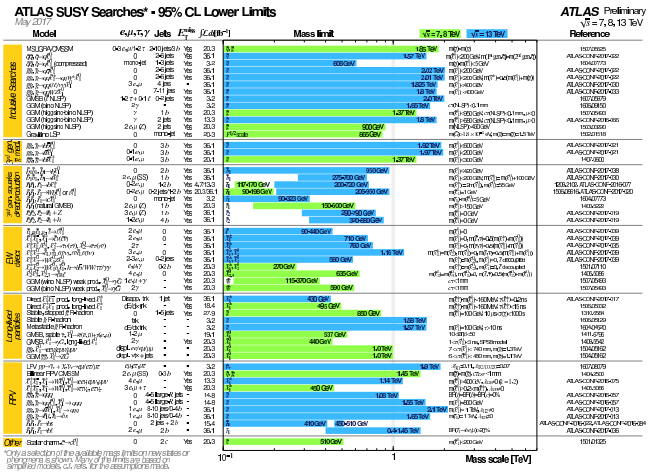

Figure 110.9: Overview of the current landscape of SUSY searches at the LHC. The plot shows exclusion mass limits of ATLAS for different searches and interpretation assumptions [177]. The corresponding results of the CMS experiment are similar [178].

made in these models. The recent addition of more comprehensive interpretations in the pMSSM will complement those derived from simplified models and, thus, will enable an even more refined understanding of the probed SUSY parameter space.

In this context, the limit range of $1.5 - 2.0$ TeV on generic colored SUSY particles only holds for light neutralinos, in the R-parity conserving MSSM. Limits on third generation squarks and electroweak gauginos also only hold for light neutralinos, and under specific assumptions for decay modes and slepton masses.

The ongoing LHC run at $\sqrt{s} = 13$ TeV, and future runs at 14 TeV with significantly larger integrated luminosities (Run 3, and the High-Luminosity LHC), will provide a large data sample for future SUSY searches. As mentioned above, the improvement in sensitivity will largely have to come from the larger statistics, and evolution of trigger and analysis techniques, since there will be no significant energy increase at the LHC anymore. Although the sensitivity for colored sparticles will increase somewhat as well, the expanded data set will be particularly beneficial for electroweak gaugino searches, and for the more difficult final states presented by compressed particle spectra, stealth SUSY, long-lived sparticles, or R-parity violating scenarios.

References:

1. H. Miyazawa, Prog. Theor. Phys. **36**, 1266 (1966).
2. Yu. A. Golfand and E.P. Likhtman, Sov. Phys. JETP Lett. **13**, 323 (1971).
3. J.L. Gervais and B. Sakita, Nucl. Phys. **B34**, 632 (1971).
4. D.V. Volkov and V.P. Akulov, Phys. Lett. **B46**, 109 (1973).
5. J. Wess and B. Zumino, Phys. Lett. **B49**, 52 (1974).
6. J. Wess and B. Zumino, Nucl. Phys. **B70**, 39 (1974).
7. A. Salam and J.A. Strathdee, Nucl. Phys. **B76**, 477 (1974).
8. H.P. Nilles, Phys. Reports **110**, 1 (1984).
9. H.E. Haber and G.L. Kane, Phys. Reports **117**, 75 (1987).
10. E. Witten, Nucl. Phys. **B188**, 513 (1981).
11. S. Dimopoulos and H. Georgi, Nucl. Phys. **B193**, 150 (1981).
12. M. Dine, W. Fischler, and M. Srednicki, Nucl. Phys. **B189**, 575 (1981).
13. S. Dimopoulos and S. Raby, Nucl. Phys. **B192**, 353 (1981).
14. N. Sakai, Z. Phys. **C11**, 153 (1981).
15. R.K. Kaul and P. Majumdar, Nucl. Phys. **B199**, 36 (1982).
16. H. Goldberg, Phys. Rev. Lett. **50**, 1419 (1983).
17. J.R. Ellis *et al.*, Nucl. Phys. **B238**, 453 (1984).
18. G. Jungman and M. Kamionkowski, Phys. Reports **267**, 195 (1996).

19. S. Dimopoulos, S. Raby, and F. Wilczek, Phys. Rev. **D24**, 1681 (1981).
20. W.J. Marciano and G. Senjanović, Phys. Rev. **D25**, 3092 (1982).
21. M.B. Einhorn and D.R.T. Jones, Nucl. Phys. **B196**, 475 (1982).
22. L.E. Ibanez and G.G. Ross, Phys. Lett. **B105**, 439 (1981).
23. N. Sakai, Z. Phys. **C11**, 153 (1981).
24. U. Amaldi, W. de Boer, and H. Furstenau, Phys. Lett. **B260**, 447 (1991).
25. P. Langacker and N. Polonsky, Phys. Rev. **D52**, 3081 (1995).
26. P. Fayet, Phys. Lett. **B64**, 159 (1976).
27. G.R. Farrar and P. Fayet, Phys. Lett. **B76**, 575 (1978).
28. H.E. Haber, *Supersymmetry, Part I (Theory)*, in this *Review*.
29. CMS Collab. and LHCb Collab., Nature **522**, 68 (2015).
30. LHCb Collab., Phys. Rev. Lett. **118**, 191801 (2017).
31. A. Höcker and W.Marciano, *The Muon Anomalous Magnetic Moment*, in this *Review*.
32. G. Hinshaw *et al.*, Astrophys. J. Supp. **208**, 19H (2013).
33. Planck Collab., Astron. & Astrophys. **594**, A13 (2016).
34. M. Carena *et al.*, *Status of Higgs Boson Physics*, in this *Review*.
35. J.F. Grivaz, *Supersymmetry, Part II (Experiment)*, in: 2010 Review of Particle Physics, K. Nakamura *et al.*, (Particle Data Group), J. Phys. **G37**, 075021 (2010).
36. I. Hinchliffe *et al.*, Phys. Rev. **D55**, 5520 (1997).
37. L. Randall and D. Tucker-Smith, Phys. Rev. Lett. **101**, 221803 (2008).
38. CMS Collab., Phys. Lett. **B698**, 196 (2011).
39. CMS Collab., Phys. Rev. Lett. **107**, 221804 (2011).
40. CMS Collab., JHEP **1301**, 077 (2013).
41. CMS Collab., Eur. Phys. J. **C73**, 2568 (2013).
42. CMS Collab., Phys. Rev. **D85**, 012004 (2012).
43. C.G. Lester and D.J. Summers, Phys. Lett. **B463**, 99 (1999).
44. D.R. Tovey, JHEP **0804**, 034 (2008).
45. M.R. Buckley *et al.*, Phys. Rev. **D89**, 055020 (2014).
46. P. Jackson, C. Rogan, and M. Sartoni, Phys. Rev. **D95**, 035031 (2017).
47. J.M. Butterworth *et al.*, Phys. Rev. Lett. **100**, 242001 (2008).
48. A.H. Chamseddine, R. Arnowitt, and P Nath, Phys. Rev. Lett. **49**, 970 (1982).
49. E. Cremmer *et al.*, Nucl. Phys. **B212**, 413 (1983).
50. P. Fayet, Phys. Lett. **B70**, 461 (1977).
51. M. Dine, A.E. Nelson, and Yu. Shirman, Phys. Rev. **D51**, 1362 (1995).
52. P. Meade, N. Seiberg, and D. Shih, Prog. Theor. Phys. Supp. **177**, 143 (2009).
53. G.F. Giudice *et al.*, JHEP **9812**, 027 (1998).
54. L. Randall and R. Sundrum, Nucl. Phys. **B557**, 79 (1999).
55. R. Arnowitt and P Nath, Phys. Rev. Lett. **69**, 725 (1992).
56. G.L. Kane *et al.*, Phys. Rev. **D49**, 6173 (1994).
57. E. Halkiadakis, G. Redlinger, and D. Shih, Ann. Rev. Nucl. and Part. Sci. **64**, 319 (2014).
58. W. Beenakker *et al.*, Int. J. Mod. Phys. **A26**, 2637 (2011).
59. W. Beenakker *et al.*, Nucl. Phys. **B492**, 51 (1997); W. Beenakker *et al.*, Nucl. Phys. **B515**, 3 (1998); W. Beenakker *et al.*, Phys. Rev. Lett. **83**, 3780 (1999), Erratum *ibid.*, **100**, 029901 (2008); M. Spira, hep-ph/0211145 (2002);T. Plehn, Czech. J. Phys. 55, B213 (2005).
60. A. Djouadi, J-L. Kneur, and G. Moultaka, Comp. Phys. Comm. **176**, 426 (2007).
61. C.F. Berger *et al.*, JHEP **0902**, 023 (2009).
62. H. Baer *et al.*, hep-ph/9305342, 1993.
63. R.M. Barnett, H.E. Haber, and G.L. Kane, Nucl. Phys. **B267**, 625 (1986).
64. H. Baer, D. Karatas, and X. Tata, Phys. Lett. **B183**, 220 (1987).
65. J. Alwall, Ph.C. Schuster, and N. Toro, Phys. Rev. **D79**, 075020 (2009).
66. J. Alwall *et al.*, Phys. Rev. **D79**, 015005 (2009).
67. O. Buchmueller and J. Marrouche, Int. J. Mod. Phys. **A29**, 1450032 (2014).
68. LEP2 SUSY Working Group, ALEPH, DELPHI, L3 and OPAL experiments, note LEPSUSYWG/04-02.1, lepsusy.web.cern.ch/lepsusy.
69. CDF Collab., Phys. Rev. Lett. **102**, 121801 (2009).
70. D0 Collab., Phys. Lett. **B660**, 449 (2008).
71. ATLAS Collab. *Search for squarks and gluinos in final states with jets and missing transverse momentum using 36 fb^{-1} of $\sqrt{s} = 13$ TeV pp collision data with the ATLAS detector*, ATLAS-CONF-2017-022 (2017).
72. CMS Collab., *Search for new phenomena with the M_{T2} variable in the all-hadronic final state produced in proton-proton collisions at $\sqrt{s}$ =13 TeV*, arXiv:1705.04650(2017).
73. CMS Collab., Phys. Rev. **D96**, 032003 (2017).
74. ATLAS Collab., *Search for production of supersymmetric particles in final states with missing transverse momentum and multiple b-jets at $\sqrt{s} = 13$ TeV proton-proton collisions with the ATLAS detector*, ATLAS-CONF-2017-021 (2017).
75. CMS Collab., *Search for supersymmetry in pp collisions at $\sqrt{s} = 13$ TeV in the single-lepton final state using the sum of masses of large-radius jets*, arXiv:1705.04673(2017).
76. ATLAS Collab., *Constraints on promptly decaying supersymmetric particles with lepton-number- and R-parity-violating interactions using Run-1 ATLAS data*, ATLAS-CONF-2015-018 (2015).
77. CMS Collab., *Search for RPV SUSY in the four-lepton final state*, CMS-PAS-SUS-13-010 (2013).
78. ATLAS Collab., Phys. Rev. **D92**, 072004 (2015).
79. CDF Collab., Phys. Rev. Lett. **107**, 042001 (2011).
80. ATLAS Collab., *Search for massive supersymmetric particles in multi-jet final states produced in pp collisions at $\sqrt{s} = 13$ TeV using the ATLAS detector at the LHC*, ATLAS-CONF-2016-057 (2016).
81. ATLAS Collab., JHEP **1709**, 088 (2017).
82. CMS Collab., Phys. Lett. **B730**, 193 (2014).
83. CMS Collab., Phys. Lett. **B770**, 257 (2017).
84. ATLAS Collab,. Phys. Rev. Lett. **114**, 161801 (2015).
85. CDF Collab., Phys. Rev. Lett. **105**, 081802 (2010).
86. D0 Collab., Phys. Lett. **B693**, 95 (2010).
87. CMS Collab., *Search for the pair production of third-generation squarks with two-body decays to a bottom or charm quark and a neutralino in proton-proton collisions at $\sqrt{s} = 13$ TeV*, arXiv:1707.07274(2017).
88. ATLAS Collab., *Search for supersymmetry in events with b-tagged jets and missing transverse momentum in pp collisions at $\sqrt{s} = 13$ TeV with the ATLAS detector*, arXiv:1708.09266(2017).
89. ATLAS Collab., Eur. Phys. J. **C75**, 510 (2015).
90. CMS Collab., Eur. Phys. J. **C77**, 578 (2017).
91. C. Boehm, A. Djouadi, and Y. Mambrini, Phys. Rev. **D61**, 095006 (2000).
92. CDF Collab., Phys. Rev. **D82**, 092001 (2010).
93. D0 Collab., Phys. Lett. **B696**, 321 (2011).
94. CDF Collab., JHEP **1210**, 158 (2012).
95. D0 Collab., Phys. Lett. **B665**, 1 (2008).
96. CDF Collab., Phys. Rev. Lett. **104**, 251801 (2010).
97. D0 Collab., Phys. Lett. **B674**, 4 (2009).
98. CMS Collab., JHEP **1710**, 005 (2017).
99. CMS Collab., JHEP **1710**, 019 (2017).
100. ATLAS Collab., *Search for a scalar partner of the top quark in the jets+E_T^{miss} final state at $\sqrt{s} = 13$ TeV with the ATLAS detector*, arXiv:1709.04183(2017).
101. ATLAS Collab., *Search for top squarks in final states with one isolated lepton, jets and missing transverse momentum using 36.1 fb^{-1} of $\sqrt{s} = 13$ TeV pp collision data with the ATLAS detector*, ATLAS-CONF-2017-037 (2017).
102. CMS Collab., *Search for direct stop pair production in the dilepton final state at $\sqrt{s} = 13$ TeV*, CMS-PAS-SUS-17-001 (2017).
103. ATLAS Collab., *Search for direct top squark pair production in final states with two leptons in $\sqrt{s} = 13$ TeV pp collisions with the ATLAS detector*, arXiv:1708.03247(2017).

104. ATLAS Collab., *Search for dark matter and other new phenomena in events with an energetic jet and large missing transverse momentum using the ATLAS detector*, ATLAS-CONF-2017-060 (2017).
105. H1 Collab., Eur. Phys. J. **C71**, 1572 (2011).
106. CMS Collab., Phys. Rev. **D91**, 052012 (2015).
107. ZEUS Collab., Eur. Phys. J. **C50**, 269 (2007).
108. CMS Collab., Phys. Rev. Lett. **111**, 221801 (2013).
109. ATLAS Collab., *A search for $B-L$ R-parity-violating scalar tops in $\sqrt{s}=13$ TeV pp collisions with the ATLAS experiment*, arXiv:1710.05544(2017).
110. CMS Collab., Phys. Rev. Lett. **114**, 061801 (2015).
111. CMS Collab., Phys. Lett. **B760**, 178 (2016).
112. ATLAS Collab., *A search for pair-produced resonances in four-jet final states at $\sqrt{s}=13$ TeV with the ATLAS detector*, ATLAS-CONF-2017-025 (2017).
113. CMS Collab., Phys. Lett. **B747**, 98 (2015).
114. LEP2 SUSY Working Group, ALEPH, DELPHI, L3 and OPAL experiments, note LEPSUSYWG/01-03.1, lepsusy.web.cern.ch/lepsusy.
115. LEP2 SUSY Working Group, ALEPH, DELPHI, L3 and OPAL experiments, note LEPSUSYWG/02-04.1, lepsusy.web.cern.ch/lepsusy.
116. CDF Collab., *Search for trilepton new physics and chargino-neutralino production at the Collider Detector at Fermilab*, CDF Note 10636 (2011).
117. D0 Collab., Phys. Lett. **B680**, 34 (2009).
118. ATLAS Collab. *Search for electroweak production of supersymmetric particles in the two and three lepton final state at $\sqrt{s}=13$ TeV with the ATLAS detector*, ATLAS-CONF-2017-039 (2017).
119. ATLAS Collab., JHEP **1405**, 071 (2014).
120. CMS Collab., *Search for electroweak production of charginos and neutralinos in multilepton final states in pp collision data at $\sqrt{s}=13$ TeV*, arXiv:1709.05406(2017).
121. ATLAS Collab., *Search for the direct production of charginos and neutralinos in $\sqrt{s}=13$ TeV pp collisions with the ATLAS detector*, arXiv:1708.07875(2017).
122. CMS Collab., *Combined search for electroweak production of charginos and neutralinos in pp collisions at $\sqrt{s}=13$ TeV*, CMS-PAS-SUS-17-004 (2017).
123. ATLAS Collab., Eur. Phys. J. **C75**, 208 (2015).
124. ATLAS Collab., Phys. Rev. **D93**, 052002 (2016).
125. CMS Collab., JHEP **1511**, 189 (2015).
126. H. Dreiner *et al.*, Eur. Phys. J. **C62**, 547 (2009).
127. LEP2 SUSY Working Group, ALEPH, DELPHI, L3 and OPAL experiments, note LEPSUSYWG/04-07.1, lepsusy.web.cern.ch/lepsusy.
128. For a sampling of recent post-LHC global analyses, see: GAMBIT Collab, arXiv:1705.07935; E.A. Bagnaschi *et al.*, Eur. Phys. J. **C77**, 268 (2017); E.A. Bagnaschi *et al.*, Eur. Phys. J. **C77**, 104 (2017); P. Bechtle *et al.*, Eur. Phys. J. **C76**, 9, (2016); E.A. Bagnaschi *et al.*, Eur. Phys. J. **C75**, 500 (2015); O. Buchmueller *et al.*, Eur. Phys. J. **C74**, 3212 (2014); O. Buchmueller *et al.*, Eur. Phys. J. **C74**, 2922 (2014); M. Citron *et al.*, Phys. Rev. **D87**, 036012 (2013); C. Strege *et al.*, JCAP **1304**, 013 (2013); A. Fowlie *et al.*, Phys. Rev. **D86**, 075010 (2012).
129. LEP2 SUSY Working Group, ALEPH, DELPHI, L3 and OPAL experiments, note LEPSUSYWG/04-09.1, lepsusy.web.cern.ch/lepsusy.
130. CDF Collab., Phys. Rev. Lett. **104**, 011801 (2010).
131. D0 Collab., Phys. Rev. Lett. **105**, 221802 (2010).
132. ATLAS Collab., Eur. Phys. J. **C76**, 517 (2016).
133. CMS Collab., *Search for supersymmetry in events with at least one photon, missing transverse momentum, and large transverse event activity in proton-proton collisions at $\sqrt{s}=13$ TeV*, arXiv:1707.06193(2017).
134. ATLAS Collab., Eur. Phys. J. **C77**, 144 (2017).
135. CMS Collab., Phys. Rev. **D90**, 092007 (2014).
136. CMS Collab., JHEP **04**, 124 (2016).
137. ATLAS Collab., *Search for supersymmetry in events with four or more leptons in $\sqrt{s}=13$ TeV pp collisions using 13.3 fb^{-1} of ATLAS data*, ATLAS-CONF-2016-075 (2016).
138. CMS Collab., Phys. Rev. **D91**, 012007 (2015).
139. ATLAS Collab., JHEP **1510**, 134 (2015).
140. CMS Collab., JHEP **1610**, 129 (2016).
141. For a sampling of recent pMSSM analyses, see: GAMBIT Collab, arXiv:1705.07917; K. de Vries *et al.*, Eur. Phys. J. **C75**, 422 (2015); C. Strege *et al.*, JHEP **1409**, 081 (2014); M. Cahill-Rowley *et al.*, Phys. Rev. **D88**, 035002 (2013); C. Boehm *et al.*, JHEP **1306**, 113, (2013); S AbdusSalam, Phys. Rev. **D87**, 115012 (2013); A. Arbey *et al.*, Eur. Phys. J. **C72**, 2169 (2012); A. Arbey *et al.*, Eur. Phys. J. **C72**, 1847 (2012); M. Carena *et al.*, Phys. Rev. **D86**, 075025 (2012); S. Sekmen *et al.*, JHEP **1202**, 075 (2012).
142. LEP2 SUSY Working Group, ALEPH, DELPHI, L3 and OPAL experiments, note LEPSUSYWG/04-01.1, lepsusy.web.cern.ch/lepsusy.
143. ALEPH Collab., Phys. Lett. **B544**, 73 (2002).
144. LEP2 SUSY Working Group, ALEPH, DELPHI, L3 and OPAL experiments, note LEPSUSYWG/02-09.2, lepsusy.web.cern.ch/lepsusy.
145. ATLAS Collab., JHEP **1409**, 103 (2014).
146. CMS Collab., Phys. Rev. **D90**, 032006 (2014).
147. CDF Collab., Phys. Rev. Lett. **110**, 201802 (2013).
148. LEP2 SUSY Working Group, ALEPH, DELPHI, L3 and OPAL experiments, note LEPSUSYWG/02-10.1, lepsusy.web.cern.ch/lepsusy.
149. DELPHI Collab., Eur. Phys. J. **C31**, 412 (2003).
150. T. Falk, K.A. Olive, and M. Srednicki, Phys. Lett. **B339**, 248 (1994).
151. C. Arina and N. Fornengo, JHEP **0711**, 029 (2007).
152. CDF Collab., Phys. Rev. Lett. **105**, 191801 (2010).
153. D0 Collab., Phys. Rev. Lett. **105**, 191802 (2010).
154. ATLAS Collab., Phys. Rev. Lett. **115**, 031801 (2015).
155. CMS Collab., Eur. Phys. J. **C76**, 317 (2016).
156. O. Buchmueller *et al.*, *Simplified Models for Displaced Dark Matter Signatures*, arXiv:1704.06515.
157. V. Khoze *et al.*, JHEP **06**, 041 (2017).
158. CMS Collab., Phys. Rev. **D94**, 112004 (2016).
159. ATLAS Collab., Phys. Lett. **B760**, 647 (2016).
160. D0 Collab., Phys. Rev. Lett. **99**, 131801 (2007).
161. ATLAS Collab., Phys. Rev. **D88**, 112003 (2013).
162. CMS Collab., *Search for stopped long-lived particles produced in pp collisions at $\sqrt{s}=13$ TeV*, CMS-PAS-EXO-16-004 (2017).
163. CMS Collab., *Search for long-lived particles that stop in the CMS detector and decay to muons at $\sqrt{s}=13$ TeV*, CMS-PAS-EXO-17-004 (2017).
164. CDF Collab., Phys. Rev. Lett. **103**, 021802 (2009).
165. D0 Collab., Phys. Rev. **D87**, 052011 (2013).
166. ATLAS Collab., Phys. Rev. **D88**, 112006 (2013).
167. ATLAS Collab., *Search for long-lived charginos based on a disappearing-track signature in pp collisions at $\sqrt{s}=13$ TeV with the ATLAS detector*, ATLAS-CONF-2017-017 (2017).
168. CMS Collab., JHEP **1501**, 096 (2015).
169. LEP2 SUSY Working Group, ALEPH, DELPHI, L3 and OPAL experiments, note LEPSUSYWG/02-05.1, lepsusy.web.cern.ch/lepsusy.
170. CMS Collab., Eur. Phys. J. **C75**, 325 (2015).
171. LHCb Collab., Eur. Phys. J. **C75**, 595 (2015).
172. CDF Collab., Phys. Rev. **D88**, 031103 (2013).
173. CMS Collab., Phys. Lett. **B722**, 273 (2013).
174. D0 Collab., Phys. Rev. Lett. **101**, 111802 (2008).
175. ATLAS Collab, Phys. Rev. **D90**, 112005 (2014).
176. For a sampling of pre-LHC global analyses, see: O. Buchmueller *et al.*, Eur. Phys. J. **C71**, 1722 (2011); E.A. Baltz and P. Gondolo, JHEP **0410**, 052 (2004); B.C. Allanach and C.G. Lester, Phys. Rev. **D73**, 015013 (2006); R.R. de Austri *et al.*, JHEP **0605**, 002 (2006); R. Lafaye *et al.*, Eur. Phys. J. **C54**, 617 (2008); S. Heinemeyer *et al.*, JHEP **0808**, 08 (2008);

R. Trotta *et al.*, JHEP **0812**, 024 (2008); P. Bechtle *et al.*, Eur. Phys. J. **C66**, 215 (2010).
177. Supersymmetry Physics Results, ATLAS experiment, http://twiki.cern.ch/twiki/bin/view/AtlasPublic/SupersymmetryPublicResults/.
178. Supersymmetry Physics Results, CMS experiment, http://cms-results.web.cern.ch/cms-results/public-results/publications/SUS/index.html.

111. Axions and Other Similar Particles

Revised October 2017 by A. Ringwald (DESY), L.J Rosenberg and G. Rybka (U. of Washington).

111.1. Introduction

In this section, we list coupling-strength and mass limits for light neutral scalar or pseudoscalar bosons that couple weakly to normal matter and radiation. Such bosons may arise from a global spontaneously broken U(1) symmetry, resulting in a massless Nambu-Goldstone (NG) boson. If there is a small explicit symmetry breaking, either already in the Lagrangian or due to quantum effects such as anomalies, the boson acquires a mass and is called a pseudo-NG boson. Typical examples are axions (A^0) [1,2], familons [3] and majorons [4], associated, respectively, with a spontaneously broken Peccei-Quinn, family and lepton-number symmetry.

A common characteristic among these light bosons ϕ is that their coupling to Standard-Model particles is suppressed by the energy scale that characterizes the symmetry breaking, *i.e.*, the decay constant f. The interaction Lagrangian is

$$\mathcal{L} = f^{-1} J^\mu \partial_\mu \phi \,, \tag{111.1}$$

where J^μ is the Noether current of the spontaneously broken global symmetry. If f is very large, these new particles interact very weakly. Detecting them would provide a window to physics far beyond what can be probed at accelerators.

Axions are of particular interest because the Peccei-Quinn (PQ) mechanism remains perhaps the most credible scheme to preserve CP in QCD. Moreover, the cold dark matter of the universe may well consist of axions and they are searched for in dedicated experiments with a realistic chance of discovery.

Originally it was assumed that the PQ scale f_A was related to the electroweak symmetry-breaking scale $v_{\rm weak} = (\sqrt{2}G_{\rm F})^{-1/2} = 247$ GeV. However, the associated "standard" and "variant" axions were quickly excluded—we refer to the Listings for detailed limits. Here we focus on "invisible axions" with $f_A \gg v_{\rm weak}$ as the main possibility.

Axions have a characteristic two-photon vertex, inherited from their mixing with π^0 and η. This coupling allows for the main search strategy based on axion-photon conversion in external magnetic fields [5], an effect that also can be of astrophysical interest. While for axions the product "$A\gamma\gamma$ interaction strength × mass" is essentially fixed by the corresponding π^0 properties, one may consider a more general class of axion-like particles (ALPs) where the two parameters (coupling and mass) are independent. A number of experiments explore this more general parameter space. ALPs populating the latter are predicted to arise generically, in addition to the axion, in low-energy effective field theories emerging from string theory [6]. The latter often contain also very light Abelian vector bosons under which the Standard-Model particles are not charged: so-called hidden-sector photons, dark photons or paraphotons. They share a number of phenomenological features with the axion and ALPs, notably the possibility of hidden photon to photon conversion. Their physics cases and the current constraints are compiled in Ref. [7].

111.2. Theory

111.2.1. *Peccei-Quinn mechanism and axions* :

The QCD Lagrangian includes a CP-violating term $\mathcal{L}_\Theta = -\bar{\Theta}\,(\alpha_s/8\pi)\,G^{\mu\nu a}\tilde{G}^a_{\mu\nu}$, where $-\pi \le \bar{\Theta} \le +\pi$ is the effective Θ parameter after diagonalizing quark masses, $G^a_{\mu\nu}$ is the color field strength tensor, and $\tilde{G}^{a,\mu\nu} \equiv \epsilon^{\mu\nu\lambda\rho}G^a_{\lambda\rho}/2$, with $\varepsilon^{0123} = 1$, its dual. Limits on the neutron electric dipole moment [8] imply $|\bar{\Theta}| \lesssim 10^{-10}$ even though $\bar{\Theta} = \mathcal{O}(1)$ is otherwise completely satisfactory. The spontaneously broken global Peccei-Quinn symmetry $\mathrm{U(1)_{PQ}}$ was introduced to solve this "strong CP problem" [1], the axion being the pseudo-NG boson of $\mathrm{U(1)_{PQ}}$ [2]. This symmetry is broken due to the axion's anomalous triangle coupling to gluons,

$$\mathcal{L} = \left(\frac{\phi_A}{f_A} - \bar{\Theta}\right)\frac{\alpha_s}{8\pi}\,G^{\mu\nu a}\tilde{G}^a_{\mu\nu}\,, \tag{111.2}$$

where ϕ_A is the axion field and f_A the axion decay constant. Color anomaly factors have been absorbed in the normalization of f_A which is defined by this Lagrangian. Thus normalized, f_A is the quantity that enters all low-energy phenomena [9]. Non-perturbative topological fluctuations of the gluon fields in QCD induce a potential for ϕ_A whose minimum is at $\phi_A = \bar{\Theta}\,f_A$, thereby canceling the $\bar{\Theta}$ term in the QCD Lagrangian and thus restoring CP symmetry.

The resulting axion mass, in units of the PQ scale f_A, is identical to the square root of the topological susceptibility in QCD, $m_A f_A = \sqrt{\chi}$. The latter can be evaluated further [10], exploiting the chiral limit (masses of up and down quarks much smaller than the scale of QCD), yielding $m_A f_A = \sqrt{\chi} \approx f_\pi m_\pi$, where $m_\pi = 135$ MeV and $f_\pi \approx 92$ MeV. In more detail one finds, to next-to-leading order in chiral perturbation theory [11],

$$m_A = 5.70(7)\,\left(\frac{10^9\,\mathrm{GeV}}{f_A}\right)\mathrm{meV}\,. \tag{111.3}$$

This result was recently confirmed by a direct calculation of the topological susceptibility via QCD lattice simulations [12].

Originally one assumed $f_A \sim v_{\rm weak}$ [1,2]. Tree-level flavor conservation fixes the axion properties in terms of a single parameter: the ratio of the vacuum expectation values of two Higgs fields that appear as a minimal ingredient. This "standard axion" was excluded after extensive searches [13]. A narrow peak structure observed in positron spectra from heavy ion collisions [14] suggested an axion-like particle of mass 1.8 MeV that decays into e^+e^-, but extensive follow-up searches were negative. "Variant axion models" were proposed which keep $f_A \sim v_{\rm weak}$ while relaxing the constraint of tree-level flavor conservation [15], but these models are also excluded [16].

However, axions with $f_A \gg v_{\rm weak}$ evade all current experimental limits. One generic class of models invokes "hadronic axions" where new heavy quarks carry $\mathrm{U(1)_{PQ}}$ charges, leaving ordinary quarks and leptons without tree-level axion couplings. The archetype is the KSVZ model [17], where in addition the heavy quarks are electrically neutral. Another generic class requires at least two Higgs doublets and ordinary quarks and leptons carry PQ charges, the archetype being the DFSZ model [18]. All of these models contain at least one electroweak singlet scalar that acquires a vacuum expectation value and thereby breaks the PQ symmetry. The KSVZ and DFSZ models are frequently used as benchmark examples, but other models exist where both heavy quarks and Higgs doublets carry PQ charges. In supersymmetric models, the axion is part of a supermultiplet and thus inevitably accompanied by a spin-0 saxion and a spin-1 axino, which both also have couplings suppressed by f_A, and are expected to have large masses due to supersymmetry breaking [19].

111.2.2. *Model-dependent axion couplings* :

Although the generic axion interactions scale approximately with f_π/f_A from the corresponding π^0 couplings, there are non-negligible model-dependent factors and uncertainties. The axion's two-photon interaction plays a key role for many searches,

$$\mathcal{L}_{A\gamma\gamma} = -\frac{G_{A\gamma\gamma}}{4}\,F_{\mu\nu}\tilde{F}^{\mu\nu}\phi_A = G_{A\gamma\gamma}\mathbf{E}\cdot\mathbf{B}\,\phi_A\,, \tag{111.4}$$

where F is the electromagnetic field-strength tensor and $\tilde{F}^{\mu\nu} \equiv \epsilon^{\mu\nu\lambda\rho}F_{\lambda\rho}/2$, with $\varepsilon^{0123} = 1$, its dual. The coupling constant is [11]

$$G_{A\gamma\gamma} = \frac{\alpha}{2\pi f_A}\left(\frac{E}{N} - 1.92(4)\right) = \left(0.203(3)\frac{E}{N} - 0.39(1)\right)\frac{m_A}{\mathrm{GeV}^2}\,, \tag{111.5}$$

where E and N are the electromagnetic and color anomalies of the axial current associated with the axion. In grand unified models, and notably for DFSZ [18], $E/N = 8/3$, whereas for KSVZ [17] $E/N = 0$ if the electric charge of the new heavy quark is taken to vanish. In general, a broad range of E/N values is possible [20], as indicated by the yellow band in Figure 111.1. The two-photon decay width is

$$\Gamma_{A\to\gamma\gamma} = \frac{G^2_{A\gamma\gamma}m_A^3}{64\,\pi} = 1.1\times10^{-24}\ \mathrm{s}^{-1}\,\left(\frac{m_A}{\mathrm{eV}}\right)^5. \tag{111.6}$$

the second expression uses Eq. (1.5) with $E/N = 0$. Axions decay faster than the age of the universe if $m_A \gtrsim 20$ eV.

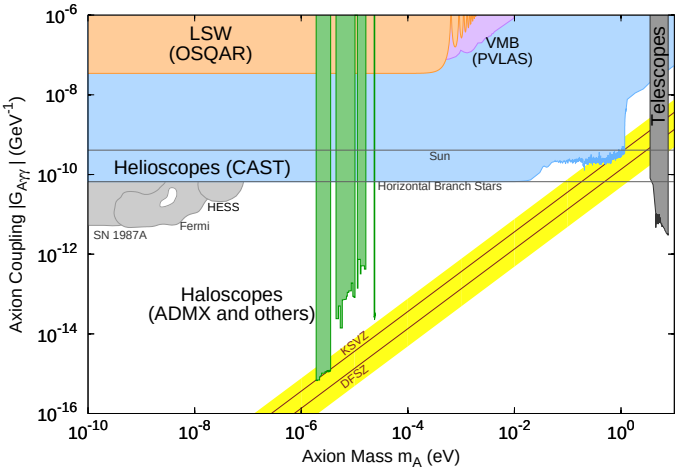

Figure 111.1: Exclusion plot for axion-like particles as described in the text.

The interaction with fermions f has derivative form and is invariant under a shift $\phi_A \to \phi_A + \phi_0$ as behooves a NG boson,

$$\mathcal{L}_{Aff} = \frac{C_f}{2f_A}\,\bar{\Psi}_f\gamma^\mu\gamma_5\Psi_f\partial_\mu\phi_A\,. \tag{111.7}$$

Here, Ψ_f is the fermion field, m_f its mass, and C_f a model-dependent coefficient. The dimensionless combination $g_{Aff} \equiv C_f m_f/f_A$ plays the role of a Yukawa coupling and $\alpha_{Aff} \equiv g^2_{Aff}/4\pi$ of a "fine-structure constant." The often-used pseudoscalar form $\mathcal{L}_{Aff} = -\mathrm{i}\,(C_f m_f/f_A)\,\bar{\Psi}_f\gamma_5\Psi_f\phi_A$ need not be equivalent to the appropriate derivative structure, for example when two NG bosons are attached to one fermion line as in axion emission by nucleon bremsstrahlung [21].

In the DFSZ model [18], the tree-level coupling coefficient to electrons is [22]

$$C_e = \frac{\sin^2\beta}{3}\,, \tag{111.8}$$

where $\tan\beta = v_u/v_d$ is the ratio of the vacuum expectation value v_u of the Higgs field H_u giving masses to the up-type quarks and the vacuum expectation value v_d of the Higgs field H_d giving masses to the down-type quarks.

For nucleons, $C_{n,p}$ have recently been determined as [11]

$$\begin{aligned} C_p &= -0.47(3) + 0.88(3)C_u - 0.39(2)C_d - 0.038(5)C_s \\ &\quad - 0.012(5)C_c - 0.009(2)C_b - 0.0035(4)C_t\,, \\ C_n &= -0.02(3) + 0.88(3)C_d - 0.39(2)C_u - 0.038(5)C_s \\ &\quad - 0.012(5)C_c - 0.009(2)C_b - 0.0035(4)C_t\,, \end{aligned} \tag{111.9}$$

in terms of the corresponding model-dependent quark couplings C_q, $q = u, d, s, c, b, t$.

Note, that the model-independent contribution of the neutron is compatible with zero. For hadronic axions $C_q = 0$, so that $C_n = -0.02(3)$. Therefore it is well possible that $C_n = 0$ whereas C_p does not vanish. In the DFSZ model, $C_u = C_c = C_t = \frac{1}{3}\cos^2\beta$ and $C_d = C_s = C_b = \frac{1}{3}\sin^2\beta$, and C_n and C_p, as functions of β,

$$\begin{aligned} C_p &= -0.435\sin^2\beta + (-0.182 \pm 0.025)\,, \\ C_n &= 0.414\sin^2\beta + (-0.16 \pm 0.025)\,, \end{aligned} \tag{111.10}$$

do not vanish simultaneously.

The axion-pion interaction is given by the Lagrangian [23]

$$\mathcal{L}_{A\pi} = \frac{C_{A\pi}}{f_\pi f_A}\left(\pi^0\pi^+\partial_\mu\pi^- + \pi^0\pi^-\partial_\mu\pi^+ - 2\pi^+\pi^-\partial_\mu\pi^0\right)\partial_\mu\phi_A\,, \tag{111.11}$$

where $C_{A\pi} = (1-z)/[3(1+z)]$ in hadronic models, with $0.38 < z = m_u/m_d < 0.58$ [24,25]. The chiral symmetry-breaking Lagrangian provides an additional term $\mathcal{L}'_{A\pi} \propto (m^2_\pi/f_\pi f_A)\,(\pi^0\pi^0 + 2\pi^-\pi^+)\,\pi^0\phi_A$. For hadronic axions it vanishes identically, in contrast to the DFSZ model (Roberto Peccei, private communication).

111.3. Laboratory Searches

111.3.1. *Light shining through walls* :

Searching for "invisible axions" is extremely challenging due to its extraordinarily feeble coupling to normal matter and radiation. Currently, the most promising approaches rely on the axion-two-photon vertex, allowing for axion-photon conversion in external electric or magnetic fields [5]. For the Coulomb field of a charged particle, the conversion is best viewed as a scattering process, $\gamma + Ze \leftrightarrow Ze + A$, called Primakoff effect [26]. In the other extreme of a macroscopic field, usually a large-scale B-field, the momentum transfer is small, the interaction coherent over a large distance, and the conversion is best viewed as an axion-photon oscillation phenomenon in analogy to neutrino flavor oscillations [27].

Photons propagating through a transverse magnetic field, with incident $\mathbf{E}_\gamma$ and magnet $\mathbf{B}$ parallel, may convert into axions. For $m_A^2 L/2\omega \ll 2\pi$, where L is the length of the B field region and ω the photon energy, the resultant axion beam is coherent with the incident photon beam and the conversion probability is $\Pi \sim (1/4)(G_{A\gamma\gamma}BL)^2$. A practical realization uses a laser beam propagating down the bore of a superconducting dipole magnet (like the bending magnets in high-energy accelerators). If another magnet is in line with the first, but shielded by an optical barrier, then photons may be regenerated from the pure axion beam [28]. The overall probability is $P(\gamma \to A \to \gamma) = \Pi^2$.

The first such experiment utilized two magnets of length $L = 4.4$ m and $B = 3.7$ T and found $|G_{A\gamma\gamma}| < 6.7 \times 10^{-7}$ GeV^{-1} at 95% CL for $m_A < 1$ meV [29]. More recently, several such experiments were performed (see Listings) [30,31]. The current best limit, $|G_{A\gamma\gamma}| < 3.5 \times 10^{-8}$ GeV^{-1} at 95% CL for $m_A \lesssim 0.3$ meV (see Figure 111.1), has been achieved by the OSQAR (Optical Search for QED Vacuum Birefringence, Axions, and Photon Regeneration) experiment, which exploited two 9 T LHC dipole magnets and an 18.5 W continuous wave laser emitting at the wavelength of 532 nm [31]. Some of these experiments have also reported limits for scalar bosons where the photon $\mathbf{E}_\gamma$ must be chosen perpendicular to the magnet $\mathbf{B}$.

The concept of resonantly enhanced photon regeneration may open unexplored regions of coupling strength [32]. In this scheme, both the production and detection magnets are within Fabry-Perot optical cavities and actively locked in frequency. The $\gamma \to A \to \gamma$ rate is enhanced by a factor $\mathcal{F}\mathcal{F}'/\pi^2$ relative to a single-pass experiment, where $\mathcal{F}$ and $\mathcal{F}'$ are the finesses of the two cavities. The resonant enhancement could be of order $10^{(10-12)}$, improving the $G_{A\gamma\gamma}$ sensitivity by $10^{(2.5-3)}$. The experiment ALPS II (Any Light Particle Search II) is based on this concept and aims at an improvement of the current laboratory bound on $G_{A\gamma\gamma}$ by a factor $\sim 10^3$ in the year 2020 [33].

Resonantly enhanced photon regeneration has already been exploited in experiments searching for "radiowaves shining through a shielding" [34,35]. For $m_A \lesssim 10^{-5}$ eV, the upper bound on $G_{A\gamma\gamma}$ established by the CROWS (CERN Resonant Weakly Interacting sub-eV Particle Search) experiment [36] is slightly less stringent than the one set by OSQAR.

111.3.2. *Photon polarization* :

An alternative to regenerating the lost photons is to use the beam itself to detect conversion: the polarization of light propagating through a transverse B field suffers dichroism and birefringence [37]. Dichroism: The $E_\parallel$ component, but not $E_\perp$, is depleted by axion production, causing a small rotation of linearly polarized light. For $m_A^2 L/2\omega \ll 2\pi$, the effect is independent of m_A. For heavier axions, it oscillates and diminishes as m_A increases, and it vanishes for $m_A > \omega$. Birefringence: This rotation occurs because there is mixing of virtual axions in the $E_\parallel$ state, but not for $E_\perp$. Hence, linearly

polarized light will develop elliptical polarization. Higher-order QED also induces vacuum magnetic birefringence (VMB). A search for these effects was performed in the same dipole magnets in the early experiment above [38]. The dichroic rotation gave a stronger limit than the ellipticity rotation: $|G_{A\gamma\gamma}| < 3.6 \times 10^{-7}$ GeV^{-1} at 95% CL for $m_A < 5 \times 10^{-4}$ eV. The ellipticity limits are better at higher masses, as they fall off smoothly and do not terminate at m_A.

In 2006 the PVLAS collaboration reported a signature of magnetically induced vacuum dichroism that could be interpreted as the effect of a pseudoscalar with $m_A = 1$–1.5 meV and $|G_{A\gamma\gamma}| = (1.6$–$5) \times 10^{-6}$ GeV^{-1} [39]. Since then, these findings are attributed to instrumental artifacts [40]. This particle interpretation is also excluded by the above photon regeneration searches that were inspired by the original PVLAS result. Recently, the fourth generation setup of the PVLAS experiment has published new results on searches for VMB (see Figure 111.1) and dichroism [41]. The bounds from the non-observation of the latter on $G_{A\gamma\gamma}$ are slightly weaker than the ones from OSQAR.

111.3.3. *Long-range forces* :

New bosons would mediate long-range forces, which are severely constrained by "fifth force" experiments [42]. Those looking for new mass-spin couplings provide significant constraints on pseudoscalar bosons [43]. Presently, the most restrictive limits are obtained from combining long-range force measurements with stellar cooling arguments [44]. For the moment, any of these limits are far from realistic values expected for axions. Still, these efforts provide constraints on more general low-mass bosons.

Recently, a method was proposed that can extend the search for axion-mediated spin-dependent forces by several orders of magnitude [45]. By combining techniques used in nuclear magnetic resonance and short-distance tests of gravity, this method appears to be sensitive to axions in the μeV – meV mass range, independent of the cosmic axion abundance, if axions have a CP-violating interaction with nuclei as large as the current experimental bound on the electric dipole moment of the neutron allows.

111.4. Axions from Astrophysical Sources

111.4.1. *Stellar energy-loss limits* :

Low-mass weakly-interacting particles (neutrinos, gravitons, axions, baryonic or leptonic gauge bosons, *etc.*) are produced in hot astrophysical plasmas, and can thus transport energy out of stars. The coupling strength of these particles with normal matter and radiation is bounded by the constraint that stellar lifetimes or energy-loss rates not conflict with observation [46–48].

We begin this discussion with our Sun and concentrate on hadronic axions. They are produced predominantly by the Primakoff process $\gamma + Ze \to Ze + A$. Integrating over a standard solar model yields the axion luminosity [49]

$$L_A = G_{10}^2\, 1.85 \times 10^{-3}\, L_\odot\,, \tag{111.12}$$

where $G_{10} = |G_{A\gamma\gamma}| \times 10^{10}$ GeV. The maximum of the spectrum is at 3.0 keV, the average at 4.2 keV, and the number flux at Earth is $G_{10}^2\ 3.75 \times 10^{11}$ cm^{-2} s^{-1}. The solar photon luminosity is fixed, so axion losses require enhanced nuclear energy production and thus enhanced neutrino fluxes. The all-flavor measurements by SNO together with a standard solar model imply $L_A \lesssim 0.10\, L_\odot$, corresponding to $G_{10} \lesssim 7$ [50], mildly superseding a similar limit from helioseismology [51]. Recently, the limit was improved to $G_{10} < 4.1$ (at $3\,\sigma$), see Figure 111.1 (Sun), exploiting a new statistical analysis that combined helioseismology (sound speed, surface helium and convective radius) and solar neutrino observations, including theoretical and observational errors, and accounting for tensions between input parameters of solar models, in particular the solar element abundances [52].

A more restrictive limit derives from globular-cluster (GC) stars that allow for detailed tests of stellar-evolution theory. The stars on the horizontal branch (HB) in the color-magnitude diagram have reached helium burning with a core-averaged energy release of about 80 erg g^{-1} s^{-1}, compared to Primakoff axion losses of $G_{10}^2\, 30$ erg g^{-1} s^{-1}. The accelerated consumption of helium reduces the HB lifetime by about $80/(80 + 30\, G_{10}^2)$. Number counts of HB stars in a large sample of 39 Galactic GCs compared with the number of red giants (that are not much affected by Primakoff losses) give a weak indication of non-standard losses which may be accounted by Primakoff-like axion emission, if the photon coupling is in the range $|G_{A\gamma\gamma}| = (2.9 \pm 1.8) \times 10^{-11}$ GeV^{-1} [53]. Still, the upper bound found in this analysis,

$$|G_{A\gamma\gamma}| < 6.6 \times 10^{-11}\,\text{GeV}^{-1}\ (95\%\,\text{CL}), \tag{111.13}$$

represents the strongest limit on $G_{A\gamma\gamma}$ for a wide mass range, see Figure 111.1.

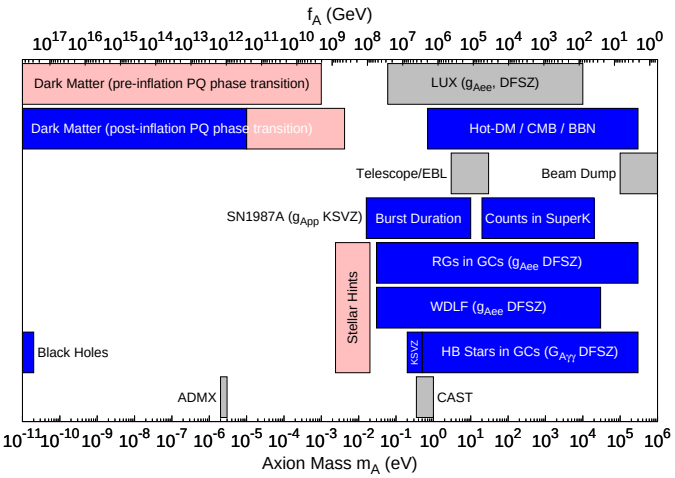

Figure 111.2: Exclusion ranges as described in the text. The intervals in the bottom row are the approximate ADMX and CAST search ranges. Limits on coupling strengths are translated into limits on m_A and f_A using the KSVZ values for the coupling strengths, if not indicated otherwise. The "Beam Dump" bar is a rough representation of the exclusion range for standard or variant axions. The limits for the axion-electron coupling are determined for the DFSZ model with an axion-electron coupling corresponding to $\sin^2\beta = 1/2$.

We translate the conservative constraint, Equation 111.13, on $G_{A\gamma\gamma}$ to $f_A > 3.4 \times 10^7$ GeV ($m_A < 0.2$ eV), using $E/N = 0$ as in the KSVZ model, and show the excluded range in Figure 111.2. For the DFSZ model with $E/N = 8/3$, the corresponding limits are slightly less restrictive, $f_A > 1.3 \times 10^7$ GeV ($m_A < 0.5$ eV).

If axions couple directly to electrons, the dominant emission processes are atomic axio-recombination and axio-deexcitation, axio-bremsstrahlung in electron-ion or electron-electron collisions, and Compton scattering [54]. Stars in the red giant (RG) branch of the color-magnitude diagram of GCs are particularly sensitive to these processes. In fact, they would lead to an extension of the latter to larger brightness. A recent analysis provided high-precision photometry for the Galactic globular cluster M5 (NGC 5904), allowing for a detailed comparison between the observed tip of the RG branch with predictions based on state-of-the-art stellar evolution theory [55]. It was found that, within the uncertainties, the observed and predicted tip of the RG branch brightness agree reasonably well within uncertainties, leading to the bound

$$\alpha_{Aee} < 1.5 \times 10^{-26} \quad (95\%\ \text{CL}), \tag{111.14}$$

implying an upper bound on the axion mass in the DFSZ model,

$$m_A \sin^2\beta < 15\ \text{meV} \quad (95\%\ \text{CL}), \tag{111.15}$$

see Figure 111.2. Intriguingly, the agreement would improve with a small amount of extra cooling that slightly postpones helium

ignition, prefering an electron coupling around $\alpha_{Aee} \sim 2.8 \times 10^{-27}$, corresponding to $m_A \sin^2\beta \sim 7$ meV.

Bremsstrahlung is also efficient in white dwarfs (WDs), where the Primakoff and Compton processes are suppressed by the large plasma frequency. A comparison of the predicted and observed luminosity function of WDs can be used to put limits on α_{Aee} [56]. A recent analysis, based on detailed WD cooling treatment and new data on the WD luminosity function (WDLF) of the Galactic Disk, found that electron couplings above $\alpha_{Aee} \gtrsim 6 \times 10^{-27}$, corresponding to a DFSZ axion mass $m_A \sin^2\beta \gtrsim 10$ meV, are disfavoured [57], see Figure 111.2. Lower couplings can not be discarded from the current knowledge of the WDLF of the Galactic Disk. On the contrary, features in some WDLFs can be interpreted as suggestions for electron couplings in the range $4.1 \times 10^{-28} \lesssim \alpha_{Aee} \lesssim 3.7 \times 10^{-27}$, corresponding to 2.5 meV $\lesssim m_A \sin^2\beta \lesssim$ 7.5 meV [57,58]. For pulsationally unstable WDs (ZZ Ceti stars), the period decrease $\dot{P}/P$ is a measure of the cooling speed. The corresponding observations of the pulsating WDs G117-B15A and R548 imply additional cooling that can be interpreted also in terms of similar axion losses [59].

Similar constraints derive from the measured duration of the neutrino signal of the supernova SN 1987A. Numerical simulations for a variety of cases, including axions and Kaluza-Klein gravitons, reveal that the energy-loss rate of a nuclear medium at the density 3×10^{14} g cm^{-3} and temperature 30 MeV should not exceed about 1×10^{19} erg g^{-1} s^{-1} [47]. The energy-loss rate from nucleon bremsstrahlung, $N + N \to N + N + A$, is $(C_N/2f_A)^2(T^4/\pi^2 m_N)\,F$. Here F is a numerical factor that represents an integral over the dynamical spin-density structure function because axions couple to the nucleon spin. For realistic conditions, even after considerable effort, one is limited to a heuristic estimate leading to $F \approx 1$ [48]. The SN 1987A limits are of particular interest for hadronic axions where the bounds on α_{Aee} are moot. Using a proton fraction of 0.3, $g_{Ann} = 0$, $F = 1$, and $T = 30$ MeV, one finds $f_A \gtrsim 4 \times 10^8$ GeV and $m_A \lesssim 16$ meV [48], see Figure 111.2. A more detailed numerical calculation [60] with state of the art SN models, again assuming $g_{Ann} = 0$, found that a coupling larger than $|g_{App}| \gtrsim 6 \times 10^{-10}$, would shorten significantly the timescale of the neutrino emission. This result is, not surprisingly, rather close to the estimate in Ref. [48].

The case of a general axion model, interacting with both protons and neutrons, is more complicated. A numerical study in Ref. [61], using the same SN models exploited in Ref. [60], inferred that the combination $g_{App}^2 + g_{Ann}^2$ would be the most appropriate to describe the axion interaction with the nuclear medium, in the regions where the axion emission rate is peaked. In combination with the results in Ref. [60], this suggests the bound

$$g_{App}^2 + g_{Ann}^2 < 3.6 \times 10^{-19}\,. \tag{111.16}$$

Note, however, that no conclusion was drawn in Ref. [60] in terms of a robust constraint from SN 1987A, and that Equation 111.16 should be taken as an indicative result, in absence of a more definite study.

If axions interact sufficiently strongly they are trapped. Only about three orders of magnitude in g_{ANN} or m_A are excluded, a range shown somewhat schematically in Figure 111.2. For even larger couplings, the axion flux would have been negligible, yet it would have triggered additional events in the detectors, excluding a further range [62]. A possible gap between these two SN 1987A arguments was discussed as the "hadronic axion window" under the assumption that $G_{A\gamma\gamma}$ was anomalously small [63]. This range is now excluded by hot dark matter bounds (see below).

There is another hint for excessive stellar energy losses from the neutron star (NS) in the supernova remnant Cassiopeia A (Cas A): its surface temperature measured over 10 years reveals an unusually fast cooling rate. This may be interpreted as a hint for extra cooling by axion neutron bremsstrahlung, requiring a coupling to the neutron of size [64]

$$g_{Ann}^2 = (1.4 \pm 0.5) \times 10^{-19} \tag{111.17}$$

corresponding to an axion mass

$$m_A = (2.3 \pm 0.4)\,\mathrm{meV}/C_n, \tag{111.18}$$

see Figure 111.2. The hint is compatible with the state-of-the-art upper limit on this coupling,

$$g_{Ann}^2 < 6 \times 10^{-19}, \tag{111.19}$$

from NS cooling [65]. In fact, as recently pointed out, the more rapid cooling of the superfluid core in the neutron star may also arise from a phase transition of the neutron condensate into a multicomponent state [66].

Recently, it has been pointed out that the hints of excessive cooling of WDs, RGs and HB stars can be explained at one stroke by an ALP coupling to electrons and photons, with couplings $g_{Aee} \sim 1.5 \times 10^{-13}$ and $|G_{A\gamma\gamma}| \sim 1.4 \times 10^{-11}\,\mathrm{GeV}^{-1}$, respectively [61,67]. Intriguingly, good fits to the data can be obtained employing the DFSZ axion with a mass in the range $2.4\,\mathrm{meV} \lesssim m_A \lesssim 20\,\mathrm{meV}$ $(2\,\sigma)$, if the SN 1987A constraint is taken into account [61], see Figure 111.2.

Finally, let us note that if the interpretation of the various hints for additional cooling of stars reported in this section in terms of emission of axions with $m_A \sim$ meV were correct, SNe would lose a large fraction of their energy as axions. This would lead to a diffuse SN axion background in the universe with an energy density comparable to the extra-galactic background light [68]. However, there is no apparent way of detecting it or the axion burst from the next nearby SN. On the other hand, neutrino detectors such as IceCube, Super-Kamiokande or a future mega-ton water Cerenkov detector will probe exactly the mass region of interest by measuring the neutrino pulse duration of the next galactic SN [60].

111.4.2. *Searches for solar axions and ALPs* :

Instead of using stellar energy losses to derive axion limits, one can also search directly for these fluxes, notably from the Sun. The main focus has been on axion-like particles with a two-photon vertex. They are produced by the Primakoff process with a flux given by Equation 111.12 and an average energy of 4.2 keV, and can be detected at Earth with the reverse process in a macroscopic B-field ("axion helioscope") [5]. In order to extend the sensitivity in mass towards larger values, one can endow the photon with an effective mass in a gas, $m_\gamma = \omega_{\mathrm{plas}}$, thus matching the axion and photon dispersion relations [69].

An early implementation of these ideas used a conventional dipole magnet, with a conversion volume of variable-pressure gas with a xenon proportional chamber as x-ray detector [70]. The conversion magnet was fixed in orientation and collected data for about 1000 s/day. Axions were excluded for $|G_{A\gamma\gamma}| < 3.6 \times 10^{-9}$ GeV^{-1} for $m_A <$ 0.03 eV, and $|G_{A\gamma\gamma}| < 7.7 \times 10^{-9}$ GeV^{-1} for $0.03 < m_A < 0.11$ eV at 95% CL.

Later, the Tokyo axion helioscope used a superconducting magnet on a tracking mount, viewing the Sun continuously. They reported $|G_{A\gamma\gamma}| < 6 \times 10^{-10}$ GeV^{-1} for $m_A < 0.3$ eV [71]. This experiment was recommissioned and a similar limit for masses around 1 eV was reported [72].

The most recent helioscope CAST (CERN Axion Solar Telescope) uses a decommissioned LHC dipole magnet on a tracking mount. The hardware includes grazing-incidence x-ray optics with solid-state x-ray detectors, as well as a novel x-ray Micromegas position-sensitive gaseous detector. CAST has established a 95% CL limit $|G_{A\gamma\gamma}| < 6.6 \times 10^{-11}$ GeV^{-1} for $m_A < 0.02$ eV [73], exploiting a IAXO (see below) pathfinder system. To cover larger masses, the magnet bores are filled with a gas at varying pressure. The runs with ^{4}He cover masses up to about 0.4 eV [74], providing the ^{4}He limits shown in Figure 111.1. To cover yet larger masses, ^{3}He was used to achieve a larger pressure at cryogenic temperatures. Limits up to 1.17 eV allowed CAST to "cross the axion line" for the KSVZ model [75], see Figure 111.1.

Dark matter direct detection experiments searching for dark matter consisting of weakly interacting massive particles, such as EDELWEISS-II, LUX, and XENON100, have also the capability to search for solar axions and ALPs [76,77]. Recently, the LUX experiment [77] has put a bound on the axion-electron coupling constant by exploiting the axio-electric effect in liquid xenon,

$$g_{Aee} < 3.5 \times 10^{-12} \quad (90\%\ \mathrm{CL}), \tag{111.20}$$

excluding the DFSZ model with $m_A \sin^2\beta > 0.12\,\mathrm{eV}$, cf. see Figure 111.2.

Going to yet larger masses in a helioscope search is not well motivated because of the cosmic hot dark matter bound of $m_A \lesssim 1$ eV (see below). Sensitivity to significantly smaller values of $G_{A\gamma\gamma}$ can be achieved with a next-generation axion helioscope with a much larger magnetic-field cross section. Realistic design options for this "International Axion Observatory" (IAXO) have been studied in some detail [78]. Such a next-generation axion helioscope may also push the sensitivity in the product of couplings to photons and to electrons, $G_{A\gamma\gamma}g_{Aee}$, into a range beyond stellar energy-loss limits and test the hypothesis that WD, RG, and HB cooling is dominated by axion emission [61,79].

Other Primakoff searches for solar axions and ALPs have been carried out using crystal detectors, exploiting the coherent conversion of axions into photons when the axion angle of incidence satisfies a Bragg condition with a crystal plane [80]. However, none of these limits is more restrictive than the one derived from the constraint on the solar axion luminosity ($L_A \lesssim 0.10\,L_\odot$) discussed earlier.

Another idea is to look at the Sun with an x-ray satellite when the Earth is in between. Solar axions and ALPs would convert in the Earth magnetic field on the far side and could be detected [81]. The sensitivity to $G_{A\gamma\gamma}$ could be comparable to CAST, but only for much smaller m_A. Deep solar x-ray measurements with existing satellites, using the solar magnetosphere as conversion region, have reported preliminary limits on $G_{A\gamma\gamma}$ [82].

111.4.3. *Conversion of astrophysical photon fluxes* :

Large-scale B fields exist in astrophysics that can induce axion-photon oscillations. In practical cases, B is much smaller than in the laboratory, whereas the conversion region L is much larger. Therefore, while the product BL can be large, realistic sensitivities are usually restricted to very low-mass particles, far away from the "axion band" in a plot like Figure 111.1.

One example is SN 1987A, which would have emitted a burst of axion-like particles (ALPs) due to the Primakoff production in its core. They would have partially converted into γ-rays in the galactic B-field. The lack of a gamma-ray signal in the GRS instrument of the SMM satellite in coincidence with the observation of the neutrinos emitted from SN1987A therefore provides a strong bound on their coupling to photons [83]. Recently, this bound has been revisited and the underlying physics has been brought to the current state-of-the-art, as far as modelling of the supernova and the Milky-Way magnetic field are concerned, resulting in the limit [84]

$$|G_{A\gamma\gamma}| < 5.3\times10^{-12}\ \mathrm{GeV}^{-1},\ \text{for}\ \ m_A \lesssim 4.4\times10^{-10}\ \mathrm{eV}.$$

Magnetically induced oscillations between photons and axion-like particles (ALPs) can modify the photon fluxes from distant sources in various ways, featuring (i) frequency-dependent dimming, (ii) modified polarization, and (iii) avoiding absorption by propagation in the form of axions.

For example, dimming of SNe Ia could influence the interpretation in terms of cosmic acceleration [85], although it has become clear that photon-ALP conversion could only be a subdominant effect [86]. Searches for linearly polarised emission from magnetised white dwarfs [87] and changes of the linear polarisation from radio galaxies (see, e.g., Ref. [88]) provide limits close to $G_{A\gamma\gamma} \sim 10^{-11}\ \mathrm{GeV}^{-1}$, for masses $m_A \lesssim 10^{-7}$ eV and $m_A \lesssim 10^{-15}$ eV, respectively, albeit with uncertainties related to the underlying assumptions. Even stronger limits, $G_{A\gamma\gamma} \lesssim 2\times10^{-13}\ \mathrm{GeV}^{-1}$, for $m_A \lesssim 10^{-14}$ eV, have been obtained by exploiting high-precision measurements of quasar polarisations [89].

Remarkably, it appears that the universe could be too transparent to TeV γ-rays that should be absorbed by pair production on the extra-galactic background light [90]. The situation is not conclusive at present [91], but the possible role of photon-ALP oscillations in TeV γ-ray astronomy is tantalizing [92]. Fortunately, the region in ALP parameter space, $G_{A\gamma\gamma} \sim 10^{-12} - 10^{-10}\ \mathrm{GeV}^{-1}$ for $m_A \lesssim 10^{-7}$ eV [93], required to explain the anomalous TeV transparency of the universe, could be conceivably probed by the next generation of laboratory experiments (ALPS II) and helioscopes (IAXO) mentioned above. This parameter region can also be probed by searching for an irregular behavior of the gamma ray spectrum of distant active galactic nuclei (AGN), expected to arise from photon-ALP mixing in a limited energy range. The H.E.S.S. collaboration has set a limit of $|G_{A\gamma\gamma}| \lesssim 2.1\times10^{-11}\ \mathrm{GeV}^{-1}$, for $1.5\times10^{-8}\ \mathrm{eV} \lesssim m_A \lesssim 6.0\times10^{-8}$ eV, from the non-observation of an irregular behavior of the spectrum of the AGN PKS 2155 [94], see Figure 111.1. Recently, the Fermi-LAT collaboration has put an even more stringent limit on the ALP-photon coupling [95] from observations of the gamma ray spectrum of NGC 1275, the central galaxy of the Perseus cluster, see Figure 111.1.

At smaller masses, $m_A \lesssim 10^{-12}\,\mathrm{eV}$, galaxy clusters become highly efficient at interconverting ALPs and photons at x-ray energies. Constraints on spectral irregularities in the spectra of luminous x-ray sourced located in or behind galaxy clusters then lead to stringent upper limits on the ALP-photon coupling. Using Chandra and XMM-Newton observations of several local sources in galaxy clusters (Hydra A, M87, NGC 1275, NGC 3862, Seyfert galaxy 2E3140) leads to bounds $|G_{A\gamma\gamma}| \lesssim 1.5\times10^{-12}\ \mathrm{GeV}^{-1}$ [96].

111.4.4. *Superradiance of black holes* :

Light bosonic fields such as axions or ALPs can affect the dynamics and gravitational wave emission of rapidly rotating astrophysical black holes through the superradiance mechanism. When their Compton wavelength is of order of the black hole size, they form gravitational bound states around the black hole. Their occupation number grows exponentially by extracting energy and angular momentum from the black hole, forming a coherent axion or ALP bound state emitting gravitational waves. When accretion cannot replenish the spin of the black hole, superradiance dominates the black hole spin evolution; this is true for both supermassive and stellar mass black holes. The existence of destabilizing light bosonic fields thus leads to gaps in the mass vs. spin plot of rotating black holes. Stellar black hole spin measurements exploiting well-studied binaries and two independent techniques exclude a mass range $6\times10^{-13}\,\mathrm{eV} < m_A < 2\times10^{-11}\,\mathrm{eV}$ at $2\,\sigma$, which for the axion excludes $3\times10^{17}\,\mathrm{GeV} < f_A < 1\times10^{19}\,\mathrm{GeV}$ [97]. These bounds apply when gravitational interactions dominate over the axion self-interaction, which is true for the QCD axion in this mass range. Long lasting, monochromatic gravitational wave signals, which can be distinguished from ordinary astrophysical sources by their clustering in a narrow frequency range, are expected to be produced by axions or ALPs annihilating to gravitons. Gravitational waves could also be sourced by axions/ALPs transitioning between gravitationally bound levels. Accordingly, the gravitational wave detector Advanced LIGO should be sensitive to the axion in the $m_A \lesssim 10^{-10}\,\mathrm{eV}$ region. LIGO measurements of black hole spins in binary merger events could also provide statistical evidence for the presence of an axion [98]. Similar signatures could arise for supermassive black holes for particle with masses $\lesssim 10^{-15}\,\mathrm{eV}$. Gravitational waves from such sources could be detected at lower-frequency observatories such as LISA.

111.5. Cosmic Axions

111.5.1. *Cosmic axion populations* :

In the early universe, axions are produced by processes involving quarks and gluons [99]. After color confinement, the dominant thermalization process is $\pi + \pi \leftrightarrow \pi + A$ [23]. The resulting axion population would contribute a hot dark matter component in analogy to massive neutrinos. Cosmological precision data provide restrictive constraints on a possible hot dark-matter fraction that translate into $m_A \lesssim 1$ eV [100], but in detail depend on the used data set and assumed cosmological model. In the future, data from a EUCLID-like survey combined with Planck CMB data can detect hot dark matter axions with a mass $m_A \gtrsim 0.15\,\mathrm{eV}$ at very high significance [101].

For $m_A \gtrsim 20$ eV, axions decay fast on a cosmic time scale, removing the axion population while injecting photons. This excess radiation provides additional limits up to very large axion masses [102]. An anomalously small $G_{A\gamma\gamma}$ provides no loophole because suppressing

decays leads to thermal axions overdominating the mass density of the universe.

The main cosmological interest in axions derives from their possible role as cold dark matter (CDM). In addition to thermal processes, axions are abundantly produced by the "re-alignment mechanism" [103].

The axion dark matter abundance crucially depends on the cosmological history. Let us first consider the so called *pre-inflationary PQ symmetry breaking scenario*, in which the PQ symmetry is broken before and during inflation and not restored afterwards. After the breakdown of the PQ symmetry, the axion field relaxes somewhere in the bottom of the "mexican hat" potential. Near the QCD epoch, topological fluctuations of the gluon fields such as instantons explicitly break the PQ symmetry. This tilting of the"mexican hat" drives the axion field toward the CP-conserving minimum, thereby exciting coherent oscillations of the axion field that ultimately represent a condensate of CDM. The fractional cosmic mass density in this homogeneous field mode, created by this "vacuum realignment" (vr) mechanism, is [12,104,105,106],

$$\begin{aligned}\Omega_A^{\rm vr}h^2 &\approx 0.12\left(\frac{f_A}{9\times 10^{11}\ {\rm GeV}}\right)^{1.165} F\,\bar\Theta_{\rm i}^2\\ &\approx 0.12\left(\frac{6\ \mu{\rm eV}}{m_A}\right)^{1.165} F\,\Theta_{\rm i}^2\,,\end{aligned}\qquad (111.21)$$

where h is the present-day Hubble expansion parameter in units of 100 km s^{-1} Mpc^{-1}, and $-\pi \le \Theta_{\rm i} \le \pi$ is the initial "misalignment angle" relative to the CP-conserving position attained in the causally connected region which evolved into today's observable universe. $F = F(\Theta_{\rm i}, f_A)$ is a factor accounting for anharmonicities in the axion potential. For $F\Theta_{\rm i}^2 = \mathcal{O}(1)$, m_A should be above $\sim 6\,\mu$eV in order that the cosmic axion density does not exceed the observed CDM density, $\Omega_{\rm CDM}h^2 = 0.12$. However, much smaller axion masses (much higher PQ scales) are still possible if the initial value $\Theta_{\rm i}$ just happens to be small enough in today's observable universe ("anthropic axion window" [107]) .

Since the axion field is then present during inflation and thus subject to quantum fluctuations, the non-observation of the associated isocurvature fluctuations in the CMB puts severe constraints in the (f_A, r) plane, where r is the ratio of the power in tensor to the one in scalar fluctuations [108]. In fact, isocurvature constraints, combined with a future measurement of a sizeable r, would strongly disfavor axions with [109]

$$f_A \gtrsim 1.3\times 10^{13}\,{\rm GeV}\left(\frac{r}{0.1}\right)^{1/2},\ m_A \lesssim 0.4\ \mu{\rm eV}\left(\frac{r}{0.1}\right)^{-1/2}.$$

In the *post-inflationary PQ symmetry breaking scenario*, on the other hand, $\Theta_{\rm i}$ will take on different values in different patches of the present universe. The average contribution is [12,104,105,106]

$$\Omega_A^{\rm vr}h^2 \approx 0.12\left(\frac{30\ \mu{\rm eV}}{m_A}\right)^{1.165}. \qquad (111.22)$$

However, the presence of cosmic strings can decrease this quantity [106,110]. In fact, the decay of cosmic strings and domain walls gives rise to a different population of cold dark matter axions, whose abundance suffers from significant uncertainties. According to Sikivie and collaborators, these populations are comparable to the re-alignment contribution [111]. Other groups find a significantly enhanced axion density [105,106,112,113] or rather, a larger m_A value for axions providing CDM, namely

$$m_A \approx (50-200)\ \mu{\rm eV}, \qquad (111.23)$$

for models with short-lived (requiring unit color anomaly $N = 1$) domain walls, such as the KSVZ model. Very recently, a value of $m_A = (26.2 \pm 3.4)\,\mu$eV was predicted from an improved calculation including the effect of the large string tension and treating the re-alignment and string-wall contribution in a unified way [110]. For models with long-lived ($N > 1$) domain walls, such as an accidental DFSZ model [114], where the PQ symmetry is broken by higher dimensional Planck suppressed operators, the mass is predicted to be significantly higher [113,115],

$$m_A \approx (0.6-4)\,{\rm meV}, \qquad (111.24)$$

see Figure 111.2

In this post-inflationary PQ symmetry breakdown scenario, the spatial axion density variations are large at the QCD transition and they are not erased by free streaming. Gravitationally bound "axion miniclusters" form around and before matter-radiation equality [116]. A significant fraction of CDM axions can reside in these bound objects. Remarkably, the minicluster fraction can be bounded by gravitational lensing [117].

In the above predictions of the fractional cosmic mass density in axions, the exponent, 1.165, arises from the non-trivial temperature dependence of the topological susceptibility $\chi(T) = m_A^2(T)f_A^2$ at temperatures slighty above the QCD quark-hadron phase transition. Recent lattice QCD calculations of this exponent [12,118] found it to be remarkably close to the prediction of the dilute instanton gas approximation (see however [119]) which was previously exploited. Therefore, the state-of-the-art prediction of the axion mass relevant for dark matter for a fixed initial misalignment angle $\Theta_{\rm i}$ differs from the previous prediction by just a factor of order one.

The non-thermal production mechanisms attributed to axions are generic to light bosonic weakly interacting particles such as ALPs [120]. The relic abundance is set by the epoch when the axion mass becomes significant, $3H(t) \approx m_A(t)$, and ALP field oscillations begin. For ALPs to contribute to the dark matter density this epoch must occur before matter radiation equality. For a temperature independent ALP mass this leads to the bound:

$$m_A \gtrsim 7\times 10^{-28}\,{\rm eV}\left(\frac{\Omega_m\,h^2}{0.15}\right)^{1/2}\left(\frac{1+z_{\rm eq}}{3.4\times 10^3}\right)^{3/2}. \qquad (111.25)$$

ALPs lighter than this bound are allowed if their cosmic energy density is small, but they are quite distinct from other forms of dark matter [121]. Ignoring anharmonicities in the ALP potential, and taking the ALP mass to be temperature independent, the relic density in dark matter ALPs due to re-alignment is given by

$$\Omega_{\rm ALP}^{\rm vr}h^2 = 0.12\left(\frac{m_A}{4.7\times 10^{-19}\,{\rm eV}}\right)^{1/2}\left(\frac{f_A}{10^{16}\,{\rm GeV}}\right)^2\left(\frac{\Omega_m h^2}{0.15}\right)^{3/4}\left(\frac{1+z_{\rm eq}}{3.4\times 10^3}\right)^{-3/4}\Theta_{\rm i}^2\,.$$

An ALP decay constant near the GUT scale gives the correct relic abundance for *ultralight ALPs* (ULAs), which we now define. Extended discussions of ULAs can be found in Refs. [122,123].

The standard CDM model treats dark matter as a distribution of cold, collisionless particles interacting only via gravity. Below the Compton wavelength, $\lambda_c = 2\pi/m_A$, the particle description of ALPs breaks down. For large occupation numbers we can model ALPs below the Compton wavelength as a coherent classical field. Taking as a reference length scale the Earth radius, $R_\oplus = 6371\,$km, we define ULAs to be those axions with $\lambda_c > R_\oplus$, leading to the defining bound

$$m_{\rm ULA} < 2\times 10^{-13}\,{\rm eV}\,. \qquad (111.26)$$

ULAs encompass the entire Earth in a single coherent field. The coherence time of the ULA field on Earth can be estimated from the crossing time of the de Broglie wavelength at the virial velocity in the Milky Way, $\tau_{\rm coh.} \sim 1/m_A v_{\rm vir.}^2$.

We notice that by the definition, Equation 111.26, an ultralight QCD axion must have a super-Planckian decay constant, $f_A > 3\times 10^{19}\,$GeV and would require fine tuning of θ_i to provide the relic abundance. Natural models for ULAs can be found in string and M-theory compactifications [6], in field theory with accidental symmetries [124], or new hidden strongly coupled sectors [125].

In addition to the gravitational potential energy, the ULA field also carries gradient energy. On scales where the gradient energy is non-negligible, ULAs acquire an effective pressure and do not behave as CDM. The gradient energy opposes gravitational collapse, leading to a Jeans scale below which perturbations are stable [126]. The Jeans scale suppresses linear cosmological structure formation relative to CDM [127]. The Jeans scale at matter-radiation equality in the case that ULAs make up all of CDM is:

$$k_{\rm J,eq} = 8.7\,{\rm Mpc}^{-1}\left(\frac{1+z_{\rm eq}}{3.4\times10^3}\right)^{-1/4}\left(\frac{\Omega^{\rm vr}_{\rm ALP}}{0.12}\right)^{1/4}\left(\frac{m_A}{10^{-22}\,{\rm eV}}\right)^{1/2}$$

On non-linear scales the gradient energy leads to the existence of a class of pseudo-solitons known as oscillatons, or axion stars [128].

Cosmological and astrophysical observations are consistent with the CDM model, and departures from it are only allowed on the scales of the smallest observed dark matter structures with $M \sim 10^{6-8} M_\odot$. The CMB power spectrum and galaxy auto-correlation power spectrum limit the ULA mass to $m_{\rm ULA} > 10^{-24}\,{\rm eV}$ from linear theory of structure formation [121,129]. Analytic models [130] and N-body simulations [131] for non-linear structures show that halo formation is suppressed in ULA models relative to CDM. This leads to constraints on the ULA mass of $m_{\rm ULA} > 10^{-22}\,{\rm eV}$ from observations of high-z galaxies [131,132], and $m_{\rm ULA} > 10^{-21}\,{\rm eV}$ from the Lyman-alpha forest flux power spectrum [133]. Including the effects of anharmonicities on structure formation with ALPs can weaken these bounds if the misalignment angle $\Theta_{\rm i} \approx \pi$ [134]. Cosmological simulations that treat gradient energy in the ULA field beyond the N-body approximation have just recently become available [135,136], and show, among other things, evidence for the formation of axion stars in the centres of ULA halos. These central axion stars have been conjectured to play a role in the apparently cored density profiles of dwarf spheroidal galaxies [135,137], and may have many other observational consequences [138].

111.5.2. *Telescope searches* :

The two-photon decay is extremely slow for axions with masses in the CDM regime, but could be detectable for eV masses. The signature would be a quasi-monochromatic emission line from galaxies and galaxy clusters. The expected optical line intensity for DFSZ axions is similar to the continuum night emission. An early search in three rich Abell clusters [139], and a recent search in two rich Abell clusters [140], exclude the "Telescope" range in Figure 111.1 and Figure 111.2 unless the axion-photon coupling is strongly suppressed. Of course, axions in this mass range would anyway provide an excessive hot DM contribution.

Very low-mass axions in halos produce a weak quasi-monochromatic radio line. Virial velocities in undisrupted dwarf galaxies are very low, and the axion decay line would therefore be extremely narrow. A search with the Haystack radio telescope on three nearby dwarf galaxies provided a limit $|G_{A\gamma\gamma}| < 1.0\times10^{-9}$ GeV^{-1} at 96% CL for $298 < m_A < 363$ μeV [141]. However, this combination of m_A and $G_{\rm A\gamma\gamma}$ does not exclude plausible axion models.

111.5.3. *Microwave cavity experiments* :

The limits of Figure 111.2 suggest that axions, if they exist, provide a significant fraction or even perhaps all of the cosmic CDM. In a broad range of the plausible m_A range for CDM, galactic halo axions may be detected by their resonant conversion into a quasi-monochromatic microwave signal in a high-Q electromagnetic cavity permeated by a strong static B field [5,142]. The cavity frequency is tunable, and the signal is maximized when the frequency is the total axion energy, rest mass plus kinetic energy, of $\nu = (m_A/2\pi)\,[1+\mathcal{O}(10^{-6})]$, the width above the rest mass representing the virial distribution in the galaxy. The frequency spectrum may also contain finer structure from axions more recently fallen into the galactic potential and not yet completely virialized [143].

The feasibility of this technique was established in early experiments of relatively small sensitive volume, $\mathcal{O}(1$ liter), with HFET-based amplifiers, setting limits in the range $4.5 < m_A < 16.3$ μeV [144], but lacking by 2–3 orders of magnitude the sensitivity required to detect realistic axions. Later, ADMX ($B \sim 8$ T, $V \sim 200$ liters) has achieved sensitivity to KSVZ axions, assuming they saturate the local dark matter density and are well virialized, over the mass range 1.9–3.3 μeV [145]. Should halo axions have a significant component not yet virialized, ADMX is sensitive to DFSZ axions [146]. The corresponding 90% CL exclusion regions shown in Figure 111.3 are normalized to an assumed local CDM density of 7.5×10^{-25} g cm^{-3} (450 MeV cm^{-3}). More recently the ADMX experiment commissioned an upgrade [147] that replaces the microwave HFET amplifiers by near quantum-limited low-noise dc SQUID microwave amplifiers [148], allowing for a significantly improved sensitivity. This apparatus is also sensitive to other hypothetical light bosons, such as hidden photons or chameleons, over a limited parameter space [120,149]. Recently, the HAYSTAC experiment reported on first results from a new microwave cavity search for dark matter axions with masses above 20 μeV. They exclude axions with two-photon coupling $|G_{A\gamma\gamma}| \gtrsim 2\times10^{-14}\,{\rm GeV}^{-1}$ over the range $23.55\,\mu{\rm eV} < m_A < 24.0\,\mu{\rm eV}$ [150]. Exploiting a Josephson parametric amplifier, this experiment has demonstrated total noise approaching the standard quantum limit for the first time in an axion search. A Rydberg atom single-photon detector [151] can in principle evade the standard quantum limit for coherent photon detection. The ORGAN experiment is designed to probe axions in the mass range $60\,\mu{\rm eV} < m_A < 210\,\mu{\rm eV}$. In a pathfinding run, it has set a limit on $|G_{A\gamma\gamma}| < 2\times10^{-12}\,{\rm GeV}^{-1}$ at 110 μeV, in a span of 2.5 neV [152]. There are further microwave cavity axion dark matter experiment in construction (CULTASK [153]) or proposed (KLASH [154]) .

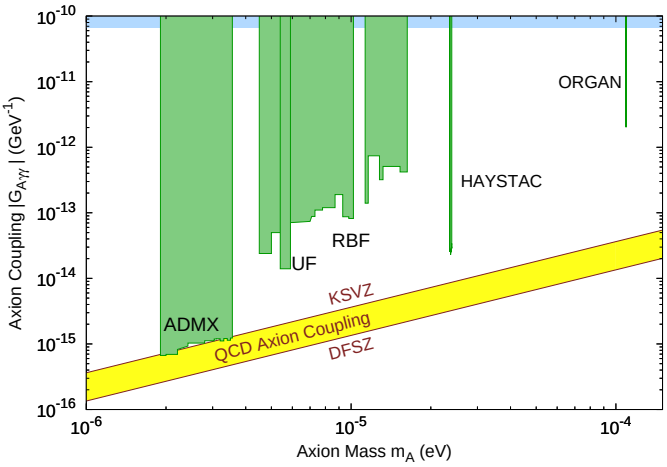

Figure 111.3: Exclusion region reported from the microwave cavity experiments RBF and UF [144], ADMX [145,147], HAYSTAC [150] and ORGAN [152]. A local dark-matter density of 450 MeV cm^{-3} is assumed.

111.5.4. *New concepts for axion dark matter direct detection* :

Other new concepts for searching for axion dark matter are also being investigated. An alternative to the microwave cavity technique is based on a novel detector architecture consisting of an open, Fabry-Perot resonator and a series of current-carrying wire planes [155]. The Orpheus detector has demonstrated this new technique, excluding dark matter ALPs with masses between 68.2 and 76.5 μeV and axion-photon couplings greater than $4\times10^{-7}\,{\rm GeV}^{-1}$. This technique may be able to probe dark matter axions in the mass range from 40 to 700 μeV. Another detector concept exploits the fact that a magnetized mirror would radiate photons in the background of axion dark matter, which could be collected like in a dish antenna [156]. Searches for hidden photon dark matter exploiting this technique are already underway [157]. The proposed MADMAX experiment will place a stack of dielectric layers in front of the magnetized mirror in

order to resonantly enhance the photon signal, aiming a sensitivity to probe the mass range $50\,\mu\text{eV} \lesssim m_A \lesssim 200\,\mu\text{eV}$ [158]. Another proposed axion dark matter search method sensitive in the 100 μeV mass range is to cool a kilogram-sized sample to mK temperatures and count axion induced atomic transitions using laser techniques [159].

The oscillating galactic dark matter axion field induces oscillating nuclear electric dipole moments (EDMs). These EDMs cause the precession of nuclear spins in a nucleon spin polarized sample in the presence of an electric field. The resulting transverse magnetization can be searched for by exploiting magnetic-resonance (MR) techniques, which are most sensitive in the range of low oscillation frequencies corresponding to sub-neV axion masses. The aim of the corresponding Cosmic Axion Spin Precession Experiment (CASPEr) [160] is to probe axion dark matter in the anthropic window, $f_A \gtrsim 10^{15}\,\text{GeV}$, corresponding to $m_A \lesssim$neV, complementary to the classic axion window probed by the RF cavity technique.

In the intermediate mass region, $\text{neV} \lesssim m_A \lesssim 0.1\,\mu\text{eV}$, one may exploit a cooled LC circuit and precision magnetometry to search for the oscillating electric current induced by dark matter axions in a strong magnetic field [161]. A similar approach is followed by the proposed ABRACADABRA [162] and DM-Radio Pathfinder [163] experiments.

An eventually non-zero axion electron coupling g_{Aee} will lead to an electron spin precession about the axion dark matter wind [164]. The QUAX (QUaerere AXions) experiment aims at exploiting MR inside a magnetized material [165]. Because of the higher Larmor frequency of the electron, it is sensitive in the classic window.

111.6. Conclusions

There is a strengthening physics case for very weakly coupled light particles beyond the Standard Model. The elegant solution of the strong CP problem proposed by Peccei and Quinn yields a particularly strong motivation for the axion. In many theoretically appealing ultraviolet completions of the Standard Model axions and axion-like particles occur automatically. Moreover, they are natural cold dark matter candidates. Perhaps the first hints of their existence have already been seen in the anomalous excessive cooling of stars and the anomalous transparency of the Universe for VHE gamma rays. Interestingly, a significant portion of previously unexplored, but phenomenologically very interesting and theoretically very well motivated axion and ALP parameter space can be tackled in the foreseeable future by a number of terrestrial experiments searching for axion/ALP dark matter, for solar axions/ALPs, and for light apparently shining through a wall.

References:

1. R.D. Peccei and H. Quinn, Phys. Rev. Lett. **38**, 1440 (1977); Phys. Rev. **D16**, 1791 (1977).
2. S. Weinberg, Phys. Rev. Lett. **40**, 223 (1978); F. Wilczek, Phys. Rev. Lett. **40**, 279 (1978).
3. F. Wilczek, Phys. Rev. Lett. **49**, 1549 (1982).
4. Y. Chikashige, R.N. Mohapatra, and R.D. Peccei, Phys. Lett. **B98**, 265 (1981); G.B. Gelmini and M. Roncadelli, Phys. Lett. **B99**, 411 (1981).
5. P. Sikivie, Phys. Rev. Lett. **51**, 1415 (1983) and Erratum *ibid.*, **52**, 695 (1984).
6. E. Witten, Phys. Lett. **B149**, 351 (1984); J.P. Conlon, JHEP **0605**, 078 (2006); P. Svrcek and E. Witten, JHEP **0606**, 051 (2006); K.-S. Choi *et al.*, Phys. Lett. **B675**, 381 (2009); A. Arvanitaki *et al.*, Phys. Rev. **D81**, 123530 (2010); B.S. Acharya, K. Bobkov, and P. Kumar, JHEP **1011**, 105 (2010); M. Cicoli, M. Goodsell, and A. Ringwald, JHEP **1210**, 146 (2012); J. Halverson, C. Long and P. Nath, Phys. Rev. **D96**, 056025 (2017).
7. J. Jaeckel and A. Ringwald, Ann. Rev. Nucl. and Part. Sci. **60**, 405 (2010); A. Ringwald, Phys. Dark Univ. **1**, 116 (2012); J. Jaeckel, Frascati Phys. Ser. **56**, 172 (2013).
8. C.A. Baker *et al.*, Phys. Rev. Lett. **97**, 131801 (2006).
9. H. Georgi, D.B. Kaplan, and L. Randall, Phys. Lett. **B169**, 73 (1986).
10. R.J. Crewther, Phys. Lett. **B70**, 349 (1977); P. Di Vecchia and G. Veneziano, Nucl. Phys. **B171**, 253 (1980).
11. G.G. di Cortona *et al.*, JHEP **1601**, 034 (2016).
12. S. Borsanyi *et al.*, Nature **539**, 69 (2016).
13. T.W. Donnelly *et al.*, Phys. Rev. **D18**, 1607 (1978); S. Barshay *et al.*, Phys. Rev. Lett. **46**, 1361 (1981); A. Barroso and N.C. Mukhopadhyay, Phys. Lett. **B106**, 91 (1981); R.D. Peccei, in *Proceedings of Neutrino '81*, Honolulu, Hawaii, Vol. 1, p. 149 (1981); L.M. Krauss and F. Wilczek, Phys. Lett. **B173**, 189 (1986).
14. J. Schweppe *et al.*, Phys. Rev. Lett. **51**, 2261 (1983); T. Cowan *et al.*, Phys. Rev. Lett. **54**, 1761 (1985).
15. R.D. Peccei, T.T. Wu, and T. Yanagida, Phys. Lett. **B172**, 435 (1986).
16. W.A. Bardeen, R.D. Peccei, and T. Yanagida, Nucl. Phys. **B279**, 401 (1987).
17. J.E. Kim, Phys. Rev. Lett. **43**, 103 (1979); M.A. Shifman, A.I. Vainstein, and V.I. Zakharov, Nucl. Phys. **B166**, 493 (1980).
18. M. Dine, W. Fischler, and M. Srednicki, Phys. Lett. **B104**, 199 (1981); A.R. Zhitnitsky, Sov. J. Nucl. Phys. **31**, 260 (1980).
19. J.E. Kim and G. Carosi, Rev. Mod. Phys. **82**, 557 (2010).
20. J.E. Kim, Phys. Rev. **D58**, 055006 (1998); L. Di Luzio, F. Mescia and E. Nardi, Phys. Rev. Lett. **118**, 031801 (2017).
21. G. Raffelt and D. Seckel, Phys. Rev. Lett. **60**, 1793 (1988); M. Carena and R.D. Peccei, Phys. Rev. **D40**, 652 (1989); K. Choi, K. Kang, and J.E. Kim, Phys. Rev. Lett. **62**, 849 (1989).
22. M. Srednicki, Nucl. Phys. **B260**, 689 (1985).
23. S. Chang and K. Choi, Phys. Lett. **B316**, 51 (1993).
24. H. Leutwyler, Phys. Lett. **B378**, 313 (1996).
25. Mini review on Quark Masses in C. Patrignani *et al.* (Particle Data Group), Chin. Phys. C **40**, 100001 (2016).
26. D.A. Dicus *et al.*, Phys. Rev. **D18**, 1829 (1978).
27. G. Raffelt and L. Stodolsky, Phys. Rev. **D37**, 1237 (1988).
28. A.A. Anselm, Yad. Fiz. **42**, 1480 (1985); K. van Bibber *et al.*, Phys. Rev. Lett. **59**, 759 (1987).
29. G. Ruoso *et al.*, Z. Phys. **C56**, 505 (1992); R. Cameron *et al.*, Phys. Rev. **D47**, 3707 (1993).
30. M. Fouche *et al.* (BMV Collab.), Phys. Rev. **D78**, 032013 (2008); P. Pugnat *et al.* (OSQAR Collab.), Phys. Rev. **D78**, 092003 (2008); A. Chou *et al.* (GammeV T-969 Collab), Phys. Rev. Lett. **100**, 080402 (2008); A. Afanasev *et al.* (LIPSS Collab.), Phys. Rev. Lett. **101**, 120401 (2008); K. Ehret *et al.* (ALPS Collab.), Phys. Lett. **B689**, 149 (2010); P. Pugnat *et al.* (OSQAR Collab.), Eur. Phys. J. **C74**, 3027 (2014).
31. R. Ballou *et al.* (OSQAR Collab.), Phys. Rev. **D92**, 092002 (2015).
32. F. Hoogeveen and T. Ziegenhagen, Nucl. Phys. **B358**, 3 (1991); P. Sikivie, D. Tanner, and K. van Bibber, Phys. Rev. Lett. **98**, 172002 (2007); G. Mueller *et al.*, Phys. Rev. **D80**, 072004 (2009).
33. R. Baehre *et al.* (ALPS Collab.), JINST **1308**, T09001 (2013).
34. F. Hoogeveen, Phys. Lett. **B288**, 195 (1992); J. Jaeckel and A. Ringwald, Phys. Lett. **B659**, 509 (2008); F. Caspers, J. Jaeckel, and A. Ringwald, JINST **0904**, P11013 (2009).
35. R. Povey, J. Hartnett, and M. Tobar, Phys. Rev. **D82**, 052003 (2010); A. Wagner *et al.*, Phys. Rev. Lett. **105**, 171801 (2010).
36. M. Betz *et al.*, Phys. Rev. **D88**, 075014 (2013).

37. L. Maiani *et al.*, Phys. Lett. **B175**, 359 (1986).
38. Y. Semertzidis *et al.*, Phys. Rev. Lett. **64**, 2988 (1990).
39. E. Zavattini *et al.* (PVLAS Collab.), Phys. Rev. Lett. **96**, 110406 (2006).
40. E. Zavattini *et al.* (PVLAS Collab.), Phys. Rev. **D77**, 032006 (2008).
41. F. Della Valle *et al.* (PVLAS Collab.), Eur. Phys. J. **C76**, 24 (2016).
42. E. Fischbach and C. Talmadge, Nature **356**, 207 (1992).
43. J.E. Moody and F. Wilczek, Phys. Rev. **D30**, 130 (1984);
A.N. Youdin *et al.*, Phys. Rev. Lett. **77**, 2170 (1996);
Wei-Tou Ni *et al.*, Phys. Rev. Lett. **82**, 2439 (1999);
D.F. Phillips *et al.*, Phys. Rev. **D63**, 111101 (2001);
B.R. Heckel *et al.* (Eöt-Wash Collab.), Phys. Rev. Lett. **97**, 021603 (2006);
S.A. Hoedl *et al.*, Phys. Rev. Lett. **106**, 041801 (2011).
44. G. Raffelt, Phys. Rev. **D86**, 015001 (2012).
45. A. Arvanitaki and A.A. Geraci, Phys. Rev. Lett. **113**, 161801 (2014).
46. M.S. Turner, Phys. Reports **197**, 67 (1990);
G.G. Raffelt, Phys. Reports **198**, 1 (1990).
47. G.G. Raffelt, *Stars as Laboratories for Fundamental Physics*, (Univ. of Chicago Press, Chicago, 1996).
48. G.G. Raffelt, Lect. Notes Phys. **741**, 51 (2008).
49. S. Andriamonje *et al.* (CAST Collab.), JCAP **0704**, 010 (2007).
50. P. Gondolo and G. Raffelt, Phys. Rev. **D79**, 107301 (2009).
51. H. Schlattl, A. Weiss, and G. Raffelt, Astropart. Phys. **10**, 353 (1999).
52. N. Vinyoles *et al.*, JCAP **1510**, 015 (2015).
53. A. Ayala *et al.*, Phys. Rev. Lett. **113**, 191302 (2014);
O. Straniero *et al.*, doi:10.3204/DESY-PROC-2015-02/straniero_oscar.
54. J. Redondo, JCAP **1312**, 008 (2013).
55. N. Viaux *et al.*, Phys. Rev. Lett. **111**, 231301 (2013).
56. G.G. Raffelt, Phys. Lett. **B166**, 402 (1986);
S.I. Blinnikov and N.V. Dunina-Barkovskaya, Mon. Not. R. Astron. Soc. **266**, 289 (1994).
57. M.M. Miller Bertolami *et al.*, JCAP **1410**, 069 (2014).
58. J. Isern *et al.*, Astrophys. J. Lett. **682**, L109 (2008);
J. Isern *et al.*, J. Phys. Conf. Ser. **172**, 012005 (2009).
59. J. Isern *et al.*, Astron. & Astrophys. **512**, A86 (2010);
A.H. Córsico *et al.*, Mon. Not. Roy. Astron. Soc. **424**, 2792 (2012);
A.H. Córsico *et al.*, JCAP **1212**, 010 (2012).
60. T. Fischer *et al.*, Phys. Rev. **D94**, 085012 (2016).
61. M. Giannotti *et al.*, JCAP **1710**, 010 (2017).
62. J. Engel, D. Seckel, and A.C. Hayes, Phys. Rev. Lett. **65**, 960 (1990).
63. T. Moroi and H. Murayama, Phys. Lett. **B440**, 69 (1998).
64. L.B. Leinson, JCAP **1408**, 031 (2014).
65. J. Keller and A. Sedrakian, Nucl. Phys. **A897**, 62 (2013);
A. Sedrakian, Phys. Rev. **D93**, 065044 (2016).
66. L.B. Leinson, Phys. Lett. **B741**, 87 (2015).
67. M. Giannotti *et al.*, JCAP **1605**, 057 (2016).
68. G.G. Raffelt, J. Redondo, and N. Viaux Maira, Phys. Rev. **D84**, 103008 (2011).
69. K. van Bibber *et al.*, Phys. Rev. **D39**, 2089 (1989).
70. D. Lazarus *et al.*, Phys. Rev. Lett. **69**, 2333 (1992).
71. S. Moriyama *et al.*, Phys. Lett. **B434**, 147 (1998);
Y. Inoue *et al.*, Phys. Lett. **B536**, 18 (2002).
72. M. Minowa *et al.*, Phys. Lett. **B668**, 93 (2008).
73. V. Anastassopoulos *et al.*, Nature Phys. **13**, 584 (2017).
74. E. Arik *et al.* (CAST Collab.), JCAP **0902**, 008 (2009).
75. S. Aune *et al.* (CAST Collab.), Phys. Rev. Lett. **107**, 261302 (2011);
M. Arik *et al.* (CAST Collab.), Phys. Rev. Lett. **112**, 091302 (2014);
M. Arik *et al.* (CAST Collab.), Phys. Rev. **D92**, 021101 (2015).
76. E. Armengaud *et al.* (EDELWEISS-II Collab.), JCAP **1311**, 067 (2013);
E. Aprile *et al.* (XENON100 Collab.), Phys. Rev. **D90**, 062009 (2014) and Erratum *ibid.*, **95**,029904(2017).
77. D. S. Akerib *et al.* (LUX Collab.), Phys. Rev. Lett. **118**, 261301 (2017).
78. E. Armengaud *et al.*, JINST **9**, T05002 (2014).
79. K. Barth *et al.*, JCAP **1305**, 010 (2013).
80. F.T. Avignone III *et al.*, Phys. Rev. Lett. **81**, 5068 (1998);
S. Cebrian *et al.*, Astropart. Phys. **10**, 397 (1999);
A. Morales *et al.* (COSME Collab.), Astropart. Phys. **16**, 325 (2002);
R. Bernabei *et al.*, Phys. Lett. **B515**, 6 (2001);
Z. Ahmed *et al.* (CDMS Collab.), Phys. Rev. Lett. **103**, 141802 (2009);
E. Armengaud *et al.* (EDELWEISS Collab.), JCAP **1311**, 067 (2013).
81. H. Davoudiasl and P. Huber, Phys. Rev. Lett. **97**, 141302 (2006).
82. H.S. Hudson *et al.*, ASP Conf. Ser. **455**, 25 (2012).
83. J.W. Brockway, E.D. Carlson, and G.G. Raffelt, Phys. Lett. **B383**, 439 (1996);
J.A. Grifols, E.Massó, and R. Toldrà, Phys. Rev. Lett. **77**, 2372 (1996).
84. A. Payez *et al.*, JCAP **1502**, 006 (2015).
85. C. Csaki, N. Kaloper, and J. Terning, Phys. Rev. Lett. **88**, 161302 (2002).
86. A. Mirizzi, G.G. Raffelt, and P.D. Serpico, Lect. Notes Phys. **741**, 115 (2008).
87. R. Gill and J. S. Heyl, Phys. Rev. **D84**, 085001 (2011).
88. D. Horns *et al.*, Phys. Rev. **D85**, 085021 (2012).
89. A. Payez, J.R. Cudell, and D. Hutsemekers, JCAP **1207**, 041 (2012).
90. D. Horns and M. Meyer, JCAP **1202**, 033 (2012).
91. J. Biteau and D.A. Williams, Astrophys. J. **812**, 60 (2015).
92. A. De Angelis, G. Galanti, and M. Roncadelli, Phys. Rev. **D84**, 105030 (2011);
M. Simet, D. Hooper, and P.D. Serpico, Phys. Rev. **D77**, 063001 (2008);
M.A. Sanchez-Conde *et al.*, Phys. Rev. **D79**, 123511 (2009).
93. M. Meyer, D. Horns, and M. Raue, Phys. Rev. **D87**, 035027 (2013).
94. A. Abramowski *et al.* (H.E.S.S. Collab.), Phys. Rev. **D88**, 102003 (2013).
95. M. Ajello *et al.* (Fermi-LAT Collab.), Phys. Rev. Lett. **116**, 161101 (2016).
96. D. Wouters and P. Brun, Astrophys. J. **772**, 44 (2013);
M. Berg *et al.*, `arXiv:1605.01043` [astro-ph.HE];
M. C. D. Marsh *et al.*, `arXiv:1703.07354` [hep-ph];
J. P. Conlon *et al.*, JCAP **1707**, 005 (2017).
97. A. Arvanitaki *et al.*, Phys. Rev. **D81**, 123530 (2010);
A. Arvanitaki and S. Dubovsky, Phys. Rev. **D83**, 044026 (2011);
A. Arvanitaki, M. Baryakhtar, and X. Huang, Phys. Rev. **D91**, 084011 (2015).
98. A. Arvanitaki *et al.*, Phys. Rev. **D95**, 043001 (2017).
99. M.S. Turner, Phys. Rev. Lett. **59**, 2489 (1987) and Erratum *ibid.*, **60**, 1101 (1988);
E. Massó, F. Rota, and G. Zsembinszki, Phys. Rev. **D66**, 023004 (2002);
P. Graf and F. D. Steffen, Phys. Rev. **D83**, 075011 (2011).
100. S. Hannestad *et al.*, JCAP **1008**, 001 (2010);
M. Archidiacono *et al.*, JCAP **1310**, 020 (2013);
E. Di Valentino *et al.*, Phys. Lett. **B752**, 182 (2016).
101. M. Archidiacono *et al.*, JCAP **1505**, 050 (2015).
102. E. Massó and R. Toldra, Phys. Rev. **D55**, 7967 (1997);
D. Cadamuro and J. Redondo, JCAP **1202**, 032 (2012).
103. J. Preskill, M.B. Wise, and F. Wilczek, Phys. Lett. **B120**, 127 (1983);
L.F. Abbott and P. Sikivie, Phys. Lett. **B120**, 133 (1983);
M. Dine and W. Fischler, Phys. Lett. **B120**, 137 (1983).
104. K.J. Bae, J.-H. Huh, and J.E. Kim, JCAP **0809**, 005 (2008).
105. O. Wantz and E.P.S. Shellard, Phys. Rev. **D82**, 123508 (2010).

106. G. Ballesteros, J. Redondo, A. Ringwald and C. Tamarit, JCAP **1708**, 001 (2017).
107. M. Tegmark *et al.*, Phys. Rev. **D73**, 023505 (2006).
108. M. Beltrán, J. García-Bellido, and J. Lesgourgues, Phys. Rev. **D75**, 103507 (2007);
M.P. Hertzberg, M. Tegmark, and F. Wilczek, Phys. Rev. **D78**, 083507 (2008);
J. Hamann *et al.*, JCAP **0906**, 022 (2009);
P.A.R. Ade *et al.* [Planck Collab.], Astron. & Astrophys. **571**, A22 (2014);
P.A.R. Ade *et al.* [Planck Collab.], Astrophys. Space Sci. **361**, 58 (2016).
109. P. Fox, A. Pierce, and S.D. Thomas, `hep-th/0409059`;
D.J.E. Marsh *et al.*, Phys. Rev. Lett. **113**, 011801 (2014);
L. Visinelli and P. Gondolo, Phys. Rev. Lett. **113**, 011802 (2014).
110. V. B. Klaer and G. D. Moore, `arXiv:1708.07521` [hep-ph].
111. S. Chang, C. Hagmann and P. Sikivie, Phys. Rev. **D59**, 023505 (1999);
C. Hagmann, S. Chang and P. Sikivie, Phys. Rev. **D63**, 125018 (2001).
112. T. Hiramatsu *et al.*, Phys. Rev. **D83**, 123531 (2011);
T. Hiramatsu *et al.*, Phys. Rev. **D85**, 105020 (2012) and Erratum *ibid.*, **86**, 089902 (2012).
113. M. Kawasaki, K. Saikawa, and T. Sekiguchi, Phys. Rev. **D91**, 065014 (2015).
114. A. Ringwald and K. Saikawa, Phys. Rev. **D94**, 049908 (2016) and Addendum *ibid.*, **94**, 049908 (2016).
115. T. Hiramatsu, M. Kawasaki, K. Saikawa and T. Sekiguchi, JCAP **1301**, 001 (2013).
116. E.W. Kolb and I.I. Tkachev, Phys. Rev. Lett. **71**, 3051 (1993);
K.M. Zurek, C.J. Hogan, and T.R. Quinn, Phys. Rev. **D75**, 043511 (2007).
117. E.W. Kolb and I.I. Tkachev, Astrophys. J. **460**, L25 (1996);
M. Fairbairn, D. J. E. Marsh and J. Quevillon, Phys. Rev. Lett. **119**, 021101 (2017).
118. E. Berkowitz, M. I. Buchoff and E. Rinaldi, Phys. Rev. **D92**, 034507 (2015);
S. Borsanyi *et al.*, Phys. Lett. **B752**, 175 (2016);
R. Kitano and N. Yamada, JHEP **1510**, 136 (2015);
P. Petreczky, H. P. Schadler and S. Sharma, Phys. Lett. **B762**, 498 (2016);
Y. Taniguchi *et al.*, Phys. Rev. **D95**, 054502 (2017).
119. C. Bonati *et al.*, JHEP **1603**, 155 (2016).
120. P. Arias *et al.*, JCAP **1206**, 013 (2012).
121. R. Hlozek *et al.*, Phys. Rev. **D91**, 103512 (2015).
122. D. J. E. Marsh, Phys. Rept. **643**, 1 (2016).
123. L. Hui, J. P. Ostriker, S. Tremaine and E. Witten, Phys. Rev. **D95**, 043541 (2017).
124. A. G. Dias *et al.*, JHEP **1406**, 037 (2014);
J. E. Kim and D. J. E. Marsh, Phys. Rev. **D93**, 025027 (2016).
125. H. Davoudiasl and C. W. Murphy, Phys. Rev. Lett. **118**, 141801 (2017).
126. M. Khlopov *et al.*, Mon. Not. Roy. Astron. Soc. **215**, 575 (1985)..
127. W. Hu, R. Barkana and A. Gruzinov, Phys. Rev. Lett. **85**, 1158 (2000);
L. Amendola and R. Barbieri, Phys. Lett. **B642**, 192 (2006);
D. J. E. Marsh and P. G. Ferreira, Phys. Rev. **D82**, 103528 (2010).
128. E. Seidel and W. M. Suen, Phys. Rev. Lett. **66**, 1659 (1991).
129. R. Hlozek, D. J. E. Marsh and D. Grin, `arXiv:1708.05681` [astro-ph.CO].
130. D. J. E. Marsh and J. Silk, Mon. Not. Roy. Astron. Soc. **437**, 2652 (2014).
131. H. Y. Schive, T. Chiueh, T. Broadhurst and K. W. Huang, Astrophys. J. 818,89(2016).
132. B. Bozek *et al.*, Mon. Not. Roy. Astron. Soc. **450**, 209 (2015);
P. S. Corasaniti, *et al.*, Phys. Rev. **D95**, 083512 (2017).
133. E. Armengaud *et al.*, Mon. Not. Roy. Astron. Soc. **471**, 4606 (2017);
V. Irsic *et al.*, Phys. Rev. Lett. **119**, 031302 (2017);
T. Kobayashi *et al.*, `arXiv:1708.00015` [astro-ph.CO].
134. H. Y. Schive and T. Chiueh, `arXiv:1706.03723` [astro-ph.CO].
135. H. Y. Schive, T. Chiueh and T. Broadhurst, Nature Phys. **10**, 496 (2014).
136. B. Schwabe, J. C. Niemeyer and J. F. Engels, Phys. Rev. **D94**, 043513 (2016);
J. Veltmaat and J. C. Niemeyer, Phys. Rev. **D94**, 123523 (2016);
P. Mocz *et al.*, `1705.05845` [astro-ph.CO].
137. D. J. E. Marsh and A. R. Pop, Mon. Not. Roy. Astron. Soc. **451**, 2479 (2015);
S. R. Chen *et al.*, Mon. Not. Roy. Astron. Soc. **468**, 1338 (2017);
A. X. Gonzles-Morales *et al.*, Mon. Not. Roy. Astron. Soc. **472**, 1346 (2017).
138. D. G. Levkov, A. G. Panin and I. I. Tkachev, Phys. Rev. Lett. **118**, 011301 (2017);
T. Helfer *et al.*, JCAP **1703**, 055 (2017);
J. Eby, M. Ma, P. Suranyi and L. C. R. Wijewardhana, `1705.05385` [hep-ph].
139. M. Bershady *et al.*, Phys. Rev. Lett. **66**, 1398 (1991);
M. Ressell, Phys. Rev. **D44**, 3001 (1991).
140. D. Grin *et al.*, Phys. Rev. **D75**, 105018 (2007).
141. B.D. Blout *et al.*, Astrophys. J. **546**, 825 (2001).
142. P. Sikivie, Phys. Rev. **D32**, 2988 (1985);
L. Krauss *et al.*, Phys. Rev. Lett. **55**, 1797 (1985);
R. Bradley *et al.*, Rev. Mod. Phys. **75**, 777 (2003).
143. P. Sikivie and J. Ipser, Phys. Lett. **B291**, 288 (1992);
P. Sikivie *et al.*, Phys. Rev. Lett. **75**, 2911 (1995).
144. S. DePanfilis *et al.*, Phys. Rev. Lett. **59**, 839 (1987);
W. Wuensch *et al.*, Phys. Rev. **D40**, 3153 (1989);
C. Hagmann *et al.*, Phys. Rev. **D42**, 1297 (1990).
145. S. Asztalos *et al.*, Phys. Rev. **D69**, 011101 (2004).
146. L. Duffy *et al.*, Phys. Rev. Lett. **95**, 091304 (2005);
J. Hoskins *et al.*, Phys. Rev. **D84**, 121302 (2011).
147. S.J. Asztalos *et al.* (ADMX Collab.), Phys. Rev. Lett. **104**, 041301 (2010).
148. S.J. Asztalos *et al.*, Nucl. Instrum. Methods **A656**, 39 (2011).
149. G. Rybka *et al.*, Phys. Rev. Lett. **105**, 051801 (2010);
A. Wagner *et al.*, Phys. Rev. Lett. **105**, 171801 (2010).
150. B. M. Brubaker *et al.*, Phys. Rev. Lett. **118**, 061302 (2017).
151. I. Ogawa, S. Matsuki, and K. Yamamoto, Phys. Rev. **D53**, 1740 (1996);
Y. Kishimoto *et al.*, Phys. Lett. **A303**, 279 (2002);
M. Tada *et al.*, Phys. Lett. **A303**, 285 (2002);
T.Haseyama *et al.*, J. Low Temp. Phys. **150**, 549 (2008).
152. B. T. McAllister *et al.*, `arXiv:1706.00209` [physics.ins-det].
153. W. Chung, PoS CORFU **2015**, 047 (2016).
154. D. Alesini *et al.*, `arXiv:1707.06010` [physics.ins-det].
155. G. Rybka *et al.*, Phys. Rev. **D91**, 011701 (2015).
156. D. Horns *et al.*, JCAP **1304**, 016 (2013).
157. J. Suzuki *et al.*, JCAP **1509**, 042 (2015);
B. Döbrich *et al.*, `arXiv:1510.05869` [physics.ins-det].
158. A. Caldwell *et al.*[MADMAX Working Group], Phys. Rev. Lett. **118**, 091801 (2017).
159. P. Sikivie, Phys. Rev. Lett. **113**, 201301 (2014).
160. D. Budker *et al.*, Phys. Rev. **X4**, 021030 (2014).
161. P. Sikivie, N. Sullivan, and D. B. Tanner, Phys. Rev. Lett. **112**, 131301 (2014).
162. Y. Kahn, B. R. Safdi and J. Thaler, Phys. Rev. Lett. **117**, 141801 (2016).
163. M. Silva-Feaver *et al.*, `arXiv:1610.09344` [astro-ph.IM].
164. L. Krauss *et al.*, Phys. Rev. Lett. **55**, 1797 (1985);
R. Barbieri *et al.*, Phys. Rev. **B226**, 357 (1989).
165. R. Barbieri *et al.*, Phys. Dark Univ. **15**, 135 (2017).

112. Searches for Quark and Lepton Compositeness

Revised 2017 by K. Hikasa (Tohoku University), M. Tanabashi (Nagoya University), K. Terashi (University of Tokyo), and N. Varelas (University of Illinois at Chicago)

112.1. Limits on contact interactions

If quarks and leptons are made of constituents, then at the scale of constituent binding energies (compositeness scale) there should appear new interactions among them. At energies much below the compositeness scale (Λ), these interactions are suppressed by inverse powers of Λ. The dominant effect of the compositeness of fermion ψ should come from the lowest dimensional interactions with four fermions (contact terms), whose most general flavor-diagonal color-singlet chirally invariant form reads [1,2]

$$\mathcal{L} = \mathcal{L}_{LL} + \mathcal{L}_{RR} + \mathcal{L}_{LR} + \mathcal{L}_{RL},$$

with

$$\mathcal{L}_{LL} = \frac{g^2_{\rm contact}}{2\Lambda^2} \sum_{i,j} \eta^{ij}_{LL} (\bar\psi^i_L \gamma_\mu \psi^i_L)(\bar\psi^j_L \gamma^\mu \psi^j_L),$$

$$\mathcal{L}_{RR} = \frac{g^2_{\rm contact}}{2\Lambda^2} \sum_{i,j} \eta^{ij}_{RR} (\bar\psi^i_R \gamma_\mu \psi^i_R)(\bar\psi^j_R \gamma^\mu \psi^j_R),$$

$$\mathcal{L}_{LR} = \frac{g^2_{\rm contact}}{2\Lambda^2} \sum_{i,j} \eta^{ij}_{LR} (\bar\psi^i_L \gamma_\mu \psi^i_L)(\bar\psi^j_R \gamma^\mu \psi^j_R),$$

$$\mathcal{L}_{RL} = \frac{g^2_{\rm contact}}{2\Lambda^2} \sum_{i,j} \eta^{ij}_{RL} (\bar\psi^i_R \gamma_\mu \psi^i_R)(\bar\psi^j_L \gamma^\mu \psi^j_L), \qquad (112.1)$$

where i, j are the indices of fermion species. Color and other indices are suppressed in Eq. (112.1). Chiral invariance provides a natural explanation why quark and lepton masses are much smaller than their inverse size Λ. Note $\eta^{ij}_{\alpha\beta} = \eta^{ji}_{\beta\alpha}$, therefore, in order to specify the contact interaction among the same fermion species $i = j$, it is enough to use η_{LL}, η_{RR} and η_{LR}. We will suppress the indices of fermion species hereafter. We may determine the scale Λ unambiguously by using the above form of the effective interactions; the conventional method [1] is to fix its scale by setting $g^2_{\rm contact}/4\pi = g^2_{\rm contact}(\Lambda)/4\pi = 1$ for the new strong interaction coupling and by setting the largest magnitude of the coefficients $\eta_{\alpha\beta}$ to be unity. In the following, we denote

$$\Lambda = \Lambda^\pm_{LL} \quad \text{for} \quad (\eta_{LL}, \eta_{RR}, \eta_{LR}) = (\pm 1, 0, 0)\ ,$$
$$\Lambda = \Lambda^\pm_{RR} \quad \text{for} \quad (\eta_{LL}, \eta_{RR}, \eta_{LR}) = (0, \pm 1, 0)\ ,$$
$$\Lambda = \Lambda^\pm_{VV} \quad \text{for} \quad (\eta_{LL}, \eta_{RR}, \eta_{LR}) = (\pm 1, \pm 1, \pm 1)\ ,$$
$$\Lambda = \Lambda^\pm_{AA} \quad \text{for} \quad (\eta_{LL}, \eta_{RR}, \eta_{LR}) = (\pm 1, \pm 1, \mp 1)\ ,$$
$$\Lambda = \Lambda^\pm_{V-A} \quad \text{for} \quad (\eta_{LL}, \eta_{RR}, \eta_{LR}) = (0, 0, \pm 1)\ . \qquad (112.2)$$

Such interactions can arise by interchanging constituents (when the fermions have common constituents), and/or by exchanging the binding quanta (whenever binding quanta couple to constituents of both particles).

Fermion scattering amplitude [2] induced from the contact interaction in Eq. (112.1) interferes with the Standard Model (SM) amplitude destructively or constructively. The sign of interference depends on the sign of $\eta_{\alpha\beta}$ ($\alpha, \beta = L, R$). For instance, in the parton level $qq \to qq$ scattering cross section in the $\Lambda^\pm_{LL}$ model, the contact interaction amplitude and the SM gluon exchange amplitude interfere destructively for $\eta_{LL} = +1$, while they interfere constructively for $\eta_{LL} = -1$. In models of quark compositeness, the quark scattering cross sections induced from the contact interactions receive sizable QCD radiative corrections. Ref. 3 provides the exact next-to-leading order (NLO) QCD corrections to the contact interaction induced quark scattering cross sections.

Over the last three decades experiments at the CERN Sp$\bar{\rm p}$S [4,5], the Fermilab Tevatron [6,7], and the CERN LHC [8–12] have searched for quark contact interactions, characterized by the four-fermion effective Lagrangian in Eq. (112.1), using jet final states. These searches have been performed primarily by studying the angular distribution of the two highest transverse momentum, $p_{\rm T}$, jets (dijets), and the inclusive jet $p_{\rm T}$ spectrum. The variable $\chi = \exp(|(y_1 - y_2)|)$ is used to measure the dijet angular distribution, where y_1 and y_2 are the rapidities of the two jets with the highest transverse momenta. For collinear massless parton scattering, χ is related to the polar scattering angle θ^* in the partonic center-of-mass frame by $\chi = (1 + |\cos\theta^*|)/(1 - |\cos\theta^*|)$. The choice of χ is motivated by the fact that the angular distribution for Rutherford scattering, which is proportional to $1/(1 - \cos\theta^*)^2$, is independent of χ. In perturbative QCD the χ distributions are relatively uniform and only mildly modified by higher-order QCD or electroweak corrections. Signatures of quark contact interactions exhibit more isotropic angular distribution than QCD and they can be identified as an excess at low values of χ. In the inclusive jet cross section measurement, quark contact interaction effects are searched as deviations from the predictions of perturbative QCD in the tails of the high-$p_{\rm T}$ jet spectrum [11].

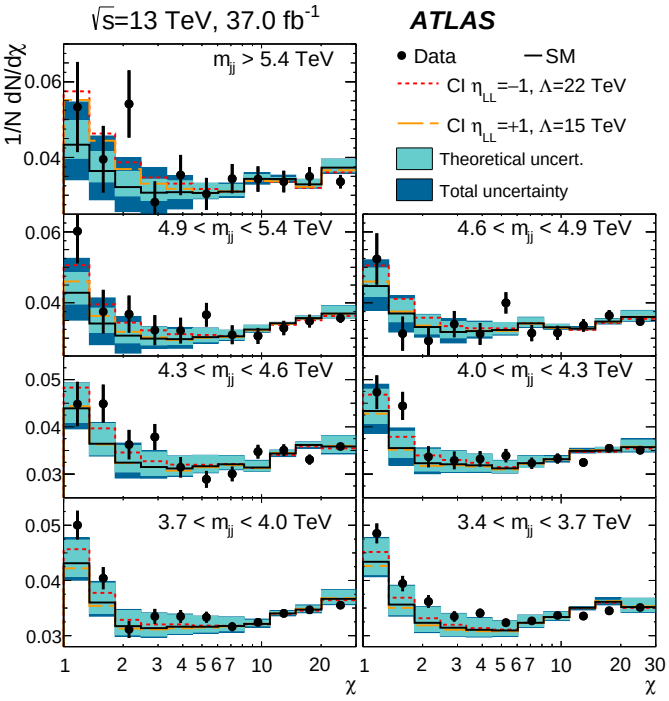

Figure 112.1: Normalized dijet angular distributions in several dijet mass (m_{jj}) ranges. The data distributions are compared to PYTHIA8 predictions with NLO and electroweak corrections applied (solid line) and with the predictions including a contact interaction (CI) term in which only left-handed quarks participate of compositeness scale $\Lambda^+_{LL} = 15$ TeV (dashed line) and $\Lambda^-_{LL} = 22$ TeV (dotted line). The theoretical uncertainties and the total theoretical and experimental uncertainties in the predictions are displayed as shaded bands around the SM prediction. Figure adopted from Ref. 9.

Recent results from the LHC, using data collected at proton-proton center-of-mass energy of $\sqrt{s} = 13$ TeV, extend previous limits on quark contact interactions. Figure 112.1 shows the normalized dijet angular distributions for several dijet mass ranges measured in ATLAS [9] at $\sqrt{s} = 13$ TeV. The data distributions are compared with SM predictions, estimated using PYTHIA8 [13] with GEANT4-based [14] ATLAS detector simulation and corrected to NLO QCD calculation provided by NLO Jet++ [15] including electroweak corrections [16],

and with predictions including a contact interaction term in which only left-handed quarks participate at compositeness scale $\Lambda^+_{LL} = 15$ TeV ($\Lambda^-_{LL} = 22$ TeV) with destructive (constructive) interference. Over a wide range of χ and dijet mass the data are well described by the SM predictions. Using the dijet angular distributions measured at high dijet masses and $\sqrt{s} = 13$ TeV, the ATLAS [9] and CMS [12] Collaborations have set 95% confidence level (C.L.) lower limits on the contact interaction scale Λ, ranging from 9.1 to 29.5 TeV for different quark contact interaction models that correspond to various combinations of (η_{LL}, η_{RR}, η_{LR}), as summarized in Figure 112.2. The contact interaction scale limits extracted using the dijet angular distributions include the exact NLO QCD corrections to dijet production induced by contact interactions [3]. In proton-proton collisions, the $\Lambda^{\pm}_{LL}$ and $\Lambda^{\pm}_{RR}$ contact interaction models result in identical tree-level cross sections and NLO QCD corrections and yield the same exclusion limits. For $\Lambda^{\pm}_{VV}$ and $\Lambda^{\pm}_{AA}$, the contact interaction predictions are identical at tree level, but exhibit different NLO QCD corrections and yield different exclusion limits.

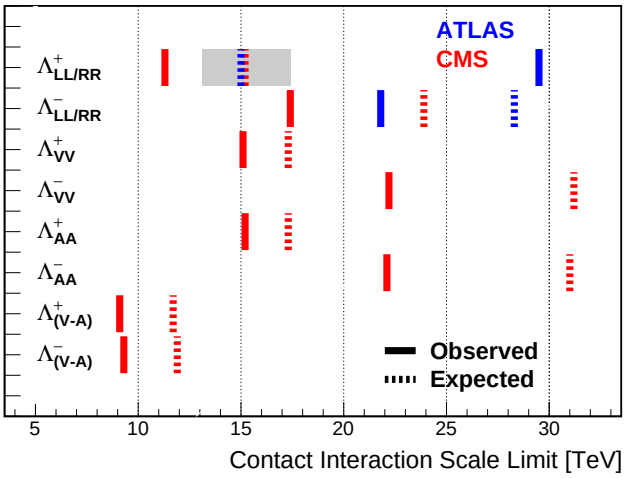

Figure 112.2: Observed (solid lines) and expected (dashed lines) 95% C.L. lower limits on the contact interaction scale Λ for different contact interaction models from ATLAS [9] and CMS preliminary [12] using the dijet angular distributions. The contact interaction models used for the dijet angular distributions include the exact NLO QCD corrections to dijet production. The shaded band for the $\Lambda^+_{LL/RR}$ model indicates the range of contact interaction scale that was not excluded in ATLAS [9] due to statistical fluctuation of observed data.

If leptons (l) and quarks (q) are composite with common constituents, the interaction of these constituents will manifest itself in the form of a $llqq$-type four-fermion contact interaction Lagrangian at energies below the compositeness scale Λ. The $llqq$ terms in the contact interaction Lagrangian can be expressed as

$$\mathcal{L}_{LL} = \frac{g^2_{\rm contact}}{\Lambda^2} \sum_{i,j} \eta^{ij}_{LL} (\bar{q}^i_L \gamma_\mu q^i_L)(\bar{l}^j_L \gamma^\mu l^j_L),$$

$$\mathcal{L}_{RR} = \frac{g^2_{\rm contact}}{\Lambda^2} \sum_{i,j} \eta^{ij}_{RR} (\bar{q}^i_R \gamma_\mu q^i_R)(\bar{l}^j_R \gamma^\mu l^j_R),$$

$$\mathcal{L}_{LR} = \frac{g^2_{\rm contact}}{\Lambda^2} \sum_{i,j} \eta^{ij}_{LR} (\bar{q}^i_L \gamma_\mu q^i_L)(\bar{l}^j_R \gamma^\mu l^j_R),$$

$$\mathcal{L}_{RL} = \frac{g^2_{\rm contact}}{\Lambda^2} \sum_{i,j} \eta^{ij}_{RL} (\bar{q}^i_R \gamma_\mu q^i_R)(\bar{l}^j_L \gamma^\mu l^j_L). \qquad (112.3)$$

Searches on quark-lepton compositeness have been reported from experiments at LEP [17–20], HERA [21,22], the Tevatron [23–24], and recently from the ATLAS [25–26] and CMS [27–28] experiments at the LHC. The most stringent searches for $llqq$ contact interactions are performed by the LHC experiments using high-mass oppositely-charged lepton pairs produced through the $q\bar{q} \to l^+l^-$ Drell-Yan process. The contact interaction amplitude of the $u\bar{u} \to l^+l^-$ process ($l = e$ or μ) interferes with the corresponding SM amplitude constructively (destructively) for $\eta^{ul}_{\alpha\beta} = -1$ ($\eta^{ul}_{\alpha\beta} = +1$). The ATLAS Collaboration has extracted limits on the $llqq$ contact interaction at $\sqrt{s} = 13$ TeV for the right-right ($\eta_{RR} = \pm 1$, $\eta_{LL} = \eta_{LR} = \eta_{RL} = 0$), left-left ($\eta_{LL} = \pm 1$, $\eta_{RR} = \eta_{LR} = \eta_{RL} = 0$), and left-right ($\eta_{LR} = \eta_{RL} = \pm 1$, $\eta_{RR} = \eta_{LL} = 0$) models. Combining the dielectron and dimuon channels, the 95% C.L. lower limits on the $llqq$ contact interaction scale Λ are 35.2 TeV (27.7 TeV) for the right-right model, 40.1 TeV (25.4 TeV) for the left-left model, and 35.7 TeV (27.5 TeV) for the left-right model, each with constructive (destructive) interference [26]. The CMS Collaboration, using the full 8-TeV dataset has set a 95% C.L. lower limit on the scale Λ of 16.9 TeV (13.1 TeV) for the benchmark left-left $llqq$ contact interaction model with constructive (destructive) interference [28].

Note that the contact interactions arising from the compositeness of quarks and leptons in Eq. (112.1) can also be regarded as a part of more general dimension six operators in the context of low energy standard model effective theory. For a complete list of these dimension six operators see Refs. 29,30.

Interactions of hypothetical dark matter candidate particles with SM particles through mediators can also be described as contact interactions at low energy. See *"Searches for WIMPs and Other Particles"* in this volume for limits on the interactions involving dark matter candidate particles.

112.2. Limits on excited fermions

Another typical consequence of compositeness is the appearance of excited leptons and quarks (l^* and q^*). Phenomenologically, an excited lepton is defined to be a heavy lepton which shares a leptonic quantum number with one of the existing leptons (an excited quark is defined similarly). For example, an excited electron e^* is characterized by a nonzero transition-magnetic coupling with electrons. Smallness of the lepton mass and the success of QED prediction for $g - 2$ suggest chirality conservation, *i.e.,* an excited lepton should not couple to both left- and right-handed components of the corresponding lepton [31–33].

Excited leptons may be classified by $SU(2) \times U(1)$ quantum numbers. Typical examples are:

1. Sequential type

$$\begin{pmatrix} \nu^* \\ l^* \end{pmatrix}_L, \qquad [\nu^*_R], \qquad l^*_R.$$

   ν^*_R is necessary unless ν^* has a Majorana mass.

2. Mirror type

$$[\nu^*_L], \qquad l^*_L, \qquad \begin{pmatrix} \nu^* \\ l^* \end{pmatrix}_R.$$

3. Homodoublet type

$$\begin{pmatrix} \nu^* \\ l^* \end{pmatrix}_L, \qquad \begin{pmatrix} \nu^* \\ l^* \end{pmatrix}_R.$$

Similar classification can be made for excited quarks.

Excited fermions can be pair produced via their minimal gauge couplings. The couplings of excited leptons with Z are given by

$$\frac{e}{2\sin\theta_W \cos\theta_W}(-1 + 2\sin^2\theta_W)\bar{l^*}\gamma^\mu l^* Z_\mu$$

$$+ \frac{e}{2\sin\theta_W \cos\theta_W}\bar{\nu^*}\gamma^\mu \nu^* Z_\mu$$

in the homodoublet model. The corresponding couplings of excited quarks can be easily obtained. Although form factor effects can be present for the gauge couplings at $q^2 \neq 0$, they are usually neglected.

Excited fermions may also be produced via the contact interactions with ordinary quarks and leptons [34]

$$\mathcal{L} = \frac{g^2_{\rm contact}}{\Lambda^2}\left[\eta'_{LL}(\bar{\psi}_L\gamma_\mu\psi_L)(\bar{\psi}^*_L\gamma^\mu\psi^*_L) + (\eta''_{LL}(\bar{\psi}_L\gamma_\mu\psi_L)(\bar{\psi}^*_L\gamma^\mu\psi_L) + \text{h.c.}) + \cdots\right]. \quad (112.4)$$

Again, the coefficient is conventionally taken $g^2_{\rm contact} = 4\pi$. It is widely assumed $\eta'_{LL} = \eta''_{LL} = 1$, $\eta'_{LR} = \eta''_{LR} = \eta'_{RL} = \eta''_{RL} = \eta'_{RR} = \eta''_{RR} = 0$ in experimental analyses for simplicity.

In addition, transition-magnetic type couplings with a gauge boson are expected. These couplings can be generally parameterized as follows:

$$\begin{aligned}\mathcal{L} =& \frac{\lambda^{(\psi^*)}_\gamma e}{2m_{\psi^*}}\bar{\psi}^*\sigma^{\mu\nu}(\eta_L\frac{1-\gamma_5}{2} + \eta_R\frac{1+\gamma_5}{2})\psi F_{\mu\nu} \\ &+ \frac{\lambda^{(\psi^*)}_Z e}{2m_{\psi^*}}\bar{\psi}^*\sigma^{\mu\nu}(\eta_L\frac{1-\gamma_5}{2} + \eta_R\frac{1+\gamma_5}{2})\psi Z_{\mu\nu} \\ &+ \frac{\lambda^{(l^*)}_W g}{2m_{l^*}}\bar{l}^*\sigma^{\mu\nu}\frac{1-\gamma_5}{2}\nu W_{\mu\nu} \\ &+ \frac{\lambda^{(\nu^*)}_W g}{2m_{\nu^*}}\bar{\nu}^*\sigma^{\mu\nu}(\eta_L\frac{1-\gamma_5}{2} + \eta_R\frac{1+\gamma_5}{2})lW^\dagger_{\mu\nu} \\ &+ \text{h.c.}, \end{aligned} \quad (112.5)$$

where $g = e/\sin\theta_W$, $\psi = \nu$ or l, $F_{\mu\nu} = \partial_\mu A_\nu - \partial_\nu A_\mu$ is the photon field strength, $Z_{\mu\nu} = \partial_\mu Z_\nu - \partial_\nu Z_\mu$, *etc.*. The normalization of the coupling is chosen such that

$$\max(|\eta_L|, |\eta_R|) = 1.$$

Chirality conservation requires

$$\eta_L\eta_R = 0. \quad (112.6)$$

These couplings in Eq. (112.5) can arise from $SU(2) \times U(1)$-invariant higher-dimensional interactions. A well-studied model is the interaction of homodoublet type l^* with the Lagrangian (see Refs. 35,36)

$$\mathcal{L} = \frac{1}{2\Lambda}\bar{L}^*\sigma^{\mu\nu}(gf\frac{\tau^a}{2}W^a_{\mu\nu} + g'f'YB_{\mu\nu})\frac{1-\gamma_5}{2}L + \text{h.c.}, \quad (112.7)$$

where L denotes the lepton doublet (ν, l), Λ is the compositeness scale, g, g' are $SU(2)$ and $U(1)_Y$ gauge couplings, and $W^a_{\mu\nu}$ and $B_{\mu\nu}$ are the field strengths for $SU(2)$ and $U(1)_Y$ gauge fields. These couplings satisfy the relation

$$\lambda_W = -\sqrt{2}\sin^2\theta_W(\lambda_Z\cot\theta_W + \lambda_\gamma), \quad (112.8)$$

with $\lambda_{W,Z,\gamma}$ being defined in Eq. (112.5) with $\lambda_{W,Z,\gamma} = \lambda^{(\ell^*)}_{W,Z,\gamma}$ or $\lambda_{W,Z,\gamma} = \lambda^{(\nu^*)}_{W,Z,\gamma}$. Here $(\eta_L, \eta_R) = (1, 0)$ is assumed. It should be noted that the electromagnetic radiative decay of l^* (ν^*) is forbidden if $f = -f'$ ($f = f'$).

Additional coupling with gluons is possible for excited quarks:

$$\mathcal{L} = \frac{1}{2\Lambda}\bar{Q}^*\sigma^{\mu\nu}\left(g_s f_s\frac{\lambda^a}{2}G^a_{\mu\nu} + gf\frac{\tau^a}{2}W^a_{\mu\nu} + g'f'YB_{\mu\nu}\right) \times \frac{1-\gamma_5}{2}Q + \text{h.c.}, \quad (112.9)$$

where Q denotes a quark doublet, g_s is the QCD gauge coupling, and $G^a_{\mu\nu}$ the gluon field strength.

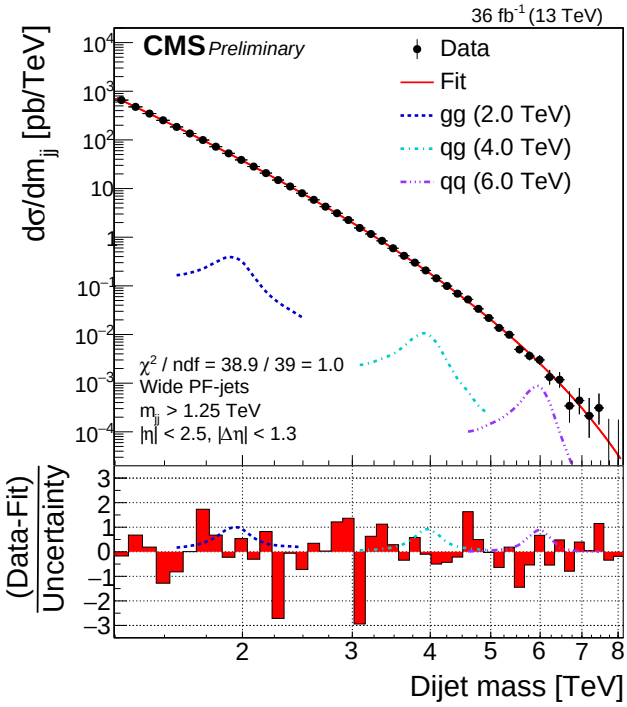

Figure 112.3: Dijet mass distribution measured by CMS using wide jets reconstructed from two highest transverse momentum jets by adding nearby jets within $\Delta R = \sqrt{\Delta\eta^2 + \Delta\phi^2} < 1.1$. The data distribution is compared to a fit representing a smooth background spectrum (solid curve). The excited quark signal with mass of 4.0 TeV (labeled as qg) is shown together with other benchmark signals. Shown at the bottom panel is the difference between the data and the fitted parametrization divided by the statistical uncertainty of the data. Figure adopted from Ref. 60.

If leptons are made of color triplet and antitriplet constituents, we may expect their color-octet partners. Transitions between the octet leptons (l_8) and the ordinary lepton (l) may take place via the dimension-five interactions

$$\mathcal{L} = \frac{1}{2\Lambda}\sum_l\{\bar{l}^\alpha_8 g_S F^\alpha_{\mu\nu}\sigma^{\mu\nu}(\eta_L l_L + \eta_R l_R) + \text{h.c.}\} \quad (112.10)$$

where the summation is over charged leptons and neutrinos. The leptonic chiral invariance implies $\eta_L\eta_R = 0$ as before.

Searches for the excited quarks and leptons have been performed over the last decades in experiments at the LEP [37–40], HERA [41–42], Tevatron [43–44], and LHC [45–67]. Most stringent constraints, which are described below at 95% confidence level, come from the LHC experiments.

The signature of excited quarks q^* at hadron colliders is characterized by a narrow resonant peak in the reconstructed invariant mass distribution of the q^* decay products. The decays via the transition-magnetic type operator in Eq. (112.9) are considered for excited quarks in LHC searches, and the final states to search for are dijet (qg) [45, 46, 57–60] or a jet in association with a photon ($q\gamma$) [47, 48, 61, 62] or a weak gauge boson (qW, qZ) [63, 64]. All analyses consider only spin-1/2 excited states of first generation quarks (u^*, d^*) with degenerate masses, expected to be predominantly produced in proton-proton collisions except for the excited b quark searches described below. Only the minimal gauge interactions and the transition-magnetic couplings with the form given in Eq. (112.9) are considered in the production process, and hence the contact interactions in Eq. (112.4) are not considered. The compositeness scale Λ is taken to be the same as the excited quark mass m_{q^*}. The transition-magnetic coupling coefficients f_s, f and f' are assumed to be equal to 1 (denoted by f).

With proton-proton collision data recorded at $\sqrt{s} = 13$ TeV at the LHC, the excited quark masses are excluded in dijet resonance searches up to 6.0 TeV in both ATLAS [46] and CMS [60]. Figure 112.3 shows the dijet mass distribution measured in CMS [60] by using the two highest $p_{\rm T}$ jets reconstructed with the anti-$k_{\rm T}$ algorithm [68] of a distance parameter of 0.4, and by combining nearby jets within $\Delta R = \sqrt{\Delta\eta^2 + \Delta\phi^2} < 1.1$ around the leading two jets. The measured dijet mass spectrum is compared to a fit with smoothly falling background shape (solid curve) to look for a narrow resonance; an excited quark signal with mass of 4.0 TeV is shown in the figure (denoted by qg) as one of the benchmark signals considered in the analysis.

The photon + jet resonance searches, targeting excited quarks decaying into a quark and a photon ($q^* \to q + \gamma$), have excluded q^* masses up to 5.3 TeV in ATLAS [48] and 5.5 TeV in CMS [62] using collision data at $\sqrt{s} = 13$ TeV. The W/Z boson + jet final states are examined to look for the $q^* \to q + W$ and $q + Z$ signal in CMS [64], exploiting jet substructure technique designed to provide sensitivity for highly-boosted hadronically decaying W and Z bosons. The lower mass limit of 5.0 (4.8) TeV is obtained from the W + jet (Z + jet) search using dataset recorded at $\sqrt{s} = 13$ TeV.

The excited b quarks (b^*) are also considered in the present searches at the LHC. Assuming the similar production processes to the first-generation excited quarks, the b^* has been searched for in final states containing at least one jet identified as originating from a b quark (b-tagging). The searches using two jets including at least one b-tagged jet have been performed at 8 and 13 TeV [49, 50, 58], resulting in b^* lower mass limits of 2.3 TeV in ATLAS using 13.3 fb^{-1} at $\sqrt{s} = 13$ TeV [49] and 1.6 TeV in CMS using 19.7 fb^{-1} at $\sqrt{s} = 8$ TeV [58]. The CMS Collaboration also performed a search for $b^* \to b + \gamma$ in events with a b-tagged jet in association with a photon using data at $\sqrt{s} = 13$ TeV [62], and excluded b^* masses up to 1.8 TeV. Excited b quarks with charged-current decay into a W-boson and a top quark ($b^* \to t + W$) were looked for in both ATLAS and CMS using the full 8 TeV data[51, 65]. ATLAS excluded b^* masses below 1.5 TeV for the b^* with left- and right-handed couplings [51] while CMS excluded the masses below 1.39(1.43) TeV for the left(right)-handed couplings [65].

Searches for excited leptons l^* are also performed at the LHC using proton-proton collision data recorded at $\sqrt{s} = 7$ and 8 TeV [53–56, 66, 67]. Considering single l^* production in contact interactions (Eq. (112.4)) and electromagnetic radiative decay to a SM lepton and a photon ($l^* \to l + \gamma$ where $l = e, \mu$), both the excited electron and excited muon masses below 2.2 TeV are excluded for $\Lambda = m_{l^*}$ using 13 fb^{-1} at $\sqrt{s} = 8$ TeV in ATLAS [54]. With the full 20.3 fb^{-1} data at $\sqrt{s} = 8$ TeV, the inclusive search on multi-lepton signatures with 3 or more charged leptons in ATLAS [55] further constrains the excited charged leptons and neutrinos. Considering both the transition-magnetic (Eq. (112.7)) and contact interaction (Eq. (112.4)) processes, the lower mass limits for the e^*, μ^*, τ^* and ν^* (for every excited neutrino flavor) are obtained to be 3.0, 3.0, 2.5 and 1.6 TeV, respectively, for $\Lambda = m_{e^*}$, m_{μ^*}, m_{τ^*} and m_{ν^*}. The rate of pair-produced excited leptons is independent of Λ for the minimal gauge interaction processes, and it allows to improve search sensitivity with multi-lepton signatures at high Λ, especially for excited neutrinos because the predominant $\nu_l^* \to l + W$ decays result in a higher acceptance for ≥ 3 charged lepton final states.

The ATLAS Collaboration performed a search [56] for single excited muons both produced and decayed in contact interaction processes (Eq. (112.4)), being characterized by the final state with two muons and two jets ($q\bar{q} \to \mu\mu^* \to \mu\mu q\bar{q}$). With the full 8 TeV data the lower mass limit of 2.8 TeV was set for the μ^* at $\Lambda = m_{\mu^*}$.

A search for excited leptons with $l^* \to l + \gamma$ decays ($l = e, \mu$) produced in contact interactions by the CMS Collaboration using the full data at $\sqrt{s} = 8$ TeV [67] resulted in mass exclusions of 2.45 TeV for the e^* and 2.47 TeV for the μ^* at $\Lambda = m_{l^*}$. The CMS Collaboration also performed an excited lepton search in the final states containing a Z boson [67], probing the excited leptons produced in contact interactions and decayed in neutral-current processes ($l^* \to l + Z$) with $f = f' = 1$ or $f = -f' = 1$. The latter ($f = -f' = 1$) is forbidden in the radiative decay $l^* \to l + \gamma$. The leptonic and hadronic decays of

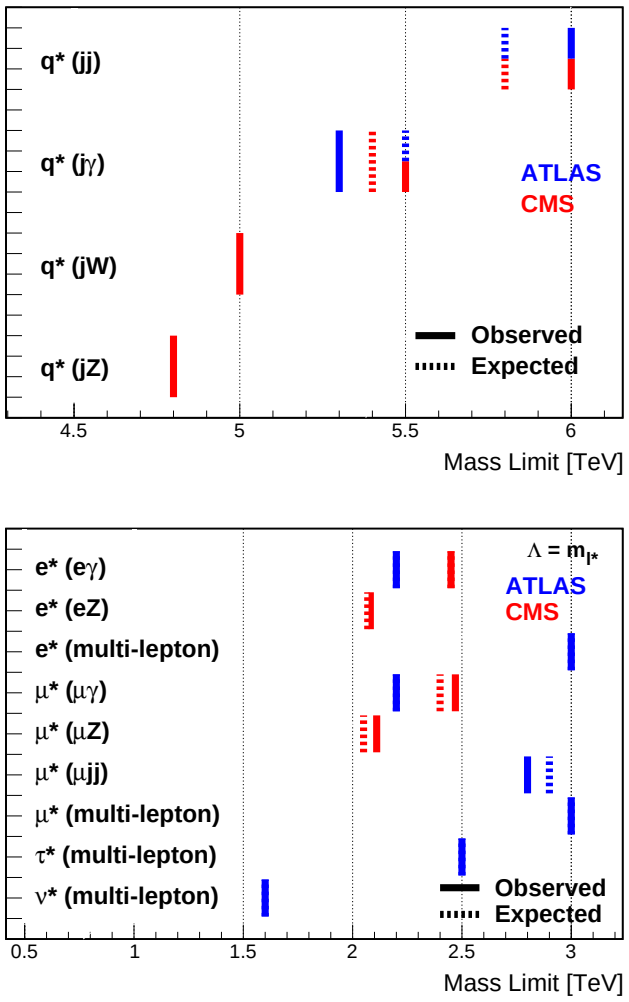

Figure 112.4: 95% C.L. lower mass limits for the excited quarks (top) and excited leptons (bottom) at ATLAS [46,48,54–56] and CMS [60,62,64] [67] experiments. Refs. [60] and [62] are CMS preliminary. Shown are the most stringent limits for each final state (denoted in parentheses) of the excited fermions from both experiments. Only first generation quarks (u, d) with transition-magnetic type interactions with $f_s = f = f' = 1$ are considered for the excited quarks. The excited lepton limits are given for the production via contact interactions with $\Lambda = m_{l^*}$. For the $q^* \to q + g$ ATLAS and CMS have the same observed and expected limits. Also, for the $q^* \to q + \gamma$ the CMS observed and ATLAS expected limits are same. For the excited leptons, the observed and expected limits are same in the ATLAS $l + \gamma$, ATLAS multi-lepton and the CMS $e + \gamma$ searches and hence the expected limit lines are not visible.

Z bosons have been considered in the search, and the most stringent limits are obtained from the hadronic Z decay to be 2.08 (2.34) TeV and 2.11 (2.37) TeV for the e^* and μ^*, respectively, with $f = f' = 1$ ($f = -f' = 1$) at $\Lambda = m_{l^*}$.

Figure 112.4 summarizes the most stringent 95% C.L. lower mass limits for excited quarks and leptons obtained from the LHC experiments.

References:

1. E.J. Eichten, K.D. Lane, and M.E. Peskin, Phys. Rev. Lett. **50**, 811 (1983).
2. E.J. Eichten *et al.*, Rev. Mod. Phys. **56**, 579 (1984); Erratum *ibid.* **58**, 1065 (1986).
3. J. Gao *et al.*, Phys. Rev. Lett. **106**, 142001 (2011).
4. G. Arnison *et al.* [UA1 Collab.], Phys. Lett. **B177**, 244 (1986).

5. J.A. Appel *et al.* [UA2 Collab.], Phys. Lett. **B160**, 349 (1985).
6. F. Abe *et al.* [CDF Collab.], Phys. Rev. Lett. **62**, 613 (1989);
F. Abe *et al.* [CDF Collab.], Phys. Rev. Lett. **69**, 2896 (1992);
F. Abe *et al.* [CDF Collab.], Phys. Rev. Lett. **77**, 5336 (1996);
F. Abe *et al.* [CDF Collab.], Erratum Phys. Rev. Lett. **78**, 4307 (1997).
7. B. Abbott *et al.* [DØ Collab.], Phys. Rev. Lett. **80**, 666 (1998);
B. Abbott *et al.* [DØ Collab.], Phys. Rev. Lett. **82**, 2457 (1999);
B. Abbott *et al.* [DØ Collab.], Phys. Rev. **D62**, 031101 (2000);
B. Abbott *et al.* [DØ Collab.], Phys. Rev. **D64**, 032003 (2001);
B. Abbott *et al.* [DØ Collab.], Phys. Rev. Lett. **103**, 191803 (2009).
8. G. Aad *et al.* [ATLAS Collab.], Phys. Lett. **B694**, 327 (2011);
G. Aad *et al.* [ATLAS Collab.], New J. Phys. **13**, 053044 (2011);
G. Aad *et al.* [ATLAS Collab.], JHEP **01**, 029 (2013);
G. Aad *et al.* [ATLAS Collab.], Phys. Rev. Lett. **114**, 221802 (2015);
G. Aad *et al.* [ATLAS Collab.], Phys. Lett. **B754**, 302 (2016).
9. G. Aad *et al.* [ATLAS Collab.], submitted to Phys. Rev. **D**, arXiv:1703.09127.
10. V. Khachatryan *et al.* [CMS Collab.], Phys. Rev. Lett. **105**, 262001 (2010);
V. Khachatryan *et al.* [CMS Collab.], Phys. Rev. Lett. **106**, 201804 (2011);
S. Chatrchyan *et al.* [CMS Collab.], JHEP **1205**, 055 (2012);
V. Khachatryan *et al.* [CMS Collab.], Phys. Lett. **B746**, 79 (2015);
A.M. Sirunyan *et al.* [CMS Collab.], JHEP **07**, 013 (2017).
11. S. Chatrchyan *et al.* [CMS Collab.], Phys. Rev. **D87**, 052017 (2013).
12. CMS Collaboration, CMS-PAS-EXO-16-046 (2017).
13. T. Sjöstrand, S. Mrenna, and P. Skands, Comp. Phys. Comm. **178**, 852 (2008).
14. S. Agostinelli *et al.* [GEANT4 Collab.], GEANT4: a simulation toolkit, Nucl. Instrum. Methods **A506**, 250 (2003).
15. Z. Nagy, Phys. Rev. Lett. **88**, 122003 (2002);
Z. Nagy, Phys. Rev. **D68**, 094002, (2003).
16. S. Dittmaier, A. Huss, and C. Speckner, JHEP **1211**, 095 (2012).
17. S. Schael *et al.* [ALEPH Collab.], Eur. Phys. J. **C49**, 411 (2007).
18. J. Abdallah *et al.* [DELPHI Collab.], Eur. Phys. J. **C45**, 589 (2006).
19. M. Acciarri *et al.* [L3 Collab.], Phys. Lett. **B489**, 81 (2000).
20. K. Ackerstaff *et al.* [OPAL Collab.], Phys. Lett. **B391**, 221 (1997);
G. Abbiendi *et al.* [OPAL Collab.], Eur. Phys. J. **C33**, 173 (2004).
21. F.D. Aaron *et al.* [H1 Collab.], Phys. Lett. **B705**, 52 (2011).
22. S. Chekanov *et al.* [ZEUS Collab.], Phys. Lett. **B591**, 23 (2004).
23. F. Abe *et al.* [CDF Collab.], Phys. Rev. Lett. **68**, 1463 (1992);
F. Abe *et al.* [CDF Collab.], Phys. Rev. Lett. **79**, 2198 (1997);
T. Affolder *et al.* [CDF Collab.], Phys. Rev. Lett. **87**, 231803 (2001);
A. Abulencia *et al.* [CDF Collab.], Phys. Rev. Lett. **96**, 211801 (2006).
24. B. Abbott *et al.* [DØ Collab.], Phys. Rev. Lett. **82**, 4769 (1999).
25. G. Aad *et al.* [ATLAS Collab.], Phys. Rev. **D84**, 011101 (2011);
G. Aad *et al.* [ATLAS Collab.], Phys. Lett. **B712**, 40 (2012);
G. Aad *et al.* [ATLAS Collab.], Phys. Rev. **D87**, 015010 (2013);
G. Aad *et al.* [ATLAS Collab.], Eur. Phys. J. **C74**, 3134 (2014);
M. Aaboud *et al.* [ATLAS Collab.], Phys. Lett. **B761**, 372 (2016).
26. M. Aaboud *et al.* [ATLAS Collab.], submitted to JHEP, arXiv:1707.02424.
27. S. Chatrchyan *et al.* [CMS Collab.], Phys. Rev. **D87**, 032001 (2013).
28. V. Khachatryan *et al.* [CMS Collab.], JHEP **04**, 025 (2015).
29. W. Buchmuller and D. Wyler, Nucl. Phys. **B268**, 621 (1986).
30. B. Grzadkowski *et al.*, JHEP **1010**, 085 (2010).
31. F.M. Renard, Phys. Lett. **B116**, 264 (1982).
32. F. del Aguila, A. Mendez, and R. Pascual, Phys. Lett. **B140**, 431 (1984).
33. M. Suzuki, Phys. Lett. **B143**, 237 (1984).
34. U. Baur, M. Spira, and P.M. Zerwas, Phys. Rev. **D42**, 815 (1990).
35. K. Hagiwara, D. Zeppenfeld, and S. Komamiya, Z. Phys. **C29**, 115 (1985).
36. N. Cabibbo, L. Maiani, and Y. Srivastava, Phys. Lett. **B139**, 459 (1984).
37. D. Decamp *et al.* [ALEPH Collab.], Phys. Reports **216**, 253 (1992);
P. Barate *et al.* [ALEPH Collab.], Eur. Phys. J. **C4**, 571 (1998).
38. P. Abreu *et al.* [DELPHI Collab.], Nucl. Phys. **B367**, 511 (1991);
J. Abdallah *et al.* [DELPHI Collab.], Eur. Phys. J. **C37**, 405 (2004).
39. O. Adriani *et al.* [L3 Collab.], Phys. Reports **236**, 1 (1993);
P. Achard *et al.* [L3 Collab.], Phys. Lett. **B531**, 28 (2002);
P. Achard *et al.* [L3 Collab.], Phys. Lett. **B568**, 23 (2003).
40. G. Abbiendi *et al.* [OPAL Collab.], Phys. Lett. **B544**, 57 (2002);
G. Abbiendi *et al.* [OPAL Collab.], Phys. Lett. **B602**, 167 (2004).
41. C. Adloff *et al.* [H1 Collab.], Phys. Lett. **B525**, 9 (2002);
F.D. Aaron *et al.* [H1 Collab.], Phys. Lett. **B663**, 382 (2008);
F.D. Aaron *et al.* [H1 Collab.], Phys. Lett. **B666**, 131 (2008).
42. S. Chekanov *et al.* [ZEUS Collab.], Phys. Lett. **B549**, 32 (2002).
43. D. Acosta *et al.* [CDF Collab.], Phys. Rev. Lett. **94**, 101802 (2005);
A. Abulencia *et al.* [CDF Collab.], Phys. Rev. Lett. **97**, 191802 (2006);
T. Aaltonen *et al.* [CDF Collab.], Phys. Rev. **D79**, 112002 (2009).
44. V.M. Abazov *et al.* [DØ Collab.], Phys. Rev. **D73**, 111102 (2006);
V.M. Abazov *et al.* [DØ Collab.], Phys. Rev. **D77**, 091102 (2008);
V.M. Abazov *et al.* [DØ Collab.], Phys. Rev. Lett. **103**, 191803 (2009).
45. G. Aad *et al.* [ATLAS Collab.], Phys. Lett. **B708**, 37 (2012);
G. Aad *et al.* [ATLAS Collab.], JHEP **1301**, 29 (2013);
G. Aad *et al.* [ATLAS Collab.], Phys. Rev. **D91**, 052007 (2015);
G. Aad *et al.* [ATLAS Collab.], Phys. Lett. **B754**, 302 (2016).
46. M. Aaboud *et al.* [ATLAS Collab.], submitted to Phys. Rev. **D**, arXiv:1703.09127.
47. G. Aad *et al.* [ATLAS Collab.], Phys. Rev. Lett. **108**, 211802 (2012);
G. Aad *et al.* [ATLAS Collab.], Phys. Lett. **B728**, 562 (2014).
48. M. Aaboud *et al.* [ATLAS Collab.], CERN-EP-2017-148.
49. ATLAS Collaboration, ATLAS-CONF-2016-060 (2016).
50. M. Aaboud *et al.* [ATLAS Collab.], Phys. Lett. **B759**, 229 (2016).
51. G. Aad *et al.* [ATLAS Collab.], JHEP **1602**, 110 (2016).
52. G. Aad *et al.* [ATLAS Collab.], Phys. Lett. **B721**, 171 (2013).
53. G. Aad *et al.* [ATLAS Collab.], Phys. Rev. **D85**, 072003 (2012).
54. G. Aad *et al.* [ATLAS Collab.], New J. Phys. **15**, 093011 (2013).
55. G. Aad *et al.* [ATLAS Collab.] JHEP **1508**, 138 (2015).
56. G. Aad *et al.* [ATLAS Collab.], New J. Phys. **18**, 073021 (2016).
57. S. Chatrchyan *et al.* [CMS Collab.], Phys. Lett. **B704**, 123 (2011);
S. Chatrchyan *et al.* [CMS Collab.], JHEP **1301**, 13 (2013);
S. Chatrchyan *et al.* [CMS Collab.], Phys. Rev. **D87**, 114015 (2013).
58. V. Khachatryan *et al.* [CMS Collab.], Phys. Rev. **D91**, 052009 (2015).
59. V. Khachatryan *et al.* [CMS Collab.], Phys. Rev. Lett. **116**, 071801 (2016);
V. Khachatryan *et al.* [CMS Collab.], Phys. Rev. Lett. **117**, 031802 (2016);
A.M. Sirunyan *et al.* [CMS Collab.], Phys. Lett. **B769**, 520 (2017).
60. CMS Collaboration, CMS-PAS-EXO-16-056 (2017).
61. V. Khachatryan *et al.* [CMS Collab.], Phys. Lett. **B738**, 274 (2014).
62. CMS Collaboration, CMS-PAS-EXO-17-002 (2017).

63. S. Chatrchyan *et al.* [CMS Collab.], Phys. Lett. **B722**, 28 (2013);
S. Chatrchyan *et al.* [CMS Collab.], Phys. Lett. **B723**, 280 (2013);
V. Khachatryan *et al.* [CMS Collab.], JHEP **1408**, 173 (2014).
64. A.M. Sirunyan *et al.* [CMS Collab.], submitted to Phys. Rev. **D**, arXiv:1708.05379.
65. V. Khachatryan *et al.* [CMS Collab.], JHEP **1601**, 166 (2016).
66. S. Chatrchyan *et al.* [CMS Collab.], Phys. Lett. **B704**, 143 (2011);
S. Chatrchyan *et al.* [CMS Collab.], Phys. Lett. **B720**, 309 (2013).
67. V. Khachatryan *et al.* [CMS Collab.], JHEP **1603**, 125 (2016).
68. M. Cacciari, G.P. Salam, and G. Soyez, JHEP **0804**, 063 (2008).
69. T. Sjöstrand *et al.*, Comp. Phys. Comm. **135**, 238 (2001).

113. Dynamical Electroweak Symmetry Breaking: Implications of the H^0

Updated August 2017 by K.M. Black (Boston University), R.S. Chivukula (Michigan State University), and M. Narain (Brown University).

113.1. Introduction and Phenomenology

In theories of dynamical electroweak symmetry breaking, the electroweak interactions are broken to electromagnetism by the vacuum expectation value of a composite operator, typically a fermion bilinear. In these theories, the longitudinal components of the massive weak bosons are identified with composite Nambu-Goldstone bosons arising from dynamical symmetry breaking in a strongly-coupled extension of the standard model. Viable theories of dynamical electroweak symmetry breaking must also explain (or at least accommodate) the presence of an additional composite scalar state to be identified with the H^0 scalar boson [1,2] – a state unlike any other observed so far.

Theories of dynamical electroweak symmetry breaking can be classified by the nature of the composite singlet state to be associated with the H^0, and the corresponding dimensional scales f, the analog of the pion decay-constant in QCD, and Λ, the scale of the underlying strong dynamics.[1] Of particular importance is the ratio v/f, where $v^2 = 1/(\sqrt{2}G_F) \approx (246\,\text{GeV})^2$, since this ratio measures the expected size of the deviations of the couplings of a composite Higgs boson from those expected in the standard model. The basic possibilities, and the additional states that they predict, are described below.

113.1.1. *Technicolor, $v/f \simeq 1$, $\Lambda \simeq 1$ TeV*:

Technicolor models [8–10] incorporate a new asymptotically free gauge theory ("technicolor") and additional massless fermions ("technifermions" transforming under a vectorial representation of the gauge group). The global chiral symmetry of the fermions is spontaneously broken by the formation of a technifermion condensate, just as the approximate chiral symmetry in QCD is broken down to isospin by the formation of a quark condensate. The $SU(2)_W \times U(1)_Y$ interactions are embedded in the global technifermion chiral symmetries in such a way that the only unbroken gauge symmetry after chiral symmetry breaking is $U(1)_{em}$.[2] These theories naturally provide the Nambu-Goldstone bosons "eaten" by the W and Z boson. There would also typically be additional heavy states (e.g. vector mesons, analogous to the ρ and ω mesons in QCD) with TeV masses [14,15], and the WW and ZZ scattering amplitudes would be expected to be strong at energies of order 1 TeV.

There are various possibilities for the scalar H^0 in technicolor models, as described below.[3] In all of these cases, however, to the extent that the H^0 has couplings consistent with those of the standard model [16], these theories are very highly constrained.

a) H^0 **as a singlet scalar resonance:** The strongly-interacting fermions which make up the Nambu-Goldstone bosons eaten by the weak bosons would naturally be expected to also form an isoscalar neutral bound state, analogous to the σ particle expected in pion-scattering in QCD [17]. However, in this case, there is no symmetry protecting the mass of such a particle – which would therefore generically be of order the energy scale of the underlying strong dynamics Λ. In the simplest theories of this kind – those with a global $SU(2)_L \times SU(2)_R$ chiral symmetry which is spontaneously broken to $SU(2)_V$ – the natural dynamical scale Λ would be of order a TeV, resulting in a particle too heavy and broad to be identified with the H^0. The scale of the underlying interactions could naturally be smaller than 1 TeV if the global symmetries of the theory are larger than $SU(2)_L \times SU(2)_R$, but in this case there would be additional (pseudo-)Nambu-Goldstone bosons (more on this below). A theory of this kind would only be viable, therefore, if some choice of the parameters of the high energy theory could give rise to sufficiently light state without the appearance of additional particles that should have already been observed. Furthermore, while a particle with these quantum numbers could have Higgs-like couplings to any electrically neutral spin-zero state made of quarks, leptons, or gauge-bosons, there is no symmetry insuring that the coupling strengths of such a composite singlet scalar state would be precisely the same as those of the standard model Higgs [18].

b) H^0 **as a dilaton:** It is possible that the underlying strong dynamics is approximately scale-invariant, as inspired by theories of "walking technicolor" [19–23], and that both the scale and electroweak symmetries are spontaneously broken at the TeV energy scale [24]. In this case, due to the spontaneous breaking of approximate scale invariance, one might expect a corresponding (pseudo-) Nambu-Goldstone boson [20] with a mass less than a TeV, the dilaton.[4] A dilaton couples to the trace of the energy momentum tensor, which leads to a similar pattern of two-body couplings as the couplings of the standard model Higgs boson [29–31]. Scale-invariance is a space-time symmetry, however, and is unrelated to the global symmetries that we can identify with the electroweak group. Therefore the decay-constants associated with the breaking of the scale and electroweak symmetries will not, in general, be the same.[5] In other words, if there are no large anomalous dimensions associated with the W- and Z-bosons or the top- or bottom-quarks, the ratios of the couplings of the dilaton to these particles would be the same as the ratios of the same couplings for the standard model Higgs boson, but the overall strength of the dilaton couplings would be expected to be different [32,33]. Furthermore, the couplings of the dilaton to gluon- and photon-pairs can be related to the beta functions of the corresponding gauge interactions in the underlying high-energy theory, and will not in general yield couplings with the exactly the same strengths as the standard model [34,35].

c) H^0 **as a singlet Pseudo-Nambu-Goldstone Boson:** If the global symmetries of the technicolor theory are larger than $SU(2)_L \times SU(2)_R$, there can be extra singlet (pseudo-) Nambu-Goldstone bosons which could be identified with the H^0. In this case, however, the coupling strength of the singlet state to WW and ZZ pairs would be comparable to the couplings to gluon and photon pairs, and these would all arise from loop-level couplings in the underlying technicolor theory [36]. This pattern of couplings is not supported by the data.

113.1.2. *The Higgs doublet as a pseudo-Nambu-Goldstone Boson, $v/f < 1$, $\Lambda > 1$ TeV*:

In technicolor models, the symmetry-breaking properties of the underlying strong dynamics necessarily breaks the electroweak gauge symmetries. An alternative possibility is that the underlying strong dynamics itself does not break the electroweak interactions, and that the entire quartet of bosons in the Higgs doublet (including the state associated with the H^0) are composite (pseudo-) Nambu-Goldstone particles [37,38], In this case, the underlying dynamics can occur at energies larger than 1 TeV and additional interactions with the top-quark mass generating sector (and possibly with additional weakly-coupled gauge bosons) cause the vacuum energy to be minimized when the composite Higgs doublet gains a vacuum expectation value [39,40]. In these theories, the couplings of the remaining singlet scalar state would naturally be equal to that of the standard model Higgs boson up to corrections of order $(v/f)^2$ and, therefore, constraints on the

[1] In a strongly interacting theory "Naive Dimensional Analysis" [3,4] implies that, in the absence of fine-tuning, $\Lambda \simeq g^* f$ where $g^* \simeq 4\pi$ is the typical size of a strong coupling in the low-energy theory [5,6]. This estimate is modified in the presence of multiple flavors or colors [7].

[2] For a review of technicolor models, see [11–13].

[3] In these models, the self-coupling of the H^0 scalar is not related to its mass, as it is in the SM – though there are currently no experimental constraints on this coupling.

[4] Even in this case, however, a dilaton associated with electroweak symmetry breaking will likely not *generically* be as light as the H^0 [25–28].

[5] If both the electroweak symmetry and the approximate scale symmetry are broken only by electroweak doublet condensate(s), then the decay-constants for scale and electroweak symmetry breaking may be approximately equal – differing only by terms formally proportional to the amount of explicit scale-symmetry breaking.

size of deviations of the H^0 couplings from that of the standard model Higgs [16] give rise to lower bounds on the scales f and Λ.[6]

The electroweak gauge interactions, as well as the interactions responsible for the top-quark mass, explicitly break the chiral symmetries of the composite Higgs model, and lead generically to sizable corrections to the mass-squared of the Higgs-doublet – the so-called "Little Hierarchy Problem" [41]. "Little Higgs" theories [42–45] are examples of composite Higgs models in which the (collective) symmetry-breaking structure is selected so as to suppress these contributions to the Higgs mass-squared.

Composite Higgs models typically require a larger global symmetry of the underlying theory, and hence additional relatively light (compared to Λ) scalar particles, extra electroweak vector bosons (e.g. an additional $SU(2) \times U(1)$ gauge group), and vector-like partners of the top-quark of charge $+2/3$ and possibly also $+5/3$ [46]. In addition to these states, one would expect the underlying dynamics to yield additional scalar and vector resonances with masses of order Λ. If the theory respects a custodial symmetry [47], the couplings of these additional states to the electroweak and Higgs boson will be related – and, for example, one might expect a charged vector resonance to have similar branching ratios to WZ and WH. Different composite Higgs models utilize different mechanisms for arranging for the hierarchy of scales $v < f$ and arranging for a scalar Higgs self-coupling small enough to produce an H^0 of mass of order 125 GeV, for a review see [48]. If the additional states in these models carry color, they can provide additional contributions to Higgs production via gluon fusion [49]. The extent to which Higgs production at the LHC conforms with standard model predictions provides additional constraints (typically lower bounds on the masses of the additional colored states of order 0.7 TeV) on these models.

In addition, if the larger symmetry of the underlying composite Higgs theory does not commute with the standard model gauge group, then the additional states found in those models – especially those related to the top-quark, which tend to have the largest couplings to the electroweak sector – may be *colorless*. For example, in twin Higgs models [50], the top-partners carry no standard model charges. The phenomenology of the additional states such theories are rather different, since lacking color the production these particles at the LHC will be suppressed – and, their decays may occur only via the electroweak symmetry breaking sector, leading to their being long-lived.

113.1.3. *Top-Condensate, Top-Color, Top-Seesaw and related theories, $v/f < 1$, $\Lambda > 1$ TeV* :

A final alternative is to consider a strongly interacting theory with a high (compared to a TeV) underlying dynamical scale that *would* naturally break the electroweak interactions, but whose strength is adjusted ("fine-tuned") to produce electroweak symmetry breaking at 1 TeV. This alternative is possible if the electroweak (quantum) phase transition is continuous (second order) in the strength of the strong dynamics [51]. If the fine tuning can be achieved, the underlying strong interactions will produce a light composite Higgs bound state with couplings equal to that of the standard model Higgs boson up to corrections of order $(1\ \text{TeV}/\Lambda)^2$. As in theories in which electroweak symmetry breaking occurs through vacuum alignment, therefore, constraints on the size of deviations of the H^0 couplings from that of the standard model Higgs give rise to lower bounds on the scale Λ. Formally, in the limit $\Lambda \to \infty$ (a limit which requires arbitrarily fine adjustment of the strength of the high-energy interactions), these theories are equivalent to a theory with a fundamental Higgs boson – and the fine adjustment of the coupling strength is a manifestation of the hierarchy problem of theories with a fundamental scalar particle.

In many of these theories the top-quark itself interacts strongly (at high energies), potentially through an extended color gauge sector [52–56]. In these theories, top-quark condensation (or the condensation of an admixture of the top with additional vector-like quarks) is responsible for electroweak symmetry breaking, and the H^0 is identified with a bound state involving the third generation of quarks. These theories typically include an extra set of massive color-octet vector bosons (top-gluons), and an extra $U(1)$ interaction (giving rise to a top-color Z') which couple preferentially to the third generation and whose masses define the scale Λ of the underlying physics.

113.1.4. *Flavor* :

In addition to the electroweak symmetry breaking dynamics described above, which gives rise to the masses of the W and Z particles, additional interactions must be introduced to produce the masses of the standard model fermions. Two general avenues have been suggested for these new interactions. In one case, e.g. "extended technicolor" (ETC) theories [57,58], the gauge interactions in the underlying strongly interacting theory are extended to incorporate flavor. This extended gauge symmetry is broken down (possibly sequentially, at several different mass scales) to the residual strong interaction responsible for electroweak symmetry breaking. The massive gauge-bosons corresponding to the broken symmetries then mediate interactions between mass operators for the quarks/leptons and the corresponding bilinears of the strongly-interacting fermions, giving rise to the masses of the ordinary fermions after electroweak symmetry breaking. An an alternative proposal, "partial compositeness" [59], the additional interactions giving rise to mixing between the ordinary quarks and leptons and massive composite fermions in the strongly-interacting underlying theory. Theories incorporating partial compositeness include additional vector-like partners of the ordinary quarks and leptons, typically with masses of order a TeV or less.

In both cases, the effects of these flavor interactions on the electroweak properties of the ordinary quarks and leptons are likely to be most pronounced in the third generation of fermions.[7] The additional particles present, especially the additional scalars, often couple more strongly to heavier fermions.

Moreover, since the flavor interactions must give rise to quark mixing, we expect that a generic theory of this kind could give rise to large flavor-changing neutral-currents [58]. In ETC theories, these constraints are typically somewhat relaxed if the theory incorporates approximate generational flavor symmetries [60], the theory "walks" [19–23], or if $\Lambda > 1$ TeV [61]. In theories of partial compositeness, the masses of the ordinary fermions depend on the scaling-dimension of the operators corresponding to the composite fermions with which they mix. This leads to a new mechanism for generating the mass-hierarchy of the observed quarks and leptons that, potentially, ameliorates flavor-changing neutral current problems and can provide new contributions to the composite Higgs potential which allows for $v/f < 1$ [62–66].

Alternatively, one can assume that the underlying flavor dynamics respects flavor symmetries ("minimal" [67,68] or "next-to-minimal" [69] flavor violation) which suppress flavor-changing neutral currents in the two light generations. Additional considerations apply when extending these arguments to potential explanation of neutrino masses (see, for example, [70,71]) .

Since the underlying high-energy dynamics in these theories are strongly coupled, there are no reliable calculation techniques that can be applied to analyze their properties. Instead, most phenomenological studies depend on the construction of a "low-energy" effective theory describing additional scalar, fermion, or vector

[6] In these models v/f is an adjustable parameter, and in the limit $v/f \to 1$ they reduce, essentially, to the technicolor models discussed in the previous subsection. Our discussion here is consistent with that given there, since we expect corrections to the SM Higgs couplings to be large for $v/f \simeq 1$. Current measurements constrain the couplings of the H^0 to equal those predicted for the Higgs in the standard model to about the 10% level [16], suggesting that f must have values of order a TeV or higher and, therefore, a dynamical scale Λ of at least several TeV.

[7] Indeed, from this point of view, the vector-like partners of the top-quark in top-seesaw and little Higgs models can be viewed as incorporating partial compositeness to explain the origin of the top quark's large mass.

boson degrees of freedom, which incorporates the relevant symmetries and, when available, dynamical principles. In some cases, motivated by the AdS/CFT correspondence [72], the strongly-interacting theories described above have been investigated by analyzing a dual compactified five-dimensional gauge theory. In these cases, the AdS/CFT "dictionary" is used to map the features of the underlying strongly coupled high-energy dynamics onto the low-energy weakly coupled dual theory [73].

More recently, progress has been made in investigating strongly-coupled models using lattice gauge theory [74]. These calculations offer the prospect of establishing which strongly coupled theories of electroweak symmetry breaking have a particle with properties consistent with those observed for the H^0 – and for establishing concrete predictions for these theories at the LHC [75].

113.2. Experimental Searches

As discussed above, the extent to which the couplings of the H^0 conform to the expectations for a standard model Higgs boson constrains the viability of each of these models. Measurements of the H^0 couplings, and their interpretation in terms of effective field theory, are summarized in the H^0 review in this volume. In what follows, we will focus on searches for the additional particles that might be expected to accompany the singlet scalar: extra scalars, fermions, and vector bosons. In some cases, detailed model-specific searches have been made for the particles described above (though generally not yet taking account of the demonstrated existence of the H^0 boson).

In most cases, however, generic searches (e.g. for extra W' or Z' particles, extra scalars in the context of multi-Higgs models, or for fourth-generation quarks) are quoted that can be used – when appropriately translated – to derive bounds on a specific model of interest.

The mass scale of the new particles implied by the interpretations of the low mass of H^0 discussed above, and existing studies from the Tevatron and lower-energy colliders, suggests that only the Large Hadron Collider has any real sensitivity. A number of analyses already carried out by ATLAS and CMS use relevant final states and might have been expected to observe a deviation from standard model expectations – in no case so far has any such deviation been reported. The detailed implications of these searches in various model frameworks are described below.

Except where otherwise noted, all limits in this section are quoted at a confidence level of 95%. The searches at $\sqrt{s}$ = 8 TeV (Run 1) are based on 20.3 fb^{-1} of data recorded by ATLAS, and an integrated luminosity of 19.7 fb^{-1} analyzed by CMS. The datasets collected at $\sqrt{s}$ = 13 TeV during Run 2 of the LHC since 2015 are based on analyses with varied integrated luminosities ranging between ∼2-36fb^{-1}.

113.2.1. *Searches for Z′ or W′ Bosons* :

Massive vector bosons or particles with similar decay channels would be expected to arise in Little Higgs theories, in theories of Technicolor, or models involving a dilaton, adjusted to produce a light Higgs boson, consistent with the observed H^0. These particles would be expected to decay to pairs of vector bosons, to third generation quarks, or to leptons. The generic searches for W' and Z' vector bosons listed below can, therefore, be used to constrain models incorporating a composite Higgs-like boson.

A general review of searches for Z' and W' bosons is also included in this volume [76,77]. In the context of the dynamical electroweak symmetry breaking models, we emphasize their decays to third generation fermions by including a detailed overview, while also briefly summarizing the other searches.

$Z' \to \ell\ell$:

ATLAS [78] and CMS [79] have both searched for Z' production with $Z' \to ee$ or $\mu\mu$. No deviation from the standard model prediction was seen in the dielectron and dimuon invariant mass spectra, by either the ATLAS or the CMS analysis, and lower limits on possible Z' boson masses were set. A $Z'_{\rm SSM}$ with couplings equal to the standard model Z (a "sequential standard model" Z') and a mass below 4.5 TeV was excluded by ATLAS, while CMS set a lower mass limit of 4.0 TeV. The experiments also place limits on the parameters of extra dimension models and in the case of ATLAS on the parameters of a minimal walking technicolor model [19–23], consistent with a 125 GeV Higgs boson [80]. For a general review of searches in these channels see the PDG review of Z prime in this volume [76].

In addition, both experiments have also searched for Z' decaying to a ditau final state [81,82]. While less sensitive than dielectron or dimuon final states, an excess in $\tau^+\tau^-$ could have interesting implications for models in which lepton universality is not a requirement and enhanced couplings to the third generation are allowed. This analysis led to lower limits on the mass of a $Z'_{\rm SSM}$ of 2.4 and 2.1 TeV from ATLAS and CMS respectively.

$Z' \to q\overline{q}$:

The ability to relatively cleanly select $t\bar{t}$ pairs at the LHC together with the existence of enhanced couplings to the third generation in many models makes it worthwhile to search for new particles decaying in this channel. Both ATLAS [84] and CMS [83] have carried out searches for new particles decaying into $t\bar{t}$.

ATLAS focused on the lepton plus jets final state, where the top quark pair decays as $t\bar{t} \to WbWb$ with one W boson decaying leptonically and the other hadronically; CMS used final states where both, one or neither W decays leptonically and then combined the results. The $t\bar{t}$ invariant mass spectrum was analyzed for any excess, and no evidence for any resonance was seen. ATLAS excluded a narrow (Γ/m = 1.2%) leptophobic top-color Z' boson with masses between 0.7 and 2.1 TeV and with Γ/m = 3% between 0.7 and 3.2 TeV. CMS set limits on leptophobic Z' bosons for three different assumed widths Γ/m = 1.0% , Γ/m = 10.0%, and Γ/m = 30.0% of 3.9 TeV to 4.0 TeV and exclude RS KK gluons up to 3.3 TeV.

Both ATLAS [85] and CMS [86] have also searched for resonances decaying into $q\overline{q}$, qg or gg using the dijet invariant mass spectrum. Model-independent upper limits on cross sections were set; ATLAS excluded Z' bosons below 2.1 TeV, W' bosons below 3.6 TeV and chiral W^* bosons below 3.4 TeV. CMS was able to exclude W' bosons below 2.7 TeV; Z' bosons below 2.1 TeV and between 2.3 and 2.6 TeV; color octet scalars below 3.0 TeV; and g_{KK} gravitons below 1.9 TeV. Searches were also carried out for wide resonances, assuming Γ/m up to 30%, and excluded axigluons and colorons with mass below 5.5 TeV. Additionally ATLAS [87] and CMS [88] searched for $Z' \to b\bar{b}$ selecting events where at least one of the jets is b-tagged. ATLAS excluded Z' bosons in the range of 1.1 to 1.5 TeV while CMS excluded masses between 1.2 and 1.68 TeV.

$W' \to \ell\nu$:

Both LHC experiments have also searched for massive charged vector bosons. In this section we include a summary of the results, with emphasis on final states with third generation fermions, while the details on other decays are discussed in the mini-review of W' [77]. ATLAS searched for a heavy W' decaying to $e\nu$ or $\mu\nu$ and find no excess over the standard model expectation. A sequential standard model (SSM) W' boson (assuming zero branching ratio to WZ) with mass less than 5.1 TeV was excluded [89] using 36 fb^{-1} dataset at $\sqrt{s}$ = 13 TeV, and excited chiral bosons W^* excluded up to 3.21 TeV [90](20.3 fb^{-1}, $\sqrt{}$ = 8 TeV). Based on a smaller dataset, the CMS experiment excluded a SSM W' boson with mass up to 4.1 TeV [91] and presented the upper limits on the production of generic W' bosons decaying into this final state using a model-independent approach.

CMS [92] has carried out a complementary search in the $\tau\nu$ final state. As noted above, such searches place interesting limits on models with enhanced couplings to the third generation. No excess was observed and limits between 2.0 and 2.7 TeV were set on the mass of a W' decaying preferentially to the third generation; a W' with universal fermion couplings was also excluded for masses less than 2.7 TeV.

$W' \to t\overline{b}$:

Heavy new gauge bosons can couple to left-handed fermions like the SM W boson or to right-handed fermions. W' bosons that couple only to right-handed fermions (W'_R) may not have leptonic decay modes, depending on the mass of the right-handed neutrino. For these W' bosons, the $t\overline{b}$ ($t\overline{b} + \overline{t}b$) decay mode is especially important because in many models the W' boson is expected to have enhanced couplings

to the third generation of quarks relative to those in the first and second generations. It is also the hadronic decay mode with the best signal-to-background. ATLAS and CMS have performed searches for W' bosons via the $W' \to$ tb decay channel in the lepton+jets and all-hadronic final state.

The CMS lepton+jets search [93,94,95,96], $W' \to$ tb $\to$ Wbb $\to \ell\nu$bb, proceeded via selecting events with an isolated lepton (electron or muon), and at least two jets, one of which is identified to originate from a b-quark. The mass of the W' boson ($M_{\rm tb}$) was reconstructed using the four-momentum vectors of the final state objects (bb$\ell\nu$). The distribution of $M_{\rm tb}$ is used as the search discriminant. A search [96] using 35.9fb^{-1} of data, collected at $\sqrt{s} = 13$ TeV, led to an exclusion of W'_R bosons with masses below 3.4 TeV (3.6 TeV) if $M_{W'_R} >> M_{\nu_R}$ ($M_{W'_R} < M_{\nu_R}$), where M_{ν_R} is the mass of the right-handed neutrino.

The CMS search for $W' \to$tb decays using the all-hadronic final state focused on W' masses above 1 TeV [95]. In this region, the top quark gets a large Lorentz boost and hence the three hadronic products from its decay merge into a single large-radius jet. Techniques which rely on substructure information of the jets [97] are employed to identify boosted W and top quark jets and compute the mass of the jet. W' candidate mass was computed from back-to-back boosted top tagged jet and a low mass b tagged jet. From this all-hadronic search, W' bosons were excluded for masses up to 2.02 TeV.

ATLAS has searched for W'_R bosons in the $t\bar{b}$ final state both for lepton+jets [98] and all-hadronic [99] decays of the top. No significant deviations from the standard model were seen in either analysis and limits were set on the $W' \to t\bar{b}$ cross section times branching ratio and W' bosons with purely left-handed (right-handed) couplings to fermions were excluded for masses below 1.70 (1.92) TeV.

In addition, the above studies also provided upper limits on the W' effective couplings to right- and left-handed fermions. In Fig. 113.1 (bottom) the upper limits on W' couplings normalized to the SM W couplings derived by ATLAS [98] are shown. The top panel of Fig. 113.1 shows the upper limits for arbitrary combinations of left- and right-handed couplings of the W' boson to fermions set using a model independent approach by CMS [96].

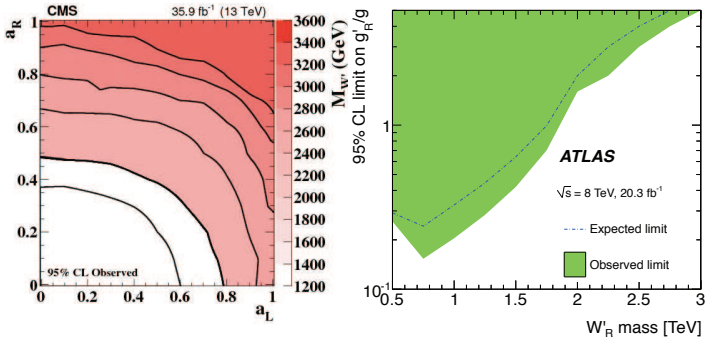

Figure 113.1: Left panel: Observed limits on the W' boson mass as function of the left-handed ($a_{\rm L}$) and right-handed ($a_{\rm R}$) couplings. Black lines represent contours of equal W' boson mass [96]. Right panel: Observed and expected regions, on the g$'$/g vs mass of the W' -boson plane, that are excluded at 95% CL, for right-handed W' bosons [98].

113.2.2. *Searches for Resonances decaying to Vector Bosons and/or Higgs Bosons* :

$X \to WW, WZ, ZZ$:

Both the ATLAS and CMS experiments have used the data collected at $\sqrt{s} = 8$ TeV and $\sqrt{s} = 13$ TeV to search for resonances decaying to pairs of bosons. Overall no significant excesses were seen in the full datasets that were analyzed and the results are interpreted in models with heavy vector triplets (HVT) [100], models with strong gravity and extra spatial dimensions, as well as setting model independent limits as a function of mass. For a full review of models including extra spatial dimensions including the interpretation of many of these results in that context please see the review of extra dimensions in this volume [73].

Utilizing data collected at $\sqrt{s} = 8$ TeV, ATLAS [101] and CMS [102] have both looked for a resonant state (such as a W') decaying to WZ in the fully-leptonic channel, $\ell\nu\ell'\ell'$ (where $\ell, \ell' = e, \mu$). The WZ invariant mass distribution reconstructed from the observed lepton momenta missing transverse energy. The backgrounds arise mainly from standard model WZ, ZZ and $t\bar{t} + W/Z$ production. No significant deviation from the standard model prediction is observed by either experiment. A W' with mass less than 1.55 (1.52) TeV is excluded by CMS (ATLAS); ATLAS also sets limits on the production cross section for HVT particles, and CMS sets limits on the production of low-scale technimesons ρ_{TC} from the reconstructed WZ mass spectrum and cross section.

ATLAS [103,104] and CMS [105] have also searched for narrow resonances decaying to WW, WZ or ZZ in $\ell\nu jj$ and $\ell\ell jj$ final states (where one boson decays leptonically and the other to jets) in data recorded at $\sqrt{s} = 13$ TeV. No deviation from the standard model is seen by either experiment; resonance masses below 2.750 TeV for a HVT model decaying into WW and 2.820 TeV decaying into WZ by ATLAS and below 2.4 TeV by CMS.

Searches have also been conducted in fully hadronic final states. ATLAS [106] and CMS [107] have searched for massive resonance in dijet systems with one or both jets identified as a W or a Z boson using jet-substructure techniques. Limits are set by both experiments on the production cross section times branching ratio for new HVT particles decaying to WZ and ZZ and for g_{KK} gravitons decaying to WW or ZZ. ATLAS excludes HVT particles between 1.2 and 3.5 TeV while CMS excludes W' bosons below 3.6 TeV and Z' bosons below 2.7 TeV.

$X \to W/Z + H^0$ and $X \to H^0H^0$:

With the existence and decay properties of the Higgs boson established, and the significant datasets now available, it is possible to use searches for anomalous production of the Higgs as a potential signature for new physics. ATLAS [108,109] and CMS [110,111] have both searched in the data collected at $\sqrt{s} = 13$ TeV for new particles decaying to a vector boson plus a Higgs boson, where the vector boson decays leptonically or hadronically and the Higgs boson to $b\bar{b}$. No deviation from the standard model is seen in any of these final states and limits can be placed on the allowed production cross section times branching ratio for resonances on a heavy vector triplet model. The exact limits depend on the parameters considered but exclude HVT particles with a mass up to 3.8 TeV. Both experiments also place model-independent limits on the production cross-section as a function of mass.

Both experiments [112,113,114] have also searched for resonant production of Higgs boson pairs $X \to H^0H^0$ with $H^0 \to b\bar{b}$. No signal is observed and limits are placed on the possible production cross section for any new resonance and cross-section limits are placed between 1000 fb and 2 fb for masses between 0.3and 3.0 TeV on resonant production. ATLAS places additionally places limits on non-resonant Standard Model Higgs production constrained to be less than 330 fb.

$Y \to W/Z + X$ with $X \to jj$:

ATLAS has searched for a dijet resonance [115] with an invariant mass in the range $130 - 300$ GeV, produced in association with a W or a Z boson. The analysis used 20.3 fb^{-1} of data recorded at $\sqrt{s} = 8$ TeV. The W or Z boson is required to decay leptonically ($\ell = e, \mu$). No significant deviation from the standard model prediction is observed and limits are set on the production cross section times branching ratio for a hypothetical technipion produced in association with a W or Z boson from the decay of a technirho particle in the context of Low Scale Technicolor models.

ATLAS [116] has searched for a resonance (Y) decaying into XH where $H \to bb$ and a new particle X decays into dijet pairs ($X \to jj$). A two dimensional scan in both Y, between 1 and 4 TeV, and X masses, between 0.05 and 1 TeV is performed. No significant excesses are seen and upper limits on the cross-section of this process are set as a function of X and Y.

Summary of Searches with Diboson Final States:

Both ATLAS [117] and CMS [118] provide plots summarizing the various searches results and limits. The results are shown in the context of HVT models and models of strong gravity with extra spatial dimensions. No excess is seen in any search and limits on the W' are placed up to 3.5 TeV and 2.7 TeV on Z' particles in the HVT model as seen in Fig. 113.2

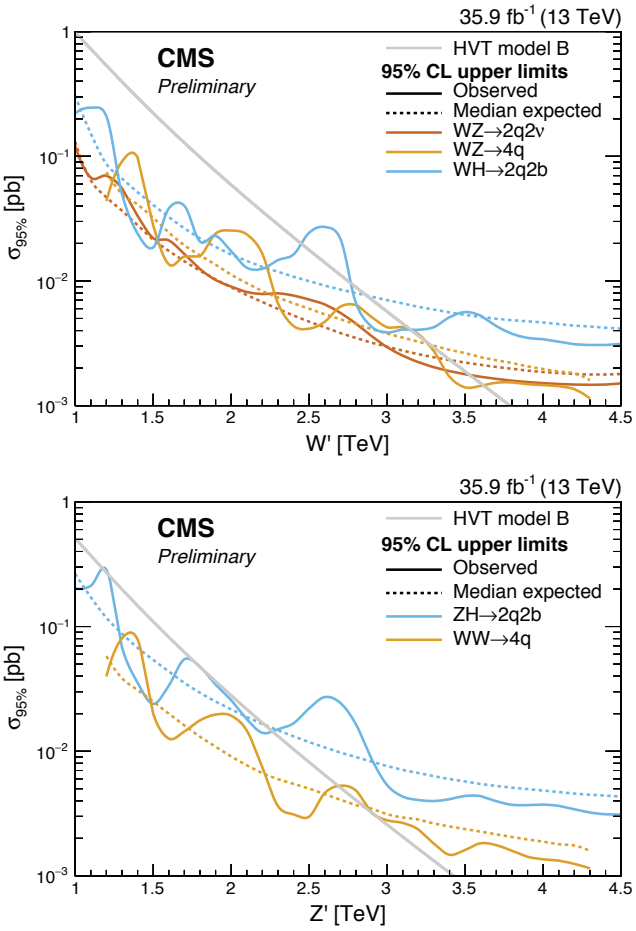

Figure 113.2: Top panel: Observed limits from W' to diboson from CMS [118]. Bottom panel: Observed limits from Z' to diboson decays from CMS [118]. Note in both cases ATLAS provides similar summary plots which are available [117].

113.2.3. *Vector-like third generation quarks* :

Vector-like quarks (VLQ) have non-chiral couplings to W bosons, i.e. their left- and right-handed components couple in the same way. They therefore have vectorial couplings to W bosons. Vector-like quarks arise in Little Higgs theories, top-coloron-models, and theories of a composite Higgs boson with partial compositeness. In the following, the notation T quark refers to a vector-like quark with charge 2/3 and the notation B quark refers to a vector-like quark with charge $-1/3$, the same charges as the SM top and b quarks respectively. The X and Y have charges 5/3, and $-4/3$ respectively. Vector-like quarks couple with SM quarks with Yukawa interactions and may exist as SU(2) singlets (T, and B), doublets $[(X,T),(T,B),(B,Y)]$, or triplets $[(X,T,B),\ (T,B,Y)]$. At the LHC, VLQs can be pair produced via the dominant gluon-gluon fusion. VLQs can also be produced singly by their electroweak effective couplings to a weak boson and a standard model quark. Single production rate is expected to dominate over the rate of pair production at large VLQ masses. T quarks can decay to bW, tZ, or tH^0. Weak isospin singlets are expected to decay to all three final states with (asymptotic) branching fractions of 50%, 25%, 25%, respectively. Weak isospin doublets are expected to decay exclusively to tZ and to tH^0 [119] with equal branching ratios. Analogously, B quarks can decay to tW, bZ, or bH^0. The Y and X quarks decay exclusively to bW and to tW. While these are taken as the benchmark scenarios, other representations are possible and hence the final results are interpreted for many allowed branching fraction combinations.

Given the multiple decay modes of the VLQs, the final state signatures of both pair produced and the singly produced VLQs are fairly rich with leptons, jets, b-jets, and missing energy. Depending on the mass of the VLQ, the top quarks and $W/Z/H^0$ bosons may be Lorentz boosted and identified using jet substructure techniques. Thus the searches are performed using lepton+jets signatures, multi-lepton and all-hadronic decays. In addition, T or B quarks with their antiparticles can result in events with same-sign leptons, for example if the decay $T \to tH \to bWW^+W^-$ is present, followed by leptonic decays of two same-sign W bosons. In the following subsections, while we describe the searches for each of the decay modes of the VLQs, the same analysis can be re-interpreted to obtain the sensitivity to a combination with varied branching fractions to the different decay modes.

In the following sections, the results obtained for T (B) quarks assuming 100% branching ratio to Wb (Wt) are also applicable to heavy vector-like Y (X) with charge 4/3 (5/3).

113.2.3.1. *Searches for T quarks that decay to W, Z and H^0 bosons:*

$T/Y \to bW$:

CMS has searched for pair production of heavy T quarks that decay exclusively to bW [120,121,122]. The analysis selected events with exactly one charged lepton, assuming that the W boson from the second T quark decays hadronically. Under this hypothesis, a 2-constraint kinematic fit can be performed to reconstruct the mass of the T quark. In Ref. 121 and Ref. 122, the two-dimensional distribution of reconstructed mass vs S_T was used to test for the signal. S_T is the scalar sum of the missing p_T and the transverse momenta of the lepton and the leading four jets. This analysis, when combined with the search in the fully hadronic final state [123] excluded new quarks that decay 100% to bW for masses below 0.89 TeV [122]. At times the hadronically-decaying W boson is produced with a large Lorentz boost, leading to the W decay products merged into a wide single jet also known as a fat jet. Algorithms such as jet pruning [124] were used to resolve the substructure of the fat jets from the decays of the heavy particles. If the mass of the boosted jet was compatible with the W boson mass, then the W boson candidate jet and its subjets were used in the kinematic reconstruction of the T quark. No excess over standard model backgrounds was observed. Upper limits on the production cross section as a function of the mass of T quarks were measured. By comparing them with the predicted cross section for vector like quark pair production, the strong pair production of T quarks was excluded for masses below 1.30 TeV (1.28 TeV expected) [120].

An analogous search has been carried out by ATLAS [125], [126] for the pair production of heavy T quarks. It used the lepton+jets final state with an isolated electron or muon and at least four jets, including a b-jet and required reconstruction of the T quark mass. Given the mass range of the T quark being explored was from a 0.4 TeV to a couple of TeV, the W boson from the T quark may fall in two categories: those with a high boost leading to merged decay products, and others where the two jets from the W boson were resolved. In addition, the selection was optimized to require large angular separation between the high p_T W bosons and the b-jets. The $T \to Wb$ candidates were constructed from both the leptonically and hadronically decaying W bosons by pairing them with the two highest p_T b-tagged jets in the event. The pairing of b-jets with W bosons which minimizes the difference between the masses of leptonically decaying T ($m_{lep}(T)$) and the hadronic T ($m_{had}(T)$) was chosen. Finally, $m_{lep}(T)$ was used as the discriminating variable in a signal region defined by high S_T, the scalar sum of the missing p_T, the p_T of the lepton and jets, and the opening angle between the lepton and the neutrino ($\Delta\ R(e,\nu)$). With the 36.1fb^{-1} data collected during

Run 2 at $\sqrt{s}$ = 13 TeV, assuming 100% branching ratio to the Wb decay, the observed lower limit on the T mass was 1.35 TeV, and in the SU(2) singlet scenario, the lower mass limit was obtained to be 1.17 TeV [125].

A targeted search for a T quark, produced singly in association with a light flavor quark and a b quark and decaying into bW, was carried out by CMS at $\sqrt{s}$=13 teV and a dataset corresponding to 2.3fb^{-1} [127]. The anlaysis used lepton+jets events, with at least one b-tagged jet with large transverse momentum, and a jet in the forward η region. Selected events were required to have $S_T > 500$ GeV, where S_T is defined as the scalar sum of the transverse momenta of the lepton, the leading central jet, and the missing transverse momentum. The invariant mass of the T candidate was used as the discriminating variable and was reconstructed using the four-vectors of the leptonically decaying W boson and the leading central jet. No excess over the standard model prediction was observed. As the VLQ width is proportional to the square of the coupling, upper limits were set on the production cross section assuming a narrow width VLQ with coupling greater than 0.5. For Y/T quarks with a coupling of 0.5 and a 100% branching fraction for the decay to bW the excluded masses were in the range from 0.85 to 1.40 TeV [127]. A similar search [128,129] performed by ATLAS, for singlet T quarks, with coupling of $\sqrt{(c_L{}^{Wb})2 + (c_R{}^{Wb})^2} = \frac{1}{\sqrt{2}}$, and $\mathcal{B}(T \to bW) = 0.5$, led to exclusion limits on T/Y masses below 1.44 TeV. This search also provided limits, as a function of the Y quark mass, on the coupling of the Y quark to bW, and the mixing parameter $|sin\theta_R|$ for a (Y,B) doublet model [128]. For a VLQ mass around 1 TeV, the smallest excluded coupling-strength values are obtained, with $|c_L^{Wb}|$=0.45 for a T quark and $\sqrt{(c_L{}^{Wb})2 + (c_R{}^{Wb})^2}$=0.33 for a Y quark. The limit on $|sin\theta_R|$ is around 0.23, and close to the constraints from electroweak precision observables.

$T \to tH^0$:

ATLAS has performed a search for $T\overline{T}$ production with $T \to tH^0$ [126], [130]. Given the dominant decay mode $H^0 \to b\overline{b}$, these events are characterized by a large number of jets, many of which are b-jets. Thus the event selection required one isolated electron or muon and high jet multicplicity (including b tagged jets). The sample is categorized by the jet multiplicity (5 and ≥6 jets in the 1-lepton channel; 6 and ≥7 jets in the 0-lepton channel), b-tag multiplicity (2, 3 and ≥4) and mass-tagged jet multiplicity (0, 1 and ≥2). The distribution of $m_{\rm eff}$, defined as the scalar sum of the lepton and jet p_Ts and the missing E_T, for each category were used as the discriminant for the final signal and background separation. No excess of events were found. Weak isospin doublet T quarks were excluded below 1.16 TeV.

The CMS search for $T\overline{T}$ production, with $T \to tH^0$ decays has been performed in both lepton+jets, multilepton and all hadronic final states. The lepton+jets analysis [131] emphasizes the presence of large number of b-tagged jets, and combined with other kinematic variables in a Boosted Decision Tree (BDT) for enhancing signal to background discrimination. The multilepton analysis [131] was optimized for the presence of b-jets and the large hadronic activity. For $\mathcal{B}(T \to Wb) = 1$, the combined lepton+jets and multilepton analyses led to a lower limit on T quark masses of 0.71 TeV. A search for $T \to tH^0$ in all hadronic decays [132], optimized for a high mass T quark, and based on identifying boosted top quark jets has been carried out by CMS. This search aimed to resolve sub-jets within the jets arising from boosted top quark decays, including b-tagging of the sub-jets. A likelihood discriminator was defined based on the distributions of H_T, and the invariant mass of the two b-jets in the events for signal and background. No excess above background expectations was observed. Assuming 100% branching ratio for $T \to tH^0$, this analysis led to a lower limit of 0.75 TeV on the mass of the T quark.

Searches for T quarks at $\sqrt{s}$=13 TeV, based on a 2.6fb^{-1} dataset [133] have been performed by CMS using the lepton+jets final state. This search has been optimized for high mass T quarks by exploiting techniques to identify W or Higgs bosons decaying hadronically with large transverse momenta. The boosted W channel excluded T quarks decaying only to bW with masses below 0.91 TeV, and the boosted tH channel excluded T quarks decaying only to tH for masses below 0.89 TeV.

A CMS search for $T \to tH^0$ with $H^0 \to \gamma\gamma$ decays has been performed [134] in pair production of T quarks. To identify the Higgs boson produced in the decay of the heavy T quark, and the subsequent $H^0 \to \gamma\gamma$ decay, the analysis focused on identification of two photons in events with one or more high p_T lepton+jets or events with no leptons and large hadronic activity. A search for a resonance in the invariant mass distribution of the two photons in events with large hadronic activity defined by the H_T variable showed no excess above the prediction from standard model processes. The analysis resulted in exclusion of T quark masses below 0.54 TeV.

A search for electroweak single production of T quark decaying to tH^0 using boosted topologies in fully hadronic [135] and lepton+jets [136] in the final states has been performed by CMS. The electroweak couplings of the T quarks to the SM third generation quarks are highly model dependent and hence these couplings determine the rates of the single T quark production. In both analyses, T quark candidate invariant mass was reconstructed using the boosted Higgs boson jets and the top quark. Higgs boson jets were identified using jet substructure techniques and subjet b tagging. For the lepton+jets analysis the top quark was reconstructed from the leptonically decaying W and the b jet, while in the all hadronic analysis the top quark jet was tagged using substructure analysis. There was no excess of events observed above background. Exclusion limits on the product of the production cross section and the branching fraction ($\sigma(pp \to Tqt/b) \times \mathcal{B}(T \to tH^0)$ were derived for the T quark masses in the range 0.70-1.8 TeV. From the lepton+jets analysis, for a mass of 1.0 TeV, values of ($\sigma(pp \to Tqt/b) \times \mathcal{B}(T \to tH^0)$ greater than 0.8 and 0.7 pb were excluded assuming left- and right-handed coupling of the T quark to standard model fermions, respectively [136]. For the all-hadronic analysis, upper limits between 0.31 and 0.93 pb were obtained on ($\sigma(pp \to Tqt/b) \times \mathcal{B}(T \to tH^0)$ for T quark masses in the range 1.0-1.8 TeV [135].

$T \to tZ$:

Both ATLAS and CMS search for T quarks that decay exclusively into tZ in pp collisons at $\sqrt{s}$ = 13 TeV. No excesses were found in either search.

ATLAS performed a search [137] for optimized pair production of vector-like top quarks decaying into tZ where the Z boson subsequently decays into neutrino pairs utilizing 36.1 fb^{-1} of data. The search selected events with one lepton, multiple jets, and significant missing transverse momentum. No significant excesses were found and lower limits on the mass of a vector like top quark were placed, excluding masses below 0.87 TeV (weak-isopsin singlet) , 1.05 TeV (weak-isospin doublet), and 1.16 TeV (pure Zt mode). CMS searched [138] for single production of T quarks decaying into tZ with the Z boson decaying to pairs of charged leptons (electrons and muons) and the top quark decaying hadronically usig 35.9 fb^{-1} of data. Limits were placed on T quarks with masses between 0.7 and 1.7 TeV excluding the product of cross-section and branching fraction above values of 0.27 to 0.04 pb. Additionally, limits on a Z' boson decaying into tZ were set.

Combined searches for $T \to bW/tZ/tH^0$:

Most of the analyses described above targeted an individual decay mode of the T quark, with 100% branching ratio to either bW, tZ or tH^0 and were optimized accordingly. However, they have varied sensitivity to all three decay modes and the results can be interpreted as a function of branching ratios to each of the three decay modes, with the total adding up to unity ($\mathcal{B}(tH) + \mathcal{B}(tZ) + \mathcal{B}(Wb) = 1$).

Combinations of analyses are performed by both ATLAS and CMS. The limits set by ATLAS searches in lepton+jets, dileptons with same-sign charge, and final states with Z boson have been combined and the results obtained for various sets of branching fractions for T quark decays to bW, tH^0 and tZ are shown in Fig. 113.3. In the combined analysis, ATLAS set lower T quarks mass limits that ranged from 0.6 to 1.35 TeV for all possible values of the branching fractions to the three decay modes [125,139]. In Fig. 113.3, exclusion is shown in the plane of $\mathcal{B}(T \to Ht)$ versus $\mathcal{B}(T \to Wb)$, for different values of

the T quark mass from the lepton+jets analyses optimized for bW, tH, Zt modes and the same-sign leptons analysis. The grey (light shaded) area in the figure corresponds to the unphysical region where the sum of branching ratios exceeds unity, or is smaller than zero. The default branching ratio values for the weak-isospin singlet and doublet cases are also shown in Fig. 113.3 as cross and square symbols respectively. A similar combination was also performed by CMS.

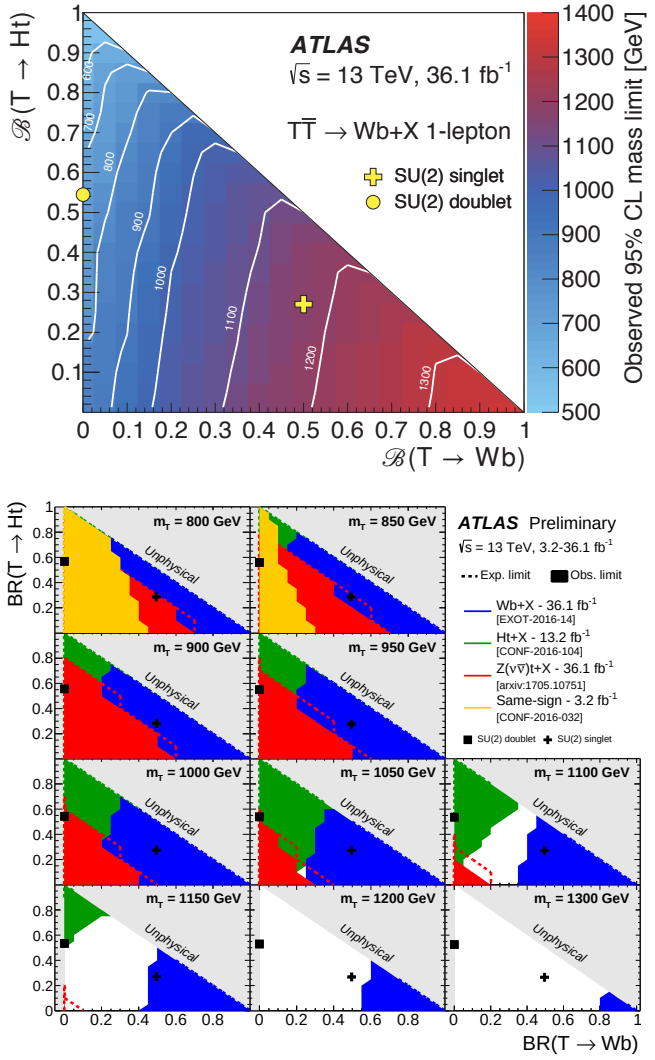

Figure 113.3: Observed limits on the mass of the T quark in the plane of $\mathcal{B}(T \to tH^0)$ versus $\mathcal{B}(T \to bW)$ from all ATLAS searches for TT production. The markers indicate the default branching ratios for the SU(2) singlet and doublet scenarios with masses above 0.8 TeV, where they are approximately independent of the VLQ T mass. Top panel: Summary from the $T \to Wb$ analysis [125]. Bottom panel: Exclusions for different values of the T quark mass for the Wb+X (blue), the tH^0+X (green), the $Z(\nu\bar{\nu})t$+X (red) and the same-sign leptons (yellow) analyses. Similar combination plots are also made by CMS.

An inclusive search by CMS targeted at heavy T quarks decaying to any combination of bW, tZ, or tH^0 is described in Ref. 131. Selected events have at least one isolated charged lepton. Events were categorized according to number and flavour of the leptons, the number of jets, and the presence of hadronic vector boson and top quark decays that are merged into a single jet. The use of jet substructure to identify hadronic decays significantly increases the acceptance for high T quark masses. No excess above standard model backgrounds was observed. Limits on the pair production cross section of the new quarks are set, combining all event categories, for all combinations of branching fractions into the three final states. For T quarks that exclusively decay to $bW/tZ/tH^0$, masses below 0.70/0.78/0.71 TeV are excluded.

113.2.3.2. *Searches for B quarks that decay to W, Z and H^0 bosons:*

ATLAS and CMS have performed searches for pair production of heavy B quarks which subsequently decay to Wt, bZ or bH^0. The searches have been carried out in final states with single leptons, di-leptons (with same charge or opposite charge), multileptons, as well as in fully hadronic final states.

$B \to WtX$:

A search for $B \to tW$ has been performed by the ATLAS experiment [125] using lepton+jets events with one hadronically decaying W and one leptonically decaying W utilizing 36.1 fb^{-1} of data at $\sqrt{s} = 13$ TeV. The search was optimized for T production decaying into Wb. Since the analysis was optimized for $T \to Wb$ rather than Wt decays the analysis does not reconstruct the full B mass. As discussed earlier, the hadronically and leptonically decaying heavy quarks were required to have similar reconstructed masses (within 300 GeV). The interpretation of the $T \to Wb$ in the context of $B \to tW$ production led to the exclusion of Heavy B like VLQs for masses less than 1.25 TeV and 1.08 TeV, assuming a 100% branching fraction to tW or SU(2) singlet B scenario, respectively.

A similar search by CMS [140], using 19.8 fb^{-1} of $\sqrt{s} = 8$ TeV data, selected events with one lepton and four or more jets, with at least one b-tagged jet, significant missing p_T, and further categorizes them based on the number of jets tagged as arising from the decay of boosted W, Z or H^0 bosons. The S_T distributions of the events in different categories showed no excess of events above the expected background and yielded a lower limit on the B quark mass of 0.73 TeV for $BR(B \to Wt) = 1$.

CMS [133] also searches for pair production of both TT and BB with collisions from 2.5 fb^{-1} of $\sqrt{s} = 13$ TeV data. The analysis searches for events with one high p_T lepton , multiple jets, and highly boosted W or Higgs bosons decaying hadronically. The analysis focuses on pair production and selects events with either a boosted W or Higgs candidate and then proceeds to search for anomalous production in excess of standard model production. Seeing no significant excesses CMS then proceeded to set limits in many different interpretations. The strongest was from the the $B \to Wt$ interpretation leading to excluding heavy vector like B's less than 0.73 TeV.

$B \to bZX$:

A search by CMS [141] for the pair-production of a heavy B quark and its antiparticle, one of which decays to bZ, selected events with a Z-boson decay to e^+e^- or $\mu^+\mu^-$ and a jet identified as originating from a b quark. The signal from $B \to bZ$ decays would appear as a local enhancement in the bZ mass distribution. No such enhancement was found and B quarks that decay 100% into bZ are excluded below 0.70 TeV. This analysis also set upper limits on the branching fraction for $B \to bZ$ decays of 30-100% in the B quark mass range 0.45-0.70 TeV. A complementary search has been carried out by ATLAS for new heavy quarks decaying into a Z boson and a b-quark [142]. Selected dilepton events contain a high transverse momentum Z boson that decays leptonically, together with two b-jets. If the dilepton events have an extra lepton in addition to those from the Z boson, then only one b-jet is required. No significant excess of events above the standard model expectation was observed, and mass limits were set depending on the assumed branching ratios, see Fig. 113.4. In a weak-isospin singlet scenario, a B quark with mass lower than 0.65 TeV was excluded, while for a particular weak-isospin doublet scenario, a B quark with mass lower than 0.73 TeV was ruled out.

ATLAS has searched for the electroweak production of single B quarks, which is accompanied by a b-jet and a light jet [142]. The dilepton selection for double B production was modified for the single B production study by requiring the presence of an additional energetic jet in the forward region. An upper limit of 200 fb was

obtained for the process $\sigma(pp \to B\bar{b}q) \times B(B \to Zb)$ with a heavy B quark mass at 0.70 TeV. This search indicated that the electroweak mixing parameter X_{Bb} below 0.5 is neither expected or observed to be excluded for any values of B quark mass.

Combination $B \to tW/bZ/bH^0$:

The ATLAS experiment has combined the various analyses targeted for specific decay modes to obtain the most sensitive limits on the pair production of B quarks [126]. The analyses using single lepton events, same sign charge dilepton events, events with opposite sign dilepton events, and multilepton events are combined to obtain lower limits on the mass of the B quark in the plane of $BR(B \to Wt)$ vs $BR(B \to bH)$. The searches were optimized for 100% branching fractions and hence are most sensitive at large $BR(B \to Wt)$, and also at large $BR(B \to bH^0)$. For all possible values of branching ratios in the three decay modes tW, bZ, or bH^0, the lower limits on the B quark mass was found to be between 0.58 TeV and 0.81 TeV and as shown in Fig. 113.4. Analyses were also combined by the ATLAS experiment to provide the most sensitive limits on the pair production of B quarks to produce limits as a function of both B mass and branching ratio [125]. CMS provided similar combinations of their analyses.

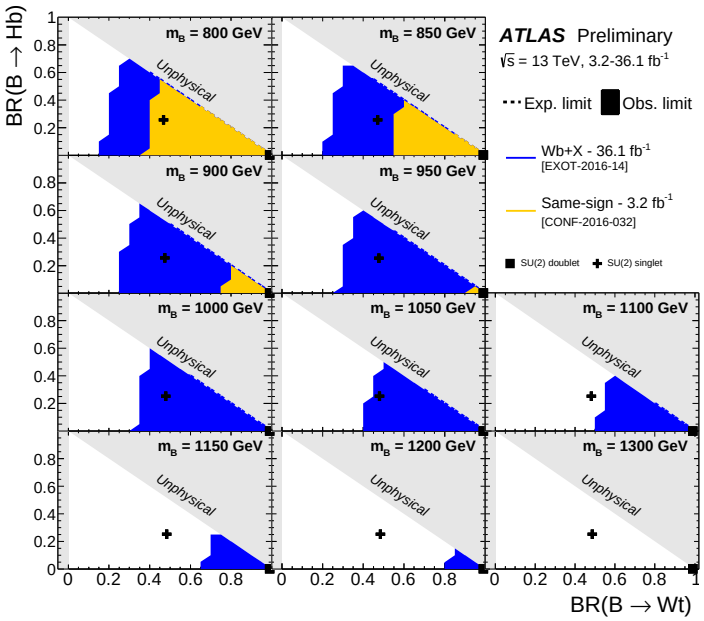

Figure 113.4: Observed limits on the mass of the B quark in the plane of $BR(B \to bH^0)$ versus $BR(B \to tW)$ from ATLAS searches for BB production [125]. Exclusion limits are drawn sequentially for each of the analyses and overlaid (rather than combined).

113.2.3.3. *Searches for top-partner quark X:*

Searches for a heavy top vector-like quark X, with exotic charge 5/3, such as that proposed in Refs. 143,144, have been performed by both ATLAS and CMS [125,145].

The analyses assumed pair-production or single-production of X with X decaying with 100% branching fraction to to tW. Searches for X have been performed using two final state signatures: same-sign leptons and lepton+jets.

The analysis based on searching for same-sign leptons, from the two W bosons from one of the X, has smaller backgrounds compared to the lepton+jets signature. Requiring same-sign leptons eliminates most of the standard model background processes, leaving those with smaller cross sections: $t\bar{t}$, W, $t\bar{t}Z$, WWW, and same-sign WW. In addition, backgrounds from instrumental effects due to charge misidentification were considered. Assuming pair production of X, the analyses by CMS using H_T as the discriminating variable restrict the X mass to be higher than 1.16 (1.10) TeV for a right (left) handed chirality particle [145,146,147]. The limits obtained by ATLAS, by classifying the signal region by number of b-jets, H_T, and missing p_T in the event, corresponded to a lower mass limit on X of 0.99 TeV [148,149].

Searches for X using leptons+jets final state signatures are based on either full or partial reconstruction of the T mass from the lepton, jets (including b jets) and missing p_T. The CMS search [145,150] also utilized jet substructure techniques to identify boosted X topologies. The discriminating variable used was the mass constructed from the lepton and b-tagged jet, $M_{(\ell,b)}$, which corresponds to the visible mass of leptonically decaying top quark. To optimize the search sensitivity, the events were further separated into categories based on lepton flavor (e, μ), the number of b-tagged jets, the number of W-tagged jets, and the number of t-tagged jets. In the absence of a signal, the CMS analysis excluded X quark masses with right-handed (left-handed) couplings below 1.32 (1.30) TeV [150].

The ATLAS lepton+jets search for X utilized events with high p_T W bosons and b-jets. The search described earlier for T pair production, with $T \to Wb$ decays, can be reinterpreted as a search for $X \to tW$. This analysis excluded X with masses below 1.25 TeV [125].

The single X production cross section depends on the coupling constant λ of the tWX vertex. ATLAS has performed an analysis of same-sign dileptons which includes both the single and pair production. This analysis led to a lower limit on the mass of the X of 0.75 TeV for both values of $\lambda = 0.5$ and 1.0 [151].

113.2.4. ***Colorons and Colored Scalars*** : These particles are associated with top-condensate and top-seesaw models, which involve an enlarged color gauge group. The new particles decay to dijets, $t\bar{t}$, and $b\bar{b}$.

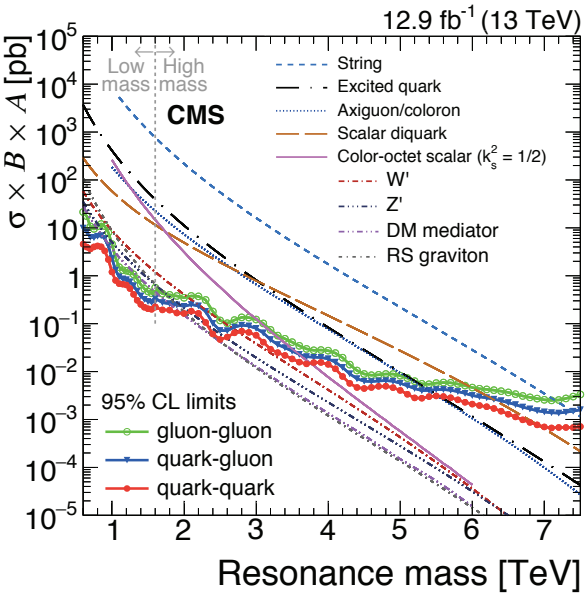

Figure 113.5: Observed 95% C.L. limits on $\sigma \times B \times A$ for string resonances, excited quarks, axigluons, colorons, E6 diquarks, s8 resonances, W' and Z' bosons, and Randall-Sundrum gravitons g_{KK} from [156].

Direct searches for colorons, color-octect scalars and other heavy objects decaying to $q\bar{q}$, qg, qq, or gg has been performed using LHC data from pp collisions at $\sqrt{s}$ =7, 8 and 13 TeV. Based on the analysis of dijet events from a data sample corresponding to a luminosity of 19.6 fb^{-1}, at $\sqrt{s}$ = 8 TeV the CMS experiment excluded pair production of colorons with mass between $1.20 - 3.60$ and $3.90 - 4.08$ TeV [152]. Analyses of inclusive 8- and 10-jet final states with low missing transverse momentum by CMS [153], set limits in several benchmark models. Colorons (axigluons) with masses

between 0.6 and 0.75 (up to 1.15) TeV were excluded, and gluinos in R-parity violating supersymmetric scenarios were ruled out from 0.6 up to 1.1 TeV.

A search for pair-produced colorons based on an integrated luminosity of 5.0 fb^{-1} at $\sqrt{s} = 7$ TeV by CMS excluded colorons with masses between 0.25 TeV and 0.74 TeV, assuming colorons decay 100% into $q\overline{q}$ [154]. This analysis was based on events with at least four jets and two dijet combinations with similar dijet mass. Color-octet scalars (s8) with masses between $1.20 - 2.79$ TeV were excluded by CMS [152], and below 2.7 TeV by ATLAS [155].

These studies have now been extended to take advantage of the increased center-of-mass energy during Run 2 of the LHC. Using the 12.6fb^{-1} of data collected at $\sqrt{s}$ =13 TeV, searches for narrow resonances have been performed by CMS. An analysis of the dijet invariant mass spectrum formed using wide jets [156,157], separated by $\Delta\eta_{jj} \leq 1.3$, led to limits on new particles decaying to parton pairs (qq, qg, gg). Specific exclusions on the masses of colorons and color-octet scalars were obtained and are shown in Fig. 113.5.

113.3. Conclusions

As the above analyses have demonstrated, there is already substantial sensitivity to possible new particles predicted to accompany the H^0 in dynamical frameworks of electroweak symmetry breaking. No hints of any deviations from the standard model have been observed, and limits typically at the scale of a few hundred GeV to a few TeV are set.

Given the need to better understand the H^0 and to determine in detail how it behaves, such analyses continue to be a major theme of Run 2 the LHC, and we look forward to increased sensitivity as a result of the higher luminosity at the increased centre of mass energy of collisions.

References:

1. ATLAS Collab., Phys. Lett. **B716**, 1 (2012).
2. CMS Collab., Phys. Lett. **B716**, 30 (2012).
3. S. Weinberg, Physica A **96**, 327 (1979).
4. A. Manohar and H. Georgi, Nucl. Phys. **B234**, 189 (1984).
5. H. Georgi, Nucl. Phys. **B266**, 274 (1986).
6. R.S. Chivukula, hep-ph/0011264 (2000).
7. R.S. Chivukula, M.J. Dugan, and M. Golden, Phys. Rev. **D47**, 2930 (1993).
8. S. Weinberg, Phys. Rev. **D13**, 974 (1976).
9. S. Weinberg, Phys. Rev. **D19**, 1277 (1979).
10. L. Susskind, Phys. Rev. **D20**, 2619 (1979).
11. K. Lane, hep-ph/0202255 (2002).
12. C.T. Hill and E.H. Simmons, Phys. Reports **381**, 235 (2003), [Erratum-ibid. **390**, 553 (2004)].
13. R. Shrock, hep-ph/0703050 (2007).
14. E. Eichten *et al.*, Rev. Mod. Phys. **56**, 579 (1984) [Addendum-ibid. **58**, 1065 (1986)].
15. E. Eichten *et al.*, Phys. Rev. **D34**, 1547 (1986).
16. See "Status of Higgs Boson Physics" review in this volume..
17. R.S. Chivukula and V. Koulovassilopoulos, Phys. Lett. **B309**, 371 (1993).
18. R. Foadi, M.T. Frandsen, and F. Sannino, Phys. Rev. **D87**, 095001 (2013).
19. B. Holdom, Phys. Lett. **B150**, 301 (1985).
20. K. Yamawaki, M. Bando, and K.-i. Matumoto, Phys. Rev. Lett. **56**, 1335 (1986).
21. T.W. Appelquist, D. Karabali, and L.C.R. Wijewardhana, Phys. Rev. Lett. **57**, 957 (1986).
22. T. Appelquist and L.C.R. Wijewardhana, Phys. Rev. **D35**, 774 (1987).
23. T. Appelquist and L.C.R. Wijewardhana, Phys. Rev. **D36**, 568 (1987).
24. E. Gildener and S. Weinberg, Phys. Rev. **D13**, 3333 (1976).
25. Z. Chacko, R. Franceschini and R. K. Mishra, JHEP **1304**, 015 (2013).
26. B. Bellazzini *et al.*, Eur. Phys. J. **C73**, 2333 (2013).
27. B. Bellazzini *et al.*, Eur. Phys. J. **C74**, 2790 (2014).
28. Z. Chacko, R.K. Mishra, and D. Stolarski, JHEP **1309**, 121 (2013).
29. J.R. Ellis, M.K. Gaillard, and D.V. Nanopoulos, Nucl. Phys. **B106**, 292 (1976).
30. M.A. Shifman *et al.*, Sov. J. Nucl. Phys. **30**, 711 (1979) [Yad. Fiz. **30**, 1368 (1979)].
31. A.I. Vainshtein, V.I. Zakharov, and M.A. Shifman, Sov. Phys. Usp. **23**, 429 (1980) [Usp. Fiz. Nauk **131**, 537 (1980)].
32. M. Bando, K.-i. Matumoto, and K. Yamawaki, Phys. Lett. **B178**, 308 (1986).
33. W.D. Goldberger, B. Grinstein, and W. Skiba, Phys. Rev. Lett. **100**, 111802 (2008).
34. S. Matsuzaki and K. Yamawaki, Phys. Rev. **D85**, 095020 (2012).
35. S. Matsuzaki and K. Yamawaki, Phys. Rev. **D86**, 035025 (2012).
36. E. Eichten, K. Lane, and A. Martin, arXiv:1210.5462 (2012).
37. D.B. Kaplan and H. Georgi, Phys. Lett. **B136**, 183 (1984).
38. D.B. Kaplan, H. Georgi, and S. Dimopoulos, Phys. Lett. **B136**, 187 (1984).
39. M.E. Peskin, Nucl. Phys. **B175**, 197 (1980).
40. J. Preskill, Nucl. Phys. **B177**, 21 (1981).
41. R. Barbieri and A. Strumia, hep-ph/0007265 (2000).
42. N. Arkani-Hamed, A.G. Cohen, and H. Georgi, Phys. Lett. **B513**, 232 (2001).
43. N. Arkani-Hamed *et al.*, JHEP **0208**, 020 (2002).
44. N. Arkani-Hamed *et al.*, JHEP **0207**, 034 (2002).
45. M. Schmaltz and D. Tucker-Smith, Ann. Rev. Nucl. and Part. Sci. **55**, 229 (2005).
46. K. Agashe *et al.*, Phys. Lett. **B641**, 62 (2006).
47. P. Sikivie *et al.*, Nucl. Phys. **B173**, 189 (1980).
48. B. Bellazzini, C. Csaki, and J. Serra, Eur. Phys. J. **C74**, 2766 (2014).
49. R. Essig *et al.*, arxiv:1707.03399.
50. Z. Chacko, H. S. Goh and R. Harnik, Phys. Rev. Lett. **96**, 231802 (2006).
51. R.S. Chivukula, A.G. Cohen, and K.D. Lane, Nucl. Phys. **B343**, 554 (1990).
52. V.A. Miransky, M. Tanabashi, and K. Yamawaki, Phys. Lett. **B221**, 177 (1989) and Mod. Phys. Lett. **A4**, 1043 (1989).
53. W.A. Bardeen, C.T. Hill, and M. Lindner, Phys. Rev. **D41**, 1647 (1990).
54. C.T. Hill, Phys. Lett. **B266**, 419 (1991).
55. B.A. Dobrescu and C.T. Hill, Phys. Rev. Lett. **81**, 2634 (1998).
56. R.S. Chivukula *et al.*, Phys. Rev. **D59**, 075003 (1999).
57. S. Dimopoulos and L. Susskind, Nucl. Phys. **B155**, 237 (1979).
58. E. Eichten and K.D. Lane, Phys. Lett. **B90**, 125 (1980).
59. D.B. Kaplan, Nucl. Phys. **B365**, 259 (1991).
60. T. Appelquist, M. Piai, and R. Shrock, Phys. Rev. **D69**, 015002 (2004).
61. R.S. Chivukula, B.A. Dobrescu, and E.H. Simmons, Phys. Lett. **B401**, 74 (1997).
62. Y. Grossman and M. Neubert, Phys. Lett. **B474**, 361 (2000).
63. S.J. Huber and Q. Shafi, Phys. Lett. **B498**, 256 (2001).
64. T. Gherghetta and A. Pomarol, Nucl. Phys. **B586**, 141 (2000).
65. K. Agashe, R. Contino, and A. Pomarol, Nucl. Phys. **B719**, 165 (2005).
66. G.F. Giudice *et al.*, JHEP **0706**, 045 (2007).
67. R.S. Chivukula and H. Georgi, Phys. Lett. **B188**, 99 (1987).
68. G. D'Ambrosio *et al.*, Nucl. Phys. **B645**, 155 (2002).
69. K. Agashe *et al.*, hep-ph/0509117 (2005).
70. T. Appelquist and R. Shrock, Phys. Lett. **B548**, 204 (2002).
71. B. Keren-Zur *et al.*, Nucl. Phys. **B867**, 429 (2013).
72. J.M. Maldacena, Adv. Theor. Math. Phys. **2**, 231 (1998).
73. For a review, see C. Csaki, J. Hubisz, and P. Meade, hep-ph/0510275 (2005), and "Extra Dimensions" review in this volume.
74. C. Pica, PoS LATTICE **2016**, 015 (2016), arXiv:1701.07782.
75. T. Appelquist *et al.*, Phys. Rev. **D93**, 114514 (2016).
76. PDG review of Zprime boson in this volume.
77. PDG review of Wprime boson in this volume.

78. ATLAS Collab., arXiv:1707.02424 [hep-ex] , submitted to JHEP.
79. CMS Collab., CMS-PAS-EXO-16-031 (2016).
80. ATLAS Collab., Phys. Rev. **D90**, 052005 (2014).
81. ATLAS Collab., arXiv:1709.07242 [hep-ex] (2017).
82. CMS Collab., JHEP **0217**, 48 (2017).
83. CMS Collab., JHEP **0717**, 001 (2016).
84. ATLAS Collab., ATLAS-CONF-2016-014 (2016).
85. ATLAS Collab.,arXiv:1703.09127 [hep-ex], submitted to PRD.
86. CMS Collab., Phys. Lett. B 769,520(2017).
87. ATLAS Collab., Phys. Lett. B 759, 229 (2016).
88. CMS Collab., CMS-PAS-EXO-12-023 (2014).
89. ATLAS Collab., arXiv:1706.04786 [hep-ex] (2017).
90. ATLAS Collab., JHEP **1409**, 037 (2014).
91. CMS Collab., Phys. Lett. **B770**, 278 (2017).
92. CMS Collab., Phys. Lett. **B755**, 196 (2016).
93. CMS Collab., JHEP **1405**, 108 (2014).
94. CMS Collab., JHEP **1602**, 122 (2016).
95. CMS Collab., JHEP **1708**, 029 (2017).
96. CMS Collab., arXiv:arXiv:1708.08539 , submitted to Phys. Lett. B.
97. CMS Collab., CMS-PAS-JME-15-002, (2015), cds.cern.ch/record/2126325.
98. ATLAS Collab., Phys. Lett. **B743**, 235 (2015).
99. ATLAS Collab., Eur. Phys. J. **C75**, 165 (2015).
100. D. Pappadopulo, A. Thamm,R. Torre, and A. Wulzer, JHEP **1409**, 060 (2014).
101. ATLAS Collab., Phys. Lett. **B737**, 223 (2014).
102. CMS Collab., Phys. Lett. **B740**, 83 (2015).
103. ATLAS Collab., JHEP **1609**, 173 (2016).
104. ATLAS Collab., ATLAS-CONF-2017-051.
105. CMS Collab., arXiv:1705.09171 [hep-ex], submitted to Phys. Lett. B.
106. ATLAS Collab., arXiv:1708.04445 [hep-ex], submitted to Phys. Lett. B.
107. CMS Collab., arXiv:1708.05379 [hep-ex], submitted to Physical Review D.
108. ATLAS Collab., Phys. Lett. **B765**, 32 (2016).
109. ATLAS Collab., arXiv:1707.06958 [hep-ex], submitted to Phys. Lett. B.
110. CMS Collab., Phys. Lett. **B768**, 137 (2017).
111. CMS Collab., Eur. Phys. J. **C77**, 636 (2017).
112. ATLAS Collab., Eur. Phys. J. **C75**, 412 (2015).
113. ATLAS Collab., ATLAS-CONF-2016-049 (2016).
114. CMS Collab., CMS-EXO-12-053 (2015).
115. ATLAS Collab., ATLAS-CONF-2013-074 (2013).
116. ATLAS Collab., arXiv:1709.06783 [hep-ex], submitted to PLB (2017).
117. ATLAS Collab., atlas.web.cern.ch/Atlas/GROUPS/PHYSICS/CombinedSummaryPlots/EXOTICS/index.html.
118. CMS Collab., twiki.cern.ch/twiki/bin/view/CMSPublic/PhysicsResultsB2GDibosons.
119. F. del Aguila *et al.*, Nucl. Phys. **B334**, 1 (1990).
120. CMS Collab., CMS-PAS-B2G-17-003 (2017).
121. CMS Collab., CMS-PAS-B2G-12-017 (2014).
122. CMS Collab., Phys. Rev. **D93**, 012003 (2016) arXiv:1509.04177.
123. CMS Collab., CMS-PAS-B2G-12-013 (2015).
124. S.D. Ellis, C.K. Vermilion, and J.R. Walsh, Phys. Rev. **D80**, 051501 (2009).
125. ATLAS Collab., arXiv:1707.03347 [hep-ex].
126. ATLAS Collab., JHEP **1508**, 105 (2015).
127. CMS Collab., Phys. Lett. **B772**, 634 (2017).
128. ATLAS Collab., ATLAS-CONF-16-072 (2016), http://cds.cern.ch/record/1480052.
129. ATLAS Collab., Eur. Phys. J. **C76**, 442 (2016).
130. ATLAS Collab., ATLAS-CONF-2016-104 (2016), http://cds.cern.ch/record/2220371.
131. CMS Collab., Phys. Lett. **B729**, 149 (2014).
132. CMS Collab., JHEP **1506**, 080 (2015).
133. CMS Collab., arXiv:1706.03408 [hep-ex].
134. CMS Collab., cds.cern.ch/record/1709129 (2014).
135. CMS Collab, JHEP **1704**, 136 (2017).
136. CMS Collab, Phys. Lett. **B771**, 80 (2017).
137. ATLAS Collab., JHEP **1700**, 052 (2017) CERN-EP-2017-075, submitted to JHEP.
138. CMS Collab., arXiv:1708.01062 [hep-ex], Submitted to Phys. Lett. B.
139. ATLAS Collab., JHEP **1708**, 052, (2017).
140. CMS Collab., CMS-PAS-B2G-12-019 (2012), http://cds.cern.ch/record/1599436.
141. CMS Collab., Phys. Rev. **D93**, 112009 (2016) arXiv:1507.07129.
142. ATLAS Collab., JHEP **1411**, 104 (2014).
143. R. Contino and G. Servant, JHEP **0806**, 026 (2008).
144. J. Mrazek, A. Wulzer, Phys. Rev. **D81**, 075006 (2010).
145. CMS Collab., JHEP **1708**, 073 (2017).
146. CMS Collab., CMS-PAS-B2G-16-019 (2017), https://cds.cern.ch/record/2256747.
147. CMS Collab., Phys. Rev. Lett. **112**, 171801 (2014).
148. ATLAS Collab., ATLAS-CONF-16-03 (2016), http://cds.cern.ch/record/2161545.
149. ATLAS Collab., Phys. Rev. **D91**, 112011 (2015).
150. CMS Collab., CMS-PAS-B2G-17-008 (2017), http://cds.cern.ch/record/2264686.
151. ATLAS Collab., JHEP **1510**, 150 (2015).
152. V. Khachatryan *et al.* [CMS Collab.], Phys. Rev. **D91**, 052009 (2015).
153. CMS Collaboration, Phys. Lett. **B770**, 257 (2017).
154. CMS Collab., Phys. Rev. Lett. **110**, 141802 (2013).
155. ATLAS Collab., Phys. Rev. **D91**, 052007 (2015).
156. CMS Collaboration, Phys. Lett. **B769**, 520 (2017).
157. CMS Collab., CMS-PAS-EXO-15-001 (2015), https://cds.cern.ch/record/2048099.

114. Grand Unified Theories

Revised August 2017 by A. Hebecker (U. Heidelberg) and J. Hisano (Nagoya U.)

114.1. The standard model

The Standard Model (SM) may be defined as the renormalizable field theory with gauge group $G_{SM} = SU(3)_C \times SU(2)_L \times U(1)_Y$, with 3 generations of fermions in the representation

$$(\mathbf{3},\mathbf{2})_{1/3} + (\bar{\mathbf{3}},\mathbf{1})_{-4/3} + (\bar{\mathbf{3}},\mathbf{1})_{2/3} + (\mathbf{1},\mathbf{2})_{-1} + (\mathbf{1},\mathbf{1})_{2}\ , \quad (114.1)$$

and a scalar Higgs doublet H transforming as $(\mathbf{1},\mathbf{2})_1$. Here and below we use boldface numbers to specify the dimension of representations of non-Abelian groups (in this case fundamental and antifundamental) and lower indices for $U(1)$ charges. The fields of Eq. (114.1) should also be familiar as $[Q, u^c, d^c, L, e^c]$, with $Q = (u, d)$ and $L = (\nu, e)$ being the quark and lepton $SU(2)$-doublets and u^c, d^c, e^c charge conjugate $SU(2)$-singlets.† Especially after the recent discovery of the Higgs, this model is remarkably complete and consistent with almost all experimental data.

A notable exception are neutrino masses, which are known to be non-zero but are absent in the SM even after the Higgs acquires its vacuum expectation value (VEV). The minimalist attitude is to allow for the dimension-five operator $(HL)^2$, which induces (Majorana) neutrino masses. In the seesaw mechanism [1,2,3] this operator is generated by integrating out heavy singlet fermions (right-handed (r.h.) neutrinos). Alternatively, neutrinos can have Dirac masses if light singlet neutrinos are added to the SM spectrum.

Conceptual problems of the SM include the absence of a Dark Matter candidate, of a mechanism for generating the baryon asymmetry of the universe, and of any reason for the observed smallness of the θ parameter of QCD (θ_{QCD}). In addition, the apparently rather complex group-theoretic data of Eq. (114.1) remains unexplained. Together with the abundance of seemingly arbitrary coupling constants, this disfavors the SM as a candidate fundamental theory, even before quantum gravity problems arise at energies near the Planck mass M_P.

To be precise, there are 19 SM parameters which have to be fitted to data: Three gauge couplings* g_3, g_2 and g_1, 13 parameters associated with the Yukawa couplings (9 charged fermion masses, three mixing angles and one CP phase in the CKM matrix.), the Higgs mass and quartic coupling, and θ_{QCD}. In addition, Majorana neutrinos introduce 3 more masses and 6 mixing angles and phases. As we will see, the paradigm of grand unification addresses mainly the group theoretic data of Eq. (114.1) and the values of the three gauge couplings. In many concrete realizations, it then impacts also the other mentioned issues of the SM, such as the family structure and fermion mass hierarchy.

More specifically, after precision measurements of the Weinberg angle θ_W in the LEP experiments, supersymmetric GUTs (SUSY GUTs) have become the leading candidates in the search for 'Physics beyond the SM'. Supersymmetry (SUSY) is a symmetry between bosons and fermions which requires the addition of superpartners to the SM spectrum, thereby leading to the noted prediction of θ_W [4]. The measured Higgs mass ($\sim$ 125 GeV) is in principle consistent with this picture, assuming superpartners in the region of roughly 10 TeV. Such heavy superpartners then induce radiative corrections raising the Higgs mass above the Z boson mass m_Z [5,6]. However, if SUSY is motivated as a solution to the gauge hierarchy problem (i.e. to the naturalness problem of the Higgs mass) [7], its minimal incarnation in terms of the MSSM is becoming questionable. Indeed, compared to expectations based on the minimal SUSY SM (MSSM) with superpartner masses below about 1 TeV, the Higgs mass is somewhat too high [8]. Independently, the LHC has disfavored light colored superpartners. These facts represent new hints for future work on SUSY GUTs or on GUTs without TeV-scale supersymmetry.

† In our convention the electric charge is $Q = T_3 + Y/2$ and all our spinor fields are left-handed (l.h.).

* Equivalently, the $SU(2)_L$ and $U(1)_Y$ couplings are denoted as $g = g_2$ and $g' = \sqrt{3/5}\ g_1$. One also uses $\alpha_s = \alpha_3 = (g_3^2/4\pi)$, $\alpha_{\rm EM} = (e^2/4\pi)$ with $e = g\ \sin\theta_W$ and $\sin^2\theta_W = (g')^2/(g^2 + (g')^2)$.

114.2. Basic group theory and charge quantization

Historically, the first attempt at unification was the Pati-Salam model with gauge group $G_{PS} = SU(4)_C \times SU(2)_L \times SU(2)_R$ [9]. It unifies SM fermions in the sense that one generation (plus an extra SM singlet) now comes from the $(\mathbf{4},\mathbf{2},\mathbf{1}) + (\bar{\mathbf{4}},\mathbf{1},\mathbf{2})$ of G_{PS}. This is easy to verify from the breaking pattern $SU(4)_C \to SU(3)_C \times U(1)_{B-L}$ together with the identification of SM hypercharge as a linear combination between $B - L$ (baryon minus lepton number) and the T_3 generator of $SU(2)_R$. This model explains charge quantization, that is, why all electric charges are integer multiples of some smallest charge in the SM. However, G_{PS} is not simple (containing three simple factors), and thus it does not predict gauge coupling unification.

Since G_{SM} has rank four (two for $SU(3)_C$ and one for $SU(2)_L$ and $U(1)_Y$, respectively), the rank-four group $SU(5)$ is the minimal choice for unification in a simple group [10]. The three SM gauge coupling constants derive from a universal coupling α_G at the GUT scale M_G. Explicitly embedding G_{SM} in $SU(5)$ is straightforward, with $SU(3)_C$ and $SU(2)_L$ corresponding e.g. to the upper-left 3×3 and lower-right 2×2 blocks, respectively, in traceless 5×5 matrices for $SU(5)$ generators of the fundamental representation. The $U(1)_Y$ corresponds to matrices generated by $\mathrm{diag}(-2/3, -2/3, -2/3, 1, 1)$ and hence commutes with $SU(3)_C \times SU(2)_L \subset SU(5)$. It is then easy to derive how one SM generation precisely comes from the $\mathbf{10} + \bar{\mathbf{5}}$ of $SU(5)$ (where $\mathbf{10}$ is the antisymmetric rank-2 tensor):

$$\mathbf{10}: \begin{pmatrix} 0 & u_b^c & -u_g^c & u_r & d_r \\ -u_b^c & 0 & u_r^c & u_g & d_g \\ u_g^c & -u_r^c & 0 & u_b & d_b \\ -u_r & -u_g & -u_b & 0 & e^c \\ -d_r & -d_g & -d_b & -e^c & 0 \end{pmatrix} \quad \text{and} \quad \bar{\mathbf{5}}: \begin{pmatrix} d_r^c \\ d_g^c \\ d_b^c \\ e \\ -\nu_e \end{pmatrix}. \quad (114.2)$$

Since $SU(5)$ has 24 generators, $SU(5)$ GUTs have 12 new gauge bosons known as X bosons (or X/Y bosons) in addition to the SM. X bosons form an $SU(3)_C$-triplet and $SU(2)_L$-doublet. Their interaction connects quarks and leptons such that baryon and lepton numbers are not conserved and nucleon decay is predicted. Furthermore, $U(1)_Y$ hypercharge is automatically quantized since it is embedded in $SU(5)$.

In order to break the electroweak symmetry at the weak scale and give mass to quarks and leptons, Higgs doublets are needed. In the minimal $SU(5)$ model, they can sit in either a $\mathbf{5_H}$ or $\bar{\mathbf{5}}_\mathbf{H}$. The three additional states are referred to as color-triplet Higgs scalars. Their couplings also violate baryon and lepton numbers, inducing nucleon decay. In order not to violently disagree with the non-observation of nucleon decay, the triplet mass must be greater than $\sim 10^{11}$ GeV [11]. Moreover, in SUSY GUTs [12], in order to cancel anomalies as well as give mass to both up and down quarks, both Higgs multiplets $\mathbf{5_H}$ and $\bar{\mathbf{5}}_\mathbf{H}$ are required. As we shall discuss later, nucleon decay now constrains the Higgs triplets to have mass significantly greater than M_G in the minimal SUSY $SU(5)$ GUT since integrating out the Higgs triplets generates dimension-five baryon-number-violating operators [13]. The mass splitting between doublet and triplet in the $\mathbf{5_H}$ (and $\bar{\mathbf{5}}_\mathbf{H}$) comes from their interaction with the $SU(5)$ breaking sector.

While $SU(5)$ allows for the minimal GUT models, unification is not complete: Two independent representations, $\mathbf{10}$ and $\bar{\mathbf{5}}$, are required for one SM generation. A further representation, an SU(5) singlet, has to be added to serve as r.h. neutrino in the seesaw mechanism. In this case, the r.h. neutrino masses are not necessarily related to the GUT scale. By contrast, a single $\mathbf{16}$-dimensional spinor representation of $SO(10)$ accommodates a full SM generation together with an extra singlet, potentially providing a r.h. neutrino [14]. This is most easily understood from the breaking pattern $SO(10) \to SU(5) \times U(1)_X$ and the associated branching rule* $\mathbf{16} = \mathbf{10}_{-5} + \bar{\mathbf{5}}_3 + \mathbf{1}_{-1}$. Here the indices refer to charges under the $U(1)_X$ subgroup, which is orthogonal to $SU(5)$ and reflects the fact that $SO(10)$ has rank five. From the above, it is easy to see that $U(1)_X$ charges can be given as $2Y - 5(B - L)$. Intriguingly, all representations of $SO(10)$ are anomaly free in four

* Useful references on group theory in the present context include [15] and refs. therein.

dimensions (4d). Thus, the absence of anomalies in an $SU(5)$-GUT or a SM generation can be viewed as deriving from this feature.

Table 114.1 presents the states of one family of quarks and leptons, as they appear in the **16**. To understand this, recall that the Γ-matrices of the 10d Clifford algebra give rise to five independent, anticommuting 'creation-annihilation' operators $\Gamma^{a\pm} = (\Gamma^{2a-1} \pm i\Gamma^{2a})/2$ with $a = 1, ..., 5$. These correspond to five fermionic harmonic oscillators or "spin" 1/2 systems. The 32-dimensional tensor product of those is reducible since the 10d rotation generators $M_{mn} = -i[\Gamma^m, \Gamma^n]/4$ $(m, n = 1, ..., 10)$ always flip an even number of "spins". This gives rise to the **16** as displayed in Table 114.1.

Next, one also recalls that the natural embedding of $SU(5)$ in $SO(10)$ relies on 'pairing up' real dimensions, $R^{10} \equiv C^5$, similarly to the paring up of Γ^ms used above. This makes it clear how to associate one $|\pm>$ system to each complex dimension of $SU(5)$, which explains the labeling of the "spin" columns in Table 114.1: The first three and last two "spins" correspond to $SU(3)_C$ and $SU(2)_L$, respectively. In fact, an $SU(3)_C$ rotation just raises one color index and lowers another, changing colors $\{r,\ g,\ b\}$, or changes relative phases between the three spin states. Similarly, an $SU(2)_L$ rotation raises one weak index and lowers another, thereby flipping the weak isospin from up to down or vice versa, or changes the relative phase between the two spin states. In this representation $U(1)_Y$ hypercharge is simply given by $Y = -2/3(\sum$ color spins$) + (\sum$ weak spins$)$. $SU(5)$ rotations corresponding to X bosons then raise (or lower) a color index, while at the same time lowering (or raising) a weak index. It is easy to see that such rotations can mix the states $\{Q,\ u^c,\ e^c\}$ and $\{d^c, L\}$ among themselves and ν^c is a singlet. Since $SO(10)$ has 45 generators, additional 21 gauge bosons are introduced including the $U(1)_X$ above. The 20 new $SO(10)$ rotations not in $SU(5)$ are then given by either raising any two spins or lowering them. With these rotations, **1** and **5** are connected with **10**. The last $SO(10)$ rotation changes phases of states with weight $2(\sum$ color spins$) + 2(\sum$ weak spins$)$, which corresponds to $U(1)_X$.

Table 114.1: Quantum numbers of **16**-dimensional representation of $SO(10)$.

state	Y	Color	Weak	$SU(5)$	$SO(10)$
ν^c	0	$---$	$--$	**1**	
e^c	2	$---$	$++$		
u_r	1/3	$+--$	$-+$		
d_r	1/3	$+--$	$+-$		
u_g	1/3	$-+-$	$-+$		
d_g	1/3	$-+-$	$+-$	**10**	
u_b	1/3	$--+$	$-+$		
d_b	1/3	$--+$	$+-$		**16**
u_r^c	$-4/3$	$-++$	$--$		
u_g^c	$-4/3$	$+-+$	$--$		
u_b^c	$-4/3$	$++-$	$--$		
d_r^c	2/3	$-++$	$++$		
d_g^c	2/3	$+-+$	$++$		
d_b^c	2/3	$++-$	$++$	$\bar{\mathbf{5}}$	
ν	-1	$+++$	$-+$		
e	-1	$+++$	$+-$		

$SO(10)$ has two inequivalent maximal subgroups and hence breaking patterns, $SO(10) \to SU(5) \times U(1)_X$ and $SO(10) \to SU(4)_C \times SU(2)_L \times SU(2)_R$. In the first case, one can carry on breaking to $G_{SM} \subset SU(5)$ precisely as in the minimal $SU(5)$ case above. Alternatively, one can identify $U(1)_Y$ as an appropriate linear combination of $U(1)_X$ and the $U(1)$ factor from $SU(5)$, leading to the so-called flipped $SU(5)$ [16] as an intermediate step in breaking $SO(10)$ to G_{SM}. In the second case, we have an intermediate Pati-Salam model thanks to the branching rule $\mathbf{16} = (\mathbf{4}, \mathbf{2}, \mathbf{1}) + (\overline{\mathbf{4}}, \mathbf{1}, \mathbf{2})$. Finally, $SO(10)$ can break directly to the SM at M_G. Gauge coupling unification remains intact in the case of this 'direct' breaking and for the breaking pattern $SO(10) \to SU(5) \to G_{SM}$ (with $SU(5)$ broken at M_G). In the case of intermediate-scale Pati-Salam or flipped $SU(5)$ models, gauge coupling predictions are modified. The Higgs multiplets in the minimal $SO(10)$ come from the fundamental representation, $\mathbf{10_H} = \mathbf{5_H} + \bar{\mathbf{5}}_\mathbf{H}$. Note, only in $SO(10)$ does the representation type distinguish SM matter from Higgs fields.

Finally, larger symmetry groups can be considered. For example, the exceptional group E_6 has maximal subgroup $SO(10) \times U(1)$ [17]. Its fundamental representation branches as $\mathbf{27} = \mathbf{16}_1 + \mathbf{10}_{-2} + \mathbf{1}_4$. Another maximal subgroup is $SU(3)_C \times SU(3)_L \times SU(3)_R \subset E_6$ with branching rule $\mathbf{27} = (\mathbf{3}, \mathbf{3}, \mathbf{1}) + (\bar{\mathbf{3}}, \mathbf{1}, \bar{\mathbf{3}}) + (\mathbf{1}, \bar{\mathbf{3}}, \mathbf{3})$. Independently of any underlying E_6, the group $[SU(3)]^3$ with additional permutation symmetry Z_3 interchanging the three factors can be considered. This is known as "trinification" [18]. The $E_6 \to [SU(3)]^3$ breaking pattern has been used in phenomenological analyses of the heterotic string [19]. However, in larger symmetry groups, such as E_6, $SU(6)$, etc., there are now many more states which have not been observed and must be removed from the effective low-energy theory.

Intriguingly, the logic by which G_{SM} is a maximal subgroup of $SU(5)$, which together with $U(1)_X$ is a maximal subgroup of $SO(10)$, continues in a very elegant and systematic way up to the largest exceptional group. The resulting famous breaking chain $E_8 \to E_7 \to E_6 \to SO(10) \to SU(5) \to G_{SM}$ together with the special role played by E_8 in group and in string theory is a tantalizing hint at deeper structures. However, since all representations of E_8 and E_7 are real and can not lead to 4d chiral fermions, this is necessarily outside the 4d GUT framework.

114.3. GUT breaking and doublet-triplet splitting

In the standard, 4d field-theoretic approach to GUTs, the unified gauge group is broken spontaneously by an appropriate GUT Higgs sector. Scalar potentials (or superpotentials in SUSY GUTs) exist whose vacua spontaneously break $SU(5)$ or $SO(10)$. While these potentials are ad hoc (just like the Higgs potential in the SM), the most naive expectation is that all their dimensionful parameters are $O(M_G)$. In the simplest case of $SU(5)$, the **24** (adjoint) GUT Higgs develops a VEV along the G_{SM}-singlet direction as $\langle\Phi\rangle \propto \mathrm{diag}(-2/3, -2/3, -2/3, 1, 1)$. In order for $SO(10)$ to break to $SU(5)$, the **16** or **126**, which have a G_{SM}-singlet with non-zero $U(1)_X$ charge, get a VEV.

The masses of doublet and triplet in the $\mathbf{5_H}$ (and $\bar{\mathbf{5}}_\mathbf{H}$) generically split due to their coupling to the GUT Higgs. In addition, both the doublet and the triplet masses also get an equal contribution from an $SU(5)$-invariant GUT-scale mass term. Without any further structure, an extreme fine-tuning between two large effects is then necessary to keep the doublet mass at the electroweak scale. Supersymmetry plays an important role in forbidding large radiative correction to the doublet mass due to the non-renormalization theorem [7]. However, even in this case we have to fine tune parameters at tree level. This is the doublet-triplet splitting problem which, in the SUSY context, is clearly related the μ-term problem of the MSSM (the smallness of the coefficient of $\mu H_u\ H_d$).

Several mechanisms for natural doublet-triplet splitting have been suggested under the assumption of supersymmetry, such as the sliding singlet [20], missing partner [21] missing VEV [22], and pseudo-Nambu-Goldstone boson mechanisms [23]. Particular examples of the missing partner mechanism for $SU(5)$ [24], the missing VEV mechanism for $SO(10)$ [25,26] and the pseudo-Nambu-Goldstone boson mechanism for $SU(6)$ [27] have been shown to be consistent with gauge coupling unification and nucleon decay. From the GUT-scale perspective, one is satisfied if the triplets are naturally heavy and the doublets are massless ($\mu \simeq 0$). There are also several mechanisms for

resolving the subsequent issue of why μ is of order the SUSY breaking scale [28]. * For a review of the μ problem and some suggested solutions in SUSY GUTs and string theory, see [29,30,31,32] and references therein.

In general, GUT-breaking sectors successfully resolving the doublet-triplet splitting problem, dynamically stabilizing all GUT-scale VEVs and allowing for realistic neutrino masses and Yukawa couplings (including the GUT-symmetry violation in the latter) require a number of ingredients. However, for validity of the effective theory, introduction of higher or many representations is limited, otherwise a Landau pole may appear below the Planck scale. In addition, GUTs are only effective theories below the Planck scale in the 4d field-theoretic approach. Since M_G is close to this scale, the effects of higher-dimension operators are not obviously negligible. In particular, operators including the GUT-breaking Higgs may affect low-energy predictions, such as quark and lepton masses.

Thus, especially in the context of GUT breaking and doublet-triplet splitting, models beyond 4d field theory appear attractive. While this is mainly the subject of the next section, some advantages can already be noted: In models with extra dimensions, in particular string constructions, GUT breaking may occur due to boundary conditions in the compactified dimensions [33,34,35,36]. No complicated GUT breaking sector is then required. Moreover, boundary conditions can give mass only to the triplet, leaving the doublet massless. This is similar to the 'missing partner mechanism' since the effective mass term does not 'pair up' the triplets from $\mathbf{5_H}$ and $\overline{\mathbf{5}}_\mathbf{H}$ but rather each of them with further fields which are automatically present in the higher-dimensional theory. This can eliminate dimension-five nucleon decay (cf. Sec. 114.6).

114.4. String-theoretic and higher-dimensional unified models

As noted earlier, the GUT scale is dangerously close to the scale of quantum gravity. It may hence be necessary to discuss unified models of particle physics in the latter, more ambitious context. Among the models of quantum gravity, superstring or M-theory stands out as the best-studied and technically most developed proposal, possessing in particular a high level internal, mathematical consistency. For our purposes, it is sufficient to know that five 10d and one 11d low-energy effective supergravity theories arise in this setting (cf. [37] and refs. therein).

Grand unification is realized most naturally in the context of the two 'heterotic' theories with gauge groups $\mathrm{E_8}\times\mathrm{E_8}$ and $SO(32)$, respectively [35] (see [38] for some of the more recent results). Justified in part by the intriguing breaking path $\mathrm{E_8} \to \cdots \to G_{SM}$ mentioned above, the focus has historically largely been on $\mathrm{E_8}\times\mathrm{E_8}$. To describe particle physics, solutions of the 10d theory with geometry $R^{1,3} \times M_6$ are considered, where M_6 is a Calabi-Yau (CY) 3-fold (with 6 real dimensions). The background solution involves expectation values of higher-dimensional components of the $\mathrm{E_8}\times\mathrm{E_8}$ gauge fields. This includes both Wilson lines [33] and non-vanishing field-strength and leads, in general, to a reduced gauge symmetry and to chirality in the resulting 4d effective theory. The 4d fermions arise from 10d gauginos.

Given an appropriate embedding of G_{SM} in $\mathrm{E_8}\times\mathrm{E_8}$, gauge coupling unification is automatic at leading order. Corrections arise mainly through (string)-loop effects and are similar to the familiar field-theory thresholds of 4d GUTs [39]. Thus, one may say that coupling unification is a generic prediction in spite of the complete absence* of a 4d GUT at any energy scale. This absence is both an advantage and a weakness. On the up side, GUT breaking and doublet-triplet splitting [41] are more naturally realized and dimension-five nucleon decay is relatively easy to avoid. On the down side, there is no reason to expect full GUT representations in the matter sector and flavor model building is much less tied to the GUT structure than in 4d.

One technical problem of heterotic constructions is the dependence on the numerous size and shape parameters of M_6 (the so-called moduli), the stabilization of which is poorly understood (see [42] for recent developments). Another is the sheer mathematical complexity of the analysis, involving in particular the study of (non-Abelian) gauge-bundles on CY spaces [43] (see however [44]) .

An interesting sub-chapter of heterotic string constructions is represented by orbifold models [34]. Here the internal space is given by a six-torus, modded out by a discrete symmetry group (e.g. T^6/Z_n). More recent progress is reported in [45,46], including in particular the systematic exploration of the phenomenological advantages of so-called 'non-prime' (referring to n) orbifolds. The symmetry breaking to G_{SM} as well as the survival of Higgs doublets without triplet partners is ensured by the appropriate embedding of the discrete orbifold group in $\mathrm{E_8}\times\mathrm{E_8}$. String theory on such spaces, which are locally flat but include singularities, is much more calculable than in the CY case. The orbifold geometries can be viewed as singular limits of CYs.

An even simpler approach to unified models, which includes many of the advantages of full-fledged string constructions, is provided by Orbifold GUTs [36]. These are (mostly) 5d or 6d SUSY field theories with unified gauge group (e.g. $SU(5)$ or $SO(10)$), broken in the process of compactifying to 4d. To give a particularly simple example, consider $SU(5)$ on $R^{1,3}\times S^1/(Z_2 \times Z_2')$. Here the compact space is an interval of length $\pi R/2$ and the embedding of Z_2' in the hypercharge direction of $SU(5)$ realizes the breaking to G_{SM}. Concretely, 5d X bosons are given Dirichlet BCs at one endpoint of the interval and thus have no Kaluza-Klein (KK) zero mode. Their lightest modes have mass $\sim 1/R$, making the KK-scale the effective GUT scale. As an implication, the boundary theory has no $SU(5)$ invariance. Nevertheless, since the $SU(5)$-symmetric 5d bulk dominates 4d gauge couplings, unification remains a prediction. Many other features but also problems of 4d GUTs can be circumvented, especially doublet-triplet splitting is easily realized.

With the advent of the string-theory 'flux landscape' [47], which is best understood in 10d type-IIB supergravity, the focus in string model building has shifted to this framework. While type II string theories have no gauge group in 10d, brane-stacks support gauge dynamics. A particularly appealing setting (see e.g. [48]) is provided by type IIB models with D7 branes (defining 8d submanifolds). However, in the $SO(10)$ context the **16** is not available and, for $SU(5)$, the top-Yukawa coupling vanishes at leading order [49]. As a crucial insight, this can be overcome on the non-perturbative branch of type IIB, also known as F-theory [50,51]. This setting allows for more general branes, thus avoiding constraints of the Dp-brane framework. GUT breaking can be realized using hypercharge flux (the VEV of the $\mathrm{U}(1)_Y$ field strength), an option not available in heterotic models. The whole framework combines the advantages of the heterotic or higher-dimensional unification approach with the more recent progress in understanding moduli stabilization. It thus represents at this moment the most active and promising branch of theory-driven GUT model building (see e.g. [52] and refs. therein).

As a result of the flux-breaking, a characteristic 'type IIB' or 'F-theoretic' tree-level correction to gauge unification arises [53]. The fact that this correction can be rather significant numerically is occasionally held against the framework of F-theory GUTs. However, at a parametric level, this correction nevertheless behaves like a 4d threshold, i.e., it provides $\mathcal{O}(1)$ additive contributions to the inverse 4d gauge coupling $\alpha_i^{-1}(M_G)$.

A final important issue in string GUTs is the so-called string-scale/GUT-scale problem [54]. It arises since, in heterotic compactifications, the Planck scale and the high-scale value of the gauge coupling unambiguously fix the string-scale to about 10^{18} GeV. As the compactification radius R is raised above the string length, the GUT scale (identified with $1/R$) goes down and the string coupling goes up. Within the domain of perturbative string theory, a gap of about a factor ~ 20 remains between the lowest GUT scale achievable in this way and the phenomenological goal of 2×10^{16} GeV. The situation

* The solution of [28] relies on the absence of the fundamental superpotential term $\mu H_u\, H_d$ (or $\mu\, \mathbf{5}_H \overline{\mathbf{5}}_H$). This is ensured by a $U(1)_R$. The latter clashes with typical superpotentials for the GUT breaking sector. However, higher-dimensional or stringy GUTs, where the triplet Higgs is simply projected out, can be consistent with the $U(1)_R$ symmetry.

* See however [40].

can be improved by venturing into the non-perturbative regime [54] or by considering 'anisotropic' geometries with hierarchically different radii R [54,55].

In F-theory GUTs, the situation is dramatically improved since the gauge theory lives only in four out of the six compact dimensions. This allows for models with a 'decoupling limit', where the GUT scale is parametrically below the Planck scale [51]. However, moduli stabilization may not be without problems in such constructions, in part due to a tension between the required large volume and the desirable low SUSY breaking scale.

114.5. Gauge coupling unification

The quantitative unification of the three SM gauge couplings at the energy scale M_G is one of the cornerstones of the GUT paradigm. It is obviously of direct phenomenological relevance. Gauge coupling unification is best understood in the framework of effective field theory (EFT) [56]. In the simplest case, the relevant EFT at energies $\mu \gg M_G$ has a unified gauge symmetry (say $SU(5)$ for definiteness) and a single running gauge coupling $\alpha_G(\mu)$. At energies $\mu \ll M_G$, states with mass $\sim M_G$ (such as X bosons, GUT Higgs, color-triplet Higgs) have to be integrated out. The EFT now has three independent couplings and SM (or SUSY SM) matter content. One-loop renormalization group equations readily allow for an extrapolation to the weak scale,

$$\alpha_i^{-1}(m_Z) = \alpha_G^{-1}(M_G) + \frac{b_i}{2\pi}\log\left(\frac{M_G}{m_Z}\right) + \delta_i\,, \qquad (114.3)$$

(i = 1-3). Here we defined δ_i to absorb all sub-leading effects, including threshold corrections at or near the weak scale (e.g. from superpartners and the additional Higgs bosons in the case of the MSSM). We will discuss them momentarily.

It is apparent from Eq. (114.3) that the three low-scale couplings can be very different. This is due to the large energy range $m_Z \ll \mu \ll M_G$ and the non-universal β-function coefficients ($b_i^{\rm SM} = \{41/10, -19/6, -7\}$ or $b_i^{\rm MSSM} = \{33/5, 1, -3\}$). Incomplete GUT multiplets, such as gauge and Higgs bosons in the SM and also their superpartners and the additional Higgs bosons in the MSSM, contribute to the differences between the β functions. Inverting the argument, one expects that extrapolating the measured couplings to the high scale, we find quantitative unification at $\mu \sim M_G$. While this fails in the SM, it works intriguingly well in the MSSM (cf. Fig. 1).

The three equations contained in (Eq. (114.3)) can be used to determine the three 'unknowns' $\alpha_3(m_Z)$, $\alpha_G(M_G)$ and M_G, assuming that all other parameters entering the equations are given. Focusing on the SUSY case and using the $\overline{\rm MS}$ coupling constants $\alpha_{\rm EM}^{-1}(m_Z)$ and $\sin^2\theta_W(m_Z)$ from [57],

$$\alpha_{\rm EM}^{-1}(m_Z) = 127.950 \pm 0.017\,, \qquad (114.4)$$

$$\sin^2\theta_W(m_Z) = 0.23129 \pm 0.00005\,, \qquad (114.5)$$

as input, one determines $\alpha_{1,2}^{-1}(m_Z)$, which then gives

$$\alpha_G^{-1}(M_G) \simeq 24.3 \qquad \text{and} \qquad M_G \simeq 2\times 10^{16}\ \text{GeV}\,. \qquad (114.6)$$

Here we have set $\delta_i = 0$ for simplicity. Crucially, one in addition obtains a prediction for the low-energy observable α_3,

$$\alpha_3^{-1}(m_Z) = -\frac{5}{7}\alpha_1^{-1}(m_Z) + \frac{12}{7}\alpha_2^{-1}(m_Z) + \Delta_3\,, \qquad (114.7)$$

where

$$\Delta_3 = \frac{5}{7}\delta_1 - \frac{12}{7}\delta_2 + \delta_3\,. \qquad (114.8)$$

Here we followed the elegant formulation in Ref. [58] of the classical analyses of [4]. Of course, it is a matter of convention which of the three low-energy gauge coupling parameters one 'predicts' and indeed, early works on the subject discussed the prediction of $\sin^2\theta_W$ in terms of $\alpha_{\rm EM}$ and α_3 [59,60].

Remarkably, the leading order result (i.e. Eq. (114.7) with $\delta_i = 0$) is in excellent agreement with experiments [57]:

$$\alpha_3^{\rm LO}(m_Z) = 0.117 \qquad \text{vs.} \qquad \alpha_3^{\rm EXP}(m_Z) = 0.1181 \pm 0.0011\,. \qquad (114.9)$$

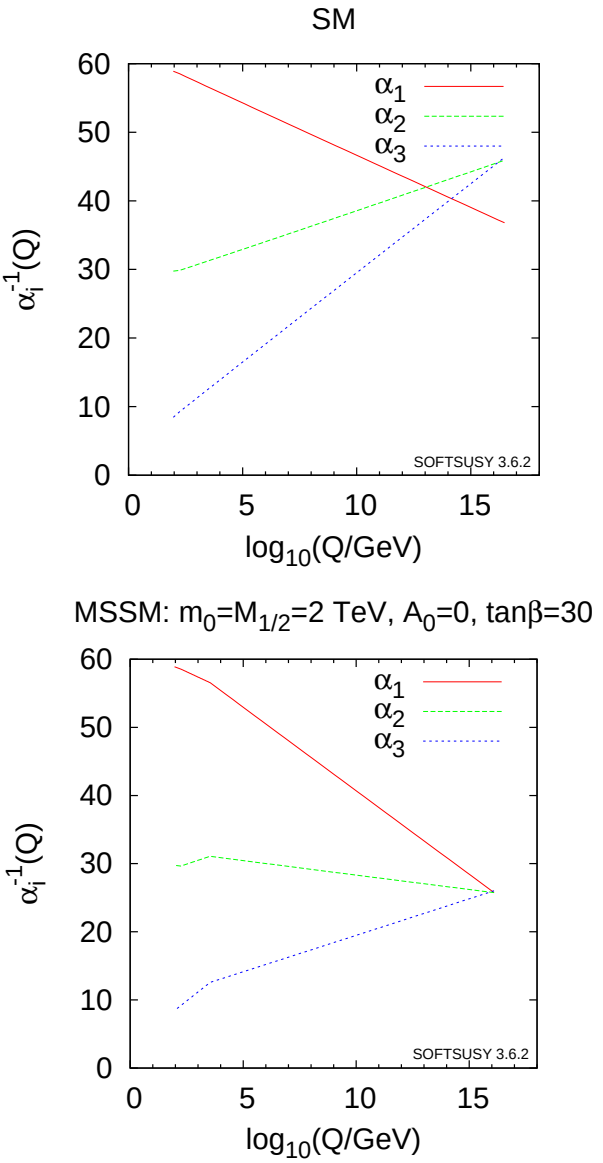

Figure 114.1: Running couplings in SM and MSSM using two-loop RG evolution. The SUSY threshold at 2 TeV is clearly visible on the MSSM side. (We thank Ben Allanach for providing the plots created using SOFTSUSY [62].)

However, this near perfection is to some extent accidental. To see this, we now discuss the various contributions to the δ_i (and hence to Δ_3).

The two-loop running correction from the gauge sector $\Delta_3^{(2)}$ and the low-scale threshold correction $\Delta_3^{(l)}$ from superpartners can be summarized as [58]

$$\Delta_3^{(2)} \simeq -0.82 \qquad \text{and} \qquad \Delta_3^{(l)} \simeq \frac{19}{28\pi}\log\left(\frac{m_{\rm SUSY}}{m_Z}\right)\,. \qquad (114.10)$$

The relevant scale $m_{\rm SUSY}$ can be estimated as [61]

$$m_{\rm SUSY} \;\to\; m_H^{3/19} m_{\widetilde{H}}^{12/19} m_{\widetilde{W}}^{4/19} \times \left(\frac{m_{\widetilde{W}}}{m_{\widetilde{g}}}\right)^{28/19}\left(\frac{m_{\widetilde{l}}}{m_{\widetilde{q}}}\right)^{3/19}\,, \qquad (114.11)$$

where m_H stands for the masses of non-SM Higgs states and superpartner masses are given in self-evident notation. Detailed analyses including the above effects are best done using appropriate software packages, such as SOFTSUSY [62], (or alternatively SuSpect [63] or SPheno [64]) . See also [62] for references to the underlying theoretical two-loop analyses.

To get a very rough feeling for these effects, let us assume that all superpartners are degenerate at $m_{\rm SUSY} = 1$ TeV, except for heavier gluinos: $m_{\widetilde{W}}/m_{\widetilde{g}} \simeq 1/3$. This gives $\Delta_3^{(l)} \simeq -0.35 + 0.22\ln(m_{\rm SUSY}/m_Z) \simeq 0.18$. The resulting prediction of $\alpha_3(m_Z) \simeq 0.126$ significantly upsets the perfect one-loop agreement found earlier. Before discussing this issue further, it is useful to introduce yet another important type of correction, the high or GUT scale thresholds.

To discuss high scale thresholds, let us set all other corrections to zero for the moment and write down a version of Eq. (114.3) that captures the running near and above the GUT scale more correctly. The threshold correction at one-loop level can be evaluated accurately by the simple step-function approximation for the β functions in the $\overline{\rm DR}$ scheme* [68],

$$\alpha_i^{-1}(m_Z) = \alpha_G^{-1}(\mu) + \frac{1}{2\pi}\left[b_i \ln\frac{\mu}{m_Z} + b_i^C \ln\frac{\mu}{M_C} + b_i^X \ln\frac{\mu}{M_X} + b_i^\Phi \ln\frac{\mu}{M_\Phi}\right] . \quad (114.12)$$

Here we started the running at some scale $\mu \gg M_G$, including the contribution of the minimal set of states relevant for the transition from the high-scale $SU(5)$ model to the MSSM. These are the color-triplet Higgs multiplets with mass M_C, massive vector multiplets of X-bosons with mass M_X (including GUT Higgs degrees of freedom), and the remaining GUT-Higgs fields and superpartners with mass M_Φ. The coefficients $b_i^{C,X,\Phi}$ can be found in Ref. [69]. Crucially, the b_i in Eq. (114.12) conspire to make the running GUT-universal at high scales, such that the resulting prediction for α_3 does not depend on the value of μ.

To relate this to our previous discussion, we can, for example, define $M_G \equiv M_X$ and then choose $\mu = M_G$ in Eq. (114.12). This gives the high-scale threshold corrections

$$\delta_i^{(h)} = \frac{1}{2\pi}\left[b_i^C \ln\frac{M_G}{M_C} + b_i^\Phi \ln\frac{M_G}{M_\Phi}\right] , \quad (114.13)$$

and a corresponding correction $\Delta_3^{(h)}$. To get some intuition for the magnitude, one can furthermore assume $M_\Phi = M_G$, finding (with $b_i^C = \{2/5, 0, 1\}$)

$$\Delta_3^{(h)} = \frac{9}{14\pi}\ln\left(\frac{M_G}{M_C}\right) . \quad (114.14)$$

To obtain the desired effect of $-\Delta_3^{(2)} - \Delta_3^{(l)} \simeq +0.64$, the triplet Higgs would have to be by about a factor 20 lighter than the GUT scale. While this is ruled out by nucleon decay in the minimal model [70] as will be discussed Sec. 114.6, it is also clear that threshold corrections of this order of magnitude can, in general, be realized with a certain amount of GUT-scale model building, e.g. in specific $SU(5)$ [24] or $SO(10)$ [25,26] constructions. It is, however, a significant constraint on the 4d GUT sector of the theory.

The above analysis implicitly assumes universal soft SUSY breaking masses at the GUT scale, which directly affect the spectrum of SUSY particles at the weak scale. In the simplest case we have a universal gaugino mass $M_{1/2}$, a universal mass for squarks and sleptons m_{16} and a universal Higgs mass m_{10}, as motivated by $SO(10)$. In some cases, threshold corrections to gauge coupling unification can be exchanged for threshold corrections to soft SUSY parameters (see [71] and refs. therein). For example, if gaugino masses were not unified at M_G and, in particular, gluinos were lighter than winos at the weak scale (cf. Eq. (114.11))), then it is possible that, due to weak scale threshold corrections, a much smaller or even slightly negative threshold correction at the GUT scale would be consistent with gauge coupling unification [72].

It is also noteworthy that perfect unification can be realized without significant GUT-scale corrections, simply by slightly raising the (universal) SUSY breaking scale. In this case the dark matter abundance produced by thermal processes in the early universe (if the lightest neutralino is the dark matter particle) is too high. However, even if the gaugino mass in the MSSM is about 1 TeV to explain the dark matter abundance, if the Higgsino and the non-SM Higgs boson masses are about 10-100 TeV, the effective SUSY scale can be raised [73]. This setup is realized in split SUSY [74] or the pure gravity mediation model [75] based on anomaly mediation [76]. Since the squarks and sleptons are much heavier than the gaugino masses in those setups, a gauge hierarchy problem is reintroduced. The facts that no superpartners have so far been seen at the LHC and that the observed Higgs mass favors heavier stop masses than about 1 TeV force one to accept a certain amount of fine-tuning anyway.

For non-SUSY GUTs or GUTs with a very high SUSY breaking scale to fit the data, new light states in incomplete GUT multiplets or multiple GUT breaking scales are required. For example, non-SUSY models $SO(10) \to SU(4)_C \times SU(2)_L \times SU(2)_R \to$ SM, with the second breaking scale of order an intermediate scale, determined by light neutrino masses using the see-saw mechanism, can fit the low-energy data for gauge couplings [77] and at the same time survive nucleon decay bounds [78]. Alternatively, one can appeal to string-theoretic corrections discussed in Sec. 114.4 to compensate for a high SUSY breaking scale. This has, for example, been concretely analyzed in the context of F-theory GUTs in [79].

In 5d or 6d orbifold GUTs, certain "GUT scale" threshold corrections come from the Kaluza-Klein modes between the compactification scale, $M_c \sim 1/R$, and the effective cutoff scale M_*. In string theory, this cutoff scale is the string scale. Gauge coupling unification at two loops then constrains the values of M_c and M_*.* Typically, one finds M_c to be lower than the 4d GUT scale. Since the X-bosons, responsible for nucleon decay, get mass at the compactification scale, this has significant consequences for nucleon decay.

Finally, it has been shown that non-supersymmetric GUTs in warped 5d orbifolds can be consistent with gauge coupling unification. This assumes (in 4d language) that the r.h. top quark and the Higgs doublets are composite-like objects with a compositeness scale in the TeV range [81].

114.6. Nucleon decay

Quarks and leptons are indistinguishable in any 4d GUT, and both the baryon (B) and lepton number (L) are not conserved. This leads to baryon-number-violating nucleon decay. In addition to baryon-number violation, lepton-number violation is also required for nucleon decay since, in the SM, leptons are the only free fermions which are lighter than nucleons. The lowest-dimension operators relevant for nucleon decay are $(B+L)$ violating dimension-six four-fermion-terms in the SM, and all baryon-violating operators with dimension less than seven preserve $(B-L)$ [82]. In $SU(5)$ GUTs, the dimension-six operators are induced by X boson exchange. These operators are suppressed by $(1/M_G^2)$, and the nucleon lifetime is given by $\tau_N \propto M_G^4/(\alpha_G^2\, m_p^5)$ (m_p is proton mass). The dominant decay mode of the proton (and the baryon-violating decay mode of the neutron), via X boson exchange, is $p \to e^+\,\pi^0$ ($n \to e^+\,\pi^-$). In any simple gauge symmetry, with one universal GUT coupling α_G and scale M_G, the nucleon lifetime from gauge boson exchange is calculable. Hence, the GUT scale may be directly observed via the extremely rare decay of the nucleon. Experimental searches for nucleon decay began with the Kolar Gold Mine, Homestake, Soudan, NUSEX, Frejus, HPW, IMB, and Kamiokande detectors [59]. The present experimental bounds come from Super-Kamiokande. The null result on search for $p \to e^+\pi^0$ constrains M_G to be be larger than $O(10^{15})$ GeV. Non-SUSY GUTs are constrained by the non-observation of nucleon decay, while a precise and general statement is hard to make. The reason is that gauge couplings do not unify with just the SM particle content. Once extra states or large thresholds are included to ensure precision unification, a certain range of unification scales is allowed. By contrast,

* The $\overline{\rm DR}$ scheme is frequently used in a supersymmetric regularization [65]. The renormalization transformation of the gauge coupling constants from $\overline{\rm MS}$ to $\overline{\rm DR}$ scheme is given in Ref. [66]. For an alternative treatment using holomorphic gauge couplings and NSVZ β-functions see e.g. [67].

* It is interesting to note that a ratio $M_*/M_c \sim 100$, needed for gauge coupling unification to work in orbifold GUTs, is typically the maximum value for this ratio consistent with perturbativity [80].

in SUSY GUTs one generically has $M_G \sim 2\times10^{16}$ GeV from the gauge coupling unification. Hence dimension-six baryon-number-violating operators are predicted to induce a lifetime of about $\tau_p \sim 10^{36}$ years.

However, in SUSY GUTs there are additional sources for baryon and/or lepton-number violation – dimension-four and five operators [13]. These arise since, in the SUSY SM, quarks and leptons have scalar partners (squarks and sleptons). Although our notation does not change, when discussing SUSY models our fields are chiral superfields and both fermionic and bosonic matter is implicitly represented by those. In this language, baryon- and/or lepton-number-violating dimension-four and five operators are given as so-called F terms of products of chiral superfields, which contain two fermionic components and the rest scalars or products of scalars. Within the context of $SU(5)$ the dimension-four and five operators have the form

$$(\mathbf{10}\ \bar{\mathbf{5}}\ \bar{\mathbf{5}}) \supset (u^c\ d^c\ d^c) + (Q\ L\ d^c) + (e^c\ L\ L),$$

$$(\mathbf{10}\ \mathbf{10}\ \mathbf{10}\ \bar{\mathbf{5}}) \supset (Q\ Q\ Q\ L) + (u^c\ u^c\ d^c\ e^c)$$

$$+B\text{- and } L\text{-conserving terms},$$

respectively. The dimension-four operators are renormalizable, with dimensionless couplings similar to Yukawa couplings. By contrast, the dimension-five operators have a dimensionful coupling of order $(1/M_G)$. They are generated by integrating out the color-triplet Higgs with GUT-scale mass. Note that both triplet Higgsinos (due to their fermionic nature) and Higgs scalars (due to their mass-enhanced trilinear coupling with matter) contribute to the operators.

The dimension-four operators violate either baryon number or lepton number. The nucleon lifetime is extremely short if both types of dimension-four operators are present in the SUSY SM since squark or slepton exchange induces the dangerous dimension-six SM operators. Even in the case that they violate baryon number or lepton number only but not both, they are constrained by various phenomena [83]. For example, the primordial baryon number in the universe is washed out unless the dimensionless coupling constants are less than 10^{-7}. Both types of operators can be eliminated by requiring R parity, which distinguishes Higgs from ordinary matter multiplets. R parity [84] or its cousin, matter parity [12,85], act as $F \to -F$, $H \to H$ with $F = \{\mathbf{10},\ \bar{\mathbf{5}}\}$, $H = \{\bar{\mathbf{5}}_\mathbf{H},\ \mathbf{5}_\mathbf{H}\}$ in $SU(5)$. This forbids the dimension-four operator $(\mathbf{10}\ \bar{\mathbf{5}}\ \bar{\mathbf{5}})$, but allows the Yukawa couplings for quark and lepton masses of the form $(\mathbf{10}\ \bar{\mathbf{5}}\ \bar{\mathbf{5}}_\mathbf{H})$ and $(\mathbf{10}\ \mathbf{10}\ \mathbf{5}_\mathbf{H})$. It also forbids the dimension-three, lepton-number-violating operator $(\bar{\mathbf{5}}\ \mathbf{5}_\mathbf{H}) \supset (L\ H_u)$ as well as the dimension-five, baryon-number-violating operator $(\mathbf{10}\ \mathbf{10}\ \mathbf{10}\ \bar{\mathbf{5}}_\mathbf{H}) \supset (Q\ Q\ Q\ H_d) + \cdots$. In $SU(5)$, the Higgs multiplet $\bar{\mathbf{5}}_\mathbf{H}$ and the matter multiplets $\bar{\mathbf{5}}$ have identical gauge quantum numbers. In E_6, Higgs and matter multiplets could be unified within the fundamental **27** representation. Only in $SO(10)$ are Higgs and matter multiplets distinguished by their gauge quantum numbers. The Z_4 center of $SO(10)$ distinguishes **10**s from **16**s and can be associated with R parity [86].

The dimension-five baryon-number-violating operators may also be forbidden at tree level by certain symmetries consistent with $SU(5)$ [13]. However, these symmetries are typically broken by the VEVs responsible for the color-triplet Higgs masses. Consequently the dimension-five operators are generically generated via the triplet Higgs exchange in SUSY $SU(5)$ GUTs, as mentioned above. Hence, the triplet partners of Higgs doublets must necessarily obtain mass of order the GUT scale. In addition, it is also important to note that Planck or string scale physics may independently generate the dimension-five operators, even without a GUT. These contributions must be suppressed by some underlying symmetry; for example, the same flavor symmetry which may be responsible for hierarchical fermion Yukawa matrices.

Dimension-five operators include squarks and/or sleptons. To allow for nucleon decay, these must be converted to light quarks or leptons by exchange of a gaugino or Higgsino in the SUSY SM. The nucleon lifetime is proportional to $M_G^2\ m_{\rm SUSY}^2/m_p^5$, where $m_{\rm SUSY}$ is the SUSY breaking scale. Thus, dimension-five operators may predict a shorter nucleon lifetime than dimension-six operators. Unless accidental cancellations are present, the dominant decay modes from dimension-five operators include a K meson, such as $p \to K^+\ \bar{\nu}$ ($n \to K^0\ \bar{\nu}$). This is due to a simple symmetry argument: The operators are given as $(Q_i\ Q_j\ Q_k\ L_l)$ and $(u_i^c\ u_j^c\ d_k^c\ e_l^c)$, where $i, j, k, l\,(=1\text{–}3)$ are family indices and color and weak indices are implicit. They must be invariant under $SU(3)_C$ and $SU(2)_L$ so that their color and weak doublet indices must be anti-symmetrized. Since these operators are given by bosonic superfields, they must be totally symmetric under interchange of all indices. Thus the first operator vanishes for $i = j = k$ and the second vanishes for $i = j$. Hence a second or third generation member exists in the dominant modes of nucleon decay unless these modes are accidentally suppressed [85].

Recent Super-Kamiokande bounds on the proton lifetime severely constrain the dimension-six and five operators. With 306 kton-years of data they find $\tau_p/{\rm Br}(p \to e^+\pi^0) > 1.67\times10^{34}$ years and $\tau_p/{\rm Br}(p \to K^+\bar{\nu}) > 6.61\times10^{33}$ years at 90% CL [87]. The hadronic matrix elements for baryon-number-violating operators are evaluated with lattice QCD simulations [88]. The lower bound on the X boson mass from null results in nucleon decay searches is approaching 10^{16} GeV in SUSY $SU(5)$ GUTs [89]. In the minimal SUSY $SU(5)$, $\tau_p/{\rm Br}(p \to K^+\bar{\nu})$ is smaller than about 10^{31} years if the triplet Higgs mass is 10^{16} GeV and $m_{\rm SUSY} = 1$ TeV [90]. The triplet Higgs mass bound from nucleon decay is then in conflict with gauge coupling unification so that this model is considered to be ruled out [70].

Since nucleon decay induced by the triplet Higgs is a severe problem in SUSY GUTs, various proposals for its suppression have been made. First, some accidental symmetry or accidental structure in non-minimal Higgs sectors in $SU(5)$ or $SO(10)$ theories may suppress the dimension-five operators [25,26,21,91]. As mentioned above, the triplet Higgs mass term violates symmetries which forbid the dimension-five operators. In other words, the nucleon decay is suppressed if the Higgs triplets in $\bar{\mathbf{5}}_\mathbf{H}$ and $\mathbf{5}_\mathbf{H}$ do not have a common mass term but, instead, their mass terms involve partners from other $SU(5)$ multiplets. Second, the SUSY breaking scale may be around $\mathcal{O}(10\text{–}100)$ TeV in order to explain the observed Higgs boson mass at the LHC. In this case, nucleon decay is automatically suppressed [74,92,93]. Third, accidental cancellations among diagrams due to a fine-tuned structure of squark and slepton flavor mixing might suppress nucleon decay [94]. Last, we have also implicitly assumed a hierarchical structure for Yukawa matrices in the analysis. It is however possible to fine-tune a hierarchical structure for quarks and leptons which baffles the family structure so that the nucleon decay is suppressed [95]. The upper bound on the proton lifetime from some of these theories is approximately a factor of 10 above the experimental bounds. Future experiments with larger neutrino detectors, such as JUNO [96], Hyper-Kamiokande [97] and DUNE [98], are planned and will have higher sensitivities to nucleon decay.

Appealing to global symmetries to suppress specific interactions may not always be as straightforward as it naively seems, as a general remark, while global symmetries are introduced to control the dimension-four and five operators in SUSY GUTs. Indeed, there are two possibilities: On the one hand, the relevant symmetry might be gauged at a higher scale. Effects of the VEVs responsible for the spontaneous breaking are then in principle dangerous and need to be quantified. On the other hand, the symmetry might be truly only global. This must e.g. be the case for anomalous symmetries, which are then also violated by field-theoretic non-perturbative effects. The latter can in principle be exponentially small. It is, however, widely believed that global symmetries are always broken in quantum gravity (see e.g. [99]). One then needs to understand which power or functional form the Planck scale suppression of the relevant interaction has. For example, dimension-five baryon number violating operators suppressed by just one unit of the Planck or string scale are completely excluded.

In view of the above, it is also useful to recall that in string models 4d global symmetries generally originate in higher-dimensional gauge symmetries. Here 'global' implies that the gauge boson has acquired a Stückelberg-mass. This is a necessity in the anomalous case (Green-Schwarz mechanism) but can also happen to non-anomalous symmetries. One expects no symmetry violation beyond the well-understood non-perturbative effects. Discrete symmetries arise as

subgroups of continuous gauge symmetries, such as $Z_N \subset U(1)$. In particular, non-anomalous subgroups of Stückelberg-massive $U(1)$s represent unbroken discrete gauge symmetries and as such are non-perturbatively exact (see e.g. [100]). Of course, such discrete gauge symmetries may also arise as remnants of continuous gauge symmetries after conventional 4d spontaneous breaking.

Are there ways to avoid the stringent predictions for proton decay discussed above? Orbifold GUTs and string theories, see Sec. 114.4, contain grand unified symmetries realized in higher dimensions. In the process of compactification and GUT symmetry breaking, the triplet Higgs states may be removed (projected out of the massless sector of the theory). In such models, the nucleon decay due to dimension-five operators can be severely suppressed or eliminated completely. However, nucleon decay due to dimension-six operators may be enhanced, since the gauge-bosons mediating proton decay obtain mass at the compactification scale, M_c, which is typically less than the 4d GUT scale (cf. Sec. 114.5). Alternatively, the same projections which eliminate the triplet Higgs may rearrange the quark and lepton states such that the massless states of one family come from different higher-dimensional GUT multiplets. This can suppress or completely eliminate even dimension-six proton decay. Thus, enhancement or suppression of dimension-six proton decay is model-dependent. In some complete 5d orbifold GUT models [101,58] the lifetime for the decay $\tau_p/\mathrm{Br}(p \to e^+\pi^0)$ can be near the bound of 1×10^{34} years with, however, large model-dependence and/or theoretical uncertainties. In other cases, the modes $p \to K^+\bar{\nu}$ and $p \to K^0\mu^+$ may be dominant [58]. Thus, interestingly, the observation of nucleon decay may distinguish string or higher-dimensional GUTs from 4d ones.

In orbifold GUTs or string theory, new discrete symmetries consistent with SUSY GUTs can forbid all dimension-three and four baryon- and lepton-number-violating operators. Even the μ term and dimension-five baryon- and lepton-number-violating operators can be forbidden to all orders in perturbation theory [32]. The μ term and dimension-five baryon- and lepton-number-violating operators may then be generated, albeit sufficiently suppressed, via non-perturbative effects. The simplest example of this is a Z_4^R symmetry which is the unique discrete R symmetry consistent with $SO(10)$ [32]. Even though it forbids the dimension-five proton decay operator to the desired level, it allows the required dimension-five neutrino mass term. In this case, proton decay is dominated by dimension-six operators, leading to decays such as $p \to e^+\pi^0$.

114.7. Yukawa coupling unification

In the SM, masses and mixings for quarks and leptons come from the Yukawa couplings with the Higgs doublet, but the values of these couplings remain a mystery. GUTs provide at least a partial understanding since each generation is embedded in unified multiplet(s). Specifically, since quarks and leptons are two sides of the same coin, the GUT symmetry relates the Yukawa couplings (and hence the masses) of quarks and leptons.

In $SU(5)$, there are two types of independent renormalizable Yukawa interactions given by λ_{ij} $(\mathbf{10}_i\ \mathbf{10}_j\ \mathbf{5_H}) + \lambda'_{ij}$ $(\mathbf{10}_i\ \bar{\mathbf{5}}_j\ \bar{\mathbf{5}}_{\mathbf{H}})$. These contain the SM interactions λ_{ij} $(Q_i\ u^c_j\ H_u) + \lambda'_{ij}$ $(Q_i\ d^c_j\ H_d\ + e^c_i\ L_j\ H_d)$. Here $i, j\,(=1\text{–}3)$ are, as before, family indices. Hence, at the GUT scale we have tree-level relations between Yukawa coupling constants for charged lepton and down quark masses, such as $\lambda_b = \lambda_\tau$ in which $\lambda_{b/\tau}$ are the bottom quark /τ lepton Yukawa coupling constants [102,103]. In $SO(10)$, there is only one type of independent renormalizable Yukawa interaction given by λ_{ij} $(\mathbf{16}_i\ \mathbf{16}_j\ \mathbf{10_H})$, leading to relations among all Yukawa coupling constants and quark and lepton masses within one generation [104,105] (such as $\lambda_t = \lambda_b = \lambda_\tau$, with λ_t the top quark Yukawa coupling constant).

114.7.1. *The third generation, b–τ or t–b–τ unification* :

Third generation Yukawa couplings are larger than those of the first two generations. Hence, the fermion mass relations predicted from renormalizable GUT interactions which we introduced above are expected to be more reliable. In order to compare them with data, we have to include the radiative correction to these relations from the RG evolution between GUT and fermion mass scale, from integrating out heavy particles at the GUT scale, and from weak scale thresholds.

Since testing Yukawa coupling unification is only possible in models with successful gauge coupling unification, we here focus on SUSY GUTs. In the MSSM, top and bottom quark and τ lepton masses are related to the Yukawa coupling constants at the scale m_Z as

$$m_t(m_Z) = \lambda_t(m_Z)\ v_u(1 + \delta m_t/m_t),$$

$$m_{b/\tau}(m_Z) = \lambda_{b/\tau}(m_Z)\ v_d(1 + \delta m_{b/\tau}/m_{b/\tau}),$$

where $\langle H^0_u\rangle \equiv v_u = \sin\beta\ v/\sqrt{2}$, $\langle H^0_d\rangle \equiv v_d = \cos\beta\ v/\sqrt{2}$, $v_u/v_d \equiv \tan\beta$ and $v \sim 246$ GeV is fixed by the Fermi constant, G_μ. Here, $\delta m_f/m_f$ $(f = t, b, \tau)$ represents the threshold correction due to integrating out SUSY partners. For the bottom quark mass, it is found [106] that the dominant corrections come from the gluino-sbottom and from the Higgsino-stop loops,

$$\left(\frac{\delta m_b}{m_b}\right)_{g_3} \sim \frac{g_3^2}{6\pi^2}\frac{m_{\tilde{g}}\mu}{m^2_{\mathrm{SUSY}}}\tan\beta$$

and

$$\left(\frac{\delta m_b}{m_b}\right)_{\lambda_t} \sim \frac{\lambda_t^2}{16\pi^2}\frac{A_t\mu}{m^2_{\mathrm{SUSY}}}\tan\beta\,, \qquad (114.15)$$

where $m_{\tilde{g}}$, μ, and A_t stand for gluino and Higgsino masses and trilinear stop coupling, respectively. Note that Eq. (114.15) only illustrates the structure of the corrections – non-trivial functional dependences on several soft parameters $\sim m_{\mathrm{SUSY}}$ have been suppressed. For the full one-loop correction to the bottom quark mass see, for example, Ref. [107].

Note also that the corrections do not go to zero as SUSY particles become much heavier than m_Z. They may change the bottom quark mass at the $\mathcal{O}(10)\%$ level for $\tan\beta = \mathcal{O}(10)$. The total effect is sensitive to the relative phase between gluino and Higgsino masses since $A_t \sim -m_{\tilde{g}}$ due to the infrared fixed point nature of the RG equation for A_t [108] in settings where SUSY breaking terms come from Planck scale dynamics, such as gravity mediation. The τ lepton mass also receives a similar correction, though only at the few % level. The top quark mass correction, not being proportional to $\tan\beta$, is at most 10% [109].

Including one loop threshold corrections at m_Z and additional RG running, one finds the top, bottom and τ pole masses. In SUSY GUTs, b–τ unification has two possible solutions with $\tan\beta \sim 1$ or $\mathcal{O}(10)$. The small $\tan\beta$ solution may be realized in the MSSM if superpartner masses are $\mathcal{O}(10)$ TeV, as suggested by the observed Higgs mass [92]. The large $\tan\beta$ limit such as $\tan\beta \sim 40$–50 overlaps the $SO(10)$ symmetry relation [109]. When $\tan\beta$ is large, there are significant threshold corrections to down quark masses as mentioned above, and Yukawa unification is only consistent with low-energy data in a restricted region of SUSY parameter space, with important consequences for SUSY searches [109,110]. More recent analyses of Yukawa unification after LHC Run-I are found in Ref. [111].

Gauge coupling unification is also successful in the scenario of split supersymmetry [74], in which squarks and sleptons have mass at a scale $\tilde{m} \gg m_Z$, while gauginos and/or Higgsinos have masses of order the weak scale. Unification of b–τ Yukawa couplings requires $\tan\beta$ to be fine-tuned close to 1 [92]. If by contrast, $\tan\beta \gtrsim 1.5$, b–τ Yukawa unification only works for $\tilde{m} \lesssim 10^4$ GeV. This is because the effective theory between the gaugino mass scale and $\tilde{m}$ includes only one Higgs doublet, as in the standard model. As a result, the large top quark Yukawa coupling tends to increase the ratio λ_b/λ_τ due to the vertex correction, which is absent in supersymmetric theories, as one runs down in energy below $\tilde{m}$. This is opposite to what happens in the MSSM where the large top quark Yukawa coupling lowers the ratio λ_b/λ_τ [103].

114.7.2. *Beyond leading order: three-family models* :

Simple Yukawa unification is not possible for the first two generations. Indeed, $SU(5)$ implies $\lambda_s = \lambda_\mu$, $\lambda_d = \lambda_e$ and hence $\lambda_s/\lambda_d = \lambda_\mu/\lambda_e$. This is an RG-invariant relation which extrapolates to $m_s/m_d = m_\mu/m_e$ at the weak scale, in serious disagreement with data ($m_s/m_d \sim 20$ and $m_\mu/m_e \sim 200$). An elegant solution to this

problem was given by Georgi and Jarlskog [112] (for a recent analysis in the SUSY context see [113]) .

More generally, we have to recall that in all of the previous discussion of Yukawa couplings, we assumed renormalizable interactions as well as the minimal matter and Higgs content. Since the GUT scale is close to the Planck scale, higher-dimension operators involving the GUT-breaking Higgs may modify the predictions, especially for lower generations. An example is provided by the operators $\mathbf{10}\ \bar{\mathbf{5}}\ \bar{\mathbf{5}}_{\mathbf{H}}\ \mathbf{24}_{\mathbf{H}}$ with $\mathbf{24}_{\mathbf{H}}$ the GUT-breaking Higgs of $SU(5)$. We can fit parameters to the observed fermion masses with these operators, though some fine-tuning is introduced in doing so. The SM Higgs doublet may come in part from higher representations of the GUT group. For example, the **45** of $SU(5)$ includes an $SU(2)_L$ doublet with appropriate $U(1)_Y$ charge [112]. This **45** can, in turn, come from the **120** or **126** of $SO(10)$ after its breaking to $SU(5)$ [114]. These fields may also have renormalizable couplings with quarks and leptons. The relations among the Yukawa coupling constants in the SM are modified if the SM Higgs doublet is a linear combination of several such doublets from different $SU(5)$ multiplets. Finally, the SM fermions may not be embedded in GUT multiplets in the minimal way. Indeed, if all quarks and leptons are embedded in **16**s of $SO(10)$, the renormalizable interactions with $\mathbf{10}_{\mathbf{H}}$ cannot explain the observed CKM mixing angles. This situation improves when extra matter multiplets, such as **10**, are introduced: After $U(1)_X$, which distinguishes the $\bar{\mathbf{5}}$s coming from the **16** and the **10** of $SO(10)$, is broken (e.g. by a VEV of $\mathbf{16}_{\mathbf{H}}$ or $\mathbf{126}_{\mathbf{H}}$), the r.h. down quarks and l.h. leptons in the SM can be linear combinations of components in **16**s and **10**s. As a result, $\lambda \neq \lambda'$ in $SU(5)$ [115].

To construct realistic three-family models, some or all of the above effects can be used. Even so, to achieve significant predictions for fermion masses and mixing angles grand unification alone is not sufficient. Other ingredients, for example additional global family symmetries are needed (in particular, non-abelian symmetries can strongly reduce the number of free parameters). These family symmetries constrain the set of effective higher-dimensional fermion mass operators discussed above. In addition, sequential breaking of the family symmetry can be correlated with the hierarchy of fermion masses. One simple, widely known idea in this context is to ensure that each $\mathbf{10}_i$ enters Yukawa interactions together with a suppression factor ϵ^{3-i} (ϵ being a small parameter). This way one automatically generates a stronger hierarchy in up-type quark Yukawas as compared to down-type quark and lepton Yukawas and no hierarchy for neutrinos, which agrees with observations at the $\mathcal{O}(1)$-level. Three-family models exist which fit all the data, including neutrino masses and mixing [26,116].

Finally, a particularly ambitious variant of unification is to require that the fermions of all three generations come from a single representation of a large gauge group. A somewhat weaker assumption is that the flavor group (e.g. $SU(3)$) unifies with the SM gauge group in a simple gauge group at some energy scale $M \geq M_G$. Early work on such 'flavor-unified GUTs', see e.g. [117], has been reviewed in [118,119]. For a selection of more recent papers see [120]. In such settings, Yukawa couplings are generally determined by gauge couplings together with symmetry breaking VEVs. This is reminiscent of heterotic string GUTs, where all couplings come from the 10d gauge coupling. However, while the $\mathrm{E}_8 \to SU(3)\times\mathrm{E}_6$ branching rule $\mathbf{248} = (\mathbf{8},\mathbf{1}) + (\mathbf{1},\mathbf{78}) + (\mathbf{3},\mathbf{27}) + (\bar{\mathbf{3}},\bar{\mathbf{27}})$ looks very suggestive in this context, the way in which most modern heterotic models arrive at three generations is actually more complicated.

114.7.3. *Flavor violation* :

Yukawa interactions of GUT-scale particles with quarks and leptons may leave imprints on the flavor violation induced by SUSY breaking parameters [121]. To understand this, focus first on the MSSM with universal Planck-scale boundary conditions (as e.g. in gravity mediation). Working in a basis where up-quark and lepton Yukawas are diagonal, one finds that the large top-quark Yukawa coupling reduces the l.h. squark mass squareds in the third generation radiatively. It turns out that only the l.h. down-type squark mass matrix has sizable off-diagonal terms in the flavor basis after CKM-rotation. However, in GUTs the color-triplet Higgs has flavor violating interactions from the Yukawa coupling λ_{ij} ($\mathbf{10}_i\ \mathbf{10}_j\ \mathbf{5}_{\mathbf{H}}$), such that flavor-violating r.h. slepton mass terms are radiatively generated in addition [122]. If r.h. neutrinos are introduced as $SU(5)$ singlets with interactions λ''_{ij} ($\mathbf{1}_i\ \bar{\mathbf{5}}_j\ \mathbf{5}_{\mathbf{H}}$), the doublet and color-triplet Higgses acquire another type of Yukawa coupling, respectively. They then radiatively generate flavor-violating l.h. slepton [123] and r.h. down squark masses [124]. These flavor-violating SUSY breaking terms induce new contributions to FCNC processes in quark and lepton sectors, such as $\mu \to e\gamma$ and K^0–$\bar{K}^0$ and B^0–$\bar{B}^0$ mixing. EDMs are also induced when both l.h. and r.h. squarks/sleptons have flavor-violating mass terms with relative phases, as discussed for $SO(10)$ in [125] or for $SU(5)$ with r.h. neutrinos in [126]. Thus, such low-energy observables constrain GUT-scale interactions.

114.8. Neutrino masses

We see from atmospheric and solar neutrino oscillation observations, along with long baseline accelerator and reactor experiments, that neutrinos have finite masses. By adding three "sterile" neutrinos ν_i^c with Yukawa couplings $\lambda_{\nu,ij}$ ($\nu_i^c\ L_j\ H_u$) (i,j = 1–3), one easily obtains three massive Dirac neutrinos with mass $m_\nu = \lambda_\nu\ v_u$, analogously to quark and charged lepton masses. However, in order to obtain a τ neutrino with mass of order 0.1 eV, one requires the exceedingly small coupling ratio $\lambda_{\nu_\tau}/\lambda_\tau \lesssim 10^{-10}$. By contrast, the seesaw mechanism *naturally* explains such tiny neutrino masses as follows [1,2,3]: The sterile neutrinos have no SM gauge quantum numbers so that there is no symmetry other than global lepton number which forbids the Majorana mass term $\frac{1}{2}M_{ij}\ \nu_i^c\ \nu_j^c$. Note also that sterile neutrinos can be identified with the r.h. neutrinos necessarily contained in complete families of $SO(10)$ or Pati-Salam models. Since the Majorana mass term violates $U(1)_X$ in $SO(10)$, one might expect $M_{ij} \sim M_G$. The heavy sterile neutrinos can be integrated out, defining an effective low-energy theory with only three light active Majorana neutrinos with the effective dimension-five operator

$$-\mathcal{L}_{eff} = \frac{1}{2}c_{ij}\ (L_i\ H_u)\ (L_j\ H_u)\,, \tag{114.16}$$

where $c = \lambda_\nu^T\ M^{-1}\ \lambda_\nu$. This then leads to a 3×3 Majorana neutrino mass matrix $m = m_\nu^T\ M^{-1}\ m_\nu$.

Atmospheric neutrino oscillations require neutrino masses with $\Delta m_\nu^2 \sim 2.5\times 10^{-3}$ eV^2 with maximal mixing, in the simplest scenario of two neutrino dominance. With hierarchical neutrino masses this implies $m_{\nu_\tau} = \sqrt{\Delta m_\nu^2} \sim 0.05$ eV. Next, we can try to relate the neutrino Yukawa coupling to the top quark Yukawa coupling, $\lambda_{\nu_\tau} = \lambda_t$ at the GUT scale, as in $SO(10)$ or $SU(4)\times SU(2)_L \times SU(2)_R$ models. This gives $M \sim 10^{14}$ GeV, which is remarkably close to the GUT scale.

Neutrinos pose a special problem for SUSY GUTs. The question is why the quark mixing angles in the CKM matrix are small while there are two large lepton mixing angles in the PMNS matrix (cf. however the comment at the end of Sec. 114.7). Discussions of neutrino masses and mixing angles can, for example, be found in Refs. [127] and [128]. For SUSY GUT models which fit quark and lepton masses, see Ref. [25]. Finally, for a compilation of the range of SUSY GUT predictions for neutrino mixing, see [129].

The seesaw mechanism implemented by r.h. neutrinos is sometimes called the type-I seesaw model. There are variant models in which the dimension-five operator for neutrino masses is induced in different ways: In the type-II model, an $SU(2)_L$ triplet Higgs boson Σ is introduced to have couplings ΣL^2 and also ΣH_u^2 [130]. In the type-III model, an $SU(2)_L$ triplet of fermions $\tilde{\Sigma}$ with a Yukawa coupling $\tilde{\Sigma}LH_u$ is introduced [131]. In these models, the dimension-five operator is induced by integrating out the triplet Higgs boson or fermions. Such models can also be implemented in GUTs by introducing Higgs bosons in the **15** or fermions in the **24** in $SU(5)$ GUTs or the **126** in $SO(10)$ GUTs. Notice that the gauge non-singlet fields in the type-II and III models have masses at the intermediate scale. Thus, gauge coupling unification is not automatic if they are implemented in SUSY GUTs.

114.9. Selected topics

114.9.1. *Magnetic monopoles* :

In the broken phase of a GUT there are typically localized classical solutions carrying magnetic charge under an unbroken $U(1)$ symmetry [132]. These magnetic monopoles with mass of order M_G/α_G can be produced during a possible GUT phase transition in the early universe. The flux of magnetic monopoles is experimentally found to be less than $\sim 10^{-16}$ cm^{-2} s^{-1} sr^{-1} [133]. Many more are however predicted, hence the GUT monopole problem. In fact, one of the original motivations for inflation was to solve the monopole problem by exponential expansion after the GUT phase transition [134] and hence dilution of the monopole density. Other possible solutions to the monopole problem include: sweeping them away by domain walls [135], $U(1)$ electromagnetic symmetry breaking at high temperature [136] or GUT symmetry non-restoration [137]. Parenthetically, it was also shown that GUT monopoles can catalyze nucleon decay [138]. A significantly stronger bound on the monopole flux can then be obtained by considering X-ray emission from radio pulsars due to monopole capture and the subsequent nucleon decay catalysis [139].

Note that the present upper bound on the inflationary vacuum energy density is very close to the GUT scale, $V_{inf}^{1/4} = (1.88 \times 10^{16}\,\text{GeV}) \times (r/0.10)^{1/4}$, with the scalar-to-tensor ratio constraint to $r < 0.11$ [140]. This guarantees that reheating does not lead to temperatures above M_G and hence the monopole problem is solved by inflation (unless M_G is unexpectedly low).

114.9.2. *Anomaly constraints vs. GUT paradigm* :

As emphasized at the very beginning, the fact that the SM fermions of one generation fill out the $\mathbf{10} + \overline{\mathbf{5}}$ of $SU(5)$ appears to provide overwhelming evidence for some form of GUT embedding. However, one should be aware that a counterargument can be made which is related to the issue of 'charge quantization by anomaly cancellation' (see [141,142] for some early papers and [143] for a more detailed reference list): Imagine we only knew that the low-energy gauge group were G_{SM} and the matter content included the $(\mathbf{3},\mathbf{2})_Y$, i.e. a 'quark doublet' with $U(1)$-charge Y. One can then ask which possibilities exist of adding further matter to ensure the cancellation of all triangle anomalies. It turns out that this problem has only three different, minimal* solutions [142]. One of those is precisely a single SM generation, with the apparent '$SU(5)$-ness' emerging accidentally. Thus, if one randomly picks models from the set of consistent gauge theories, preconditioning on G_{SM} and $(\mathbf{3},\mathbf{2})_Y$, one may easily end up with '$\mathbf{10} + \overline{\mathbf{5}}$' of an $SU(5)$ that is in no way dynamically present. This is precisely what happens in the context of non-GUT string model building [144].

114.9.3. *GUT baryogenesis and leptogenesis* :

During inflation, any conserved quantum number is extremely diluted. Thus, one expects the observed baryon asymmetry of the universe to originate at reheating or in the subsequent cosmological evolution. In detail, the situation is slightly more involved: Both baryon number B and lepton number L are global symmetries of the SM. However, $(B+L)$ is anomalous and violated by thermal fluctuations in the early universe, via so-called sphaleron processes. Moreover, it is violated in GUT models, as is most apparent in proton decay. By contrast, $(B-L)$ is anomaly free and preserved by both the SM as well as $SU(5)$ or $SO(10)$ gauge interactions.

Now, the old idea of GUT baryogenesis [145,146] is to generate a $(B+L)$ and hence a baryon asymmetry by the out-of-equilibrium decay of the color-triplet Higgs. However such an asymmetry, generated at GUT temperatures, is washed out by sphalerons. This can be overcome [147] using lepton-number violating interaction of neutrinos to create a $(B-L)$ from the $(B+L)$ asymmetry, before sphaleron processes become sufficiently fast at $T < 10^{12}$ GeV. This $(B-L)$ asymmetry can then survive the subsequent sphaleron dominated phase. Note that this does not work in the minimal SUSY GUT setting, with the triplet Higgs above the GUT scale. The reason is that a correspondingly high reheating temperature would be required which, as explained above, is ruled out by Planck data.

However, the most widely accepted simple way out of the dilemma is to directly generate a net $(B-L)$ asymmetry dynamically in the early universe, also using r.h. neutrinos. Indeed, we have seen that neutrino oscillations suggest a new scale of physics of order 10^{14} GeV. This scale is associated with heavy Majorana neutrinos in the seesaw mechanism. If in the early universe, the decay of the heavy neutrinos is out of equilibrium and violates both lepton number and CP, then a net lepton number may be generated. This lepton number will then be partially converted into baryon number via electroweak processes [148]. This mechanism is called leptogenesis.

If the three heavy Majorana neutrino masses are hierarchical, the net lepton number is produced by decay of the lightest one, and it is proportional to the CP asymmetry in the decay, ϵ_1. The CP asymmetry is bounded from above, and the lightest neutrino mass is required to be larger than 10^9 GeV in order to explain the observed baryon asymmetry [149]. This implies that the reheating temperature after inflation should be larger than 10^9 GeV so that the heavy neutrinos are thermally produced. In supersymmetric models, there is a tension between leptogenesis and Big Bang Nucleosynthesis (BBN) if gravitinos decay in the BBN era. The gravitino problem gives a constraint on the reheating temperature $\lesssim 10^{6-10}$ GeV though the precise value depends on the SUSY breaking parameters [150]. Recent reviews of leptogenesis can be found in Ref. [151].

114.10. Conclusion

Most conservatively, grand unification means that (some of) the SM gauge interactions of $U(1)_Y$, $SU(2)_L$ and $SU(3)_C$ become part of a larger, unifying gauge symmetry at a high energy scale. In most models, especially in the simplest and most appealing variants of $SU(5)$ and $SO(10)$ unification, the statement is much stronger: One expects the three gauge couplings to unify (up to small threshold corrections) at a unique scale, M_G, and the proton to be unstable due to exchange of gauge bosons of the larger symmetry group. Supersymmetric grand unified theories provide, by far, the most predictive and economical framework allowing for perturbative unification. For a selection of reviews, with many more details than could be discussed in the present article, see [118,152].

Thus, the three classical pillars of GUTs are gauge coupling unification at $M_G \sim 2 \times 10^{16}$ GeV, low-energy supersymmetry (with a large SUSY desert), and nucleon decay. The first of these may be viewed as predicting the value of the strong coupling – a prediction which has already been verified (see Fig. 114.1). Numerically, this prediction remains intact even if SUSY partner masses are somewhat above the weak scale. However, at the conceptual level a continuously increasing lower bound on the SUSY scale is nevertheless problematic for the GUT paradigm: Indeed, if the independent, gauge-hierarchy-based motivation for SUSY is completely abandoned, the SUSY scale and hence α_3 become simply free parameters and the first two pillars crumble. Thus, it is important to keep pushing bounds on proton decay which, although again not completely universal in all GUT constructions, is arguably a more generic part of the GUT paradigm than low-energy SUSY.

Whether or not Yukawa couplings unify is more model dependent. However, irrespective of possible (partial) Yukawa unification, there certainly exists a very interesting and potentially fruitful interplay between flavor model building and grand unification. Especially in the neutrino sector this is strongly influenced by the developing experimental situation.

Another phenomenological signature of grand unification is the strength of the direct coupling of the QCD axion to photons, relative to its coupling to gluons. It is quantified by the predicted anomaly ratio $E/N = 8/3$ (see [153,154]). This arises in field-theoretic axion models consistent with GUT symmetry (such as DFSZ [155]) and in string-theoretic GUTs [154]. In the latter, the axion does not come from the phase of a complex scalar but is a fundamental shift-symmetric real field, coupling through a higher-dimension operator

* Adding extra vector-like sets of fields, e.g. two fermions which only transform under $U(1)$ and have charges Y and $-Y$, is considered to violate minimality.

directly to the product of the GUT field-strength and its dual.

It is probably fair to say that, due to limitations of the 4d approach, including especially remaining ambiguities (free parameters or ad hoc assumptions) in models of flavor and GUT breaking, the string theoretic approach has become more important in GUT model building. In this framework, challenges include learning how to deal with the many vacua of the 'landscape' as well as, for each vacuum, developing the tools for reliably calculating detailed, phenomenological observables. Finally, due to limitations of space, the present article has barely touched on the interesting cosmological implications of GUTs. They may become more important in the future, especially in the case that a high inflationary energy scale is established observationally.

References:

1. P. Minkowski, Phys. Lett. **B67**, 421 (1977).
2. T. Yanagida, in *Proceedings of the Workshop on the Unified Theory and the Baryon Number of the Universe*, eds. O. Sawada and A. Sugamoto, KEK report No. 79-18, Tsukuba, Japan, 1979;
   S. Glashow, Quarks and leptons, published in *Proceedings of the Carg'ese Lectures*, M. Levy (ed.), Plenum Press, New York, (1980);
   M. Gell-Mann, P. Ramond and R. Slansky, in *Supergravity*, ed. P. van Nieuwenhuizen *et al.*, North-Holland, Amsterdam, (1979), p. 315 [arXiv:1306.4669].
3. F. Wilczek, eConf C **790823**, 437 (1979);
   E. Witten, Phys. Lett. **B91**, 81 (1980);
   R.N. Mohapatra and G. Senjanovic, Phys. Rev. Lett. **44**, 912 (1980).
4. U. Amaldi, W. de Boer and H. Furstenau, Phys. Lett. **B260**, 447 (1991);
   J.R. Ellis, S. Kelley and D.V. Nanopoulos, Phys. Lett. **B260**, 131 (1991);
   P. Langacker and M. Luo, Phys. Rev. **D44**, 817 (1991);
   C. Giunti, C.W. Kim and U.W. Lee, Mod. Phys. Lett. **A6**, 1745 (1991);
   P. Langacker and N. Polonsky, Phys. Rev. **D47**, 4028 (1993), [hep-ph/9210235];
   M. Carena, S. Pokorski and C.E.M. Wagner, Nucl. Phys. **B406**, 59 (1993) [hep-ph/9303202];
   See also the review by S. Dimopoulos, S.A. Raby and F. Wilczek, Physics Today, p. 25 October (1991).
5. Y. Okada, M. Yamaguchi and T. Yanagida, Prog. Theor. Phys. **85**, 1 (1991);
   J.R. Ellis, G. Ridolfi and F. Zwirner, Phys. Lett. **B257**, 83 (1991);
   H.E. Haber and R. Hempfling, Phys. Rev. Lett. **66**, 1815 (1991).
6. M.S. Carena *et al.*, Phys. Lett. **B355**, 209 (1995) [hep-ph/9504316];
   G. Degrassi *et al.*, Eur. Phys. J. **C28**, 133 (2003) [arXiv:hep-ph/0212020];
   P. Kant *et al.*, JHEP **1008**, 104 (2010) [arXiv:1005.5709].
7. M.J.G. Veltman, Acta Phys. Pol. **B12**, 437 (1981);
   L. Maiani, Gif-sur-Yvette Summer School on Particle Physics, 11th, Gif-sur-Yvette, France, 1979 (Inst. Nat. Phys. Nucl. Phys. Particules, Paris, 1979);
   E. Witten, Nucl. Phys. **B188**, 513 (1981).
8. J.L. Feng *et al.*, Phys. Rev. Lett. **111**, 131802 (2013) [arXiv:1306.2318];
   S. Heinemeyer, Lecture at 42nd ITEP winter school, Moscow, arXiv:1405.3781;
   P. Draper and H. Rzehak, Phys. Rept. **619**, 1 (2016) [arXiv:1601.01890].
9. J. Pati and A. Salam, Phys. Rev. **D8**, 1240 (1973);
   For more discussion on the standard charge assignments in this formalism, see A. Davidson, Phys. Rev. **D20**, 776 (1979) and R.N Mohapatra and R.E. Marshak, Phys. Lett. **B91**, 222 (1980); see also J. C. Pati, Int. J. Mod. Phys. A **32**, 1741013 (2017), arXiv:1706.09531 for a recent account.
10. H. Georgi and S.L Glashow, Phys. Rev. Lett. **32**, 438 (1974).
11. J.R. Ellis, M.K. Gaillard and D.V. Nanopoulos, Phys. Lett. **B80**, 360 (1979) [Phys. Lett. **B82**, 464 (1979)];
    E. Golowich, Phys. Rev. **D24**, 2899 (1981).
12. S. Dimopoulos, S. Raby, and F. Wilczek, Phys. Rev. **D24**, 1681 (1981);
    S. Dimopoulos and H. Georgi, Nucl. Phys. **B193**, 150 (1981);
    L. Ibanez and G.G. Ross, Phys. Lett. **B105**, 439 (1981);
    N. Sakai, Z. Phys. **C11**, 153 (1981);
    M.B. Einhorn and D.R.T. Jones, Nucl. Phys. **B196**, 475 (1982);
    W.J. Marciano and G. Senjanovic, Phys. Rev. **D25**, 3092 (1982).
13. S. Weinberg, Phys. Rev. **D26**, 287 (1982);
    N. Sakai and T. Yanagida, Nucl. Phys. **B197**, 533 (1982).
14. H. Georgi, Particles and Fields, *Proceedings of the APS Div. of Particles and Fields*, ed. C. Carlson, p. 575 (1975);
    H Fritzsch and P. Minkowski, Ann. Phys. **93**, 193 (1975).
15. R. Slansky, Phys. Reports **79**, 1 (1981);
    H. Georgi, Front. Phys. **54**, 1 (1982);
    R. Feger and T.W. Kephart, Comp. Phys. Comm. **192**, 166 (2015) [arXiv:1206.6379];
    N. Yamatsu, PTEP, no.4, 043B02 (2016) [arXiv:1512.05559].
16. S.M. Barr, Phys. Lett. **B112**, 219 (1982);
    J.P. Derendinger, J.E. Kim and D.V. Nanopoulos, Phys. Lett. **B139**, 170 (1984);
    I. Antoniadis *et al.*, Phys. Lett. **B194**, 231 (1987) and Phys. Lett. **B231**, 65 (1989).
17. F. Gursey, P. Ramond and P. Sikivie, Phys. Lett. **B60**, 177 (1976).
18. A. de Rujula, H. Georgi and S. L. Glashow, *5th Workshop on Grand Unification*, ed. K. Kang, H. Fried and P. Frampton, World Scientific, Singapore (1984), p. 88;
    See also earlier paper by Y. Achiman and B. Stech, p. 303, "New Phenomena in Lepton-Hadron Physics," ed. D.E.C. Fries and J. Wess, Plenum, NY (1979).
19. B.R. Greene *et al.*, Nucl. Phys. **B278**, 667 (1986) and Nucl. Phys. **B292**, 606 (1987);
    B.R. Greene, C.A. Lutken and G.G. Ross, Nucl. Phys. **B325**, 101 (1989);
    J.E. Kim, Phys. Lett. **B591**, 119 (2004) [hep-ph/0403196].
20. E. Witten, Phys. Lett. **B105**, 267 (1981).
21. A. Masiero *et al.*, Phys. Lett. **B115**, 380 (1982);
    B. Grinstein, Nucl. Phys. **B206**, 387 (1982).
22. S. Dimopoulos and F. Wilczek, *Proceedings Erice Summer School*, ed. A. Zichichi (1981);
    M. Srednicki, Nucl. Phys. **B202**, 327 (1982).
23. K. Inoue, A. Kakuto and H. Takano, Prog. Theor. Phys. **75**, 664 (1986).
24. Y. Yamada, Z. Phys. **C60**, 83 (1993);
    J. Hisano *et al.*, Phys. Lett. **B342**, 138 (1995) [hep-ph/9406417];
    G. Altarelli, F. Feruglio and I. Masina, JHEP **0011**, 040 (2000) [hep-ph/0007254].
25. K.S. Babu and S.M. Barr, Phys. Rev. **D48**, 5354 (1993) [hep-ph/9306242];
    K.S. Babu and S.M. Barr, Phys. Rev. **D50**, 3529 (1994) [hep-ph/9402291];
    K.S. Babu, J.C. Pati and Z. Tavartkiladze, JHEP **1006**, 084 (2010) [arXiv:1003.2625].
26. K.S. Babu and R.N. Mohapatra, Phys. Rev. Lett. **74**, 2418 (1995) [hep-ph/9410326];
    V. Lucas and S. Raby, Phys. Rev. **D54**, 2261 (1996) [hep-ph/9601303];
    T. Blažek *et al.*, Phys. Rev. **D56**, 6919 (1997) [hep-ph/9611217];
    S.M. Barr and S. Raby, Phys. Rev. Lett. **79**, 4748 (1997) [hep-ph/9705366];
    K.S. Babu, J.C. Pati and F. Wilczek, Nucl. Phys. **B566**, 33 (2000) [hep-ph/9812538];
    R. Dermíšek, A. Mafi and S. Raby, Phys. Rev. **D63**, 035001 (2001) [hep-ph/0007213].
27. R. Barbieri, G.R. Dvali and A. Strumia, Nucl. Phys. **B391**, 487 (1993);

Z. Berezhiani, C. Csaki and L. Randall, Nucl. Phys. **B444**, 61 (1995) [hep-ph/9501336];
Q. Shafi and Z. Tavartkiladze, Phys. Lett. **B522**, 102 (2001) [hep-ph/0105140].
28. G.F. Giudice and A. Masiero, Phys. Lett. **B206**, 480 (1988); J.E. Kim and H.P. Nilles, Mod. Phys. Lett. **A9**, 3575 (1994) [hep-ph/9406296].
29. L. Randall and C. Csaki, in *Palaiseau 1995, SUSY 95* 99-109 [hep-ph/9508208].
30. E. Witten, in *Hamburg 2002, SUSY 02* [hep-ph/0201018]; M. Dine, Y. Nir and Y. Shadmi, Phys. Rev. **D66**, 115001 (2002) [hep-ph/0206268].
31. A. Hebecker, J. March-Russell and R. Ziegler, JHEP **0908**, 064 (2009) [arXiv:0801.4101]; F. Brümmer *et al.*, JHEP **0908**, 011 (2009) [arXiv:0906.2957]; F. Brümmer *et al.*, JHEP **1004**, 006 (2010) [arXiv:1003.0084].
32. H.M. Lee *et al.*, Phys. Lett. **B694**, 491 (2011) [arXiv:1009.0905]; R. Kappl *et al.*, Nucl. Phys. **B847**, 325 (2011) [arXiv:1012.4574];
H.M. Lee *et al.*, Nucl. Phys. **B850**, 1 (2011) [arXiv:1102.3595].
33. Y. Hosotani, Phys. Lett. **B126**, 309 (1983).
34. L.J. Dixon *et al.*, Nucl. Phys. **B261**, 678 (1985) and Nucl. Phys. **B274**, 285 (1986);
L.E. Ibanez, H.P. Nilles and F. Quevedo, Phys. Lett. **B187**, 25 (1987);
L.E. Ibanez *et al.*, Phys. Lett. **B191**, 282 (1987).
35. P. Candelas *et al.*, Nucl. Phys. **B258**, 46 (1985).
36. Y. Kawamura, Prog. Theor. Phys. **103**, 613 (2000) [hep-ph/9902423] and Prog. Theor. Phys. **105**, 999 (2001) [hep-ph/0012125];
G. Altarelli and F. Feruglio, Phys. Lett. **B511**, 257 (2001) [hep-ph/0102301];
L.J. Hall and Y. Nomura, Phys. Rev. **D64**, 055003 (2001) [hep-ph/0103125];
A. Hebecker and J. March-Russell, Nucl. Phys. **B613**, 3 (2001) [hep-ph/0106166];
T. Asaka, W. Buchmuller and L. Covi, Phys. Lett. **B523**, 199 (2001) [hep-ph/0108021];
L.J. Hall *et al.*, Phys. Rev. **D65**, 035008 (2002) [hep-ph/0108071];
R. Dermisek and A. Mafi, Phys. Rev. **D65**, 055002 (2002) [hep-ph/0108139];
H.D. Kim and S. Raby, JHEP **0301**, 056 (2003) [hep-ph/0212348].
37. L.E. Ibanez and A.M. Uranga, "String theory and particle physics: An introduction to string phenomenology," Cambridge University Press 2012;
K.S. Choi and J.E. Kim, Lect. Notes Phys. **696**, 1 (2006);
R. Blumenhagen *et al.*, Phys. Reports **445**, 1 (2007) [hep-th/0610327].
38. V. Braun *et al.*, JHEP **0605**, 043 (2006) [hep-th/0512177];
V. Bouchard and R. Donagi, Phys. Lett. **B633**, 783 (2006) [hep-th/0512149];
L.B. Anderson *et al.*, Phys. Rev. **D84**, 106005 (2011) [arXiv:1106.4804].
39. L.J. Dixon, V. Kaplunovsky and J. Louis, Nucl. Phys. **B355**, 649 (1991).
40. G. Aldazabal *et al.*, Nucl. Phys. **B452**, 3 (1995) [hep-th/9410206];
Z. Kakushadze *et al.*, Int. J. Mod. Phys. **A13**, 2551 (1998) [hep-th/9710149].
41. E. Witten, Nucl. Phys. **B258**, 75 (1985).
42. S. Gukov *et al.*, Phys. Rev. **D69**, 086008 (2004) [hep-th/0310159];
G. Curio, A. Krause and D. Lust, Fortsch. Phys. **54**, 225 (2006) [hep-th/0502168];
L.B. Anderson *et al.*, Phys. Rev. **D83**, 106011 (2011) [arXiv:1102.0011].
43. R. Friedman, J. Morgan and E. Witten, Commun. Math. Phys. **187**, 679 (1997) [hep-th/9701162].
44. R. Blumenhagen, G. Honecker and T. Weigand, JHEP **0508**, 009 (2005) [hep-th/0507041];
L. B. Anderson *et al.*, JHEP **1401** (2014) 047 [arXiv:1307.4787].
45. T. Kobayashi, S. Raby and R.J. Zhang, Phys. Lett. **B593**, 262 (2004) [hep-ph/0403065].
46. S. Forste *et al.*, Phys. Rev. **D70**, 106008 (2004) [hep-th/0406208];
T. Kobayashi, S. Raby and R.J. Zhang, Nucl. Phys. **B704**, 3 (2005) [hep-ph/0409098];
W. Buchmuller *et al.*, Nucl. Phys. **B712**, 139 (2005) [hep-ph/0412318];
W. Buchmuller *et al.*, Phys. Rev. Lett. **96**, 121602 (2006) [hep-ph/0511035], and Nucl. Phys. **B785**, 149 (2007) [hep-th/0606187];
O. Lebedev, *et al.*, Phys. Lett. **B645**, 88 (2007) [hep-th/0611095];
J.E. Kim, J.H. Kim and B. Kyae, JHEP **0706**, 034 (2007) [hep-ph/0702278];
O. Lebedev, *et al.*, Phys. Rev. **D77**, 046013 (2008) [arXiv:0708.2691].
47. S.B. Giddings, S. Kachru and J. Polchinski, Phys. Rev. **D66**, 106006 (2002) [hep-th/0105097];
S. Kachru *et al.*, Phys. Rev. **D68**, 046005 (2003) [hep-th/0301240].
48. R. Blumenhagen *et al.*, Nucl. Phys. **B815**, 1 (2009) [arXiv:0811.2936].
49. R. Blumenhagen *et al.*, Nucl. Phys. **B616**, 3 (2001) [hep-th/0107138].
50. R. Donagi and M. Wijnholt, Adv. Theor. Math. Phys. **15**, 1237 (2011) [arXiv:0802.2969].
51. C. Beasley, J.J. Heckman and C. Vafa, JHEP **0901**, 058 (2009) [arXiv:0802.3391], and JHEP **0901**, 059 (2009) [arXiv:0806.0102].
52. T. Weigand, Class. Quantum Grav. **27**, 214004 (2010) [arXiv:1009.3497];
J.J. Heckman, Ann. Rev. Nucl. and Part. Sci. **160**, 237 (2010) [arXiv:1001.0577];
M. Cvetic, I. Garcia-Etxebarria and J. Halverson, JHEP **1101**, 073 (2011) [arXiv:1003.5337];
A. Maharana and E. Palti, Int. J. Mod. Phys. **A28**, 1330005 (2013) [arXiv:1212.0555];
S. Krippendorf, S. Schafer-Nameki and J.M. Wong, JHEP **1511**, 008 (2015) [arXiv:1507.05961].
53. R. Donagi and M. Wijnholt, Adv. Theor. Math. Phys. **15**, 1523 (2011) [arXiv:0808.2223];
R. Blumenhagen, Phys. Rev. Lett. **102**, 071601 (2009) [arXiv:0812.0248];
K. S. Choi and J. E. Kim, Phys. Rev. **D83**, 065016 (2011) [arXiv:1012.0847];
C. Mayrhofer, E. Palti and T. Weigand, JHEP **1309**, 082 (2013) [arXiv:1303.3589];
G. K. Leontaris and Q. Shafi, Phys. Rev. **D96**, 066023 (2017) [arXiv:1706.08372].
54. E. Witten, Nucl. Phys. **B471**, 135 (1996) [hep-th/9602070].
55. A. Hebecker and M. Trapletti, Nucl. Phys. **B713**, 173 (2005) [hep-th/0411131].
56. H. Georgi, H. R. Quinn and S. Weinberg, Phys. Rev. Lett. **33**, 451 (1974);
See also the definition of effective field theories by S. Weinberg, Phys. Lett. **B91**, 51 (1980).
57. C. Patrignani *et al.* [Particle Data Group], Chin. Phys. C **40**, 100001 (2016).
58. M.L. Alciati *et al.*, JHEP **0503**, 054 (2005) [hep-ph/0501086].
59. See talks on proposed and running nucleon decay experiments, and theoretical talks by P. Langacker, p. 131, and W.J. Marciano and A. Sirlin, p. 151, in *The Second Workshop on Grand Unification*, eds. J.P. Leveille *et al.*, Birkhäuser, Boston (1981).
60. W.J. Marciano, p. 190, *Eighth Workshop on Grand Unification*, ed. K. Wali, World Scientific Publishing Co., Singapore (1987).
61. M.S. Carena *et al.*, in Ref. [4].

62. B.C. Allanach, Comp. Phys. Comm. **143**, 305 (2002) [hep-ph/0104145].
63. A. Djouadi, J. L. Kneur and G. Moultaka, Comp. Phys. Comm. **176**, 426 (2007) [hep-ph/0211331].
64. W. Porod and F. Staub, Comp. Phys. Comm. **183**, 2458 (2012) [arXiv:1104.1573].
65. W. Siegel, Phys. Lett. **B94**, 37 (1980).
66. I. Antoniadis, C. Kounnas, and R. Lacaze, Nucl. Phys. **B221**, 377 (1983).
67. M.A. Shifman, Int. J. Mod. Phys. **A11**, 5761 (1996) [arXiv:hep-ph/9606281];
N. Arkani-Hamed and H. Murayama, JHEP **0006**, 030 (2000) [arXiv:hep-th/9707133];
I. Jack, D.R.T. Jones and A. Pickering, Phys. Lett. **B435**, 61 (1998) [arXiv:hep-ph/9805482].
68. M.B. Einhorn and D.R.T. Jones in Ref. [12];
I. Antoniadis, C. Kounnas, and K. Tamvakis, Phys. Lett. **B119**, 377 (1982).
69. J. Hisano, H. Murayama and T. Yanagida, Phys. Rev. Lett. **69**, 1014 (1992) and Nucl. Phys. **B402**, 46 (1993) [hep-ph/9207279].
70. H. Murayama and A. Pierce, Phys. Rev. **D65**, 055009 (2002) [hep-ph/0108104].
71. G. Anderson *et al.*, eConf **C960625**, SUP107 (1996) [hep-ph/9609457].
72. S. Raby, M. Ratz and K. Schmidt-Hoberg, Phys. Lett. **B687**, 342 (2010) [arXiv:0911.4249].
73. J. Hisano, T. Kuwahara and N. Nagata, Phys. Lett. **B723**, 324 (2013) [arXiv:1304.0343].
74. N. Arkani-Hamed, A. Delgado and G.F. Giudice, Nucl. Phys. **B741**, 108 (2006) [hep-ph/0601041].
75. M. Ibe, T. Moroi and T.T. Yanagida, Phys. Lett. **B644**, 355 (2007) [hep-ph/0610277].
76. G.F. Giudice *et al.*, JHEP **9812**, 027 (1998) [hep-ph/9810442]; L. Randall and R. Sundrum, Nucl. Phys. **B557**, 79 (1999) [hep-th/9810155].
77. R.N. Mohapatra and M.K. Parida, Phys. Rev. **D47**, 264 (1993) [hep-ph/9204234].
78. D.G. Lee *et al.*, Phys. Rev. **D51**, 229 (1995) [hep-ph/9404238].
79. L.E. Ibanez *et al.*, JHEP **1207**, 195 (2012) [arXiv:1206.2655].
80. K.R. Dienes, E. Dudas and T. Gherghetta, Phys. Rev. Lett. **91**, 061601 (2003) [hep-th/0210294].
81. K. Agashe, R. Contino and R. Sundrum, Phys. Rev. Lett. **95**, 171804 (2005) [hep-ph/0502222].
82. S. Weinberg, Phys. Rev. Lett. **43**, 1566 (1979);
F. Wilczek and A. Zee, Phys. Rev. Lett. **43**, 1571 (1979).
83. R. Barbier *et al.*, Phys. Rev. **420**, 1 (2005) [hep-ph/0406039].
84. G. Farrar and P. Fayet, Phys. Lett. **B76**, 575 (1978).
85. S. Dimopoulos, S. Raby and F. Wilczek, Phys. Lett. **B112**, 133 (1982);
J. Ellis, D.V. Nanopoulos and S. Rudaz, Nucl. Phys. **B202**, 43 (1982).
86. For a recent discussion, see C.S. Aulakh *et al.*, Nucl. Phys. **B597**, 89 (2001) [hep-ph/0004031].
87. K. Abe *et al.* [Super-Kamiokande Collaboration], Phys. Rev. **D95**, 012004 (2017) [arXiv:1610.03597];
S. Mine for the Super Kamiokande Collaboration, J. Phys. Conf. Ser. **718**, 062044 (2016).
88. Y. Aoki, T. Izubuchi, E. Shintani and A. Soni, Phys. Rev. **D96**, 014506 (2017) [arXiv:1705.01338 [hep-lat]].
89. For recent analysis, see J. Hisano, T. Kuwahara and Y. Omura, Nucl. Phys. **B898**, 1 (2015) [arXiv:1503.08561].
90. T. Goto and T. Nihei, Phys. Rev. **D59**, 115009 (1999) [hep-ph/9808255].
91. J.L. Chkareuli and I.G. Gogoladze, Phys. Rev. **D58**, 055011 (1998) [hep-ph/9803335].
92. G.F. Giudice and A. Romanino, Nucl. Phys. **B699**, 65 (2004) [hep-ph/0406088], [Erratum: *ibid.*, Nucl. Phys. **B706**, 65 (2005)].
93. J. Hisano *et al.*, JHEP **1307**, 038 (2013) [arXiv:1304.3651].
94. B. Bajc, P. Fileviez Perez and G. Senjanovic, Phys. Rev. **D66**, 075005 (2002) [hep-ph/0204311].
95. K.S. Choi, Phys. Lett. **B668**, 392 (2008) [arXiv:0807.2766].
96. F. An *et al.* [JUNO Collab.], J. Phys. G **43**, 030401 (2016) [arXiv:1507.05613].
97. Hyper-Kamiokande Collab., 'Hyper-Kamiokande Design Report', KEK-PREPRINT-2016-21, ICRR-REPORT-701-2016-1 (2016).
98. R. Acciarri *et al.* [DUNE Collaboration], 'The Physics Program for DUNE at LBNF', arXiv:1512.06148.
99. R. Kallosh *et al.*, Phys. Rev. **D52**, 912 (1995) [hep-th/9502069].
100. L.E. Ibanez and G.G. Ross, Nucl. Phys. **B368**, 3 (1992);
M. Berasaluce-Gonzalez *et al.*, JHEP **1112**, 113 (2011) [arXiv:1106.4169 [hep-th]].
101. L.J. Hall and Y. Nomura, Phys. Rev. **D66**, 075004 (2002) [hep-ph/0205067];
H.D. Kim, S. Raby and L. Schradin, JHEP **0505**, 036 (2005) [hep-ph/0411328].
102. M.S. Chanowitz, J.R. Ellis and M.K. Gaillard, Nucl. Phys. **B128**, 506 (1977);
A.J. Buras *et al.*, Nucl. Phys. **B135**, 66 (1978).
103. K. Inoue *et al.*, Prog. Theor. Phys. **67**, 1889 (1982);
L.E. Ibanez and C. Lopez, Phys. Lett. **B126**, 54 (1983) and Nucl. Phys. **B233**, 511 (1984).
104. H. Georgi and D.V. Nanopoulos, Nucl. Phys. **B159**, 16 (1979);
J. Harvey, P. Ramond and D.B. Reiss, Phys. Lett. **B92**, 309 (1980) and Nucl. Phys. **B199**, 223 (1982).
105. T. Banks, Nucl. Phys. **B303**, 172 (1988);
M. Olechowski and S. Pokorski, Phys. Lett. **B214**, 393 (1988);
S. Pokorski, Nucl. Phys. (Proc. Supp.) **B13**, 606 (1990);
B. Ananthanarayan, G. Lazarides and Q. Shafi, Phys. Rev. **D44**, 1613 (1991);
Q. Shafi and B. Ananthanarayan, ICTP Summer School lectures (1991);
S. Dimopoulos, L.J. Hall and S. Raby, Phys. Rev. Lett. **68**, 1984 (1992) and Phys. Rev. **D45**, 4192 (1992);
G. Anderson *et al.*, Phys. Rev. **D47**, 3702 (1993) [hep-ph/9209250];
B. Ananthanarayan, G. Lazarides and Q. Shafi, Phys. Lett. **B300**, 245 (1993);
G. Anderson *et al.*, Phys. Rev. **D49**, 3660 (1994) [hep-ph/9308333];
B. Ananthanarayan, Q. Shafi and X.M. Wang, Phys. Rev. **D50**, 5980 (1994) [hep-ph/9311225].
106. L.J. Hall, R. Rattazzi and U. Sarid, Phys. Rev. **D50**, 7048 (1994) [hep-ph/9306309, hep-ph/9306309];
M. Carena *et al.*, Nucl. Phys. **B426**, 269 (1994) [hep-ph/9402253].
107. A. Anandakrishnan, B.C. Bryant and S. Raby, JHEP **1505**, 088 (2015) [arXiv:1411.7035]..
108. M. Lanzagorta and G.G. Ross, Phys. Lett. **B364**, 163 (1995) [hep-ph/9507366].
109. K. Tobe and J.D. Wells, Nucl. Phys. **B663**, 123 (2003) [hep-ph/0301015].
110. T. Blazek, R. Dermisek and S. Raby, Phys. Rev. Lett. **88**, 111804 (2002) and Phys. Rev. **D65**, 115004 (2002) [hep-ph/0107097];
D. Auto, *et al.*, JHEP **0306**, 023 (2003) [hep-ph/0302155];
R. Dermisek *et al.*, JHEP **0304**, 037 (2003) and JHEP **0509**, 029 (2005) [hep-ph/0304101].
111. A. Anandakrishnan, S. Raby and A. Wingerter, Phys. Rev. **D87**, 055005 (2013) [arXiv:1212.0542];
M. Adeel Ajaib *et al.*, JHEP **1307**, 139 (2013) [arXiv:1303.6964];
Z. Poh and S. Raby, Phys. Rev. **D92**, 015017 (2015) [arXiv:1505.00264];
M. Badziak, M. Olechowski and S. Pokorski, JHEP **1310**, 088 (2013) [arXiv:1307.7999].
112. H. Georgi and C. Jarlskog, Phys. Lett. **B86**, 297 (1979).
113. S. Antusch and M. Spinrath, Phys. Rev. **D79**, 095004 (2009) [arXiv:0902.4644].
114. G. Lazarides, Q. Shafi and C. Wetterich, Nucl. Phys. **B181**, 287 (1981);

T.E. Clark, T.K. Kuo and N. Nakagawa, Phys. Lett. **B115**, 26 (1982);
K.S. Babu and R.N. Mohapatra, Phys. Rev. Lett. **70**, 2845 (1993) [hep-ph/9209215].
115. R. Barbieri and D.V. Nanopoulos, Phys. Lett. **B91**, 369 (1980).
116. R. Barbieri and A. Strumia, Nucl. Phys. **B493**, 3 (1997) [hep-ph/9704402];
T. Blazek, S. Raby and K. Tobe, Phys. Rev. **D60**, 113001 (1999) and Phys. Rev. **D62**, 055001 (2000) [hep-ph/9903340];
Q. Shafi and Z. Tavartkiladze, Phys. Lett. **B487**, 145 (2000) [hep-ph/0002150];
C.H. Albright and S.M. Barr, Phys. Rev. Lett. **85**, 244 (2000) [hep-ph/0002155];
Z. Berezhiani and A. Rossi, Nucl. Phys. **B594**, 113 (2001) [hep-ph/0003084];
C.H. Albright and S.M. Barr, Phys. Rev. **D64**, 073010 (2001) [hep-ph/0104294];
M.-C. Chen, K.T. Mahanthappa, Int. J. Mod. Phys. **A18**, 5819 (2003) [hep-ph/0305088];
R. Dermisek and S. Raby, Phys. Lett. **B622**, 327 (2005) [hep-ph/0507045].
117. H. Georgi, Nucl. Phys. **B156**, 126 (1979);
P.H. Frampton, Phys. Lett. **B88**, 299 (1979);
P. Frampton and S. Nandi, Phys. Rev. Lett. **43**, 1460 (1979);
J.E. Kim, Phys. Rev. Lett. **45**, 1916 (1980), Phys. Rev. **D23**, 2706 (1981) and Phys. Rev. **D26**, 674 (1982);
R. Barbieri and D.V. Nanopoulos, Phys. Lett. **B91**, 369 (1980);
Y. Fujimoto, Phys. Rev. **D26**, 3183 (1982).
118. P. Langacker, Phys. Reports **72**, 185 (1981).
119. H. Georgi, Conf. Proc. C **820726**, 705 (1982).
120. S.M. Barr, Phys. Rev. **D78**, 055008 (2008) [arXiv:0805.4808];
Y. Goto, Y. Kawamura and T. Miura, Phys. Rev. **D88**, 055016 (2013) [arXiv:1307.2631];
J.E. Kim, JHEP **1506**, 114 (2015) [arXiv:1503.03104];
C.H. Albright, R.P. Feger and T.W. Kephart, arXiv:1601.07523;
M. Reig, J. W. F. Valle, C. A. Vaquera-Araujo and F. Wilczek, arXiv:1706.03116.
121. L.J. Hall, V.A. Kostelecky and S. Raby, Nucl. Phys. **B267**, 415 (1986).
122. R. Barbieri and L.J. Hall, Phys. Lett. **B338**, 212 (1994) [hep-ph/9408406];
R. Barbieri, L.J. Hall and A. Strumia, Nucl. Phys. **B445**, 219 (1995) [hep-ph/9501334].
123. F. Borzumati and A. Masiero, Phys. Rev. Lett. **57**, 961 (1986);
J. Hisano *et al.*, Phys. Lett. **B357**, 579 (1995) [hep-ph/9501407];
J. Hisano *et al.*, Phys. Rev. **D53**, 2442 (1996) [hep-ph/9501407];
J. Hisano and D. Nomura, Phys. Rev. **D59**, 116005 (1999) [hep-ph/9810479].
124. T. Moroi, JHEP **0003**, 019 (2000) [hep-ph/0002208];
D. Chang, A. Masiero and H. Murayama, Phys. Rev. **D67**, 075013 (2003) [hep-ph/0205111].
125. S. Dimopoulos and L.J. Hall, Phys. Lett. **B344**, 185 (1995) [hep-ph/9411273].
126. J. Hisano *et al.*, Phys. Lett. **B604**, 216 (2004) [hep-ph/0407169].
127. G.L. Fogli *et al.*, Phys. Rev. **D84**, 053007 (2011) [arXiv:1106.6028].
128. T. Schwetz, M. Tortola, and J.W.F. Valle, New J. Phys. **13**, 109401 (2011) [arXiv:1108.1376].
129. C.H. Albright and M.-C. Chen, Phys. Rev. **D74**, 113006 (2006) [hep-ph/0608137].
130. M. Magg and C. Wetterich, Phys. Lett. **B94**, 61 (1980);
J. Schechter and J.W.F. Valle, Phys. Rev. **D22**, 2227 (1980);
G. Lazarides, Q. Shafi and C. Wetterich, Nucl. Phys. **B181**, 287 (1981);
R.N. Mohapatra and G. Senjanovic, Phys. Rev. **D23**, 165 (1981);
G.B. Gelmini and M. Roncadelli, Phys. Lett. **B99**, 411 (1981).
131. R. Foot, *et al.*, Z. Phys. **C44**, 441 (1989).
132. G. 't Hooft, Nucl. Phys. **B79**, 276 (1974) A.M. Polyakov, Pis'ma Zh. Eksp. Teor. Fiz. **20**, 430 (1974) [Sov. Phys. JETP Lett. **20**, 194 (1974)];
For a pedagogical introduction, see S. Coleman, in *Aspects of Symmetry*, Selected Erice Lectures, Cambridge University Press, Cambridge, (1985), and P. Goddard and D. Olive, Rept. on Prog. in Phys. **41**, 1357 (1978).
133. M. Ambrosio *et al.* [MACRO Collaboration], Eur. Phys. J. C **25** (2002) 511 [hep-ex/0207020];
S. Balestra *et al.* 'Magnetic Monopole Bibliography-II,' arXiv:1105.5587;
L. Patrizii and M. Spurio, Ann. Rev. Nucl. Part. Sci. **65** (2015) 279 [arXiv:1510.07125].
134. For a review, see A.D. Linde, *Particle Physics and Inflationary Cosmology*, Harwood Academic, Switzerland (1990).
135. G.R. Dvali, H. Liu and T. Vachaspati, Phys. Rev. Lett. **80**, 2281 (1998) [hep-ph/9710301].
136. P. Langacker and S.Y. Pi, Phys. Rev. Lett. **45**, 1 (1980).
137. G.R. Dvali, A. Melfo and G. Senjanovic, Phys. Rev. Lett. **75**, 4559 (1995) [hep-ph/9507230].
138. V. Rubakov, Nucl. Phys. **B203**, 311 (1982) and Institute of Nuclear Research Report No. P-0211, Moscow (1981), unpublished;
C. Callan, Phys. Rev. **D26**, 2058 (1982);
F. Wilczek, Phys. Rev. Lett. **48**, 1146 (1982);
See also, S. Dawson and A.N. Schellekens, Phys. Rev. **D27**, 2119 (1983).
139. K. Freese, M. S. Turner and D. N. Schramm, Phys. Rev. Lett. **51**, 1625 (1983).
140. P.A.R. Ade *et al.* [BICEP2 and Planck Collabs.], Phys. Rev. Lett. **114**, 101301 (2015) [arXiv:1502.00612];
P.A.R. Ade *et al.* [Planck Collab.], Astron. Astrophys. **594**, A20 (2016) [arXiv:1502.02114].
141. N.G. Deshpande, OITS-107;
C.Q. Geng and R.E. Marshak, Phys. Rev. **D39**, 693 (1989);
A. Font, L.E. Ibanez and F. Quevedo, Phys. Lett. **B228**, 79 (1989);
K.S. Babu and R.N. Mohapatra, Phys. Rev. Lett. **63**, 938 (1989).
142. R. Foot *et al.*, Phys. Rev. **D39**, 3411 (1989).
143. M. Nowakowski and A. Pilaftsis, Phys. Rev. **D48**, 259 (1993) [hep-ph/9304312].
144. T.P. T. Dijkstra, L.R. Huiszoon and A.N. Schellekens, Phys. Lett. **B609**, 408 (2005) [hep-th/0403196];
F. Gmeiner *et al.*, JHEP **0601**, 004 (2006) [hep-th/0510170];
B. Gato-Rivera and A.N. Schellekens, Nucl. Phys. **B883**, 529 (2014) [arXiv:1401.1782].
145. A.Y. Ignatiev *et al.*, Phys. Lett. **B76**, 436 (1978);
M. Yoshimura, Phys. Rev. Lett. **41**, 281 (1978) [Phys. Rev. Lett. **42**, 746 (1979)].
146. D. Toussaint *et al.*, Phys. Rev. **D19**, 1036 (1979);
S. Weinberg, Phys. Rev. Lett. **42**, 850 (1979);
M. Yoshimura, Phys. Lett. **B88**, 294 (1979);
S.M. Barr, G. Segre and H.A. Weldon, Phys. Rev. **D20**, 2494 (1979);
D.V. Nanopoulos and S. Weinberg, Phys. Rev. **D20**, 2484 (1979);
A. Yildiz and P.H. Cox, Phys. Rev. **D21**, 906 (1980).
147. M. Fukugita and T. Yanagida, Phys. Rev. Lett. **89**, 131602 (2002) [hep-ph/0203194].
148. M. Fukugita and T. Yanagida, Phys. Lett. **B174**, 45 (1986).
149. S. Davidson and A. Ibarra, Phys. Lett. **B535**, 25 (2002) [hep-ph/0202239];
K. Hamaguchi, H. Murayama and T. Yanagida, Phys. Rev. **D65**, 043512 (2002) [hep-ph/0109030].
150. M. Kawasaki *et al.*, Phys. Rev. **D78**, 065011 (2008) [arXiv:0804.3745].
151. W. Buchmuller, R.D. Peccei and T. Yanagida, Ann. Rev. Nucl. and Part. Sci. **55**, 311 (2005) [hep-ph/0502169];
C.S. Fong, E. Nardi and A. Riotto, Adv. High Energy Phys. **2012**, 158303 (2012) [arXiv:1301.3062].
152. G.G. Ross, "Grand Unified Theories", Benjamin/Cummings, 1984.;
K.R. Dienes, Phys. Reports **287**, 447 (1997) [hep-th/9602045];

P. Nath and P. Fileviez Perez, Phys. Reports **441**, 191 (2007) [hep-ph/0601023];
S. Raby, "Supersymmetric Grand Unified Theories" Lect. Notes Phys. **939** 1 (2017).
153. A. Ringwald, L.J. Rosenberg and G. Rybka, Review of 'Axions and other Very Light Bosons' in Ref. [57].
154. P. Svrcek and E. Witten, JHEP **0606** 051 (2006) [hep-th/0605206].
155. M. Dine, W. Fischler and M. Srednicki, Phys. Lett. **104B** 199 (1981);
A. R. Zhitnitsky, Sov. J. Nucl. Phys. **31** 260 (1980).

115. Leptoquarks

Updated August 2017 by S. Rolli (US Department of Energy) and M. Tanabashi (Nagoya U.)

Leptoquarks are hypothetical particles carrying both baryon number (B) and lepton number (L). The possible quantum numbers of leptoquark states can be restricted by assuming that their direct interactions with the ordinary SM fermions are dimensionless and invariant under the standard model (SM) gauge group. Table 115.1 shows the list of all possible quantum numbers with this assumption [1]. The columns of $SU(3)_C$, $SU(2)_W$, and $U(1)_Y$ in Table 115.1 indicate the QCD representation, the weak isospin representation, and the weak hypercharge, respectively. The spin of a leptoquark state is taken to be 1 (vector leptoquark) or 0 (scalar leptoquark).

Table 115.1: Possible leptoquarks and their quantum numbers.

Spin	$3B+L$	$SU(3)_c$	$SU(2)_W$	$U(1)_Y$	Allowed coupling
0	-2	$\bar{3}$	1	1/3	$\bar{q}_L^c \ell_L$ or $\bar{u}_R^c e_R$
0	-2	$\bar{3}$	1	4/3	$\bar{d}_R^c e_R$
0	-2	$\bar{3}$	3	1/3	$\bar{q}_L^c \ell_L$
1	-2	$\bar{3}$	2	5/6	$\bar{q}_L^c \gamma^\mu e_R$ or $\bar{d}_R^c \gamma^\mu \ell_L$
1	-2	$\bar{3}$	2	$-1/6$	$\bar{u}_R^c \gamma^\mu \ell_L$
0	0	3	2	7/6	$\bar{q}_L e_R$ or $\bar{u}_R \ell_L$
0	0	3	2	1/6	$\bar{d}_R \ell_L$
1	0	3	1	2/3	$\bar{q}_L \gamma^\mu \ell_L$ or $\bar{d}_R \gamma^\mu e_R$
1	0	3	1	5/3	$\bar{u}_R \gamma^\mu e_R$
1	0	3	3	2/3	$\bar{q}_L \gamma^\mu \ell_L$

If we do not require leptoquark states to couple directly with SM fermions, different assignments of quantum numbers become possible [2,3].

Leptoquark states are expected to exist in various extensions of SM. The Pati-Salam model [4] is an example predicting the existence of a leptoquark state. Leptoquark states also exist in grand unification theories based on $SU(5)$ [5], $SO(10)$ [6], which includes Pati-Salam color $SU(4)$, and larger gauge groups. Scalar quarks in supersymmetric models with R-parity violation may also have leptoquark-type Yukawa couplings. The bounds on the leptoquark states can therefore be applied to constrain R-parity-violating supersymmetric models. Scalar leptoquarks are expected to exist at TeV scale in extended technicolor models [7,8] where leptoquark states appear as the bound states of techni-fermions. Compositeness of quarks and leptons also provides examples of models which may have light leptoquark states [9].

Bounds on leptoquark states are obtained both directly and indirectly. Direct limits are from their production cross sections at colliders, while indirect limits are calculated from the bounds on the leptoquark-induced four-fermion interactions, which are obtained from low-energy experiments, or from collider experiments below threshold. These four-fermion interactions often cause lepton-flavor non-universalities in heavy quark decays. Anomalies observed recently in the R_K and R_D ratios [10,11] in the semi-leptonic B decays may be explained in models with TeV scale leptoquarks.

If a leptoquark couples to quarks (leptons) belonging to more than a single generation in the mass eigenbasis, it can induce four-fermion interactions causing flavor-changing neutral currents (lepton-family-number violations). The quantum number assignment of Table 1 allows several leptoquark states to couple to both left- and right-handed quarks simultaneously. Such leptoquark states are called non-chiral and may cause four-fermion interactions affecting the $(\pi \to e\nu)/(\pi \to \mu\nu)$ ratio [12]. Non-chiral scalar leptoquarks also contribute to the muon anomalous magnetic moment [13,14]. Since indirect limits provide more stringent constraints on these types of leptoquarks, it is often assumed that a leptoquark state couples only to a single generation of quarks and a single generation of leptons in a chiral interaction, for which indirect limits become much weaker. Additionally, this assumption gives strong constraints on concrete models of leptoquarks.

Refs. [15,16,17] give extensive lists of the bounds on the leptoquark-induced four-fermion interactions. For the isoscalar scalar and vector leptoquarks S_0 and V_0, for example, which couple with the first- (second-) generation left-handed quark, and the first-generation left-handed lepton, the bounds of Ref. 17 read $\lambda^2 < 0.07 \times (M_{\rm LQ}/1\ {\rm TeV})^2$ for S_0, and $\lambda^2 < 0.4 \times (M_{\rm LQ}/1\ {\rm TeV})^2$ for V_0 ($\lambda^2 < 0.7 \times (M_{\rm LQ}/1\ {\rm TeV})^2$ for S_0, and $\lambda^2 < 0.5 \times (M_{\rm LQ}/1\ {\rm TeV})^2$ for V_0) with λ being the leptoquark coupling strength. The e^+e^- experiments are sensitive to the indirect effects coming from t- and u-channel exchanges of leptoquarks in the $e^+e^- \to q\bar{q}$ process. The HERA experiments give bounds on the leptoquark-induced four-fermion interaction. For detailed bounds obtained in this way, see the Boson Particle Listings for "Indirect Limits for Leptoquarks" and its references.

Collider experiments provide direct limits on the leptoquark states through limits on the pair- and single-production cross sections. The leading-order cross sections of the parton processes

$$\begin{aligned} &q + \bar{q} \to LQ + \overline{LQ} \\ &g + g \to LQ + \overline{LQ} \\ &e + q \to LQ \end{aligned} \tag{115.1}$$

may be written as [18]

$$\begin{aligned} \hat{\sigma}_{\rm LO}\Big[q\bar{q} \to {\rm LQ} + \overline{\rm LQ}\Big] &= \frac{2\alpha_s^2\pi}{27\hat{s}}\beta^3, \\ \hat{\sigma}_{\rm LO}\Big[gg \to {\rm LQ} + \overline{\rm LQ}\Big] &= \frac{\alpha_s^2\pi}{96\hat{s}} \\ &\quad \times \Big[\beta(41 - 31\beta^2) + (18\beta^2 - \beta^4 - 17)\log\frac{1+\beta}{1-\beta}\Big], \\ \hat{\sigma}_{\rm LO}\Big[eq \to {\rm LQ}\Big] &= \frac{\pi\lambda^2}{4}\delta(\hat{s} - M_{\rm LQ}^2) \end{aligned} \tag{115.2}$$

for a scalar leptoquark. Here $\sqrt{\hat{s}}$ is the invariant energy of the parton subprocess, and $\beta \equiv \sqrt{1 - 4M_{\rm LQ}^2/\hat{s}}$. The leptoquark Yukawa coupling is given by λ. Leptoquarks are also produced singly at hadron colliders through $g + q \to LQ + \ell$ [19], which allows extending to higher masses the collider reach in the leptoquark search [20], depending on the leptoquark Yukawa coupling. See also Ref. [21] for a comprehensive review on the leptoquark phenomenology in precision experiments and particle colliders.

Leptoquark states which couple only to left- or right-handed quarks are called chiral leptoquarks. Leptoquark states which couple only to the first (second, third) generation are referred as the first- (second-, third-) generation leptoquarks.

The LHC, Tevatron and LEP experiments search for pair production of the leptoquark states, which arises from the leptoquark gauge interaction. The searches are carried on in signatures including high P_T leptons, E_T jets and large missing transverse energy, due to the typical decay of the leptoquark. The gauge couplings of a scalar leptoquark are determined uniquely according to its quantum numbers in Table 115.1. Since all of the leptoquark states belong to color-triplet representation, the scalar leptoquark pair-production cross section at the Tevatron and LHC can be determined solely as a function of the leptoquark mass without making further assumptions. This is in contrast to the indirect or single-production limits, which give constraints in the leptoquark mass-coupling plane.

Older results from the Tevatron run can be found here: [23], [24], [25] and [26].

Current results from the LHC proton-proton collider, running at a center of mass energies of 7, 8 TeV and 13 TeV, extend previous mass limits for scalar leptoquarks to > 1130 GeV (first generation, CMS, $\beta = 1$, $\sqrt{s} = 13$ TeV) and > 920 GeV(first generation, CMS, $\beta = 0.5$, $\sqrt{s} = 13$ TeV) [27]; > 1100 GeV (first generation, ATLAS, $\beta = 1$, $\sqrt{s} = 13$ TeV) [28] and > 900 GeV (first generation, ATLAS, $\beta = 0.5$, $\sqrt{s} = 8$ TeV - no update at 13 TeV is available at this time) [29]; > 1165 GeV (second generation, CMS, $\beta = 1$, $\sqrt{s} =$

13 TeV) [30] and > 960 GeV (second generation, CMS, $\beta = 0.5$, $\sqrt{s}$ = 13 TeV) [30]; and > 1050 GeV (second generation, ATLAS, $\beta = 1$, $\sqrt{s}$ = 13 TeV) [28] and > 850 GeV (second generation, ATLAS, β = 0.5, $\sqrt{s}$ = 8 TeV - no update at 13 TeV is available at this time) [29]. All limits at 95% C.L.

As for third generation leptoquarks, CMS results are the following (using both 8 and 13 TeV run data): 1) assuming that all leptoquarks decay to a top quark and a τ lepton, the existence of pair produced, third-generation leptoquarks up to a mass of 685 GeV (β =1, 8 TeV) is excluded at 95% confidence level [31]; 2) assuming that all leptoquarks decay to a bottom quark and a τ lepton, the existence of pair produced, third-generation leptoquarks up to a mass of 850 GeV (β =1, 13 TeV) is excluded at 95% confidence level [32]; 3)assuming that all leptoquarks decay to a bottom quark and a τ neutrino, the existence of pair produced, third-generation leptoquarks up to a mass of 450 GeV (β =0.5, 8 TeV)is excluded at 95% confidence level [33].

The ATLAS collaboration has a limit on third generation scalar leptoquark for the case of β =1 of 525 GeV [34] and 625 GeV for third-generation leptoquarks in the bottom τ neutrino channel, and 200 $< m_{LQ} <$ 640 GeV in the top τ neutrino channel [34].

It is also possible to consider leptoquark states which couple only with the i-th generation quarks and the j-th generation leptons ($i \neq j$) without causing conflicts with severe indirect constraints. See Ref. [35] for collider search strategies and present limits on the pair production cross sections of this class of leptoquark states.

The magnetic-dipole-type and the electric-quadrupole-type interactions of a vector leptoquark are not determined even if we fix its gauge quantum numbers as listed in the Table [36]. The production of vector leptoquarks depends in general on additional assumptions that the leptoquark couplings and their pair-production cross sections are enhanced relative to the scalar leptoquark contributions. The leptoquark pair-production cross sections in e^+e^- collisions depend on the leptoquark $SU(2) \times U(1)$ quantum numbers and Yukawa coupling with electron [37].

The most stringent searches for the leptoquark single production were performed by the HERA experiments. Since the leptoquark single-production cross section depends on its Yukawa coupling, the leptoquark mass limits from HERA are usually displayed in the mass-coupling plane. For leptoquark Yukawa coupling $\lambda = 0.1$, the ZEUS bounds on the first-generation leptoquarks range from 248 to 290 GeV, depending on the leptoquark species [39]. The H1 Collaboration released a comprehensive summary of searches for first generation leptoquarks using the full data sample collected in ep collisions at HERA (446 pb^{-1}). No evidence of production of leptoquarks was observed in final states with a large transverse momentum electron or large missing transverse momentum. For a coupling strength $\lambda = 0.3$, first generation leptoquarks with masses up to 800 GeV are excluded at 95% C.L. [41]. The CMS collaboration performed a search for single production of first and second geneation leptoquarks [42], which is complementary to the HERA searches in the high λ region (for coupling strenght $\lambda = 1.0$, first generation leptoquarks are excluded for masses up to 1.75 TeV).

The search for LQ will continue with more LHC data. Early feasability studies by the LHC experiments ATLAS [44] and CMS [45] indicate that clear signals can be established for masses up to about $M_{\rm LQ}$ 1.3 to 1.4 TeV for first- and second-generation scalar LQ, with a likely final reach 1.5 TeV, for collisions at 14 TeV in the center of mass.

References:

1. W. Buchmüller, R. Rückl, and D. Wyler, Phys. Lett. **B191**, 442 (1987).
2. K.S. Babu, C.F. Kolda, and J. March-Russell, Phys. Lett. **B408**, 261 (1997).
3. J.L. Hewett and T.G. Rizzo, Phys. Rev. **D58**, 055005 (1998).
4. J.C. Pati and A. Salam, Phys. Rev. **D10**, 275 (1974).
5. H. Georgi and S.L. Glashow, Phys. Rev. Lett. **32**, 438 (1974).
6. H. Georgi, AIP Conf. Proc. **23**, 575 (1975);
   H. Fritzsch and P. Minkowski, Ann. Phys. **93**, 193 (1975).
7. For a review, see, E. Farhi and L. Susskind, Phys. Reports **74**, 277 (1981).
8. K. Lane and M. Ramana, Phys. Rev. **D44**, 2678 (1991).
9. See, for example, B. Schremp and F. Schremp, Phys. Lett. **153B**, 101 (1985).
10. R. Aaij *et al.* [LHCb Collab.], Phys. Rev. Lett. **113**, 151601 (2014);
    R. Aaij *et al.* [LHCb Collab.], arXiv:1705.05802.
11. Y. Amhis *et al.*, arXiv:1612.07233.
12. O. Shanker, Nucl. Phys. **B204**, 375, (1982).
13. U. Mahanta, Eur. Phys. J. **C21**, 171 (2001) [Phys. Lett. **B515**, 111 (2001)].
14. K. Cheung, Phys. Rev. **D64**, 033001 (2001).
15. S. Davidson, D.C. Bailey, and B.A. Campbell, Z. Phys. **C61**, 613 (1994).
16. M. Leurer, Phys. Rev. **D49**, 333 (1994);
    Phys. Rev. **D50**, 536 (1994).
17. M. Carpentier and S. Davidson, Eur. Phys. J. **C70**, 1071 (2010).
18. T. Plehn *et al.*, Z. Phys. **C74**, 611 (1997);
    M. Kramer *et al.*, Phys. Rev. Lett. **79**, 341 (1997); and references therein.
19. J.L. Hewett and S. Pakvasa, Phys. Rev. **D37**, 3165 (1988);
    O.J.P. Eboli and A.V. Olinto, Phys. Rev. **D38**, 3461 (1988);
    A. Dobado, M.J. Herrero, and C. Muñoz, Phys. Lett. **207B**, 97 (1988);
    V.D. Barger *et al.*, Phys. Lett. **B220**, 464 (1989);
    M. De Montigny and L. Marleau, Phys. Rev. **D40**, 2869 (1989) [Erratum-*ibid.* **D56**, 3156 (1997)].
20. A. Belyaev *et al.*, JHEP **0509**, 005 (2005).
21. I. Doršner *et al.*, Phys. Reports **641**, 1 (2016).
22. D. Acosta *et al.* [CDF Collab.], Phys. Rev. **D72**, 051107 (2005).
23. V.M. Abazov *et al.* [DØCollab.], Phys. Lett. **B681**, 224 (2009).
24. A. Abulencia *et al.* [CDF Collab.], Phys. Rev. **D73**, 051102 (2006).
25. V.M. Abazov *et al.* [DØCollab.], Phys. Lett. **B671**, 224 (2009).
26. V.Abazov *et al.* [DØCollab.], Phys. Lett. **B693**, 95 (2010).
27. [CMS Collab.], CMS PAS EXO-16-043 (2016).
28. M. Aaboud, *et al.* [ATLAS Collab.], New J. Phys. **18**, 093016 (2016).
29. G.Aad *et al.* [ATLAS Collab.], arXiv:1508.04735v1.
30. [CMS Collab.], CMS PAS EXO-16-007 (2016).
31. V. Khachatryan *et al.* [CMS Collab.], JHEP **1507**, 042 (2015).
32. A.M. Sirunyan, *et al.* [CMS Collab.], JHEP **1707**, 121 (2017).
33. S. Chatrchyan *et al.* [CMS Collab.], JHEP **1212**, 055 (2012).
34. G. Aad *et al.* [ATLAS Collab.], Eur. Phys. J. **C76**, 5 (2016).
35. B. Diaz, M. Schmaltz, and Y. M. Zhong, arXiv:1706.05033.
36. J. Blümlein, E. Boos, and A. Kryukov, Z. Phys. **C76**, 137 (1997).
37. J. Blümlein and R. Ruckl, Phys. Lett. **B304**, 337 (1993).
38. G. Abbiendi *et al.* [OPAL Collab.], Eur. Phys. J. **C31**, 281 (2003).
39. S. Chekanov *et al.* [ZEUS Collab.], Phys. Rev. **D68**, 052004 (2003).
40. A. Aktas *et al.* [H1 Collab.], Phys. Lett. **B629**, 9 (2005).
41. F.D. Aaron *et al.* [H1 Collab.], Phys. Lett. **B704**, 388 (2011).
42. V. Khachatryan *et al.* [CMS Collab.], Phys. Rev. **D93**, 032005 (2016).
43. T. Aalton *et al.* [CDF Collab.], Phys. Rev. **D77**, 091105 (2008).
44. V.A. Mitsou *et al.*, Czech. J. Phys. **55**, B659 (2005).
45. S. Abdulin and F. Charles, Phys. Lett. **B464**, 223 (1999).

116. Magnetic Monopoles

Updated August 2017 by D. Milstead (Stockholm Univ.) and E.J. Weinberg (Columbia Univ.).

The symmetry between electric and magnetic fields in the source-free Maxwell's equations naturally suggests that electric charges might have magnetic counterparts, known as magnetic monopoles. Although the greatest interest has been in the supermassive monopoles that are a firm prediction of all grand unified theories, one cannot exclude the possibility of lighter monopoles, even though there is at present no strong theoretical motivation for these.

In either case, the magnetic charge is constrained by a quantization condition first found by Dirac [1]. Consider a monopole with magnetic charge Q_M and a Coulomb magnetic field

$$\mathbf{B} = \frac{Q_M}{4\pi}\frac{\hat{\mathbf{r}}}{r^2}\,. \tag{116.1}$$

Any vector potential $\mathbf{A}$ whose curl is equal to $\mathbf{B}$ must be singular along some line running from the origin to spatial infinity. This Dirac string singularity could potentially be detected through the extra phase that the wavefunction of a particle with electric charge Q_E would acquire if it moved along a loop encircling the string. For the string to be unobservable, this phase must be a multiple of 2π. Requiring that this be the case for any pair of electric and magnetic charges gives the condition that all charges be integer multiples of minimum charges $Q_E^{\rm min}$ and $Q_M^{\rm min}$ obeying

$$Q_E^{\rm min}Q_M^{\rm min} = 2\pi\,. \tag{116.2}$$

(For monopoles which also carry an electric charge, called dyons, the quantization conditions on their electric charges can be modified. However, the constraints on magnetic charges, as well as those on all purely electric particles, will be unchanged.)

Another way to understand this result is to note that the conserved orbital angular momentum of a point electric charge moving in the field of a magnetic monopole has an additional component, with

$$\mathbf{L} = m\mathbf{r}\times\mathbf{v} - 4\pi Q_E Q_M\hat{\mathbf{r}} \tag{116.3}$$

Requiring the radial component of $\mathbf{L}$ to be quantized in half-integer units yields Eq. (116.2).

If there are unbroken gauge symmetries in addition to the U(1) of electromagnetism, the above analysis must be modified [2,3]. For example, a monopole could have both a U(1) magnetic charge and a color magnetic charge. The latter could combine with the color charge of a quark to give an additional contribution to the phase factor associated with a loop around the Dirac string, so that the U(1) charge could be the Dirac charge $Q_M^D \equiv 2\pi/e$, the result that would be obtained by substituting the electron charge into Eq. (116.2). On the other hand, for monopoles without color-magnetic charge, one would simply insert the quark electric charges into Eq. (116.2) and conclude that Q_M must be a multiple of $6\pi/e$.

The prediction of GUT monopoles arises from the work of 't Hooft [4] and Polyakov [5], who showed that certain spontaneously broken gauge theories have nonsingular classical solutions that lead to magnetic monopoles in the quantum theory. The simplest example occurs in a theory where the vacuum expectation value of a triplet Higgs field ϕ breaks an SU(2) gauge symmetry down to the U(1) of electromagnetism and gives a mass M_V to two of the gauge bosons. In order to have finite energy, ϕ must approach a vacuum value at infinity. However, there is a continuous family of possible vacua, since the scalar field potential determines only the magnitude v of $\langle\phi\rangle$, but not its orientation in the internal SU(2) space. In the monopole solution, the direction of ϕ in internal space is correlated with the position in physical space; *i.e.*, $\phi^a \sim v\hat{r}^a$. The stability of the solution follows from the fact that this twisting Higgs field cannot be smoothly deformed to a spatially uniform vacuum configuration. Reducing the energetic cost of the spatial variation of ϕ requires a nonzero gauge potential, which turns out to yield the magnetic field corresponding to a charge $Q_M = 4\pi/e$. Numerical solution of the classical field equations shows that the mass of this monopole is

$$M_{\rm mon} \sim \frac{4\pi M_V}{e^2}\,. \tag{116.4}$$

The essential ingredient here was the fact that the Higgs fields at spatial infinity could be arranged in a topologically nontrivial configuration. A discussion of the general conditions under which this is possible is beyond the scope of this review, so we restrict ourselves to the two phenomenologically most important cases.

The first is the electroweak theory, with SU(2) × U(1) broken to U(1). There are no topologically nontrivial configurations of the Higgs field, and hence no topologically stable monopole solutions.

The second is when any simple Lie group is broken to a subgroup with a U(1) factor, a case that includes all grand unified theories. The monopole mass is determined by the mass scale of the symmetry breaking that allows nontrivial topology. For example, an SU(5) model with

$$\mathrm{SU(5)} \xrightarrow{M_X} \mathrm{SU(3)\times SU(2)\times U(1)} \xrightarrow{M_W} \mathrm{SU(3)\times U(1)} \tag{116.5}$$

has a monopole [6] with $Q_M = 2\pi/e$ and mass

$$M_{\rm mon} \sim \frac{4\pi M_{\rm X}}{g^2}\,, \tag{116.6}$$

where g is the SU(5) gauge coupling. For a unification scale of 10^{16} GeV, these monopoles would have a mass $M_{\rm mon} \sim 10^{17}$ – 10^{18} GeV.

In theories with several stages of symmetry breaking, monopoles of different mass scales can arise. In an SO(10) theory with

$$\mathrm{SO(10)} \xrightarrow{M_1} \mathrm{SU(4)\times SU(2)\times SU(2)} \xrightarrow{M_2} \mathrm{SU(3)\times SU(2)\times U(1)} \tag{116.7}$$

there is monopole with $Q_M = 2\pi/e$ and mass $\sim 4\pi M_1/g^2$ and a much lighter monopole with $Q_M = 4\pi/e$ and mass $\sim 4\pi M_2/g^2$ [7].

The central core of a GUT monopole contains the fields of the superheavy gauge bosons that mediate baryon number violation, so one might expect that baryon number conservation could be violated in baryon–monopole scattering. The surprising feature, pointed out by Callan [8] and Rubakov [9], is that these processes are not suppressed by powers of the gauge boson mass. Instead, the cross-sections for catalysis processes such as p + monopole → $e^+ + \pi^0$ + monopole are essentially geometric; *i.e.*, $\sigma_{\Delta B}\beta \sim 10^{-27}$ cm^2, where $\beta = v/c$. Note, however, that intermediate mass monopoles arising at later stages of symmetry breakings, such as the doubly charged monopoles of the SO(10) theory, do not catalyze baryon number violation.

116.1. Production and Annihilation

GUT monopoles are far too massive to be produced in any foreseeable accelerator. However, they could have been produced in the early universe as topological defects arising via the Kibble mechanism [10] in a symmetry-breaking phase transition. Estimates of the initial monopole abundance, and of the degree to which it can be reduced by monopole-antimonopole annihilation, predict a present-day monopole abundance that exceeds by many orders of magnitude the astrophysical and experimental bounds described below [11]. Cosmological inflation and other proposed solutions to this primordial monopole problem generically lead to present-day abundances exponentially smaller than could be plausibly detected, although potentially observable abundances can be obtained in scenarios with carefully tuned parameters.

If monopoles light enough to be produced at colliders exist, one would expect that these could be produced by analogs of the electromagnetic processes that produce pairs of electrically charged particles. Because of the large size of the magnetic charge, this is a strong coupling problem for which perturbation theory cannot be trusted. Indeed, the problem of obtaining reliable quantitative estimates of the production cross-sections remains an open one, on which there is no clear consensus.

116.2. Astrophysical and Cosmological Bounds

If there were no galactic magnetic field, one would expect monopoles in the galaxy to have typical velocities of the order of $10^{-3}c$, comparable to the virial velocity in the galaxy (relevant if the monopoles cluster with the galaxy) and the peculiar velocity of the galaxy with respect to the CMB rest frame (relevant if the monopoles are not bound to the galaxy). This situation is modified by the existence of a galactic magnetic field $B \sim 3\mu$G. A monopole with the Dirac charge and mass M would be accelerated by this field to a velocity

$$v_{\rm mag} \sim \begin{cases} c, & M \lesssim 10^{11}{\rm GeV}\ , \\ 10^{-3}c\left(\frac{10^{17}\,{\rm GeV}}{M}\right)^{1/2}, & M \gtrsim 10^{11}{\rm GeV}\ . \end{cases} \tag{116.8}$$

Accelerating these monopoles drains energy from the magnetic field. Parker [12] obtained an upper bound on the flux of monopoles in the galaxy by requiring that the rate of this energy loss be small compared to the time scale on which the galactic field can be regenerated. With reasonable choices for the astrophysical parameters (see Ref. 13 for details), this Parker bound is

$$F < \begin{cases} 10^{-15}\,{\rm cm}^{-2}\,{\rm sr}^{-1}\,{\rm sec}^{-1}\,, & M \lesssim 10^{17}\,{\rm GeV}\ , \\ 10^{-15}\left(\frac{M}{10^{17}\,{\rm GeV}}\right){\rm cm}^{-2}\,{\rm sr}^{-1}\,{\rm sec}^{-1}\,, & M \gtrsim 10^{17}\,{\rm GeV}\ . \end{cases} \tag{116.9}$$

Applying similar arguments to an earlier seed field that was the progenitor of the current galactic field leads to a tighter bound [14],

$$F < \left[\frac{M}{10^{17}{\rm GeV}} + (3\times 10^{-6})\right] 10^{-16}\,{\rm cm}^{-2}{\rm sr}^{-1}{\rm sec}^{-1}. \tag{116.10}$$

Considering magnetic fields in galactic clusters gives a bound [15] which, although less secure, is about three orders of magnitude lower than the Parker bound.

A flux bound can also be inferred from the total mass of monopoles in the universe. If the monopole mass density is a fraction Ω_M of the critical density, and the monopoles were uniformly distributed throughout the universe, there would be a monopole flux

$$F_{\rm uniform} = 1.3\times 10^{-16}\Omega_M \left(\frac{10^{17}\,{\rm GeV}}{M}\right)\left(\frac{v}{10^{-3}c}\right){\rm cm}^{-2}{\rm sr}^{-1}{\rm sec}^{-1}. \tag{116.11}$$

If we assume that $\Omega_M \sim 0.1$, this gives a stronger constraint than the Parker bound for $M \sim 10^{15}$ GeV. However, monopoles with masses $\sim 10^{17}$ GeV are not ejected by the galactic field and can be gravitationally bound to the galaxy. In this case their flux within the galaxy is increased by about five orders of magnitude for a given value of Ω_M, and the mass density bound only becomes stronger than the Parker bound for $M \sim 10^{18}$ GeV.

A much more stringent flux bound applies to GUT monopoles that catalyze baryon number violation. The essential idea is that compact astrophysical objects would capture monopoles at a rate proportional to the galactic flux. These monopoles would then catalyze proton decay, with the energy released in the decay leading to an observable increase in the luminosity of the object. A variety of bounds, based on neutron stars [16–20], white dwarfs [21], and Jovian planets [22] have been obtained. These depend in the obvious manner on the catalysis cross section, but also on the details of the astrophysical scenarios; *e.g.*, on how much the accumulated density is reduced by monopole-antimonopole annihilation, and on whether monopoles accumulated in the progenitor star survive its collapse to a white dwarf or neutron star. The bounds obtained in this manner lie in the range

$$F\left(\frac{\sigma_{\Delta B}\beta}{10^{-27}{\rm cm}^2}\right) \sim (10^{-18} - 10^{-29}){\rm cm}^{-2}{\rm sr}^{-1}{\rm sec}^{-1}. \tag{116.12}$$

It is important to remember that not all GUT monopoles catalyze baryon number nonconservation. In particular, the intermediate mass monopoles that arise in some GUTs at later stages of symmetry-breaking are examples of theoretically motivated monopoles that are exempt from the bound of Eq. (116.12).

116.3. Searches for Magnetic Monopoles

To date there have been no confirmed observations of exotic particles possessing magnetic charge. Precision measurements of the properties of known particles have led to tight limits on the values of magnetic charge they may possess. Using the induction method (see below), the electron's magnetic charge has been found to be $Q_e^m < 10^{-24}Q_M^D$ [23](where Q_M^D is the Dirac charge). Furthermore, measurements of the anomalous magnetic moment of the muon have been used to place a model dependent lower limit of 120 GeV on the monopole mass [1] [24]. Nevertheless, guided mainly by Dirac's argument and the predicted existence of monopoles from spontaneous symmetry breaking mechanisms, searches have been routinely made for monopoles produced at accelerators, in cosmic rays, and bound in matter [25]. Although the resultant limits from such searches are usually made under the assumption of a particle possessing only magnetic charge, most of the searches are also sensitive to dyons.

116.4. Search Techniques

Search strategies are determined by the expected interactions of monopoles as they pass through matter. These would give rise to a number of striking characteristic signatures. Since a complete description of monopole search techniques falls outside of the scope of this minireview, only the most common methods are described below. More comprehensive descriptions of search techniques can be found in Refs. [26,27].

The induction method exploits the long-ranged electromagnetic interaction of the monopole with the quantum state of a superconducting ring which would lead to a monopole which passes through such a ring inducing a permanent current. The induction technique typically uses Superconducting Quantum Interference Devices (SQUID) technology for detection and is employed for searches for monopoles in cosmic rays and matter. Another approach is to exploit the electromagnetic energy loss of monopoles. Monopoles with Dirac charge would typically lose energy at a rate which is several thousand times larger than that expected from particles possessing the elementary electric charge. Consequently, scintillators, gas chambers and nuclear track detectors (NTDs) have been used in cosmic ray and collider experiments. A further approach, which has been used at colliders, is to search for particles describing a non-helical path in a uniform magnetic field.

116.4.1. *Searches for Monopoles Bound in Matter* :

Monopoles have been sought in a range of bulk materials which it is assumed would have absorbed incident cosmic ray monopoles over a long exposure time of order million years. Materials which have been studied include moon rock, meteorites, manganese modules, and sea water [28]. A stringent upper limit on the monopoles per nucleon ratio of $\sim 10^{-29}$ has been obtained [28].

116.4.2. ***Searches in Cosmic Rays*** : Direct searches for monopoles in cosmic rays refer to those experiments in which the passage of the monopole is measured by an active detector. Searches made assuming a catalysis processes in which GUT monopoles could induce nucleon decay are discussed in the next section. To interpret the results of the non-catalysis searches, the cross section for the catalysis process is typically either set to zero [29] or assigned a modest value (1mb) [30].

Although early cosmic ray searches using the induction technique [31] and NTDs [32] observed monopole candidates, none of these apparent observations have been confirmed. Recent experiments have typically employed large scale detectors. The MACRO experiment at the Gran Sasso underground laboratory comprised three different types of detector: liquid scintillator, limited stream tubes, and NTDs, which provided a total acceptance of $\sim 10000{\rm m}^2$ for an isotropic flux. As shown in Fig. 116.1, this experiment has so far provided the most extensive β-dependent flux limits for GUT monopoles with Dirac charge [30]. Also shown are limits from an experiment at the OHYA mine in Japan [29], which used a $2000{\rm m}^2$ array of NTDs.

[1] Where no ambiguity is likely to arise, a reference to a monopole implies a particle possessing Dirac charge.

In Fig. 116.1, upper flux limits are also shown as a function of mass for monopole speed $\beta > 0.05$. In addition to MACRO and OYHA flux limits, results from the SLIM [33] high-altitude experiment are shown. The SLIM experiment provided a good sensitivity to intermediate mass monopoles ($10^5 \lesssim M \lesssim 10^{12}$ GeV). In addition to the results shown in Fig. 116.1, limits as low as $\sim 3 \times 10^{-18}$ cm^{-2}s^{-1}sr^{-1} and $\sim 10^{-17}$ cm^{-2}s^{-1}sr^{-1} were obtained for monopoles with $\beta > 0.8$ and $\beta > 0.625$ by the IceCube [34] and Antares [35] experiments, respectively. Stringent constraints on the flux of ultra-relativistic monopoles have been obtained at the Pierre Auger Observatory [36] which was sensitive to monopoles with γ values ranging from 10^9 to 10^{12}, leading to flux limits in the range $10^{-15} - 2.5 \times 10^{-21}$ cm^{-2}s^{-1}sr^{-1}. The RICE [37] and ANITA-II experiments [38] at the South Pole have also sought ultra-relativistic monopoles with γ values of $10^7 \lesssim \gamma \lesssim 10^{12}$ and $10^9 \lesssim \gamma \lesssim 10^{13}$, respectively, and which produced flux limits as low as 2.5×10^{-21} cm^{-2}s^{-1}sr^{-1}.

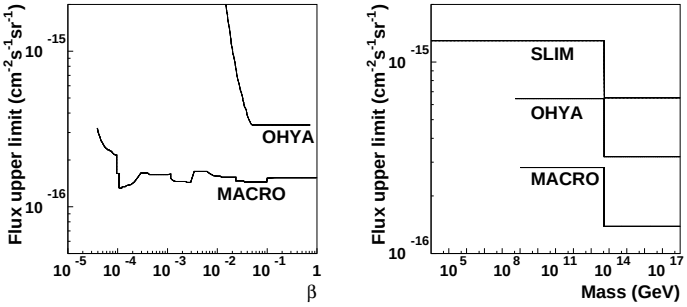

Figure 116.1: Upper flux limits for (a) GUT monopoles as a function of β (b) Monopoles as a function of mass for $\beta > 0.05$.

116.4.3. *Searches via the Catalysis of Nucleon-Decay* :

Searches have been performed for evidence of the catalysed decay of a nucleon by a monopole, as predicted by the Callan-Rubakov mechanism. The searches are thus sensitive to the assumed value of the catalysis decay cross section. Searches have been made with the Soudan [39] and Macro [40] experiments, using tracking detectors. Searches at IMB [41], the underwater Lake Baikal experiment [42] and the The IceCube experiment [43] which exploit the Cerenkov effect have also been made. The resulting β-dependent flux limits from these experiments typically vary between $\sim 10^{-18}$ and $\sim 10^{-14}$cm^{-2}sr^{-1}s^{-1}. A recent search for low energy neutrinos (assumed to be produced from induced proton decay in the sun) was made at Super-Kamiokande [44]. A model- and β-dependent of limit of $6.3 \times 10^{-24}(\frac{\beta}{10^{-3}})^2$cm^{-2}sr^{-1}s^{-1} was obtained.

116.4.4. *Searches at Colliders* :

Searches have been performed at hadron-hadron, electron-positron and lepton-hadron experiments. Collider searches can be broadly classed as being direct or indirect. In a direct search, evidence of the passage of a monopole through material, such as a charged particle track, is sought. In indirect searches, virtual monopole processes are assumed to influence the production rates of certain final states.

116.4.4.1. *Direct Searches at Colliders:*

Collider experiments typically express their results in terms of upper limits on a production cross section and/or monopole mass. To calculate these limits, ansatzes are used to model the kinematics of monopole-antimonopole pair production processes since perturbative field theory cannot be used to calculate the rate and kinematic properties of produced monopoles. Limits therefore suffer from a degree of model-dependence, implying that a comparison between the results of different experiments can be problematic, in particular when this concerns excluded mass regions. A conservative approach with as little model-dependence as possible is thus to present the upper cross-section limits as a function of one half the centre-of-mass energy of the collisions, as shown in Fig. 116.2 for recent results from high energy colliders.

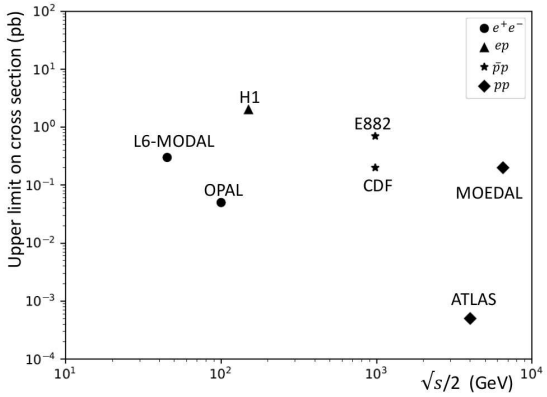

Figure 116.2: Upper limits on the production cross sections of monopoles from various collider-based experiments.

Searches for monopoles produced at the highest available energies in hadron-hadron collisions were made in pp collisions at the LHC by the ATLAS [45] and MOEDAL [46] experiments. The experiments looked for highly ionising particles leaving characteristic energy deposition profiles and stopped monopoles with the induction method, respectively. Tevatron searches have also been carried out by the CDF [47] and E882 [48] experiments. The CDF experiment used a dedicated time-of-flight system whereas the E882 experiment employed the induction technique to search for stopped monopoles in discarded detector material which had been part of the CDF and D0 detectors using periods of luminosity. Earlier searches at the Tevatron, such as [49], used NTDs and were based on comparatively modest amounts of integrated luminosity. Lower energy hadron-hadron experiments have employed a variety of search techniques including plastic track detectors [50] and searches for trapped monopoles [51].

The only LEP-2 search was made by OPAL [52] which quoted cross section limits for the production of monopoles possessing masses up to around 103 GeV. At LEP-1, searches were made with NTDs deployed around an interaction region. This allowed a range of charges to be sought for masses up to ~ 45 GeV. The L6-MODAL experiment [53] gave limits for monopoles with charges in the range $0.9Q_M^D$ and $3.6Q_M^D$, whilst an earlier search by the MODAL experiment was sensitive to monopoles with charges as low as $0.1Q_M^D$ [54]. The deployment of NTDs around the beam interaction point was also used at earlier e^+e^- colliders such as KEK [55] and PETRA [56]. Searches at e^+e^- facilities have also been made for particles following non-helical trajectories [57,58].

There has so far been one search for monopole production in lepton-hadron scattering. Using the induction method, monopoles were sought which could have stopped in the aluminium beampipe which had been used by the H1 experiment at HERA [59]. Cross section limits were set for monopoles with charges in the range $Q_M^D - 6Q_M^D$ for masses up to around 140 GeV.

116.4.4.2. *Indirect Searches at Colliders:*

It has been proposed that virtual monopoles can mediate processes which give rise to multi-photon final-states [60,61]. Photon-based searches were made by the D0 [62] and L3 [63] experiments. The D0 work led to spin-dependent lower mass limits of between 610 and 1580 GeV, while L3 reported a lower mass limit of 510 GeV. However, it should be stressed that uncertainties on the theoretical calculations which were used to derive these limits are difficult to estimate.

References:

1. P.A.M.Dirac, Proc. Royal Soc. London **A133**, 60 (1931).
2. F. Englert and P. Windey, Phys. Rev. **D14**, 2728 (1976).
3. P. Goddard, J. Nuyts, and D.I. Olive, Nucl. Phys. **B125**, 1 (1977).
4. G.'t Hooft, Nucl. Phys. **B79**, 276 (1974).

5. A.M. Polyakov, Pisma Zh. Eksp. Teor. Fiz. **20**, 194 (1974) [Pisma Zh. Eksp. Teor. Fiz. **20**, 430 (1974)].
6. C.P. Dokos and T.N. Tomaras, Phys. Rev. **D21**, 2940 (1980).
7. G. Lazarides and Q. Shafi, Phys. Lett. **B94**, 149 (1980).
8. C.G. Callan, Phys. Rev. **D26**, 2058 (1982).
9. V.A. Rubakov, Nucl. Phys. **B203**, 311 (1982).
10. T.W.B. Kibble, J. Phys. **A9**, 1387 (1976).
11. J. Preskill, Phys. Rev. Lett. **43**, 1365 (1979).
12. E.N. Parker, Astrophys. J. **160**, 383 (1970).
13. M.S. Turner, E.N. Parker, and T.J. Bogdan, Phys. Rev. **D26**, 1296 (1982).
14. F.C. Adams *et al.*, Phys. Rev. Lett. **70**, 2511 (1993).
15. Y. Rephaeli and M.S. Turner, Phys. Lett. **B121**, 115 (1983).
16. E.W. Kolb, S.A. Colgate, and J.A. Harvey, Phys. Rev. Lett. **49**, 1373 (1982).
17. S. Dimopoulos, J. Preskill, and F. Wilczek, Phys. Lett. **B119**, 320 (1982).
18. K. Freese, M.S. Turner, and D.N. Schramm, Phys. Rev. Lett. **51**, 1625 (1983).
19. E.W. Kolb and M.S. Turner, Astrophys. J. **286**, 702 (1984).
20. J.A. Harvey, Nucl. Phys. **B236**, 255 (1984).
21. K. Freese and E. Krasteva, Phys. Rev. **D59**, 063007 (1999).
22. J. Arafune, M. Fukugita, and S. Yanagita, Phys. Rev. **D32**, 2586 (1985).
23. L.L. Vant-Hull, Phys. Rev. **173**, 1412 (1968).
24. S. Graf, A. Schaefer, and W. Greiner, Phys. Lett. **B262**, 463 (1991).
25. Review of Particle Physics 2012 (*this Review*), listing on *Searches for Magnetic Monopoles*.
26. G. Giacomelli and L. Patrizii, `arXiv:hep-ex/0506014`.
27. M. Fairbairn *et al.*, Phys. Reports **438**, 1 (2007).
28. J.M. Kovalik and J.L. Kirschvink, Phys. Rev. **A33**, 1183 (1986); H. Jeon and M. J. Longo, Phys. Rev. Lett. **75**, 1443 (1995) [Erratum-ibid. **76**, 159 (1996)].
29. S. Orito *et al.*, Phys. Rev. Lett. **66**, 1951 (1991).
30. M. Ambrosio *et al.* [MACRO Collab.], Eur. Phys. J. **C25**, 511 (2002).
31. B. Cabrera, Phys. Rev. Lett. **48**, 1378 (1982).
32. P.B. Price *et al.*, Phys. Rev. Lett. **35**, 487 (1975).
33. S. Balestra *et al.*, Eur. Phys. J. **C55**, 57 (2008).
34. R. Abbasi *et al.* [IceCube Collab.], Phys. Rev. **D87**, 022001 (2013).
35. S. Adrian-Martinez *et al.* [ANTARES Collab.], Astropart. Phys. **35**, 634 (2012).
36. A. Aab *et al.* [Pierre Auger Collab.], Phys. Rev. **D98**, 082002 (2016).
37. D.P. Hogan *et al.*, Phys. Rev. **D78**, 075031 (2008).
38. M. Detrixhe *et al.*, Phys. Rev. **D83**, 023513 (2011).
39. J.E. Bartelt *et al.*, Phys. Rev. **D36**, 1990 (1987) [Erratum-ibid. **D40**, 1701 (1989)].
40. M. Ambrosio *et al.*, Eur. Phys. J. **C26**, 163 (2002).
41. R. Becker-Szendy *et al.*, Phys. Rev. **D49**, 2169 (1994).
42. V. A. Balkanov *et al.*, Prog. in Part. Nucl. Phys. **40**, 391 (1998).
43. M.G. Aartsen *et al.* [IceCube Collab.], Eur. Phys. J. **C74**, 2938 (2014).
44. K. Ueno *et al.* [Super-Kamiokande Collab.], Astropart. Phys. **36**, 131 (2012).
45. G. Aad *et al.* [ATLAS Collab.], Phys. Rev. **D93**, 052009 (2016).
46. B. Acharya *et al.*[MoEDAL Collab.], Phys. Rev. Lett. **118**, 061801 (2017).
47. A. Abulencia *et al.* [CDF Collab.], Phys. Rev. Lett. **96**, 201801 (2006).
48. G.R. Kalbfleisch *et al.*, Phys. Rev. **D69**, 052002 (2004).
49. P.B. Price, G.X. Ren, and K. Kinoshita, Phys. Rev. Lett. **59**, 2523 (1987).
50. B. Aubert *et al.*, Phys. Lett. **B120**, 465 (1983).
51. R.A. Carrigan, F.A. Nezrick, and B.P. Strauss, Phys. Rev. **D8**, 3717 (1973).
52. G. Abbiendi *et al.* [OPAL Collab.], Phys. Lett. **B663**, 37 (2008).
53. J.L. Pinfold *et al.*, Phys. Lett. **B316**, 407 (1993).
54. K. Kinoshita *et al.*, Phys. Rev. **D46**, 881 (1992).
55. K. Kinoshita *et al.*, Phys. Lett. **B228**, 543 (1989).
56. P. Musset *et al.*, Phys. Lett. **B128**, 333 (1983).
57. T. Gentile *et al.* [Cleo Collab.], Phys. Rev. **D35**, 1081 (1987).
58. W. Braunschweig *et al.* [TASSO Collab.], Z. Phys. **C38**, 543 (1988).
59. A. Aktas *et al.* [H1 Collab.], Eur. Phys. J. **C41**, 133 (2005).
60. A. De Rujula, Nucl. Phys. **B435**, 257 (1995).
61. I.F. Ginzburg and A. Schiller, Phys. Rev. **D60**, 075016 (1999).
62. B. Abbott *et al.* [D0 Collab.], Phys. Rev. Lett. **81**, 524 (1998).
63. M. Acciarri *et al.* [L3 Collab.], Phys. Lett. **B345**, 609 (1995).

INDEX

Greek letters are alphabetized by their English-language spelling. Bold page numbers signify entries in the Particle Properties Summary Tables.

Greek letters are alphabetized by their English-language spelling. Bold page numbers signify entries in the Particle Properties Summary Tables.

Greek letters are alphabetized by their English-language spelling. Bold page numbers signify entries in the Particle Properties Summary Tables.

Greek letters are alphabetized by their English-language spelling. Bold page numbers signify entries in the Particle Properties Summary Tables.

Greek letters are alphabetized by their English-language spelling. Bold page numbers signify entries in the Particle Properties Summary Tables.

Greek letters are alphabetized by their English-language spelling. Bold page numbers signify entries in the Particle Properties Summary Tables.

Greek letters are alphabetized by their English-language spelling. Bold page numbers signify entries in the Particle Properties Summary Tables.

Greek letters are alphabetized by their English-language spelling. Bold page numbers signify entries in the Particle Properties Summary Tables.

Greek letters are alphabetized by their English-language spelling. Bold page numbers signify entries in the Particle Properties Summary Tables.

Greek letters are alphabetized by their English-language spelling. Bold page numbers signify entries in the Particle Properties Summary Tables.

Greek letters are alphabetized by their English-language spelling. Bold page numbers signify entries in the Particle Properties Summary Tables.

VOLUME II: TABLE OF CONTENTS

PARTICLE LISTINGS*

*The divider sheets give more detailed indices for each main section of the Particle Listings.

INTRODUCTION TO THE PARTICLE LISTINGS

Illustrative Key to the Particle Listings

Name of particle. "Old" name used before 1986 renaming scheme also given if different. See the section "Naming Scheme for Hadrons" for details.

$a_0(1200)$

$I^G(J^{PC}) = 1^-(0^{++})$ — Particle quantum numbers (where known).

OMITTED FROM SUMMARY TABLE — Indicates particle omitted from Particle Physics Summary Table, implying particle's existence is not confirmed.

Evidence not compelling, may be a kinematic effect.

Quantity tabulated below.

$a_0(1200)$ MASS

General comments on particle.

VALUE (MeV)	EVTS	DOCUMENT ID		TECN	CHG	COMMENT
1206± 7 OUR AVERAGE						
1210± 8±9	3000	FENNER	87	MMS	−	3.5 $\pi^- p$
1198±10		PIERCE	83	ASPK	+	2.1 $K^- p$
1216±11±9	1500	[1] MERRILL	81	HBC	0	3.2 $K^- p$
• • • We do not use the following data for averages, fits, limits, etc. • • •						
1192±16	200	LYNCH	81	HBC	±	2.7 $\pi^- p$

Top line gives our best value (and error) of quantity tabulated here, based on weighted average of measurements used. Could also be from fit, best limit, estimate, or other evaluation. See next page for details.

"Document id" for this result; full reference given below.

Footnote number linking measurement to text of footnote.

[1] Systematic error was added quadratically by us in our 1986 edition.

Measurement technique. (See abbreviations on next page.)

$a_0(1200)$ WIDTH

Number of events *above background*.

VALUE (MeV)	EVTS	DOCUMENT ID		TECN	CHG	COMMENT
41±11 OUR AVERAGE Error includes scale factor of 1.8. See the ideogram below.						
50± 8		PIERCE	83	ASPK	+	2.1 $K^- p$
70^{+30}_{-20}	200	LYNCH	81	HBC	±	2.7 $\pi^- p$
25± 5±7		MERRILL	81	HBC	0	3.2 $K^- p$
• • • We do not use the following data for averages, fits, limits, etc. • • •						
<60		FENNER	87	MMS	−	3.5 $\pi^- p$

Measured value used in averages, fits, limits, etc.

Scale factor > 1 indicates possibly inconsistent data.

Reaction producing particle, or general comments.

Error in measured value (often statistical only; followed by systematic if separately known; the two are combined in quadrature for averaging and fitting.)

"Change bar" indicates result added or changed since previous edition.

Measured value *not used* in averages, fits, limits, etc. See the Introductory Text for explanations.

Charge(s) of particle(s) detected.

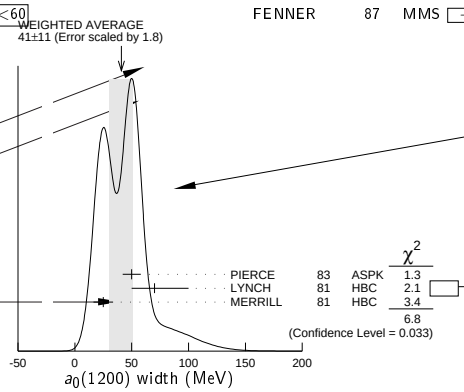

Ideogram to display possibly inconsistent data. Curve is sum of Gaussians, one for each experiment (area of Gaussian = 1/error; width of Gaussian = ±error). See Introductory Text for discussion.

Arrow points to weighted average.

Shaded pattern extends $\pm 1\sigma$ (scaled by "scale factor" S) from weighted average.

Value and error for each experiment.

Contribution of experiment to χ^2 (if no entry present, experiment not used in calculating χ^2 or scale factor because of very large error).

$a_0(1200)$ DECAY MODES

Mode	Fraction (Γ_i/Γ)	Scale factor/ Confidence level
Γ_1 3π	(65.2±1.3) %	S=1.7
Γ_2 $K\overline{K}$	(34.8±1.3) %	S=1.7
Γ_3 $\eta\pi^\pm$	< 5 $\times 10^{-4}$	CL=95%

Partial decay mode (labeled by Γ_i).

Our best value for branching fraction as determined from data averaging, fitting, evaluating, limit selection, etc. This list is basically a compact summary of results in the Branching Ratio section below.

$a_0(1200)$ BRANCHING RATIOS

Branching ratio.

$\Gamma(3\pi)/\Gamma_{total}$ — Γ_1/Γ

VALUE	DOCUMENT ID		TECN	CHG	COMMENT
0.652±0.013 OUR FIT Error includes scale factor of 1.7.					
0.643±0.010 OUR AVERAGE					
0.64 ±0.01	PIERCE	83	ASPK	+	2.1 $K^- p$
0.74 ±0.06	MERRILL	81	HBC	0	3.2 $K^- p$
• • • We do not use the following data for averages, fits, limits, etc. • • •					
0.48 ±0.15	[2] LYNCH	81	HBC	±	2.7 $\pi^- p$

Our best value (and error) of quantity tabulated, as determined from constrained fit (using *all significant* measured branching ratios for this particle).

Weighted average of measurements of this ratio only.

[2] Data has questionable background subtraction.

Footnote (referring to LYNCH 81).

$\Gamma(K\overline{K})/\Gamma_{total}$ — Γ_2/Γ

Branching ratio in terms of partial decay mode(s) Γ_i above.

VALUE	DOCUMENT ID		TECN	CHG	COMMENT
0.348±0.013 OUR FIT Error includes scale factor of 1.7.					
0.35 ±0.05	PIERCE	83	ASPK	+	2.1 $K^- p$

$\Gamma(K\overline{K})/\Gamma(3\pi)$ — Γ_2/Γ_1

VALUE	DOCUMENT ID		TECN	CHG	COMMENT
0.535±0.030 OUR FIT Error includes scale factor of 1.7.					
0.50 ±0.03	MERRILL	81	HBC	0	3.2 $K^- p$

$\Gamma(\eta(\text{neutral decay})\pi^\pm)/\Gamma_{total}$ — $0.71\Gamma_3/\Gamma$

VALUE (units 10^{-4})	CL%	DOCUMENT ID		TECN	CHG	COMMENT
<3.5	95	PIERCE	83	ASPK	+	2.1 $K^- p$

Confidence level for measured upper limit.

$a_0(1200)$ REFERENCES

References, ordered inversely by year, then author.

FENNER	87	PRL 55 14	H. Fenner *et al.*	(SLAC)
PIERCE	83	PL 123B 230	J.H. Pierce	(FNAL) UP
LYNCH	81	PR D24 610	G.R. Lynch *et al.*	(CLEO Collab.)
MERRILL	81	PRL 47 143	D.W. Merrill *et al.*	(SACL, CERN)

"Document id" used on data entries above.

Partial list of author(s) in addition to first author.

Quantum number determinations in this reference.

Journal, report, preprint, etc. (See abbreviations on next page.)

Institution(s) of author(s). (See abbreviations on next page.)

Abbreviations Used in the Particle Listings

Indicator of Procedure Used to Obtain Our Result

OUR AVERAGE	From a weighted average of selected data.
OUR FIT	From a constrained or overdetermined multiparameter fit of selected data.
OUR EVALUATION	Not from a direct measurement, but evaluated from measurements of other quantities.
OUR ESTIMATE	Based on the observed range of the data. Not from a formal statistical procedure.
OUR LIMIT	For special cases where the limit is evaluated by us from measured ratios or other data. Not from a direct measurement.

Measurement Techniques (i.e., Detectors and Methods of Analysis)

A1	A1 Collaboration at MAMI
A2MM	A2 spectrometer at the Mainz Microtron, MAMI
ACCM	ACCMOR Collaboration
ADMX	Axion Dark Matter Experiment
AEMS	Argonne effective mass spectrometer
ALEP	ALEPH – CERN LEP detector
ALPS	Photon regeneration experiment
AMND	AMANDA South Pole neutrino detector
AMY	AMY detector at KEK-TRISTAN
ANIT	Antarctic Impulsive Transient Antenna balloon mission
ANTR	ANTARES underwater neutrino telescope in the Western Mediterranean Sea
APEX	FNAL APEX Collab.
ARG	ARGUS detector at DORIS
ARGD	Fit to semicircular amplitude path on Argand diagram
ASP	Anomalous single-photon detector
ASPK	Automatic spark chambers
ASTE	ASTERIX detector at LEAR
ASTR	Astronomy
ATLS	ATLAS detector at CERN LHC
AUGE	Pierre Auger Observatory
AURG	Resonant-mass gravitational wave AURIGA detector
B787	BNL experiment 787 detector
B791	BNL experiment 791 detector
B845	BNL experiment 845 detector
B852	BNL E-852
B865	BNL E865 detector
B871	BNL experiment 871 detector
B949	BNL E949 detector at AGS
BABR	BaBar Collab.
BAIK	Lake Baikal neutrino telescope
BAKS	Baksan underground scintillation telescope
BC	Bubble chamber
BDMP	Beam dump
BEAT	CERN BEATRICE Collab.
BEBC	Big European bubble chamber at CERN
BELL	Belle Collab.
BES	BES Beijing Spectrometer at Beijing Electron-Positron Collider
BES2	BES Beijing Spectrometer at Beijing Electron-Positron Collider
BES3	BES Beijing Spectrometer at Beijing Electron-Positron Collider
BIS2	BIS-2 spectrometer at Serpukhov
BKEI	BENKEI spectrometer system at KEK Proton Synchroton
BOLO	Bolometer, a cryogenic thermal detector
BONA	Bonanza nonmagnetic detector at DORIS
BORX	BOREXINO
BPWA	Barrelet-zero partial-wave analysis
CALO	Calorimeter
CAST	CAST experiment at CERN
CBAL	Crystal Ball detector at SLAC-SPEAR or DORIS
CBAR	Crystal Barrel detector at CERN-LEAR
CBOX	Crystal Box at LAMPF
CBTP	CBELSA/TAPS Collaboration
CC	Cloud chamber
CCFR	Columbia-Chicago-Fermilab-Rochester detector
CDEX	China Dark Matter Experiment
CDF	Collider detector at Fermilab
CDF2	CDF-II Collab.
CDHS	CDHS neutrino detector at CERN
CDM2	CDMS II, Cryogenic Dark Matter Search at Soudan Underground Lab.
CDMS	CDMS Collaboration
CELL	CELLO detector at DESY
CGNT	CoGeNT dark matter search experiment
CHER	Cherenkov detector
CHM2	CHARM-II neutrino detector (glass) at CERN
CHOZ	Nuclear Power Station near Chooz, France
CHRM	CHARM neutrino detector (marble) at CERN
CHRS	CHORUS Collaboration – CERNS SPS
CIB	Cosmic Infrared Background
CIBS	CERN-IHEP boson spectrometer
CLAS	Jefferson CLAS Collab.
CLE2	CLEO II detector at CESR
CLE3	CLEO III detector at CESR
CLEC	CLEO-c detector at CESR
CLEO	Cornell magnetic detector at CESR
CMB	Cosmic Microwave Background
CMD	Cryogenic magnetic detector at VEPP-2M, Novosibirsk
CMD2	Cryogenic magnetic detector 2 at VEPP-2M, Novosibirsk
CMD3	Cryogenic magnetic detector 3 at VEPP-2000, Novosibirsk
CMS	CMS detector at CERN LHC
CNTR	Counters
COMB	Combined analysis of data from independent experiments.
COMP	COMPASS experiment at the CERN SPS
COSM	Cosmology and astrophysics
COSY	COSY-TOF Collaboration
COUP	COUPP (the Chicagoland Observatory for Underground Particle Physics) Collab.
CPLR	CPLEAR Collaboration
CRBT	Crystal Ball and TAPS detector at MAMI
CRES	CRESST cryogenic detector
CRYB	Crystal Ball at BNL
CRYM	Crystal Ball detector at Mainz Microtron MAMI
CSB2	Columbia U. - Stony Brook BGO calorimeter inserted in NaI array
CSME	COSME Collaboration
CUOR	CUORICINO experiment at Gran Sasso Laboratory.
CUSB	Columbia U. - Stony Brook segmented NaI detector at CESR
D0	D0 detector at Fermilab Tevatron Collider
DAMA	DAMA, dark matter detector at Gran Sasso National Lab.
DASP	DESY double-arm spectrometer
DAYA	Daya Bay Collaboration
DBC	Deuterium bubble chamber
DCHZ	Double Chooz Collaboration
DISP	Graviton mass measurement based on dispersion measure
DLCO	DELCO detector at SLAC-SPEAR or SLAC-PEP
DLPH	DELPHI detector at LEP
DM1	Magnetic detector no. 1 at Orsay DCI collider
DM2	Magnetic detector no. 2 at Orsay DCI collider
DMIC	DAMIC Dark Matter in CCD experiment at Fermilab
DMTP	Dark Matter Time Projection Chamber (DMTPC) directional detection experiment
DONU	DONUT Collab.
DPWA	Energy-dependent partial-wave analysis
DRFT	Directional dark matter detector at Boulby Underground Science Facility
DS50	DarkSide-50 Liquid Argon TPC at Gran Sasso National Laboratory
E621	Fermilab E621 detector
E653	Fermilab E653 detector
E665	Fermilab E665 detector
E687	Fermilab E687 detector
E691	Fermilab E691 detector
E705	Fermilab E705 Spectrometer-Calorimeter
E731	Fermilab E731 Spectrometer-Calorimeter
E756	Fermilab E756 detector
E760	Fermilab E760 detector
E761	Fermilab E761 detector
E771	Fermilab E771 detector
E773	Fermilab E773 Spectrometer-Calorimeter
E789	Fermilab E789 detector
E791	Fermilab E791 detector
E799	Fermilab E799 Spectrometer-Calorimeter
E835	Fermilab E835 detector
EDE2	EDELWEISS II dark matter search Collaboration
EDE3	EDELWEISS III dark matter search Collaboration
EDEL	EDELWEISS dark matter search Collaboration
EHS	Four-pi detector at CERN
ELEC	Electronic combination
EMC	European muon collaboration detector at CERN
EMUL	Emulsions
ESR	Electron spin resonance spectroscopy
FAST	Fiber Active Scintillator Target detector at PSI
FBC	Freon bubble chamber

Abbreviations Used in the Particle Listings

FENI FENICE (at the ADONE collider of Frascati)
FIT Fit to previously existing data
FLAT Large Area Telescope onboard the Fermi Gamma-Ray Space Telescope (Fermi-LAT)
FMPS Fermilab Multiparticle Spectrometer
FOCS FNAL E831 FOCUS Collab.
FRAB ADONE $B\overline{B}$ group detector
FRAG ADONE $\gamma\gamma$ group detector
FRAM ADONE MEA group detector
FREJ FREJUS Collaboration – modular flash chamber detector (calorimeter)
GA24 Hodoscope Cherenkov γ calorimeter (IHEP GAMS-2000) (CERN GAMS-4000)
GALX GALLEX solar neutrino detector in the Gran Sasso Underground Lab.
GAM2 IHEP hodoscope Cherenkov γ calorimeter GAMS-2000
GAM4 CERN hodoscope Cherenkov γ calorimeter GAMS-4000
GAMS IHEP hodoscope Cherenkov γ calorimeter GAMS-4π
GNO Gallium Neutrino Observatory in the Gran Sasso Underground Lab.
GOLI CERN Goliath spectrometer
GRAL GRAAL Collaboration
H1 H1 detector at DESY/HERA
HBC Hydrogen bubble chamber
HDBC Hydrogen and deuterium bubble chambers
HDES HADES Collaboration at GSI in Darmstadt
HDMO Heidelberg-Moscow Experiment
HDMS Heidelberg Dark Matter Search Experiment
HEBC Helium bubble chamber
HEPT Helium proportional tubes
HERA H1 and ZEUS Collaborations at DESY/HERA
HERB HERA-B detector at DESY/HERA
HERM HERMES detector at DESY/HERA
HESS High Energy Stereoscopic System gamma-ray instrument
HFS Hyperfine structure
HLBC Heavy-liquid bubble chamber
HOME Homestake underground scintillation detector
HPGE High-purity Germanium detector
HPW Harvard-Pennsylvania-Wisconsin detector
HRS SLAC high-resolution spectrometer
HYBR Hybrid: bubble chamber + electronics
HYCP HyperCP Collab. (FNAL E-871)
IACT Imaging Air Cherenkov Telescope
ICAR ICARUS experiment at Gran Sasso Laboratory.
ICCB IceCube neutrino detector at South Pole
IGEX IGEX Collab.
IMB Irvine-Michigan-Brookhaven underground Cherenkov detector
IMB3 Irvine-Michigan-Brookhaven underground Cherenkov detector
INDU Magnetic induction
IPWA Energy-independent partial-wave analysis
ISTR IHEP ISTRA+ spectrometer-calorimeter
JADE JADE detector at DESY
K246 KEK E246 detector with polarimeter
K2K KEK to Super-Kamiokande
K391 KEK E391a detector
K470 KEK-E470 Stopping K detector
KAM2 KAMIOKANDE-II underground Cherenkov detector
KAMI KAMIOKANDE underground Cherenkov detector
KAR2 KARMEN2 calorimeter at the ISIS neutron spallation source at Rutherford
KARM KARMEN calorimeter at the ISIS neutron spallation source at Rutherford
KEDR detector operating at VEPP-4M collider (Novosibirsk)
KIMS Korea Invisible Mass Search experiment at YangYang, Korea
KLND KamLand Collab. (Japan)
KLOE KLOE detector at DAFNE (the Frascati e+e- collider Italy)
KOLR Kolar Gold Field underground detector
KOTO KOTO experiment with K_L^0 beam at J-PARC
KTEV KTeV Collaboration
L3 L3 detector at LEP
LASR Laser
LASS Large-angle superconducting solenoid spectrometer at SLAC
LATT Lattice calculations
LEBC Little European bubble chamber at CERN
LEGS BNL LEGS Collab.
LENA Nonmagnetic lead-glass NaI detector at DORIS
LEP From combination of all 4 LEP experiments: ALEPH, DELPHI, L3, OPAL
LEPS Low-Energy Pion Spectrometer at the Paul Scherrer Institute
LGW Lead Glass Wall collaboration at SPEAR/SLAC
LHC Combined analysis of LHC experiments
LHCB LHCb detector at CERN LHC
L+P Multichannel L + P model fit
LSD Mont Blanc liquid scintillator detector
LSND Liquid Scintillator Neutrino Detector
LSW Light Shining through a Wall
LUX Large Underground Xenon experiment at SURF
MAC MAC detector at PEP/SLAC
MBNE Fermilab MiniBooNE neutrino experiment
MBR Molecular beam resonance technique
MCRO MACRO detector in Gran Sasso
MD1 Magnetic detector at VEPP-4, Novosibirsk
MDRP Millikan drop measurement
MEG Muon to electron conversion detector at PSI
MGFL MAGIC and Fermi-LAT Collaborations
MGIC MAGIC Telescopes gamma-ray observatory.
MICA Underground mica deposits
MINS Fermilab MINOS experiment
MIRA MIRABELLE Liquid-hydrogen bubble chamber
MLEV Magnetic levitation
MLS Modified Laurent Series
MMS Missing mass spectrometer
MOED MoEDAL magnetic monopoles search experiment at LHC
MPS Multiparticle spectrometer at BNL
MPS2 Multiparticle spectrometer upgrade at BNL
MPSF Multiparticle spectrometer at Fermilab
MPWA Model-dependent partial-wave analysis
MRK1 SLAC Mark-I detector
MRK2 SLAC Mark-II detector
MRK3 SLAC Mark-III detector
MRKJ Mark-J detector at DESY
MRS Magnetic resonance spectrometer
MUG2 MUON(g-2)
MWPC Multi-Wire Proportional Chamber
NA14 CERN NA14
NA31 CERN NA31 Spectrometer-Calorimeter
NA32 CERN NA32 Spectrometer
NA48 CERN NA48 Collaboration
NA49 CERN NA49 Collaboration
NA60 CERN NA60 Collaboration
NA62 CERN NA62 Experiment
NA64 CERN SPS NA64 Experiment
NAGE NEWAGE, New generation WIMP-search experiment with advanced gaseous tracking
NAIA NAIAD (NaI Advanced Detector) dark matter search experiment
ND NaI detector at VEPP-2M, Novosibirsk
NEOS NEOS Collaboration
NICE Serpukhov nonmagnetic precision spectrometer
NMR Nuclear magnetic resonance
NOMD NOMAD Collaboration, CERN SPS
NOVA NOvA experiment with Fermilabs NuMI neutrino beam
NTEV NuTeV Collab. at Fermilab
nTRV neutron Time-Reversal Violation
NUSX Mont Blanc NUSEX underground detector
OBLX OBELIX detector at LEAR
OLYA Detector at VEPP-2M and VEPP-4, Novosibirsk
OMEG CERN OMEGA spectrometer
OPAL OPAL detector at LEP
OPER OPERA experiment with emulsion tracking at Gran Sasso
OSPK Optical spark chamber
PIBE The PIBETA detector at the Paul Scherrer Institute (PSI), Switzerland.
PICA PICASSO dark matter search experiment
PICO PICO bubble chamber experiment in SNOLAB underground laboratory
PIE3 πE3 beam-line of Paul Scherrer Institute
PLAS Plastic detector
PLUT DESY PLUTO detector
PMLA PAMELA space spectrometer on Resurs-DK1 satellite
PNDX PandaX dual-phase liquid xenon dark matter experiment at Jin-Ping
PRMX The PRIMEX detector in Hall B at TJNAF
PWA Partial-wave analysis
RDK2 NIST rare radioactive decay experiment

REDE Resonance depolarization
RENO RENO Collaboration
RICE Radio Ice Cherenkov Experiment
RVUE Review of previous data
SAGE US - Russian Gallium Experiment
SCDM SuperCDMS experiment at Soudan Underground Lab.
SELX FNAL SELEX Collab.
SFM CERN split-field magnet
SHF SLAC Hybrid Facility Photon Collaboration
SIGM Serpukhov CERN-IHEP magnetic spectrometer (SIGMA)
SILI Silicon detector
SIMP SIMPLE, dark matter detector at Laboratori Nazionali del Sud
SKAM Super-Kamiokande Collab.
SLAX Solar Axion Experiment in Canfranc Underground Laboratory
SLD SLC Large Detector for $e^+ e^-$ colliding beams at SLAC
SMPL SIMPLE, Superheated Instrument for Massive ParticLe Experiments
SND Novosibirisk Spherical neutral detector at VEPP-2M
SNDR SINDRUM spectrometer at PSI
SNO SNO Collaboration (Sudbury Neutrino Observatory)
SOU2 Soudan 2 underground detector
SOUD Soudan underground detector
SPEC Spectrometer
SPED From maximum of speed plot or resonant amplitude
SPHR Bonn SAPHIR Collab.
SPNX SPHINX spectrometer at IHEP accelerator
SPRK Spark chamber
SQID SQUID device
STRC Streamer chamber
SVD2 SVD-2 experiment at IHEP, Protvino
T2K T2K Collaboration
TASS DESY TASSO detector
TEVA Combined analysis of CDF and DØ experiments
TEXO TEXONO Collab., ultra low energy Ge detector at Kuo-Sheng Laboratory
THEO Theoretical or heavily model-dependent result
TNF TNF-IHEP facility at 70 GeV IHEP accelerator
TOF Time-of-flight
TOPZ TOPAZ detector at KEK-TRISTAN
TPC TPC detector at PEP/SLAC
TPS Tagged photon spectrometer at Fermilab
TRAP Penning trap
TWST TWIST spectrometer at TRIUMF
UA1 UA1 detector at CERN
UA2 UA2 detector at CERN
UA5 UA5 detector at CERN
UCNA UCNA collaboration using polarizeed ultracold neutrons at LANSCE
UKDM UK Dark Matter Collab.
VES Vertex Spectrometer Facility at 70 GeV IHEP accelerator
VLBI Very Long Baseline Interferometer
VNS VENUS detector at KEK-TRISTAN
VRTS Very Energetic Radiation Imaging Telescope Array System (VERITAS)
WA75 CERN WA75 experiment
WA82 CERN WA82 experiment
WA89 CERN WA89 experiment
WARP Liquid argon detector for CDM searches at Gran Sasso
WASA WASA detector at CELSIUS, Uppsala and at COSY, Juelich
WIRE Wire chamber
X100 XENON100 dark matter search experiment at Gran Sasso National Laboratory
XE10 XENON10 experiment at Gran Sasso National Laboratory
XE1T XENON1T dark matter search experiment at Gran Sasso National Laboratory
XEBC Xenon bubble chamber
XMAS XMASS, liquid xenon scintillation detector at Kamioka Observatory
YUKA Graviton mass measurement based on Yukawa potential
ZEP2 ZEPLIN-II dark matter detector
ZEP3 ZEPLIN-III dark matter detector at Palmer Underground Lab.
ZEPL ZEPLIN-I galactic dark matter detector
ZEUS ZEUS detector at DESY/HERA

Conferences

Conferences are generally referred to by the location at which they were held (e.g., HAMBURG, TORONTO, CORNELL, BRIGHTON, etc.).

Journals

AA Astronomy and Astrophysics
ADVP Advances in Physics
AFIS Anales de Fisica
AJP American Journal of Physics
AL Astronomy Letters
ANP Annals of Physics
ANPL Annals of Physics (Leipzig)
ANYAS Annals of the New York Academy of Sciences
AP Atomic Physics
APAH Acta Physica Academiae Scientiarum Hungaricae
APJ Astrophysical Journal
APJS Astrophysical Journal Suppl.
APP Acta Physica Polonica
APS Acta Physica Slovaca
ARNPS Annual Review of Nuclear and Particle Science
ARNS Annual Review of Nuclear Science
ASP Astroparticle Physics
AST American Statistician
BAPS Bulletin of the American Physical Society
BASUP Bulletin of the Academy of Science, USSR (Physics)
CJNP Chinese Journal of Nuclear Physics
CJP Canadian Journal of Physics
CNPP Comments on Nuclear and Particle Physics
CP Chinese Physics
CPC Chinese Physics C
CTP Communications in Theoretical Physics
CZJP Czechoslovak Journal of Physics
DANS Doklady Akademii nauk SSSR
DP Doklady Physics (Magazine)
EPJ The European Physical Journal
EPL Europhysics Letters
FECAY Fizika Elementarnykh Chastits i Atomnogo Yadra
HADJ Hadronic Journal
IJMP International Journal of Modern Physics
JAP Journal of Applied Physics
JCAP Journal of Cosmology and Astroparticle Physics
JETP English Translation of Soviet Physics ZETF
JETPL English Translation of Soviet Physics ZETF Letters
JHEP Journal of High Energy Physics
JINR Joint Inst. for Nuclear Research
JINRRC JINR Rapid Communications
JP Journal of Physics
JPA Journal of Physics, A
JPB Journal of Physics, B
JPCRD Journal of Physical and Chemical Reference Data
JPCS Journal of Physics: Conference Series
JPG Journal of Physics, G
JPSJ Journal of the Physical Society of Japan
LNC Lettere Nuovo Cimento
MNRAS Monthly Notices of the Royal Astronomical Society
MPL Modern Physics Letters
NAST New Astronomy
NAT Nature
NATC Nature Communications (NCAOBW)
NATP Nature Physics
NC Nuovo Cimento
NIM Nuclear Instruments and Methods
NJP New Journal of Physics
NP Nuclear Physics
NPBPS Nuclear Physics B Proceedings Supplement
NPPP Nuclear and Particle Physics Proceedings
PAN Physics of Atomic Nuclei (formerly SJNP)
PD Physics Doklady (Magazine)
PDAT Physik Daten
PL Physics Letters
PN Particles and Nuclei
PPCF Plasma Physics and Controlled Fusion
PPN Physics of Particles and Nuclei (formerly SJPN)
PPNL Physics of Particles and Nuclei Letters
PPNP Progress in Particles and Nuclear Physics
PPSL Proc. of the Physical Society of London
PR Physical Review
PRAM Pramana
PRL Physical Review Letters
PRPL Physics Reports (Physics Letters C)

PRSE	Proc. of the Royal Society of Edinburgh
PRSL	Proc. of the Royal Society of London, Section A
PS	Physica Scripta
PTEP	Progress of Theoretical and Experimental Physics
PTP	Progress of Theoretical Physics
PTPS	Progress of Theoretical Physics Supplement
PTRSL	Phil. Trans. Royal Society of London
RA	Radiochimica Acta
RMP	Reviews of Modern Physics
RNC	La Rivista del Nuovo Cimento
RPP	Reports on Progress in Physics
RRP	Revue Roumaine de Physique
SCI	Science
SJNP	Soviet Journal of Nuclear Physics
SJPN	Soviet Journal of Particles and Nuclei
SPD	Soviet Physics Doklady (Magazine)
SPU	Soviet Physics - Uspekhi
UFN	Usp. Fiz. Nauk – Russian version of SPU
YAF	Yadernaya Fizika
ZETF	Zhurnal Eksperimental'noi i Teoreticheskoi Fiziki
ZETFP	Zhurnal Eksperimental'noi i Teoreticheskoi Fiziki, Pis'ma v Redakts
ZNAT	Zeitschrift fur Naturforschung
ZPHY	Zeitschrift fur Physik

Institutions

AACH	Phys. Inst. der Techn. Hochschule **Aachen** (Historical, use for general Inst. der Techn. Hochschule)	Aachen, Germany
AACH1	I Phys. Inst. B, RWTH **Aachen**	Aachen, Germany
AACH3	III Phys. Inst. A, RWTH **Aachen** Univ.	Aachen, Germany
AACHT	Inst. für Theoretische Teilchenphysik & Kosmologie, RWTH **Aachen**	Aachen, Germany
AARH	Univ. of **Aarhus**	Aarhus C, Denmark
ABO	**Åbo** Akademi Univ.	Turku, Finland
ADEL	**Adelphi** Univ.	Garden City, NY, USA
ADLD	The Univ. of **Adelaide**	Adelaide, SA, Australia
AERE	Atomic Energy Research Estab.	Didcot, United Kingdom
AFRR	**Armed Forces** Radiobiology Res. Inst.	Bethesda, MD, USA
AHMED	Physical Research Lab.	**Ahmedabad**, Gujarat, India
AICH	**Aichi** Univ. of Education	Aichi, Japan
AKIT	**Akita** Univ.	Akita, Japan
ALAH	Univ. of **Alabama (Huntsville)**	Huntsville, AL, USA
ALAT	Univ. of **Alabama (Tuscaloosa)**	Tuscaloosa, AL, USA
ALBA	**SUNY at Albany**	Albany, NY, USA
ALBE	Univ. of **Alberta**	Edmonton, AB, Canada
AMES	**Ames Lab.**	Ames, IA, USA
AMHT	**Amherst** College	Amherst, MA, USA
AMST	Univ. van **Amsterdam**	GL Amsterdam, The Netherlands
ANIK	**NIKHEF**	**Amsterdam**, The Netherlands
ANKA	**Middle East** Technical Univ.; Dept. of Physics; Experimental HEP Lab	Ankara, Turkey
ANL	**Argonne** National Lab.; High Energy Physics Division, Bldg. 362; Physics Division, Bldg. 203	Argonne, IL, USA
ANSM	**St. Anselm** Coll.	Manchester, NH, USA
ARCBO	**Arecibo** Observatory	Arecibo, PR, USA
ARIZ	Univ. of **Arizona**	Tucson, AZ, USA
ARZS	**Arizona State** Univ.	Tempe, AZ, USA
ASCI	Russian Academy of Sciences	**Moscow**, Russian Federation
AST	**Academia Sinica**	Nankang, Taipei, Taiwan
ATEN	NCSR **"Demokritos"**	**Aghia** Paraskevi , Greece
ATHU	Univ. of **Athens**	Athens, Greece
AUCK	Univ. of **Auckland**	Auckland, New Zealand
BAKU	**Natl. Azerbaijan Academy of Sciences**, Inst. of Physics	**Baku**, Azerbaijan
BANG	Indian Inst. of Science	**Bangalore**, India
BANGB	**Bangabasi** College	Calcutta, India
BARC	Univ. Autónoma de **Barcelona**	Bellaterra (Barcelona), Spain
BARI	Univ. e del Politecnico di **Bari**	Bari, Italy
BART	Univ. of **Delaware**; **Bartol** Research Inst.	Newark, DE, USA
BASL	Inst. für Physik der Univ. **Basel**	Basel, Switzerland
BAYR	Univ. **Bayreuth**	Bayreuth, Germany
BCEN	Centre d'Etudes Nucleaires de **Bordeaux-Gradignan**	Gradignan, France
BCIP	Natl. Inst. for Physics & Nuclear Eng. "Horia Hulubei" **(IFIN-HH)**	**Bucharest**-Magurele, Romania
BEIJ	**Beijing** Univ.	Beijing, China
BEIJT	**Inst. of Theoretical Physics**	**Beijing**, China
BELG	Inter-University Inst. for High Energies (ULB-VUB)	**Brussel**, Belgium
BELL	AT & T **Bell** Labs	Murray Hill, NJ, USA
BERG	Univ. of **Bergen**	Bergen, Norway
BERL	**DESY**, Deutsches Elektronen-Synchrotron	**Zeuthen**, Germany
BERN	Univ. of **Berne**	Berne, Switzerland
BGNA	Univ. di **Bologna**, & **INFN**, Sezione di Bologna; Via Irnerio, 46, I-40126 Bologna; Viale C. Berti Pichat, n. 6/2	Bologna, Italy
BHAB	**Bhabha Atomic** Research Center	Trombay, Bombay, India
BHEP	**Inst. of High Energy Physics**	**Beijing**, China
BIEL	Univ. **Bielefeld**	Bielefeld, Germany
BING	**SUNY at Binghamton**	Binghamton, NY, USA
BIRK	**Birkbeck** College, Univ. of London	London, United Kingdom
BIRM	Univ. of **Birmingham**	Edgbaston, Birmingham, United Kingdom
BLSU	**Bloomsburg** Univ.	Bloomsburg, PA, USA
BNL	**Brookhaven National Lab.**	Upton, NY, USA
BOCH	**Ruhr** Univ. **Bochum**	Bochum, Germany
BOHR	**Niels Bohr Inst.**	Copenhagen Ø, Denmark
BOIS	**Boise** State Univ.	Boise, ID, USA
BOMB	Univ. of **Bombay**	Bombay, India
BONN	**Univ. of Bonn**	Bonn, Germany
BORD	Centre d'Etudes Nucléaires de **Bordeaux** Gradignan **(CENBG)**	Gradignan, France
BOSE	S.N. **Bose** National Centre for Basis Sciences	Calcutta, India
BOSK	**"Rudjer Bošković"** Inst.	Zagreb, Croatia
BOST	**Boston** Univ.	Boston, MA, USA
BRAN	**Brandeis** Univ.	Waltham, MA, USA
BRCO	Univ. of **British Columbia**	Vancouver, BC, Canada
BRIS	Univ. of **Bristol**	Bristol, United Kingdom
BROW	**Brown** Univ.	Providence, RI, USA
BRUN	**Brunel** Univ.	Uxbridge, Middlesex, United Kingdom
BRUX	Univ. Libre de **Bruxelles**; Physique des Particules Elémentaires	Bruxelles, Belgium
BRUXT	Univ. Libre de **Bruxelles**; Physique Théorique	Bruxelles, Belgium
BUCH	Univ. of **Bucharest**	Bucharest-Magurele, Romania
BUDA	**Wigner** Research Centre for Physics	**Budapest**, Hungary
BUFF	**SUNY at Buffalo**	Buffalo, NY, USA
BURE	Inst. des Hautes Etudes Scientifiques	**Bures-sur-Yvette**, France
CAEN	Lab. de Physique Corpusculaire, **ENSICAEN**	**Caen**, France
CAGL	Univ. degli Studi di **Cagliari**	Monserrato (CA), Italy
CAIR	**Cairo** University	Orman, Giza, Cairo, Egypt
CAIW	**Carnegie Inst.** of Washington	Washington, DC, USA
CALB	Univ. della **Calabria**	Cosenza, Italy
CALC	Univ. of **Calcutta**	Calcutta, India
CAMB	**DAMTP**	Cambridge, United Kingdom

Abbreviations Used in the Particle Listings

CAMP	Univ. Estadual de **Campinas** (UNICAMP)	**Campinas**, SP, Brasil
CANB	**Australian National Univ.**	Canberra, ACT, Australia
CANTB	Inst. de Física de Cantabria (CSIC–Univ. **Cantabria**)	Santander, Spain
CAPE	University of **Cape Town**	Rondebosch, Cape Town, South Africa
CARA	Univ. Central de **Venezuela**	Caracas, Venezuela
CARL	**Carleton** Univ.	Ottawa, ON, Canada
CARLC	**Carleton** College	Northfield, MN, USA
CASE	**Case** Western Reserve Univ.	Cleveland, OH, USA
CAST	**China** Center of Advanced Science and Technology	Beijing, China
CATA	Univ. di **Catania**	Catania, Italy
CATH	**Catholic** Univ. of America	Washington, DC, USA
CAVE	**Cavendish** Lab.	Cambridge, United Kingdom
CBNM	CBNM	**Geel**, Belgium
CBPF	Centro Brasileiro de Pesquisas Físicas – **BIB/CDI/CBPF**	**Rio de Janeiro**, RJ, Brasil
CCAC	**Allegheny** College	Meadville, PA, USA
CDEF	**Univ. Paris VII, Denis Diderot**	Paris, France
CEA	Cambridge Electron Accelerator (Historical in *Review*)	**Cambridge, MA**, USA
CEADE	Center for Apl. Studies for Nuclear Physics	Havana, Cuba
CEBAF	**Jefferson Lab—Thomas Jefferson National Accelerator Facility**	**Newport News**, VA, USA
CENG	Centre d'Etudes Nucleaires	**Grenoble**, France
CERN	**CERN**, European Organization for Nuclear Research	Genève, Switzerland
CFPA	Univ. of **California, (Berkeley)**	Berkeley, CA, USA
CHIC	Univ. of **Chicago**	Chicago, IL, USA
CIAE	**State Nuclear Power Research Inst.**	**Beijing**, China
CINC	Univ. of **Cincinnati**	Cincinnati, OH, USA
CINV	**CINVESTAV-IPN** Centro de Investigacion y de Estudios Avanzados del IPN	**México**, DF, Mexico
CIT	**California Inst. of Tech.**	Pasadena, CA, USA
CLER	Univ. de **Clermont-Ferrand**	Aubière, France
CLEV	**Cleveland** State Univ.	Cleveland, OH, USA
CMNS	**Comenius** Univ. (FMFI UK)	**Bratislava**, Slovakia
CMU	**Carnegie Mellon** Univ.	Pittsburgh, PA, USA
CNEA	**Comisión Nacional de Energía Atómica**	Buenos Aires, Argentina
CNRC	Centre for Research in Particle Physics	Ottawa, ON, Canada
COIM	Univ. de Coimbra	**Coimbra**, Portugal
COLO	Univ. of **Colorado**	Boulder, CO, USA
COLU	**Columbia** Univ.	New York, NY, USA
CONC	**Concordia** University	Montreal, PQ, Canada
CORN	**Cornell** Univ.	Ithaca, NY, USA
COSU	**Colorado State** Univ.	Fort Collins, CO, USA
CPPM	Centre National de la Recherche Scientifique, Luminy	**Marseille**, France
CRAC	Henryk Niewodnicza'nski Inst. of Nuclear Physics	**Kraków**, Poland
CRNL	**Chalk River** Labs.	Chalk River, ON, Canada
CSOK	**Oklahoma** Central State Univ.	Edmond, OK, USA
CST	Univ. of **Science and Technology** of China	**Hefei**, Anhui 230026, China
CSULB	**California** State Univ.	Long Beach, CA, USA
CSUS	**California** State Univ.	Sacramento, CA, USA
CUNY	**City College** of **New York**	New York, NY, USA
CURCP	**Univ. Pierre et Marie Curie** (Paris VI), LCP	Paris, France
CURIN	**Univ. Pierre et Marie Curie** (Paris VI), LPNHE	Paris, France
CURIT	**Univ. Pierre et Marie Curie** (Paris VI), LPTHE	Paris, France
DALH	**Dalhousie** Univ.	Halifax, NS, Canada
DALI	**Dalian** Univ. of Tech.	Dalian, China
DARE	**Daresbury** Lab	Cheshire, United Kingdom
DARM	Tech. Hochschule **Darmstadt**	Darmstadt, Germany
DELA	Univ. of **Delaware**; Dept. of Physics & Astronomy	Newark, DE, USA
DELH	Univ. of **Delhi**	Delhi, India
DESY	**DESY**, Deutsches Elektronen-Synchrotron	**Hamburg**, Germany
DFAB	Escuela de Ingenieros	**Bilbao**, Spain
DOE	**Department of Energy**	Washington, DC, USA
DORT	Technische Univ. **Dortmund**	Dortmund, Germany
DUKE	**Duke** Univ.	Durham, NC, USA
DURH	Univ. of **Durham**	Durham , United Kingdom
DUUC	**University College** Dublin	Dublin, Ireland
EDIN	Univ. of **Edinburgh**	Edinburgh, United Kingdom
EFI	Univ. of Chicago, **The Enrico Fermi Inst.**	**Chicago**, IL, USA
ELMT	**Elmhurst** College	Elmhurst, IL, USA
ENSP	**l'Ecole Normale Supérieure**	**Paris**, France
EOTV	**Eötvös** University	Budapest, Hungary
EPOL	**École Polytechnique**	**Palaiseau**, France
ERLA	Univ. **Erlangen-Nurnberg**	Erlangen, Germany
ETH	**Univ. Zürich**	Zürich, Switzerland
FERR	Univ. di **Ferrara**	Ferrara, Italy
FIRZ	Univ. degli Studi di **Firenze**	Sesto Fiorentino, Italy
FISK	**Fisk** Univ.	Nashville, TN, USA
FLOR	Univ. of **Florida**	Gainesville, FL, USA
FNAL	**Fermilab**	Batavia, IL, USA
FOM	**FOM**, Stichting voor Fundamenteel Onderzoek der Materie	JP **Utrecht**, The Netherlands
FRAN	**Frankfurt Inst. for Advanced Studies (FIAS)**	Frankfurt am Main, Germany
FRAS	Lab. Nazionali di **Frascati** dell'**INFN**	Frascati (Roma), Italy
FREIB	**Albert-Ludwigs** Univ.	**Freiburg**, Germany
FREIE	**Freie Univ. Berlin**	Berlin, Germany
FRIB	Univ. de **Fribourg**	Fribourg, Switzerland
FSU	**Florida State** Univ.; High Energy Physics	Tallahassee, FL, USA
FSUSC	**Florida State** Univ.; SCS (School of Computational Science)	Tallahassee, FL, USA
FUKI	**Fukui** Univ.	Fukui, Japan
FUKU	**Fukushima** Univ.	Fukushima, Japan
GENO	Univ. di **Genova**	Genova, Italy
GEOR	**E. Andronikashvili Inst. of Physics**	Tbilisi, Republic of Georgia
GESC	**General Electric** Co.	Schenectady, NY, USA
GEVA	Univ. de **Genève**	Genève, Switzerland
GIES	Univ. **Giessen**	Giessen, Germany
GIFU	**Gifu** Univ.	Gifu, Japan
GLAS	Univ. of **Glasgow**	Glasgow, United Kingdom
GMAS	**George Mason** Univ.	Fairfax, VA, USA
GOET	Univ. **Göttingen**	Göttingen, Germany
GRAN	Univ. de **Granada**	Granada, Spain
GRAZ	Univ. **Graz**	Graz, Austria
GRON	Univ. of **Groningen**	Groningen, The Netherlands
GSCO	**Geological Survey of Canada**	Ottawa, ON, Canada
GSI	GSI Helmholtzzentrum für Schwerionenforschung GmbH	**Darmstadt**, Germany
GUAN	Univ. de **Guanajuato**	León, Gto., Mexico
GUEL	Univ. of **Guelph**	Guelph, ON, Canada
GWU	**George Washington** Univ.	Washington, DC, USA
HAHN	**Hahn-Meitner** Inst. Berlin GmbH	Berlin, Germany
HAIF	**Technion** – Israel Inst. of Tech.	Technion, Haifa, Israel
HAMB	Univ. **Hamburg**	Hamburg, Germany
HANN	Univ. **Hannover**	Hannover, Germany
HARC	**Houston Advanced Research Ctr.**	The Woodlands, TX, USA
HARV	**Harvard** Univ.	Cambridge, MA, USA
HARV	**Harvard** Univ. (LPPC)	Cambridge, MA, USA
HAWA	Univ. of **Hawai'i**	Honolulu, HI, USA
HEBR	**Hebrew** Univ.	Jerusalem, Israel
HEID	Univ. **Heidelberg**; (unspecified division) (Historical in *Review*)	Heidelberg, Germany

Abbreviations Used in the Particle Listings

HEIDH	Ruprecht-Karls Univ. **Heidelberg**	Heidelberg, Germany
HEIDP	Univ. **Heidelberg**; Physics Inst.	Heidelberg, Germany
HEIDT	Ruprecht-Karls-Univ. **Heidelberg**	Heidelberg, Germany
HELS	Univ. of **Helsinki**	University of Helsinki, Finland
HIRO	**Hiroshima** Univ.	Higashi-Hiroshima, Japan
HOUS	Univ. of **Houston**	Houston, TX, USA
HPC	**Hewlett-Packard** Corp.	Cupertino, CA, USA
HSCA	**Harvard-Smithsonian** Center for Astrophysics	Cambridge, MA, USA
IAS	**Inst. for Advanced Study**	Princeton, NJ, USA
IASD	**Dublin** Inst. for Advanced Studies	Dublin, Ireland
IBAR	**Ibaraki** Univ.	Ibaraki, Japan
IBM	**IBM** Corp.	Palo Alto, CA, USA
IBMY	**IBM**	Yorktown Heights, NY, USA
IBS	Inst. for **Boson Studies**	Pasadena, CA, USA
ICEPP	The Univ. of **Tokyo**	Tokyo, Japan
ICRR	Univ. of **Tokyo**	Chiba, Japan
ICTP	**Abdus Salam** International Centre for Theoretical Physics	**Trieste**, Italy
IFIC	**IFIC** (Instituto de Física Corpuscular)	**Paterna (Valencia)**, Spain
IFRJ	Univ. Federal do **Rio de Janeiro**	Rio de Janeiro, RJ, Brasil
IIT	**Illinois Inst. of Tech.**	Chicago, IL, USA
ILL	Univ. of **Illinois at Urbana-Champaign**	Urbana, IL, USA
ILLC	Univ. of **Illinois at Chicago**	Chicago, IL, USA
ILLG	Inst. **Laue-Langevin**	Grenoble, France
IND	**Indiana** Univ.	Bloomington, IN, USA
INEL	E G and G **Idaho**, Inc.	Idaho Falls, ID, USA
INFN	Ist. Nazionale di Fisica Nuclear (Generic INFN, unknown location)	Various places, Italy
INNS	Univ. of **Innsbruck**	**Innsbruck**, Austria
INPK	Henryk Niewodniczański Inst. of Nuclear Physics	**Kraków**, Poland
INRM	**INR**, Inst. for Nucl. Research	**Moscow**, Russian Federation
INUS	**KEK**, High Energy Accelerator Research Organization	Tokyo, Japan
IOAN	Univ. of **Ioannina**	Ioannina, Greece
IOFF	A.F. **Ioffe** Phys. Tech. Inst.	St. **Petersburg**, Russian Federation
IOWA	Univ. of **Iowa**	Iowa City, IA, USA
IPN	**IPN**, Inst. de Phys. Nucl.	**Orsay**, France
IPNP	Univ. Pierre et Marie Curie (**Paris** VI)	Paris, France
IRAD	Inst. du Radium (Historical)	**Paris**, France
ISNG	Lab. de Physique Subatomique et de Cosmologie **(LPSC)**	**Grenoble**, France
ISU	**Iowa State** Univ.	Ames, IA, USA
ISUT	Isfahan University of Technology	Isfahan, Iran
ITEP	**ITEP**, Inst. of Theor. and Exp. Physics	**Moscow**, Russian Federation
ITHA	**Ithaca** College	Ithaca, NY, USA
IUPU	**Indiana** Univ., **Purdue** Univ. **Indianapolis**	Indianapolis, IN, USA
JADA	**Jadavpur** Univ.	Calcutta, India
JAGL	**Jagiellonian** Univ.	Kraków, Poland
JHU	**Johns Hopkins** Univ.	Baltimore, MD, USA
JINR	**JINR**, Joint Inst. for Nucl. Research	**Dubna**, Russian Federation
JULI	Forschungszentrum **Jülich**	Jülich, Germany
JYV	Univ. of **Jyväskylä**	Jyväskylä, Finland
KAGO	Univ. of **Kagoshima**	Kagoshima-shi, Japan
KAIST	**Korea** Advanced Inst. of Science and Technology	Yusung ku, Daejon, Republic of Korea
KANS	Univ. of **Kansas**	Lawrence, KS, USA
KARL	Univ. **Karlsruhe** (Historical in *Review*)	Karlsruhe, Germany
KARLE	**Karlsruhe** Inst. of Technology (KIT); Inst. for Experimental Nuclear Physics	Karlsruhe, Germany
KARLK	**Karlsruhe** Inst. of Technology (KIT)	Eggenstein-Leopoldshafen, Germany
KARLT	**Karlsruhe** Inst. of Technology (KIT); Inst. for Theoretical Physics	Karlsruhe, Germany
KAZA	**Kazakh** Inst. of High Energy Physics	Alma Ata, Kazakhstan
KEK	**KEK**, High Energy Accelerator Research Organization	Ibaraki-ken, Japan
KENT	Univ. of **Kent**	Canterbury, United Kingdom
KEYN	**Open** Univ.	Milton Keynes, United Kingdom
KFTI	**Kharkov** Inst. of Physics and Tech. (NSC KIPT)	Kharkov, Ukraine
KIAE	**Kurchatov** Inst.	**Moscow**, Russian Federation
KIAM	**Keldysh** Inst. of Applied Math., Acad. Sci., Russia	Moscow, Russian Federation
KIDR	**Vinča Inst. of Nuclear Sciences**	Belgrade, Serbia
KIEV	**Institute for Nuclear Research**	**Kyiv**, Ukraine
KINK	**Kinki** Univ.	Osaka, Japan
KNTY	Univ. of **Kentucky**	Lexington, KY, USA
KOBE	**Kobe** Univ.	Kobe, Japan
KOMAB	Univ. of **Tokyo, Komaba**	Tokyo, Japan
KONAN	**Konan** Univ.	Kobe, Japan
KOSI	Inst. of Experimental Physics SAS	**Košice**, Slovakia
KYOT	**Kyoto** Univ.; Dept. of Physics, Graduate School of Science	Kyoto, Japan
KYOTU	**Kyoto** Univ.; **Yukawa** Inst. for Theor. Physics	Kyoto, Japan
KYUN	**Kyungpook** National Univ.	Daegu, Republic of Korea
KYUSH	**Kyushu** Univ.; Elementary ParticleTheory Group; Exp. Particle Physics Group; Research Center for Advanced Particle Physics	Fukuoka, Japan
LALO	**LAL**, Laboratoire de l'Accélérateur Linéaire	**Orsay**, France
LANC	**Lancaster** Univ.	Lancaster, United Kingdom
LANL	**Los Alamos National Lab.** (LANL)	Los Alamos, NM, USA
LAPL	Univ. Nacional de **La Plata**	La Plata, Argentina
LAPP	**LAPP**, Lab. d'Annecy-le-Vieux de Phys. des Particules	**Annecy-le-Vieux**, France
LASL	U.C. **Los Alamos Scientific** Lab. (Old name for LANL)	Los Alamos, NM, USA
LATV	**Latvian** State Univ.	Riga, Latvia
LAUS	EPFL **Lausanne**	Lausanne, Switzerland
LAVL	Univ. **Laval**	Quebec, QC, Canada
LBL	**Lawrence Berkeley National Lab.**	Berkeley, CA, USA
LCGT	Univ. di **Torino**	Turin, Italy
LEBD	**Lebedev** Physical Inst.	**Moscow**, Russian Federation
LECE	Univ. di **Lecce**	Lecce, Italy
LEED	Univ. of **Leeds**	Leeds, United Kingdom
LEGN	Lab. Naz. di Legnaro	**Legnaro**, Italy
LEHI	**Lehigh** Univ.	Bethlehem, PA, USA
LEHM	**Lehman** College of CUNY	Bronx, NY, USA
LEID	Univ. **Leiden**	Leiden, The Netherlands
LEMO	**Le Moyne** Coll.	Syracuse, NY, USA
LEUV	Katholieke Univ. **Leuven**	Leuven, Belgium
LIEG	Univ. de **Liège**	Liège, Belgium
LINZ	Univ. **Linz**	Linz, Austria
LISB	Inst. Nacional de Investigacion Cientifica	**Lisboa** CODEX, Portugal
LISBT	Centro de Física Teórica de Partículas **(CFTP)**	**Lisboa**, Portugal
LIVP	Univ. of **Liverpool**	Liverpool, United Kingdom
LLL	**Lawrence Livermore Lab.** (Old name for LLNL)	Livermore, CA, USA
LLNL	**Lawrence Livermore National Lab.**	Livermore, CA, USA
LOCK	**Lockheed** Palo Alto Res. Lab	Palo Alto, CA, USA
LOIC	**Imperial** College of Science Tech. & Medicine	London, United Kingdom

LOQM	Queen Mary, **Univ. of London**	London, United Kingdom
LOUC	**University College** London	London, United Kingdom
LOUV	Univ. Catholique de **Louvain**	Louvain-la-Neuve, Belgium
LOWC	**Westfield** College (Historical, see LOQM (Queen Mary and Westfield joined))	London, United Kingdom
LRL	U.C. Lawrence Radiation Lab. (Old name for LBL)	**Berkeley**, CA, USA
LSU	**Louisiana** State Univ.	Baton Rouge, LA, USA
LUND	**Fysiska Institutionen**	**Lund**, Sweden
LUND	**Lund** Univ.	Lund, Sweden
LYON	Institute de Physique Nucléaire de **Lyon** (IPN)	Villeurbanne, France
MADE	**UAM/CSIC**, Inst. de Física Teórica	**Madrid**, Cantoblanco, Spain
MADR	**C.I.E.M.A.T**	**Madrid**, Spain
MADRA	Univ. of **Madras**	Madras, India
MADU	Univ. Autónoma de **Madrid**	Cantoblanco, Madrid, Spain
MANI	Univ. of **Manitoba**	Winnipeg, MB, Canada
MANZ	**Johannes-Gutenberg-Univ.**; Inst. für Kernphysik, J.-J.-Becher-Weg 45; Inst. für Physik, Staudingerweg 7	**Mainz**, Germany
MARB	Univ. **Marburg**	Marburg, Germany
MARS	Centre de Physique des Particules de **Marseille**	Marseille, France
MASA	Univ. of **Massachusetts** Amherst	**Amherst**, MA, USA
MASB	Univ. of **Massachusetts** Boston	**Boston**, MA, USA
MASD	Univ. of **Massachusetts** Dartmouth	North **Dartmouth**, MA, USA
MCGI	**McGill** Univ.	Montreal, QC, Canada
MCHS	Univ. of **Manchester**	Manchester, United Kingdom
MCMS	**McMaster** Univ.	Hamilton, ON, Canada
MEHTA	**Harish-Chandra** Research Inst.	Allahabad, India
MEIS	**Meisei** Univ.	Tokyo, Japan
MELB	Univ. of **Melbourne**	Victoria, Australia
MEUD	Observatoire de **Meudon**	Meudon, France
MICH	Univ. of **Michigan**	Ann Arbor, MI, USA
MILA	Univ. di **Milano**	Milano, Italy
MILAI	**INFN**, Sez. di **Milano**	Milano, Italy
MINN	Univ. of **Minnesota**	Minneapolis, MN, USA
MIPT	Moscow Institute of Physics and Technology	Moscow, Russian Federation
MISS	Univ. of **Mississippi**	University, MS, USA
MISSR	Univ. of **Missouri**	Rolla, MO, USA
MIT	**MIT Massachusetts Inst. of Technology**	Cambridge, MA, USA
MIU	**Maharishi** International Univ.	Fairfield, IA, USA
MIYA	**Miyazaki** Univ.	Miyazaki-shi, Japan
MONP	Univ. de **Montpellier** II	Montpellier, France
MONS	Univ. of **Mons**	**Mons**, Belgium
MONT	Univ. de **Montréal**; Pavillon René-J.-A.-Lévesque	Montréal, PQ, Canada
MONTC	Univ. de **Montréal**; Centre de recherches mathématiques	Montréal, PQ, Canada
MOSU	**Skobeltsyn** Inst. of Nuclear Physics, Lomonosov Moscow State Univ.; Experimental HEP Division; Theoretical HEP Division	**Moscow**, Russian Federation
MPCM	Max Planck Inst. fur Chemie	**Mainz**, Germany
MPEI	**Moscow Physical Engineering** Inst.	Moscow, Russian Federation
MPIG	**Max-Planck**-Institute für Astrophysik	Garching, Germany
MPIH	**Max-Planck-Inst.** für Kernphysik	**Heidelberg**, Germany
MPIM	**Max-Planck-Inst.** für Physik	**München**, Germany
MSST	Mississippi State University	Mississippi State, MS, USA
MSU	**Michigan State** Univ.	East Lansing, MI, USA
MTHO	**Mount Holyoke** College	South Hadley, MA, USA
MULH	Centre Univ. du **Haut-Rhin**	Mulhouse, France
MUNI	**Ludwig-Maximilians-Univ. München**	Garching, Germany
MUNT	Tech. Univ. **München**	Garching, Germany
MURA	**Midwestern** Univ. Research Assoc. (Historical in *Review*)	Stroughton, WI, USA
MURC	Univ. of Murcia	Murcia, Spain
NAAS	North Americal Aviation Science Center (Historical in *Review*)	Thousand Oaks, CA, USA
NAGO	**Nagoya** Univ.	Nagoya, Japan
NANJ	**Nanjing** Univ.	Nanjing, China
NAPL	Univ. di **Napoli** "Federico II"	Napoli, Italy
NASA	**NASA**	Greenbelt, MD, USA
NBS	U.S **National Bureau of Standards** (Old name for NIST)	Gaithersburg, MD, USA
NBSB	**National Inst. Standards Tech.**	Boulder, CO, USA
NCAR	**National Center for Atmospheric Research**	Boulder, CO, USA
NCSU	**North Carolina** State Univ.	**Raleigh**, NC, USA
NDAM	Univ. of **Notre Dame**	Notre Dame, IN, USA
NEAS	**Northeastern** Univ.	Boston, MA, USA
NEBR	Univ. of **Nebraska**	Lincoln, NE, USA
NEUC	Univ. de **Neuchâtel**	Neuchâtel, Switzerland
NICEA	Univ. de **Nice**	Nice, France
NICEO	Observatoire de **Nice**	Nice, France
NIHO	**Nihon** Univ.	Tokyo, Japan
NIIG	**Niigata** Univ.	Niigata, Japan
NIJM	**Radboud** Univ. Nijmegen	AJ **Nijmegen**, The Netherlands
NIRS	Nat. Inst. Radiological Sciences	**Chiba**, Japan
NIST	**National Institute of Standards & Technology**	Gaithersburg, MD, USA
NIU	**Northern Illinois** Univ.	De Kalb, IL, USA
NMSU	**New Mexico** State Univ.; Dept. of Physics, MSC 3D; Part. & Nucl. Phys. Group, Box 30001/Dept.	Las Cruces, NM, USA
NORD	**Nordita**	Stockholm, Sweden
NOTT	Univ. of **Nottingham**	Nottingham, United Kingdom
NOVM	Inst. of Mathematics	**Novosibirsk**, Russian Federation
NOVO	BINP, **Budker** Inst. of Nuclear Physics	**Novosibirsk**, Russian Federation
NPOL	Polytechnic of **North London**	London, United Kingdom
NRL	**Naval Research** Lab	Washington, DC, USA
NSF	**National Science Foundation**	Arlington, VA, USA
NTHU	**National Tsing Hua** Univ.	Hsinchu, Taiwan
NTUA	**National Tech. Univ. of Athens**	Athens, Greece
NWES	**Northwestern** Univ.	Evanston, IL, USA
NYU	**New York** Univ.	New York, NY, USA
OBER	**Oberlin** College	Oberlin, OH, USA
OCH	**Ochanomizu** Univ.	Tokyo, Japan
OHIO	**Ohio** Univ.	Athens, OH, USA
OKAY	**Okayama** Univ.	Okayama, Japan
OKLA	Univ. of **Oklahoma**	Norman, OK, USA
OKSU	**Oklahoma State** Univ.	Stillwater, OK, USA
OREG	Univ. of **Oregon**; Inst. of Theoretical Science; U.O. Center for High Energy Physics	Eugene, OR, USA
ORNL	**Oak Ridge** National Laboratory	Oak Ridge, TN, USA
ORSAY	Univ. de **Paris Sud** 11	**Orsay** CEDEX, France
ORST	**Oregon State** Univ.	Corvallis, OR, USA
OSAK	**Osaka** Univ.	Osaka, Japan
OSKC	**Osaka City** Univ.	Osaka, Japan
OSLO	Univ. of **Oslo**	Oslo, Norway
OSU	**Ohio State** Univ.	Columbus, OH, USA
OTTA	Univ. of **Ottawa**	Ottawa, ON, Canada
OXF	University of **Oxford**	Oxford, United Kingdom
OXFTP	Univ. of **Oxford**	Oxford, United Kingdom
PADO	Univ. degli Studi di **Padova**	Padova, Italy
PARIN	**LPNHE**, IN^2P^3/CNRS	Paris, France
PARIS	Univ. de Paris (Historical)	**Paris**, France

Abbreviations Used in the Particle Listings

PARIT	**Univ. Paris VII**, LPTHE	Paris, France
PARM	**INFN**, Gruppo Collegato di **Parma**	Parma, Italy
PAST	Institut **Pasteur**	**Paris**, France
PATR	Univ. of **Patras**	Patras, Greece
PAVI	Univ. di **Pavia**	Pavia, Italy
PAVII	INFN, Sez. di **Pavia**	**Pavia**, Italy
PENN	Univ. of **Pennsylvania**	Philadelphia, PA, USA
PGIA	**INFN**, Sezione di **Perugia**	Perugia, Italy
PISA	Univ. di **Pisa**	Pisa, Italy
PISAI	**INFN**, Sez. di **Pisa**	Pisa, Italy
PITT	Univ. of **Pittsburgh**	Pittsburgh, PA, USA
PLAT	**SUNY at Plattsburgh**	Plattsburgh, NY, USA
PLRM	Univ. di **Palermo**	Palermo, Italy
PNL	**Battelle Memorial** Inst.	Richland, WA, USA
PNPI	**Petersburg** Nuclear Physics Inst. of Russian Academy of Sciences	Gatchina, Russian Federation
PPA	Princeton-Penn. Proton Accelerator (Historical in *Review*)	Princeton, NJ, USA
PRAG	Inst. of Physics, **ASCR**	**Prague**, Czech Republic
PRIN	**Princeton** Univ.	Princeton, NJ, USA
PSI	Paul Scherrer Inst.	**Villigen** PSI, Switzerland
PSLL	**Physical Science Lab**	Las Cruces, NM, USA
PSU	**Penn State** Univ.	University Park, PA, USA
PUCB	**Pontifícia Univ. Católica do Rio de Janeiro**	Rio de Janeiro, RJ, Brasil
PUEB	Univ. Autonoma de **Puebla**	**Puebla**, Pue, Mexico
PURD	**Purdue** Univ.	West Lafayette, IN, USA
QUKI	**Queen's** Univ.	Kingston, ON, Canada
RAL	**STFC Rutherford Appleton** Lab.	Chilton, Didcot, Oxfordshire, United Kingdom
REGE	Univ. **Regensburg**	Regensburg, Germany
REHO	**Weizmann** Inst. of Science	Rehovot, Israel
REZ	Nuclear Physics Inst. **AVČR**	**Řež**, Czech Republic
RGSUL	Univ. Federal do **Rio Grande do Sul** (UFRGS)	Porto Alegre, RS, Brasil
RHBL	**Royal Holloway, Univ. of London**	Egham, Surrey, United Kingdom
RHEL	**Rutherford** High Energy Lab (Old name for RAL)	Chilton, Didcot, Oxon., United Kingdom
RICE	**Rice** Univ.	Houston, TX, USA
RIKEN	**Riken** Nishina Center for Accelerator-Based Science	Saitama, Japan
RIKK	**Rikkyo** Univ.	Tokyo, Japan
RIS	**Rowland** Inst. for Science	Cambridge, MA, USA
RISC	**Rockwell** International	Thousand Oaks, CA, USA
RISL	**Universities Research Reactor**	**Risley**, Warrington, United Kingdom
RISO	**Riso** National Laboratory	Roskilde, Denmark
RL	**Rutherford** High Energy Lab (Old name for RAL)	Chilton, Didcot, Oxon., United Kingdom
RMCS	**Royal Military** Coll. of Science	Swindon, Wilts., United Kingdom
ROCH	Univ. of **Rochester**	Rochester, NY, USA
ROCK	**Rockefeller** Univ.	New York, NY, USA
ROMA	Univ. di **Roma** (Historical)	**Roma**, Italy
ROMA2	Univ. di **Roma**, "Tor Vergata"	Roma, Italy
ROMA3	**INFN, Sez. di Roma Tre**	**Roma**, Italy
ROMAI	**INFN, Sez. di Roma**	Roma, Italy
ROSE	**Rose-Hulman** Inst. of Technology	Terre Haute, IN, USA
RPI	**Rensselaer Polytechnic** Inst.	Troy, NY, USA
RUTG	**Rutgers**, the State Univ. of New Jersey	Piscataway, NJ, USA
S0GA	**Sogang** University	Seoul, Republic of Korea
SACL	**CEA Saclay**, IRFU	Gif-sur-Yvette, France
SACL5	**CEA Saclay** – IPhT	Gif-sur-Yvette, France
SACLD	**CEA Saclay** (Essonne)	Gif-sur-Yvette, France
SAGA	**Saga** Univ.	Saga-shi, Japan
SAHA	**Saha** Inst. of Nuclear Physics	Bidhan Nagar, Calcutta, India
SANG	**Kyoto Sangyo** Univ.	Kyoto-shi, Japan
SANI	Ist. Superiore di Sanità	**Roma**, Italy
SASK	Univ. of **Saskatchewan**	Saskatoon, SK, Canada
SASSO	Lab. Naz. **Gran Sasso** dell'INFN	**Assergi** (AQ), Italy
SAVO	Univ. de **Savoie**	Chambery, France
SBER	**California** State Univ.	**San Bernardino**, CA, USA
SCHAF	W.J. **Schafer** Assoc.	Livermore, DA, USA
SCIT	**Science** Univ. of **Tokyo**	Tokyo, Japan
SCOT	**Scottish** Univ. Research and Reactor Ctr.	Glasgow, United Kingdom
SCUC	Univ. of **South Carolina**	Columbia, SC, USA
SEAT	**Seattle Pacific** Coll.	Seattle, WA, USA
SEIB	Austrian Research Center, **Seibersdorf** LTD.	Seibersdorf, Austria
SEOU	**Korea** Univ.; Dept. of Physics; HEP Group	Seoul, Republic of Korea
SEOUL	**Seoul** National Univ.; Center for Theoretical Physics; Dept. of Physics & Astronomy, Coll. of Natural Sciences	Seoul, Republic of Korea
SERP	**IHEP**, Inst. for High Energy Physics	Protvino, Russian Federation
SETO	**Seton Hall** Univ.	South Orange, NJ, USA
SFLA	Univ. of **South Florida**	Tampa, FL, USA
SFRA	**Simon Fraser University**	Burnaby, BC, Canada
SFSU	**California** State Univ.	**San Francisco**, CA, USA
SHAMS	**Ain Shams** University	Abbassia, Cairo, Egypt
SHDN	**Shandong** Univ.	Jinan, Shandong, China
SHEF	Univ. of **Sheffield**	Sheffield, United Kingdom
SHMP	Univ. of **Southampton**	Southampton, United Kingdom
SHRZ	**Shiraz** Univ.	Shiraz, Iran
SIEG	Univ. **Siegen**	Siegen, Germany
SILES	Univ. of **Silesia**	Katowice, Poland
SIN	Swiss Inst. of Nuclear Research (Old name for VILL)	**Villigen**, Switzerland
SING	**National Univ.** of Singapore	Kent Ridge, Singapore
SISSA	Scuola Internazionale Superiore di Studi Avanzati	**Trieste**, Italy
SLAC	**SLAC National Accelerator Laboratory**	Menlo Park, CA, USA
SLOV	Inst. of Physics, Slovak Acad. of Sciences	**Bratislava** 45, Slovakia
SMU	**Southern Methodist** Univ.	Dallas, TX, USA
SNSP	**Scuola Normale Superiore**	**Pisa**, Italy
SOFI	Inst. for Nuclear Research and Nuclear Energy	**Sofia**, Bulgaria
SOFU	Univ. of **Sofia** "St. Kliment Ohridski"	Sofia, Bulgaria
SPAUL	Univ. de **São Paulo**	São Paulo, SP, Brasil
SPIFT	Inst. de Física Teórica (**IFT**)	**São Paulo**, SP, Brasil
SSL	Univ. of **California (Berkeley)**	Berkeley, CA, USA
STAN	**Stanford** Univ.	Stanford, CA, USA
STEV	**Stevens** Inst. of Tech.	Hoboken, NJ, USA
STFN	**Jožef Stefan** Institute	**Ljubljana**, Slovenia
STLO	**St. Louis** Univ.	St. Louis, MO, USA
STOH	**Stockholm** Univ.	Stockholm, Sweden
STON	**SUNY at Stony Brook**	Stony Brook, NY, USA
STRB	Inst. Pluridisciplinaire Hubert Curien (**CNRS**)	**Strasbourg**, France
STUT	Univ. **Stuttgart**	Stuttgart, Germany
STUTM	Max-Planck-Inst.	**Stuttgart**, Germany
SUGI	**Sugiyama Jogakuen** Univ.	Aichi, Japan
SURR	Univ. of **Surrey**	Guildford, Surrey, United Kingdom
SUSS	Univ. of **Sussex**	Brighton, United Kingdom
SVR	**Savannah** River Labs.	Aiken, SC, USA
SYDN	Univ. of **Sydney**	Sydney, NSW, Australia
SYRA	**Syracuse** Univ.	Syracuse, NY, USA
TAJK	Acad. Sci., Tadzhik SSR	**Dushanbe**, Tadzhikstan
TAMU	**Texas A&M** Univ.	College Station, TX, USA
TATA	**Tata** Inst. of Fundamental Research	Bombay, India
TBIL	**Tbilisi State University**	Tbilisi, Republic of Georgia
TELA	**Tel-Aviv** Univ.	Tel Aviv, Israel
TELE	**Teledyne Brown** Engineering	Huntsville, AL, USA
TEMP	**Temple** Univ.	Philadelphia, PA, USA
TENN	Univ. of **Tennessee**	Knoxville, TN, USA
TEXA	Univ. of **Texas** at **Austin**	Austin, TX, USA
TGAK	**Tokyo Gakugei** Univ.	Tokyo, Japan
TGU	**Tohoku Gakuin** Univ.	Miyagi, Japan

Abbreviations Used in the Particle Listings

THES	Aristotle Univ. of **Thessaloniki** (AUTh)	Thessaloniki, Greece
TINT	**Tokyo Inst. of Technology**	Tokyo, Japan
TISA	**Sagamihara** Inst. of Space & Astronautical Sci.	Kanagawa, Japan
TMSK	**Tomsk** Polytechnic Univ.	**Tomsk**, Russian Federation
TMTC	**Tokyo Metropolitan** Coll. Tech.	Tokyo, Japan
TMU	**Tokyo Metropolitan Univ.**	Tokyo, Japan
TNTO	Univ. of **Toronto**	Toronto, ON, Canada
TOHO	**Toho** Univ.	Chiba, Japan
TOHOK	**Tohoku** Univ.	Sendai, Japan
TOKA	**Tokai** Univ.	Shimizu, Japan
TOKAH	**Tokai** Univ.	Hiratsuka, Japan
TOKMS	Univ. of **Tokyo**; Meson Science Laboratory	Tokyo, Japan
TOKU	Univ. of **Tokushima**	Tokushima-shi, Japan
TOKY	Univ. of **Tokyo**; High-Energy Physics Theory Group	Tokyo, Japan
TOKYC	Univ. of **Tokyo**; Dept. of Chemistry	Tokyo, Japan
TORI	Univ. degli Studi di **Torino**	Torino, Italy
TPTI	**Uzbek** Academy of Sciences	**Tashkent**, Republic of Uzbekistan
TRIN	Trinity College **Dublin**	Dublin, Ireland
TRIU	**TRIUMF**	Vancouver, BC, Canada
TRST	Univ. di **Trieste**	Trieste, Italy
TRSTI	**INFN**, Sez. di **Trieste**	Trieste, Italy
TRSTT	Univ. degli Studi di **Trieste**	**Trieste**, Italy
TSUK	Univ. of **Tsukuba**	Ibaraki-ken, Japan
TTAM	**Tamagawa** Univ.	Tokyo, Japan
TUAT	**Tokyo** Univ. of Agriculture Tech.	Tokyo, Japan
TUBIN	Univ. **Tübingen**	Tübingen, Germany
TUFTS	**Tufts** Univ.	Medford, MA, USA
TUW	**Technische** Univ. **Wien**	Vienna, Austria
TUZL	**Tuzla** Univ.	Tuzla, Argentina
UBA	Univ. de **Buenos Aires**	Buenos Aires, Argentina
UCB	Univ. of **California (Berkeley)**	Berkeley, CA, USA
UCD	Univ. of **California (Davis)**	Davis, CA, USA
UCI	Univ. of **California (Irvine)**	Irvine, CA, USA
UCLA	Univ. of **California (Los Angeles)**	Los Angeles, CA, USA
UCND	**Union Carbide** Corp.	Oak Ridge, TN, USA
UCR	Univ. of **California (Riverside)**	Riverside, CA, USA
UCSB	Univ. of **California (Santa Barbara)**; Physics Dept., High Energy Physics Experiment	Santa Barbara, CA, USA
UCSBT	Univ. of **California (Santa Barbara)**; Kavli Inst. for Theoretical Physics	Santa Barbara, CA, USA
UCSC	Univ. of **California (Santa Cruz)**	Santa Cruz, CA, USA
UCSD	Univ. of **California (San Diego)**	La Jolla, CA, USA
UGAZ	Univ. of **Gaziantep**	Gaziantep, Turkey
UMD	Univ. of **Maryland**	College Park, MD, USA
UNAM	Univ. Nac. Autónoma de México (**UNAM**)	**México**, DF, Mexico
UNAM	Univ. Nacional Autónoma de México (**UNAM**)	**México**, DF, Mexico
UNC	Univ. of **North Carolina**	Greensboro, NC, USA
UNCCH	Univ. of **North Carolina** at **Chapel Hill**	Chapel Hill, NC, USA
UNCS	**Union** College	Schenectady, NY, USA
UNESP	UNESP	Botucatu, Brasil
UNH	Univ. of **New Hampshire**	Durham, NH, USA
UNM	Univ. of **New Mexico**	Albuquerque, NM, USA
UOEH	Univ. of Occupational and Environmental Health	**Kitakyushu**, Japan
UPNJ	**Upsala** College	East Orange, NJ, USA
UPPS	**Uppsala** Univ.	**Uppsala**, Sweden
UPR	Univ. of **Puerto Rico**	**San Juan**, PR, USA
URI	Univ. of **Rhode Island**	Kingston, RI, USA
USC	Univ. of **Southern California**	Los Angeles, CA, USA
USF	Univ. of **San Francisco**	San Francisco, CA, USA
UTAH	Univ. of **Utah**	Salt Lake City, UT, USA
UTRE	Univ. of **Utrecht**	Utrecht, The Netherlands
UTRO	**Norwegian Univ. of Science & Technology**	Trondheim, Norway
UVA	Univ. of **Virginia**	Charlottesville, VA, USA
UZINR	Acad. Sci., **Ukrainian** SSR	**Uzhgorod**, Ukraine
VALE	Univ. de **Valencia**	Burjassot, **Valencia**, Spain
VALP	**Valparaiso** Univ.	Valparaiso, IN, USA
VAND	**Vanderbilt** Univ.	Nashville, TN, USA
VASS	**Vassar** College	Poughkeepsie, NY, USA
VICT	Univ. of **Victoria**	Victoria, BC, Canada
VIEN	Inst. für Hochenergiephysik (HEPHY)	**Vienna**, Austria
VILL	**ETH Zürich**	Zürich, Switzerland
VPI	**Virginia Tech.**	Blacksburg, VA, USA
VRIJ	**Vrije** Univ.	HV **Amsterdam**, The Netherlands
WABRN	Eidgenossisches Amt für Messwesen	**Waber**, Switzerland
WARS	Univ. of **Warsaw**	Warsaw, Poland
WASCR	**Waseda** Univ.; Cosmic Ray Division	Tokyo, Japan
WASH	Univ. of **Washington**; Elem. Particle Experiment (EPE); Particle Astrophysics (PA)	Seattle, WA, USA
WASU	**Waseda** Univ.; Dept. of Physics, High Energy Physics Group	Tokyo, Japan
WAYN	**Wayne** State Univ.	Detroit, MI, USA
WESL	**Wesleyan** Univ.	Middletown, CT, USA
WIEN	Univ. **Wien**	Vienna, Austria
WILL	Coll. of **William and Mary**	Williamsburg, VA, USA
WINR	National Centre for Nuclear Research	**Warsaw**, Poland
WISC	Univ. of **Wisconsin**	Madison, WI, USA
WITW	Univ. of the **Witwatersrand**	Wits, South Africa
WMIU	**Western Michigan** Univ.	Kalamazoo, MI, USA
WONT	The Univ. of **Western Ontario**	London, ON, Canada
WOOD	**Woodstock** College (No longer in existence)	Woodstock, MD, USA
WUPP	**Bergische** Univ. Wuppertal	**Wuppertal**, Germany
WURZ	Univ. **Würzburg**	Würzburg, Germany
WUSL	**Washington** Univ.	St. Louis, MO, USA
WYOM	Univ. of **Wyoming**	Laramie, WY, USA
YALE	**Yale** Univ.	New Haven, CT, USA
YARO	**Yaroslavl** State Univ.	Yaroslavl, Russian Federation
YCC	**Yokohama** Coll. of Commerce	Yokohama, Japan
YERE	**Yerevan** Physics Inst.	Yerevan, Armenia
YOKO	**Yokohama National** Univ.	Yokohama-shi, Japan
YORKC	**York** Univ.	Toronto, Canada
ZAGR	**Zagreb** Univ.	Zagreb, Croatia
ZARA	Univ. de **Zaragoza**	Zaragoza, Spain
ZEEM	Univ. van **Amsterdam**	TV Amsterdam, The Netherlands
ZHON	**Zhongshan** (Sun Yat-Sen) Univ.	Guangzhou, China
ZHZH	**Zhengzhou** Univ.	Zhengzhou, Henan, China
ZURI	Univ. **Zürich**	Zürich, Switzerland

GAUGE AND HIGGS BOSONS

Related Reviews in Volume 1

GAUGE AND HIGGS BOSONS

γ (photon)

$I(J^{PC}) = 0,1(1^{--})$

γ MASS

Results prior to 2008 are critiqued in GOLDHABER 10. All experimental results published prior to 2005 are summarized in detail by TU 05.

The following conversions are useful: 1 eV = 1.783×10^{-33} g = 1.957×10^{-6} m_e; $\lambda\!\!\!^{-}_C = (1.973 \times 10^{-7}$ m)$\times$(1 eV/m_γ).

VALUE (eV)	CL%	DOCUMENT ID		COMMENT
<1 $\times 10^{-18}$		[1] RYUTOV	07	MHD of solar wind
• • • We do not use the following data for averages, fits, limits, etc. • • •				
$<2.2 \times 10^{-14}$		[2] BONETTI	17	Fast Radio Bursts, FRB 121102
$<1.8 \times 10^{-14}$		[3] BONETTI	16	Fast Radio Bursts, FRB 150418
$<1.9 \times 10^{-15}$		[4] RETINO	16	Ampere's Law in solar wind
$<2.3 \times 10^{-9}$	95	[5] EGOROV	14	Lensed quasar position
		[6] ACCIOLY	10	Anomalous magn. mom.
$<1 \times 10^{-26}$		[7] ADELBERGER	07A	Proca galactic field
no limit feasible		[7] ADELBERGER	07A	γ as Higgs particle
$<1 \times 10^{-19}$		[8] TU	06	Torque on rotating magnetized toroid
$<1.4 \times 10^{-7}$		ACCIOLY	04	Dispersion of GHz radio waves by sun
$<2 \times 10^{-16}$		[9] FULLEKRUG	04	Speed of 5-50 Hz radiation in atmosphere
$<7 \times 10^{-19}$		[10] LUO	03	Torque on rotating magnetized toroid
$<1 \times 10^{-17}$		[11] LAKES	98	Torque on toroid balance
$<6 \times 10^{-17}$		[12] RYUTOV	97	MHD of solar wind
$<8 \times 10^{-16}$	90	[13] FISCHBACH	94	Earth magnetic field
$<5 \times 10^{-13}$		[14] CHERNIKOV	92	Ampere's Law null test
$<1.5 \times 10^{-9}$	90	[15] RYAN	85	Coulomb's Law null test
$<3 \times 10^{-27}$		[16] CHIBISOV	76	Galactic magnetic field
$<6 \times 10^{-16}$	99.7	[17] DAVIS	75	Jupiter's magnetic field
$<7.3 \times 10^{-16}$		HOLLWEG	74	Alfven waves
$<6 \times 10^{-17}$		[18] FRANKEN	71	Low freq. res. circuit
$<2.4 \times 10^{-13}$		[19] KROLL	71A	Dispersion in atmosphere
$<1 \times 10^{-14}$		[20] WILLIAMS	71	Tests Coulomb's Law
$<2.3 \times 10^{-15}$		GOLDHABER	68	Satellite data

[1] RYUTOV 07 extends the method of RYUTOV 97 to the radius of Pluto's orbit.

[2] BONETTI 17 uses frequency-dependent time delays of repeating FRB with well-determined redshift, assuming the DM is caused by expected dispersion in IGM. There are several uncertainties, leading to mass limit 2.2×10^{-14} eV.

[3] BONETTI 16 uses frequency-dependent time delays of FRB, assuming the DM is caused by expected dispersion in IGM. There are several uncertainties, leading to mass limit 1.8×10^{-14} eV, if indeed the FRB is at the initially reported redshift.

[4] RETINO 16 looks for deviations from Ampere's law in the solar wind, using Cluster four spacecraft data. Authors quote a range of limits from 1.9×10^{-15} eV to 7.9×10^{-14} eV depending on the assumptions of the vector potential from the interplanetary magnetic field.

[5] EGOROV 14 studies chromatic dispersion of lensed quasar positions ("gravitational rainbows") that could be produced by any of several mechanisms, among them via photon mass. Limit not competitive but obtained on cosmological distance scales.

[6] ACCIOLY 10 limits come from possible alterations of anomalous magnetic moment of electron and gravitational deflection of electromagnetic radiation. Reported limits are not "claimed" by the authors and in any case are not competitive.

[7] When trying to measure m one must distinguish between measurements performed on large and small scales. If the photon acquires mass by the Higgs mechanism, the large-scale behavior of the photon might be effectively Maxwellian. If, on the other hand, one postulates the Proca regime for all scales, the very existence of the galactic field implies $m < 10^{-26}$ eV, as correctly calculated by YAMAGUCHI 59 and CHIBISOV 76.

[8] TU 06 continues the work of LUO 03, with extended LAKES 98 method, reporting the improved limit $\mu^2 A = (0.7 \pm 1.7) \times 10^{-13}$ T/m if $A = 0.2$ μG out to 4×10^{22} m. Reported result $\mu = (0.9 \pm 1.5) \times 10^{-52}$ g reduces to the frequentist mass limit 1.2×10^{-19} eV (FELDMAN 98).

[9] FULLEKRUG 04 adopted KROLL 71A method with newer and better Schumann resonance data. Result questionable because assumed frequency shift with photon mass is assumed to be linear. It is quadratic according to theorem by GOLDHABER 71B, KROLL 71, and PARK 71.

[10] LUO 03 extends LAKES 98 technique to set a limit on $\mu^2 A$, where μ^{-1} is the Compton wavelength $\lambda\!\!\!^{-}_C$ of the massive photon and A is the ambient vector potential. The important departure is that the apparatus rotates, removing sensitivity to the direction of A. They take $A = 10^{12}$ Tm, due to "cluster level fields." But see comment of GOLDHABER 03 and reply by LUO 03B.

[11] LAKES 98 reports limits on torque on a toroid Cavendish balance, obtaining a limit on $\mu^2 A < 2 \times 10^{-9}$ Tm/m^2 via the Maxwell-Proca equations, where μ^{-1} is the characteristic length associated with the photon mass and A is the ambient vector potential in the Lorentz gauge. Assuming $A \approx 1 \times 10^{12}$ Tm due to cluster fields he obtains $\mu^{-1} > 2 \times 10^{10}$ m, corresponding to $\mu < 1 \times 10^{-17}$ eV. A more conservative limit, using $A \approx (1$ μG)$\times$(600 pc) based on the galactic field, is $\mu^{-1} > 1 \times 10^{9}$ m or $\mu < 2 \times 10^{-16}$ eV.

[12] RYUTOV 97 uses a magnetohydrodynamics argument concerning survival of the Sun's field to the radius of the Earth's orbit. "To reconcile observations to theory, one has to reduce [the photon mass] by approximately an order of magnitude compared with" per DAVIS 75. "Secure limit, best by this method" (per GOLDHABER 10).

[13] FISCHBACH 94 analysis is based on terrestrial magnetic fields; approach analogous to DAVIS 75. Similar result based on a much smaller planet probably follows from more precise B field mapping. "Secure limit, best by this method" (per GOLDHABER 10).

[14] CHERNIKOV 92, motivated by possibility that photon exhibits mass only below some unknown critical temperature, searches for departure from Ampere's Law at 1.24 K. See also RYAN 85.

[15] RYAN 85, motivated by possibility that photon exhibits mass only below some unknown critical temperature, sets mass limit at $< (1.5 \pm 1.4) \times 10^{-42}$ g based on Coulomb's Law departure limit at 1.36 K. We report the result as frequentist 90% CL (FELDMAN 98).

[16] CHIBISOV 76 depends in critical way on assumptions such as applicability of virial theorem. Some of the arguments given only in unpublished references.

[17] DAVIS 75 analysis of Pioneer-10 data on Jupiter's magnetic field. "Secure limit, best by this method" (per GOLDHABER 10).

[18] FRANKEN 71 method is of dubious validity (KROLL 71A, JACKSON 99, GOLDHABER 10, and references therein).

[19] KROLL 71A used low frequency Schumann resonances in cavity between the conducting earth and resistive ionosphere, overcoming objections to resonant-cavity methods (JACKSON 99, GOLDHABER 10, and references therein). "Secure limit, best by this method" (per GOLDHABER 10).

[20] WILLIAMS 71 is landmark test of Coulomb's law. "Secure limit, best by this method" (per GOLDHABER 10).

γ CHARGE

OKUN 06 has argued that schemes in which all photons are charged are inconsistent. He says that if a neutral photon is also admitted to avoid this problem, then other problems emerge, such as those connected with the emission and absorption of charged photons by charged particles. He concludes that in the absence of a self-consistent phenomenological basis, interpretation of experimental data is at best difficult.

VALUE (e)	CHARGE	DOCUMENT ID		TECN	COMMENT
<1 $\times 10^{-46}$	**mixed**	[1] ALTSCHUL	07B	VLBI	Aharonov-Bohm effect
<1 $\times 10^{-35}$	**single**	[2] CAPRINI	05	CMB	Isotropy constraint
• • • We do not use the following data for averages, fits, limits, etc. • • •					
$<1 \times 10^{-32}$	single	[1] ALTSCHUL	07B	VLBI	Aharonov-Bohm effect
$<3 \times 10^{-33}$	mixed	[3] KOBYCHEV	05	VLBI	Smear as function of B·E$_\gamma$
$<4 \times 10^{-31}$	single	[3] KOBYCHEV	05	VLBI	Deflection as function of B·E$_\gamma$
$<8.5 \times 10^{-17}$		[4] SEMERTZIDIS	03		Laser light deflection in B-field
$<3 \times 10^{-28}$	single	[5] SIVARAM	95	CMB	For $\Omega_M = 0.3$, h^2= 0.5
$<5 \times 10^{-30}$		[6] RAFFELT	94	TOF	Pulsar $f_1 - f_2$
$<2 \times 10^{-28}$		[7] COCCONI	92		VLBA radio telescope resolution
$<2 \times 10^{-32}$		COCCONI	88	TOF	Pulsar $f_1 - f_2$ TOF

[1] ALTSCHUL 07B looks for Aharonov-Bohm phase shift in addition to geometric phase shift in radio interference fringes (VSOP mission).

[2] CAPRINI 05 uses isotropy of the cosmic microwave background to place stringent limits on possible charge asymmetry of the Universe. Charge limits are set on the photon, neutrino, and dark matter particles. Valid if charge asymmetries produced by different particles are not anticorrelated.

[3] KOBYCHEV 05 considers a variety of observable effects of photon charge for extragalactic compact radio sources. Best limits if source observed through a foreground cluster of galaxies.

[4] SEMERTZIDIS 03 reports the first laboratory limit on the photon charge in the last 30 years. Straightforward improvements in the apparatus could attain a sensitivity of 10^{-20} e.

[5] SIVARAM 95 requires that CMB photon charge density not overwhelm gravity. Result scales as Ω_M h^2.

[6] RAFFELT 94 notes that COCCONI 88 neglects the fact that the time delay due to dispersion by free electrons in the interstellar medium has the same photon energy dependence as that due to bending of a charged photon in the magnetic field. His limit is based on the assumption that the entire observed dispersion is due to photon charge. It is a factor of 200 less stringent than the COCCONI 88 limit.

[7] See COCCONI 92 for less stringent limits in other frequency ranges. Also see RAFFELT 94 note.

γ REFERENCES

BONETTI	17	PL B768 326	L. Bonetti *et al.*	(ORLEANS, CERN)
BONETTI	16	PL B757 548	L. Bonetti *et al.*	
RETINO	16	ASP 82 49	A. Retino, A.D.A.M. Spallicci, A. Vaivads	(CURCP+)
EGOROV	14	MNRAS 437 L90	P. Egorov *et al.*	(MOSU, MIPT, INRM)
ACCIOLY	10	PR D82 065026	A. Accioly, J. Helayel-Neto, E. Scatena	(LABEX+)
GOLDHABER	10	RMP 82 939	A.S. Goldhaber, M.M. Nieto	(STON, LANL)
ADELBERGER	07A	PRL 98 010402	E. Adelberger, G. Dvali, A. Gruzinov	(WASH, NYU)
ALTSCHUL	07B	PRL 98 261801	B. Altschul	(IND)
Also		ASP 29 290	B. Altschul	(SCUC)
RYUTOV	07	PPCF 49 B429	D.D. Ryutov	(LLNL)
OKUN	06	APP B37 565	L.B. Okun	(ITEP)
TU	06	PL A352 267	L.-C. Tu *et al.*	
CAPRINI	05	JCAP 0502 006	C. Caprini, P.G. Ferreira	(GEVA, OXFTP)
KOBYCHEV	05	AL 31 147	V.V. Kobychev, S.B. Popov	(KIEV, PADO)
TU	05	RPP 68 77	L.-C. Tu, J. Luo, G.T. Gillies	
ACCIOLY	04	PR D69 107501	A. Accioly, R. Paszko	
FULLEKRUG	04	PRL 93 043901	M. Fullekrug	
GOLDHABER	03	PRL 91 149101	A.S. Goldhaber, M.M. Nieto	
LUO	03	PRL 90 081801	J. Luo *et al.*	
LUO	03B	PRL 91 149102	J. Luo *et al.*	
SEMERTZIDIS	03	PR D67 017701	Y.K. Semertzidis, G.T. Danby, D.M. Lazarus	
JACKSON	99	Classical Electrodynamics	J.D. Jackson	(3rd ed., J. Wiley and Sons (1999))
FELDMAN	98	PR D57 3873	G.J. Feldman, R.D. Cousins	
LAKES	98	PRL 80 1826	R. Lakes	(WISC)
RYUTOV	97	PPCF 39 A73	D.D. Ryutov	(LLNL)

Gauge & Higgs Boson Particle Listings

γ, g, graviton, W

SIVARAM	95	AJP 63 473	C. Sivaram	(BANG)
FISCHBACH	94	PRL 73 514	E. Fischbach *et al.*	(PURD, JHU+)
RAFFELT	94	PR D50 7729	G. Raffelt	(MPIM)
CHERNIKOV	92	PRL 68 3383	M.A. Chernikov *et al.*	(ETH)
Also		PRL 69 2999 (erratum)	M.A. Chernikov *et al.*	(ETH)
COCCONI	92	AJP 60 750	G. Cocconi	(CERN)
COCCONI	88	PL B206 705	G. Cocconi	(CERN)
RYAN	85	PR D32 802	J.J. Ryan, F. Accetta, R.H. Austin	(PRIN)
CHIBISOV	76	SPU 19 624	G.V. Chibisov	(LEBD)
		Translated from UFN 119 551.		
DAVIS	75	PRL 35 1402	L. Davis, A.S. Goldhaber, M.M. Nieto	(CIT, STON+)
HOLLWEG	74	PRL 32 961	J.V. Hollweg	(NCAR)
FRANKEN	71	PRL 26 115	P.A. Franken, G.W. Ampulski	(MICH)
GOLDHABER	71B	RMP 43 277	A.S. Goldhaber, M.M. Nieto	(STON, BOHR, UCSB)
KROLL	71	PRL 26 1395	N.M. Kroll	(SLAC)
KROLL	71A	PRL 27 340	N.M. Kroll	(SLAC)
PARK	71	PRL 26 1393	D. Park, E.R. Williams	(WILC)
WILLIAMS	71	PRL 26 721	E.R. Williams, J.E. Faller, H.A. Hill	(WESL)
GOLDHABER	68	PRL 21 567	A.S. Goldhaber, M.M. Nieto	(STON)
YAMAGUCHI	59	PTPS 11 37	Y. Yamaguchi	

g
or gluon

$I(J^P) = 0(1^-)$

SU(3) color octet

Mass $m = 0$. Theoretical value. A mass as large as a few MeV may not be precluded, see YNDURAIN 95.

VALUE	DOCUMENT ID		TECN	COMMENT
• • • We do not use the following data for averages, fits, limits, etc. • • •				
	ABREU	92E	DLPH	Spin 1, not 0
	ALEXANDER	91H	OPAL	Spin 1, not 0
	BEHREND	82D	CELL	Spin 1, not 0
	BERGER	80D	PLUT	Spin 1, not 0
	BRANDELIK	80C	TASS	Spin 1, not 0

gluon REFERENCES

YNDURAIN	95	PL B345 524	F.J. Yndurain	(MADU)
ABREU	92E	PL B274 498	P. Abreu *et al.*	(DELPHI Collab.)
ALEXANDER	91H	ZPHY C52 543	G. Alexander *et al.*	(OPAL Collab.)
BEHREND	82D	PL B110 329	H.J. Behrend *et al.*	(CELLO Collab.)
BERGER	80D	PL B97 459	C. Berger *et al.*	(PLUTO Collab.)
BRANDELIK	80C	PL B97 453	R. Brandelik *et al.*	(TASSO Collab.)

graviton

$J = 2$

graviton MASS

Van Dam and Veltman (VANDAM 70), Iwasaki (IWASAKI 70), and Zakharov (ZAKHAROV 70) almost simultanously showed that "... there is a discrete difference between the theory with zero-mass and a theory with finite mass, no matter how small as compared to all external momenta." The resolution of this "vDVZ discontinuity" has to do with whether the linear approximation is valid. De Rham *etal*. (DE-RHAM 11) have shown that nonlinear effects not captured in their linear treatment can give rise to a screening mechanism, allowing for massive gravity theories. See also GOLDHABER 10 and DE-RHAM 17 and references therein. Experimental limits have been set based on a Yukawa potential or signal dispersion. h_0 is the Hubble constant in units of 100 km s^{-1} Mpc^{-1}.

The following conversions are useful: 1 eV = 1.783×10^{-33} g = 1.957×10^{-6} m_e; $\lambda\!\!\!^{-}_C = (1.973 \times 10^{-7}$ m$) \times (1$ eV$/m_g)$.

VALUE (eV)		DOCUMENT ID		TECN	COMMENT
<6 $\times 10^{-32}$		[1] CHOUDHURY 04		YUKA	Weak gravitational lensing
• • • We do not use the following data for averages, fits, limits, etc. • • •					
$<7 \times 10^{-23}$		[2] ABBOTT	17	DISP	Combined dispersion limit from three BH mergers
$<1.2 \times 10^{-22}$		[2] ABBOTT	16	DISP	Combined dispersion limit from two BH mergers
$<5 \times 10^{-23}$		[3] BRITO	13		Spinning black holes bounds
$<4 \times 10^{-25}$		[4] BASKARAN	08		Graviton phase velocity fluctuations
$<6 \times 10^{-32}$		[5] GRUZINOV	05	YUKA	Solar System observations
$<9.0 \times 10^{-34}$		[6] GERSHTEIN	04		From Ω_{tot} value assuming RTG
$>6 \times 10^{-34}$		[7] DVALI	03		Horizon scales
$<8 \times 10^{-20}$		[8,9] FINN	02	DISP	Binary pulsar orbital period decrease
		[9,10] DAMOUR	91		Binary pulsar PSR 1913+16
$<7 \times 10^{-23}$		TALMADGE	88	YUKA	Solar system planetary astrometric data
$< 2 \times 10^{-29}\ h_0^{-1}$		GOLDHABER	74		Rich clusters
$<7 \times 10^{-28}$		HARE	73		Galaxy
$<8 \times 10^{4}$		HARE	73		2γ decay

[1] CHOUDHURY 04 concludes from a study of weak-lensing data that masses heavier than about the inverse of 100 Mpc seem to be ruled out if the gravitation field has the Yukawa form.

[2] ABBOTT 16 and ABBOTT 17 assumed a dispersion relation for gravitational waves modified relative to GR.

[3] BRITO 13 explore massive graviton (spin-2) fluctuations around rotating black holes.

[4] BASKARAN 08 consider fluctuations in pulsar timing due to photon interactions ("surfing") with background gravitational waves.

[5] GRUZINOV 05 uses the DGP model (DVALI 00) showing that non-perturbative effects restore continuity with Einstein's equations as the graviton mass approaches 0, then bases his limit on Solar System observations.

[6] GERSHTEIN 04 use non-Einstein field relativistic theory of gravity (RTG), with a massive graviton, to obtain the 95% CL mass limit implied by the value of $\Omega_{tot} = 1.02 \pm 0.02$ current at the time of publication.

[7] DVALI 03 suggest scale of horizon distance via DGP model (DVALI 00). For a horizon distance of 3×10^{26} m (about age of Universe/c; GOLDHABER 10) this graviton mass limit is implied.

[8] FINN 02 analyze the orbital decay rates of PSR B1913+16 and PSR B1534+12 with a possible graviton mass as a parameter. The combined frequentist mass limit is at 90%CL.

[9] As of 2014, limits on dP/dt are now about 0.1% (see T. Damour, "Experimental tests of gravitational theory," in this *Review*).

[10] DAMOUR 91 is an analysis of the orbital period change in binary pulsar PSR 1913+16, and confirms the general relativity prediction to 0.8%. "The theoretical importance of the [rate of orbital period decay] measurement has long been recognized as a direct confirmation that the gravitational interaction propagates with velocity c (which is the immediate cause of the appearance of a damping force in the binary pulsar system) and thereby as a test of the existence of gravitational radiation and of its quadrupolar nature." TAYLOR 93 adds that orbital parameter studies now agree with general relativity to 0.5%, and set limits on the level of scalar contribution in the context of a family of tensor [spin 2]-biscalar theories.

graviton REFERENCES

ABBOTT	17	PRL 118 221101	B.P. Abbot *et al.*	(LIGO and Virgo Collabs.)
DE-RHAM	17	RMP 89 025004	C. de Rham *et al.*	
ABBOTT	16	PRL 116 061102	B.P. Abbott *et al.*	(LIGO and Virgo Collabs.)
BRITO	13	PR D88 023514	R. Brito, V. Cardoso, P. Pani	(LISB, MISS, HSCA+)
DE-RHAM	11	PRL 106 231101	C. de Rham, G. Gabadadze, A.J. Tolley	
GOLDHABER	10	RMP 82 939	A.S. Goldhaber, M.M. Nieto	(STON, LANL)
BASKARAN	08	PR D78 044018	D. Baskaran *et al.*	
GRUZINOV	05	NAST 10 311	A. Gruzinov	(NYU)
CHOUDHURY	04	ASP 21 559	S.R. Choudhury *et al.*	(DELPH, MELB)
GERSHTEIN	04	PAN 67 1596	S.S. Gershtein *et al.*	(SERP)
		Translated from YAF 67 1618.		
DVALI	03	PR D68 024012	G.R. Dvali, A. Grizinov, M. Zaldarriaga	(NYU)
FINN	02	PR D65 044022	L.S. Finn, P.J. Sutton	
DVALI	00	PL B485 208	G.R. Dvali, G. Gabadadze, M. Porrati	(NYU)
TAYLOR	93	NAT 355 132	J.N. Taylor *et al.*	(PRIN, ARCBO, BURE+) J
DAMOUR	91	APJ 366 501	T. Damour, J.H. Taylor	(BURE, MEUD, PRIN)
TALMADGE	88	PRL 61 1159	C. Talmadge *et al.*	(JPL)
GOLDHABER	74	PR D9 1119	A.S. Goldhaber, M.M. Nieto	(LANL, STON)
HARE	73	CJP 51 431	M.G. Hare	(SASK)
IWASAKI	70	PR D2 2255	Y. Iwasaki	
VANDAM	70	NP B22 397	H. van Dam, M. Veltman	(UTRE)
ZAKHAROV	70	JETPL 12 312	V.I. Zakharov *et al.*	

W

$J = 1$

See the related review(s):
Mass and Width of the W Boson

W MASS

The W-mass listed here corresponds to the mass parameter in a Breit-Wigner distribution with mass-dependent width. To obtain the world average, common systematic uncertainties between experiments are properly taken into account. The LEP-2 average W mass based on published results is 80.376 ± 0.033 GeV [SCHAEL 13A]. The combined Tevatron data yields an average W mass of 80.387 ± 0.016 GeV [AALTONEN 13N]. A combination of the LEP average with this Tevatron average and the ATLAS value [AABOUD 18J], assuming a common systematic error of 7 MeV between the latter two [Jens Erler, 52nd Rencontres de Moriond EW, March 2017], the world average W mass of 80.379 ± 0.012 GeV is obtained. OUR FIT quotes this value for the W mass.

VALUE (GeV)	EVTS	DOCUMENT ID		TECN	COMMENT
80.379± 0.012 OUR FIT					
80.370± 0.007±0.017	13.7M	[1] AABOUD	18J	ATLS	$E_{cm}^{pp} = 7$ TeV
80.375± 0.023	2177k	[2] ABAZOV	14N	D0	$E_{cm}^{p\overline{p}} = 1.96$ TeV
80.387± 0.019	1095k	[3] AALTONEN	12E	CDF	$E_{cm}^{p\overline{p}} = 1.96$ TeV
80.336± 0.055±0.039	10.3k	[4] ABDALLAH	08A	DLPH	$E_{cm}^{ee} = 161$–209 GeV
80.415± 0.042±0.031	11830	[5] ABBIENDI	06	OPAL	$E_{cm}^{ee} = 170$–209 GeV
80.270± 0.046±0.031	9909	[6] ACHARD	06	L3	$E_{cm}^{ee} = 161$–209 GeV
80.440± 0.043±0.027	8692	[7] SCHAEL	06	ALEP	$E_{cm}^{ee} = 161$–209 GeV
80.483± 0.084	49247	[8] ABAZOV	02D	D0	$E_{cm}^{p\overline{p}} = 1.8$ TeV
80.433± 0.079	53841	[9] AFFOLDER	01E	CDF	$E_{cm}^{p\overline{p}} = 1.8$ TeV
• • • We do not use the following data for averages, fits, limits, etc. • • •					
80.367± 0.026	1677k	[10] ABAZOV	12F	D0	$E_{cm}^{p\overline{p}} = 1.96$ TeV
80.401± 0.043	500k	[11] ABAZOV	09AB	D0	$E_{cm}^{p\overline{p}} = 1.96$ TeV
80.413± 0.034±0.034	115k	[12] AALTONEN	07F	CDF	$E_{cm}^{p\overline{p}} = 1.96$ TeV
82.87 ± 1.82 $^{+0.30}_{-0.16}$	1500	[13] AKTAS	06	H1	$e^{\pm}p \to \overline{\nu}_e(\nu_e)X$, $\sqrt{s} \approx 300$ GeV
80.3 ± 2.1 ± 1.2 ± 1.0	645	[14] CHEKANOV	02C	ZEUS	$e^-p \to \nu_e X$, $\sqrt{s} =$ 318 GeV
81.4 $^{+2.7}_{-2.6}$ ± 2.0 $^{+3.3}_{-3.0}$	1086	[15] BREITWEG	00D	ZEUS	$e^+p \to \overline{\nu}_e X$, $\sqrt{s} \approx$ 300 GeV
80.84 ± 0.22 ±0.83	2065	[16] ALITTI	92B	UA2	See W/Z ratio below

80.79	± 0.31	±0.84		[17] ALITTI	90B	UA2	$E_{cm}^{p\overline{p}}$ = 546,630 GeV
80.0	± 3.3	±2.4	22	[18] ABE	89I	CDF	$E_{cm}^{p\overline{p}}$ = 1.8 TeV
82.7	± 1.0	±2.7	149	[19] ALBAJAR	89	UA1	$E_{cm}^{p\overline{p}}$ = 546,630 GeV
81.8	$^{+\ 6.0}_{-\ 5.3}$	±2.6	46	[20] ALBAJAR	89	UA1	$E_{cm}^{p\overline{p}}$ = 546,630 GeV
89	± 3	±6	32	[21] ALBAJAR	89	UA1	$E_{cm}^{p\overline{p}}$ = 546,630 GeV
81.	± 5.		6	ARNISON	83	UA1	$E_{cm}^{e\overline{e}}$ = 546 GeV
80.	$^{+10.}_{-\ 6.}$		4	BANNER	83B	UA2	Repl. by ALITTI 90B

[1] AABOUD 18J select 4.61M $W^+ \to \mu^+\nu_\mu$, 3.40M $W^+ \to e^+\nu_e$, 3.23M $W^- \to \mu^-\overline{\nu}_\mu$ and 2.49M $W^- \to e^-\overline{\nu}_e$ events in 4.6 fb^{-1} pp data at 7 TeV. The W mass is determined using the transverse mass and transverse lepton momentum distributions, accounting for correlations. The systematic error includes 0.011 GeV experimental and 0.014 GeV modelling uncertainties.

[2] ABAZOV 14N is a combination of ABAZOV 09AB and ABAZOV 12F, also giving more details on the analysis.

[3] AALTONEN 12E select 470k $W \to e\nu$ decays and 625k $W \to \mu\nu$ decays in 2.2 fb^{-1} of Run-II data. The mass is determined using the transverse mass, transverse lepton momentum and transverse missing energy distributions, accounting for correlations. This result supersedes AALTONEN 07F. AALTONEN 14D gives more details on the procedures followed by the authors.

[4] ABDALLAH 08A use direct reconstruction of the kinematics of $W^+W^- \to q\overline{q}\ell\nu$ and $W^+W^- \to q\overline{q}q\overline{q}$ events for energies 172 GeV and above. The W mass was also extracted from the dependence of the WW cross section close to the production threshold and combined appropriately to obtain the final result. The systematic error includes ±0.025 GeV due to final state interactions and ±0.009 GeV due to LEP energy uncertainty.

[5] ABBIENDI 06 use direct reconstruction of the kinematics of $W^+W^- \to q\overline{q}\ell\nu_\ell$ and $W^+W^- \to q\overline{q}q\overline{q}$ events. The result quoted here is obtained combining this mass value with the results using $W^+W^- \to \ell\nu_\ell\ell'\nu_{\ell'}$ events in the energy range 183–207 GeV (ABBIENDI 03C) and the dependence of the WW production cross-section on m_W at threshold. The systematic error includes ±0.009 GeV due to the uncertainty on the LEP beam energy.

[6] ACHARD 06 use direct reconstruction of the kinematics of $W^+W^- \to q\overline{q}\ell\nu_\ell$ and $W^+W^- \to q\overline{q}q\overline{q}$ events in the C.M. energy range 189–209 GeV. The result quoted here is obtained combining this mass value with the results obtained from a direct W mass reconstruction at 172 and 183 GeV and with those from the dependence of the WW production cross-section on m_W at 161 and 172 GeV (ACCIARRI 99).

[7] SCHAEL 06 use direct reconstruction of the kinematics of $W^+W^- \to q\overline{q}\ell\nu_\ell$ and $W^+W^- \to q\overline{q}q\overline{q}$ events in the C.M. energy range 183–209 GeV. The result quoted here is obtained combining this mass value with those obtained from the dependence of the W pair production cross-section on m_W at 161 and 172 GeV (BARATE 97 and BARATE 97S respectively). The systematic error includes ±0.009 GeV due to possible effects of final state interactions in the $q\overline{q}q\overline{q}$ channel and ±0.009 GeV due to the uncertainty on the LEP beam energy.

[8] ABAZOV 02D improve the measurement of the W-boson mass including $W \to e\nu_e$ events in which the electron is close to a boundary of a central electromagnetic calorimeter module. Properly combining the results obtained by fitting $m_T(W)$, $p_T(e)$, and $p_T(\nu)$, this sample provides a mass value of 80.574 ± 0.405 GeV. The value reported here is a combination of this measurement with all previous DØ W-boson mass measurements.

[9] AFFOLDER 01E fit the transverse mass spectrum of 30115 $W \to e\nu_e$ events (M_W= 80.473 ± 0.065 ± 0.092 GeV) and of 14740 $W \to \mu\nu_\mu$ events (M_W= 80.465 ± 0.100 ± 0.103 GeV) obtained in the run IB (1994-95). Combining the electron and muon results, accounting for correlated uncertainties, yields M_W= 80.470 ± 0.089 GeV. They combine this value with their measurement of ABE 95P reported in run IA (1992-93) to obtain the quoted value.

[10] ABAZOV 12F select 1677k $W \to e\nu$ decays in 4.3 fb^{-1} of Run-II data. The mass is determined using the transverse mass and transverse lepton momentum distributions, accounting for correlations.

[11] ABAZOV 09AB study the transverse mass, transverse electron momentum, and transverse missing energy in a sample of 0.5 million $W \to e\nu$ decays selected in Run-II data. The quoted result combines all three methods, accounting for correlations.

[12] AALTONEN 07F obtain high purity $W \to e\nu_e$ and $W \to \mu\nu_\mu$ candidate samples totaling 63,964 and 51,128 events respectively. The W mass value quoted above is derived by simultaneously fitting the transverse mass and the lepton, and neutrino p_T distributions.

[13] AKTAS 06 fit the Q^2 dependence ($300 < Q^2 < 30{,}000$ GeV^2) of the charged-current differential cross section with a propagator mass. The first error is experimental and the second corresponds to uncertainties due to input parameters and model assumptions.

[14] CHEKANOV 02C fit the Q^2 dependence ($200 < Q^2 < 60000$ GeV^2) of the charged-current differential cross sections with a propagator mass fit. The last error is due to the uncertainty on the probability density functions.

[15] BREITWEG 00D fit the Q^2 dependence ($200 < Q^2 < 22500$ GeV^2) of the charged-current differential cross sections with a propagator mass fit. The last error is due to the uncertainty on the probability density functions.

[16] ALITTI 92B result has two contributions to the systematic error (±0.83); one (±0.81) cancels in m_W/m_Z and one (±0.17) is noncancelling. These were added in quadrature. We choose the ALITTI 92B value without using the LEP m_Z value, because we perform our own combined fit.

[17] There are two contributions to the systematic error (±0.84): one (±0.81) which cancels in m_W/m_Z and one (±0.21) which is non-cancelling. These were added in quadrature.

[18] ABE 89I systematic error dominated by the uncertainty in the absolute energy scale.

[19] ALBAJAR 89 result is from a total sample of 299 $W \to e\nu$ events.

[20] ALBAJAR 89 result is from a total sample of 67 $W \to \mu\nu$ events.

[21] ALBAJAR 89 result is from $W \to \tau\nu$ events.

W/*Z* MASS RATIO

VALUE	*EVTS*	*DOCUMENT ID*		*TECN*	*COMMENT*
0.88153±0.00017		[1] PDG	16		
• • • We do not use the following data for averages, fits, limits, etc. • • •					
0.8821 ±0.0011 ±0.0008	28323	[2] ABBOTT	98N	D0	$E_{cm}^{p\overline{p}}$ = 1.8 TeV
0.88114±0.00154±0.00252	5982	[3] ABBOTT	98P	D0	$E_{cm}^{p\overline{p}}$ = 1.8 TeV
0.8813 ±0.0036 ±0.0019	156	[4] ALITTI	92B	UA2	$E_{cm}^{p\overline{p}}$ = 630 GeV

[1] PDG 16 is the PDG average using the world average m_W and m_Z values as quoted in this edition of *Review of Particle Physics*. The directly measured values of m_W/m_Z are not used as their correlation with the Tevatron measured m_W is unknown.

[2] ABBOTT 98N obtain this from a study of 28323 $W \to e\nu_e$ and 3294 $Z \to e^+e^-$ decays. Of this latter sample, 2179 events are used to calibrate the electron energy scale.

[3] ABBOTT 98P obtain this from a study of 5982 $W \to e\nu_e$ events. The systematic error includes an uncertainty of ±0.00175 due to the electron energy scale.

[4] Scale error cancels in this ratio.

$m_Z - m_W$

VALUE (GeV)	*DOCUMENT ID*		*TECN*	*COMMENT*
10.803±0.015 OUR AVERAGE				
10.803±0.015	[1] PDG	16		
10.4 ±1.4 ±0.8	ALBAJAR	89	UA1	$E_{cm}^{p\overline{p}}$ = 546,630 GeV
• • • We do not use the following data for averages, fits, limits, etc. • • •				
11.3 ±1.3 ±0.9	ANSARI	87	UA2	$E_{cm}^{p\overline{p}}$ = 546,630 GeV

[1] PDG 16 value was obtained using the world average values of m_Z and m_W as listed in this publication.

$m_{W^+} - m_{W^-}$

Test of *CPT* invariance.

VALUE (GeV)	*EVTS*	*DOCUMENT ID*		*TECN*	*COMMENT*
−0.029±0.028 OUR AVERAGE					
−0.029±0.013±0.025	13.7M	[1] AABOUD	18J	ATLS	E_{cm}^{pp} = 7 TeV
−0.19 ±0.58	1722	ABE	90G	CDF	$E_{cm}^{p\overline{p}}$ = 1.8 TeV

[1] AABOUD 18J select 4.61M $W^+ \to \mu^+\nu_\mu$, 3.40M $W^+ \to e^+\nu_e$, 3.23M $W^- \to \mu^-\overline{\nu}_\mu$ and 2.49M $W^- \to e^-\overline{\nu}_e$ events in 4.6 fb^{-1} pp data at 7 TeV. The W mass is determined using the transverse mass and transverse lepton momentum distributions, accounting for correlations. The systematic error includes 0.007 GeV experimental and 0.024 GeV modelling uncertainties.

W WIDTH

The W width listed here corresponds to the width parameter in a Breit-Wigner distribution with mass-dependent width. To obtain the world average, common systematic uncertainties between experiments are properly taken into account. The LEP-2 average W width based on published results is 2.195 ± 0.083 GeV [SCHAEL 13A]. The combined Tevatron data yields an average W width of 2.046±0.049 GeV [FERMILAB-TM-2460-E].

OUR FIT uses these average LEP and Tevatron width values and combines them assuming no correlations.

VALUE (GeV)	*EVTS*	*DOCUMENT ID*		*TECN*	*COMMENT*
2.085±0.042 OUR FIT					
2.028±0.072	5272	[1] ABAZOV	09AK	D0	$E_{cm}^{p\overline{p}}$ = 1.96 GeV
2.032±0.045±0.057	6055	[2] AALTONEN	08B	CDF	$E_{cm}^{p\overline{p}}$ = 1.96 TeV
2.404±0.140±0.101	10.3k	[3] ABDALLAH	08A	DLPH	E_{cm}^{ee} = 183–209 GeV
1.996±0.096±0.102	10729	[4] ABBIENDI	06	OPAL	E_{cm}^{ee} = 170–209 GeV
2.18 ±0.11 ±0.09	9795	[5] ACHARD	06	L3	E_{cm}^{ee} = 172–209 GeV
2.14 ±0.09 ±0.06	8717	[6] SCHAEL	06	ALEP	E_{cm}^{ee} = 183–209 GeV
2.23 $^{+0.15}_{-0.14}$ ±0.10	294	[7] ABAZOV	02E	D0	$E_{cm}^{p\overline{p}}$ = 1.8 TeV
2.05 ±0.10 ±0.08	662	[8] AFFOLDER	00M	CDF	$E_{cm}^{p\overline{p}}$ = 1.8 TeV
• • • We do not use the following data for averages, fits, limits, etc. • • •					
2.152±0.066	79176	[9] ABBOTT	00B	D0	Extracted value
2.064±0.060±0.059		[10] ABE	95W	CDF	Extracted value
2.10 $^{+0.14}_{-0.13}$ ±0.09	3559	[11] ALITTI	92	UA2	Extracted value
2.18 $^{+0.26}_{-0.24}$ ±0.04		[12] ALBAJAR	91	UA1	Extracted value

[1] ABAZOV 09AK obtain this result fitting the high-end tail (100-200 GeV) of the transverse mass spectrum in $W \to e\nu$ decays.

[2] AALTONEN 08B obtain this result fitting the high-end tail (90–200 GeV) of the transverse mass spectrum in semileptonic $W \to e\nu_e$ and $W \to \mu\nu_\mu$ decays.

[3] ABDALLAH 08A use direct reconstruction of the kinematics of $W^+W^- \to q\overline{q}\ell\nu$ and $W^+W^- \to q\overline{q}q\overline{q}$ events. The systematic error includes ±0.065 GeV due to final state interactions.

[4] ABBIENDI 06 use direct reconstruction of the kinematics of $W^+W^- \to q\overline{q}\ell\nu_\ell$ and $W^+W^- \to q\overline{q}q\overline{q}$ events. The systematic error includes ±0.003 GeV due to the uncertainty on the LEP beam energy.

[5] ACHARD 06 use direct reconstruction of the kinematics of $W^+W^- \to q\overline{q}\ell\nu_\ell$ and $W^+W^- \to q\overline{q}q\overline{q}$ events in the C.M. energy range 189–209 GeV. The result quoted

here is obtained combining this value of the width with the result obtained from a direct W mass reconstruction at 172 and 183 GeV (ACCIARRI 99).

[6] SCHAEL 06 use direct reconstruction of the kinematics of $W^+W^- \to q\overline{q}\ell\nu_\ell$ and $W^+W^- \to q\overline{q}q\overline{q}$ events. The systematic error includes ± 0.05 GeV due to possible effects of final state interactions in the $q\overline{q}q\overline{q}$ channel and ± 0.01 GeV due to the uncertainty on the LEP beam energy.

[7] ABAZOV 02E obtain this result fitting the high-end tail (90–200 GeV) of the transverse-mass spectrum in semileptonic $W \to e\nu_e$ decays.

[8] AFFOLDER 00M fit the high transverse mass (100–200 GeV) $W \to e\nu_e$ and $W \to \mu\nu_\mu$ events to obtain $\Gamma(W) = 2.04 \pm 0.11(\text{stat}) \pm 0.09(\text{syst})$ GeV. This is combined with the earlier CDF measurement (ABE 95C) to obtain the quoted result.

[9] ABBOTT 00B measure $R = 10.43 \pm 0.27$ for the $W \to e\nu_e$ decay channel. They use the SM theoretical predictions for $\sigma(W)/\sigma(Z)$ and $\Gamma(W \to e\nu_e)$ and the world average for $B(Z \to ee)$. The value quoted here is obtained combining this result (2.169 ± 0.070 GeV) with that of ABBOTT 99H.

[10] ABE 95W measured $R = 10.90 \pm 0.32 \pm 0.29$. They use m_W=80.23 $\pm$ 0.18 GeV, $\sigma(W)/\sigma(Z) = 3.35 \pm 0.03$, $\Gamma(W \to e\nu) = 225.9 \pm 0.9$ MeV, $\Gamma(Z \to e^+e^-) = 83.98 \pm 0.18$ MeV, and $\Gamma(Z) = 2.4969 \pm 0.0038$ GeV.

[11] ALITTI 92 measured $R = 10.4^{+0.7}_{-0.6} \pm 0.3$. The values of $\sigma(Z)$ and $\sigma(W)$ come from $O(\alpha_s^2)$ calculations using $m_W = 80.14 \pm 0.27$ GeV, and $m_Z = 91.175 \pm 0.021$ GeV along with the corresponding value of $\sin^2\theta_W = 0.2274$. They use $\sigma(W)/\sigma(Z) = 3.26 \pm 0.07 \pm 0.05$ and $\Gamma(Z) = 2.487 \pm 0.010$ GeV.

[12] ALBAJAR 91 measured $R = 9.5^{+1.1}_{-1.0}$ (stat. + syst.). $\sigma(W)/\sigma(Z)$ is calculated in QCD at the parton level using $m_W = 80.18 \pm 0.28$ GeV and $m_Z = 91.172 \pm 0.031$ GeV along with $\sin^2\theta_W = 0.2322 \pm 0.0014$. They use $\sigma(W)/\sigma(Z) = 3.23 \pm 0.05$ and $\Gamma(Z) = 2.498 \pm 0.020$ GeV. This measurement is obtained combining both the electron and muon channels.

W^+ DECAY MODES

W^- modes are charge conjugates of the modes below.

	Mode		Fraction (Γ_i/Γ)		Confidence level
Γ_1	$\ell^+\nu$	[a]	(10.86 ± 0.09) %		
Γ_2	$e^+\nu$		(10.71 ± 0.16) %		
Γ_3	$\mu^+\nu$		(10.63 ± 0.15) %		
Γ_4	$\tau^+\nu$		(11.38 ± 0.21) %		
Γ_5	hadrons		(67.41 ± 0.27) %		
Γ_6	$\pi^+\gamma$		< 7	$\times 10^{-6}$	95%
Γ_7	$D_s^+\gamma$		< 1.3	$\times 10^{-3}$	95%
Γ_8	cX		(33.3 ± 2.6) %		
Γ_9	$c\overline{s}$		(31 $^{+13}_{-11}$) %		
Γ_{10}	invisible	[b]	(1.4 ± 2.9) %		

[a] ℓ indicates each type of lepton (e, μ, and τ), not sum over them.

[b] This represents the width for the decay of the W boson into a charged particle with momentum below detectability, p< 200 MeV.

W PARTIAL WIDTHS

Γ(invisible) Γ_{10}

This represents the width for the decay of the W boson into a charged particle with momentum below detectability, p< 200 MeV.

VALUE (MeV)	DOCUMENT ID		TECN	COMMENT
$30^{+52}_{-48} \pm 33$	[1] BARATE	99I	ALEP	E_{cm}^{ee}= 161+172+183 GeV
• • • We do not use the following data for averages, fits, limits, etc. • • •				
	[2] BARATE	99L	ALEP	E_{cm}^{ee}= 161+172+183 GeV

[1] BARATE 99I measure this quantity using the dependence of the total cross section σ_{WW} upon a change in the total width. The fit is performed to the WW measured cross sections at 161, 172, and 183 GeV. This partial width is < 139 MeV at 95%CL.

[2] BARATE 99L use W-pair production to search for effectively invisible W decays, tagging with the decay of the other W boson to Standard Model particles. The partial width for effectively invisible decay is < 27 MeV at 95%CL.

W BRANCHING RATIOS

Overall fits are performed to determine the branching ratios of the W boson. Averages on $W \to e\nu$, $W \to \mu\nu$, and $W \to \tau\nu$, and their correlations are obtained by combining results from the four LEP experiments properly taking into account the common systematic uncertainties and their correlations [SCHAEL 13A]. A first fit determines the three individual leptonic braching ratios $B(W \to e\nu)$, $B(W \to \mu\nu)$, and $B(W \to \tau\nu)$. This fit has a $\chi^2 = 6.3$ for 9 degrees of freedom. The correlation coefficients between the branching fractions are 0.14 $(e-\mu)$, −0.20 $(e-\tau)$, −0.12 $(\mu-\tau)$. A second fit assumes lepton universality and determines the leptonic branching ratio $\text{br}W \to \ell\nu$ and the hadronic branching ratio is derived as $B(W \to \text{hadrons}) = 1\text{–}3\ \text{br}W \to \ell$. This fit has a $\chi^2 = 15.4$ for 11 degrees of freedom.

$\Gamma(\ell^+\nu)/\Gamma_{\text{total}}$ Γ_1/Γ

ℓ indicates average over e, μ, and τ modes, not sum over modes.

VALUE (units 10^{-2})	EVTS	DOCUMENT ID		TECN	COMMENT
10.86±0.09 OUR FIT					
10.86±0.12±0.08	16438	ABBIENDI	07A	OPAL	E_{cm}^{ee}= 161–209 GeV
10.85±0.14±0.08	13600	ABDALLAH	04G	DLPH	E_{cm}^{ee}= 161–209 GeV
10.83±0.14±0.10	11246	ACHARD	04J	L3	E_{cm}^{ee}= 161–209 GeV
10.96±0.12±0.05	16116	SCHAEL	04A	ALEP	E_{cm}^{ee}= 183–209 GeV
• • • We do not use the following data for averages, fits, limits, etc. • • •					
11.02±0.52	11858	[1] ABBOTT	99H	D0	$E_{cm}^{p\overline{p}}$= 1.8 TeV
10.4 ±0.8	3642	[2] ABE	92I	CDF	$E_{cm}^{p\overline{p}}$= 1.8 TeV

[1] ABBOTT 99H measure $R \equiv [\sigma_W B(W \to \ell\nu_\ell)]/[\sigma_Z B(Z \to \ell\ell)] = 10.90 \pm 0.52$ combining electron and muon channels. They use $M_W = 80.39 \pm 0.06$ GeV and the SM theoretical predictions for $\sigma(W)/\sigma(Z)$ and $B(Z \to \ell\ell)$.

[2] $1216 \pm 38^{+27}_{-31}$ $W \to \mu\nu$ events from ABE 92I and 2426 $W \to e\nu$ events of ABE 91C. ABE 92I give the inverse quantity as 9.6 ± 0.7 and we have inverted.

$\Gamma(e^+\nu)/\Gamma_{\text{total}}$ Γ_2/Γ

VALUE (units 10^{-2})	EVTS	DOCUMENT ID		TECN	COMMENT
10.71±0.16 OUR FIT					
10.71±0.25±0.11	2374	ABBIENDI	07A	OPAL	E_{cm}^{ee}= 161–209 GeV
10.55±0.31±0.14	1804	ABDALLAH	04G	DLPH	E_{cm}^{ee}= 161–209 GeV
10.78±0.29±0.13	1576	ACHARD	04J	L3	E_{cm}^{ee}= 161–209 GeV
10.78±0.27±0.10	2142	SCHAEL	04A	ALEP	E_{cm}^{ee}= 183–209 GeV
• • • We do not use the following data for averages, fits, limits, etc. • • •					
10.61±0.28		[1] ABAZOV	04D	TEVA	$E_{cm}^{p\overline{p}}$= 1.8 TeV

[1] ABAZOV 04D take into account all correlations to properly combine the CDF (ABE 95W) and DØ (ABBOTT 00B) measurements of the ratio R in the electron channel. The ratio R is defined as $[\sigma_W \cdot B(W \to e\nu_e)] / [\sigma_Z \cdot B(Z \to ee)]$. The combination gives $R^{Tevatron} = 10.59 \pm 0.23$. σ_W / σ_Z is calculated at next–to–next–to–leading order (3.360 ± 0.051). The branching fraction $B(Z \to ee)$ is taken from this *Review* as (3.363 ± 0.004)%.

$\Gamma(\mu^+\nu)/\Gamma_{\text{total}}$ Γ_3/Γ

VALUE (units 10^{-2})	EVTS	DOCUMENT ID		TECN	COMMENT
10.63±0.15 OUR FIT					
10.78±0.24±0.10	2397	ABBIENDI	07A	OPAL	E_{cm}^{ee}= 161–209 GeV
10.65±0.26±0.08	1998	ABDALLAH	04G	DLPH	E_{cm}^{ee}= 161–209 GeV
10.03±0.29±0.12	1423	ACHARD	04J	L3	E_{cm}^{ee}= 161–209 GeV
10.87±0.25±0.08	2216	SCHAEL	04A	ALEP	E_{cm}^{ee}= 183–209 GeV

$\Gamma(\mu^+\nu)/\Gamma(e^+\nu)$ Γ_3/Γ_2

VALUE	EVTS	DOCUMENT ID		TECN	COMMENT
0.986±0.013 OUR AVERAGE					
0.980±0.018		[1] AAIJ	16AJ	LHCB	E_{cm}^{pp}= 8 TeV
0.993±0.019		SCHAEL	13A	LEP	E_{cm}^{ee}= 130–209 GeV
0.89 ±0.10	13k	[2] ABACHI	95D	D0	$E_{cm}^{p\overline{p}}$= 1.8 TeV
1.02 ±0.08	1216	[3] ABE	92I	CDF	$E_{cm}^{p\overline{p}}$= 1.8 TeV
1.00 ±0.14 ±0.08	67	ALBAJAR	89	UA1	$E_{cm}^{p\overline{p}}$= 546,630 GeV
• • • We do not use the following data for averages, fits, limits, etc. • • •					
1.24 $^{+0.6}_{-0.4}$	14	ARNISON	84D	UA1	Repl. by ALBAJAR 89

[1] AAIJ 16AJ make precise measurements of forward $W \to e\nu$ and $W \to \mu\nu$ production in proton-proton collisions at 8 TeV and determine the ratio of the W branching fractions $B(W \to e\nu)/B(W \to \mu\nu) = 1.020 \pm 0.002 \pm 0.019$.

[2] ABACHI 95D obtain this result from the measured $\sigma_W B(W \to \mu\nu) = 2.09 \pm 0.23 \pm 0.11$ nb and $\sigma_W B(W \to e\nu) = 2.36 \pm 0.07 \pm 0.13$ nb in which the first error is the combined statistical and systematic uncertainty, the second reflects the uncertainty in the luminosity.

[3] ABE 92I obtain $\sigma_W B(W \to \mu\nu) = 2.21 \pm 0.07 \pm 0.21$ and combine with ABE 91C $\sigma_W B((W \to e\nu))$ to give a ratio of the couplings from which we derive this measurement.

$\Gamma(\tau^+\nu)/\Gamma_{\text{total}}$ Γ_4/Γ

VALUE (units 10^{-2})	EVTS	DOCUMENT ID		TECN	COMMENT
11.38±0.21 OUR FIT					
11.14±0.31±0.17	2177	ABBIENDI	07A	OPAL	E_{cm}^{ee}= 161–209 GeV
11.46±0.39±0.19	2034	ABDALLAH	04G	DLPH	E_{cm}^{ee}= 161–209 GeV
11.89±0.40±0.20	1375	ACHARD	04J	L3	E_{cm}^{ee}= 161–209 GeV
11.25±0.32±0.20	2070	SCHAEL	04A	ALEP	E_{cm}^{ee}= 183–209 GeV

$\Gamma(\tau^+\nu)/\Gamma(e^+\nu)$ Γ_4/Γ_2

VALUE	EVTS	DOCUMENT ID		TECN	COMMENT
1.043±0.024 OUR AVERAGE					
1.063±0.027		SCHAEL	13A	LEP	E_{cm}^{ee}= 130–209 GeV
0.961±0.061	980	[1] ABBOTT	00D	D0	$E_{cm}^{p\overline{p}}$= 1.8 TeV
0.94 ±0.14	179	[2] ABE	92E	CDF	$E_{cm}^{p\overline{p}}$= 1.8 TeV
1.04 ±0.08 ±0.08	754	[3] ALITTI	92F	UA2	$E_{cm}^{p\overline{p}}$= 630 GeV
1.02 ±0.20 ±0.12	32	ALBAJAR	89	UA1	$E_{cm}^{p\overline{p}}$= 546,630 GeV